Title

THE CHARACTERIZATION AND CATALYSIS OF MODIFIED PLATINUM SURFACES

Author

Yeates, R.C.

Publication Date

1985-07-01

Thesis/dissertation

Lawrence Berkeley Laboratory
UNIVERSITY OF CALIFORNIA

Materials & Molecular Research Division

THE CHARACTERIZATION AND CATALYSIS
OF MODIFIED PLATINUM SURFACES

R.C. Yeates
(Ph.D. Thesis)

July 1985

Prepared for the U.S. Department of Energy under Contract DE-AC03-76SF00098

DISCLAIMER

LBL-20050

The Characterization and Catalysis of Modified Platinum Surfaces

Randall Clayton Yeates

Ph.D. Thesis

Lawrence Berkeley Laboratory
University of California
Berkeley, California 94720

July 1985

The Characterization and Catalysis of Modified Platinum Surfaces

By Randall C. Yeates

Materials and Molecular Research Division
Lawrence Berkeley Laboratory
and Department of Chemistry
University of California, Berkeley, CA 94720

ABSTRACT

The surface and catalytic properties of single crystal platinum surfaces of (111), (100), (553) and (13,1,1) cyrstallographic orientations modified by copper, gold and silicon were studied using combined ultra-high vacuum/high pressure techniques. The surface properties of the epitaxial and alloyed copper-platinum and gold-platinum systems were investigated by low energy electron diffraction (LEED), Auger electron spectroscopy (AES), carbon monoxide thermal desorption spectroscopy (TDS), and ultraviolet and X-ray photoelectron spectroscopies (UPS and XPS). Both gold and copper were found to grow layer-by-layer in (1 X 1) islands on all the surfaces studied. Epitaxial gold and copper simply blocked adsorption sites on the platinum surfaces. Gold-platinum and copper-platinum alloy surfaces, formed by diffusion of epitaxially deposited gold or copper into the platinum bulk, generally displayed no order other than a (1 X 1) structure (although a (2 X 2) structure could

be obtained on the Cu-Pt(111) and Cu-Pt(100) alloy surfaces with careful annealing of the sample). No electronic modification of the platinum in the gold-platinum alloys was observed. Platinum in the copper-platinum alloys, however, was electronically modified. This modification resulted in a decrease of the CO desorption energy of up to 5 kcal/mol. The n-hexane conversion reaction was used as a model reforming reaction to study the catalytic properties of these alloy surfaces. Surface structure sensitivity of the catalytic behavior was found. In addition to ensemble effects, electronic factors were also important in determining the activity and selectivities of the reaction catalyzed by these alloy surfaces. Also, mixed gold-platinum sites on the Au-Pt(111) alloy surfaces were found to be more active for the isomerization of n-hexane than pure platinum sites and the mechanism for isomerization at these mixed sites was different than the mechanism at pure platinum sites. The oscillatory behavior of the carbon monoxide oxidation reaction was also studied. The mechanism of the oscillations was found to be different at low pressure (10^{-4} torr) and high pressure (1 atm.). At low pressure oscillations were observed only on the Pt(100) surface and were driven by a surface phase transition. Oscillations were not observed at atomspheric pressure over pure platinum surfaces. When silicon was present on the platinum surface, however, oscillatory behavior in the reaction rate was observed over all the cyrstallographic orientations studied.

Oscillations at high pressure were driven by a cyclic oxidation and reduction of the catalyst surface. The role of the silicon, apparently, was to increase the rate of surface oxidation.

To My Parents

ACKNOWLEDGMENTS

When I began to think about which graduate school I would like to attend, Prof. E. M. Eyring suggested that I should consider Prof. G. A. Somorjai at UC Berkeley. After studying several of Prof. Somorjai's papers I was convinced that I wanted to do my graduate work under his direction. This is a decision I haven't regretted. Prof. Somorjai has been a constant source of ideas and encouragement (prodding) over the last four years. I am also grateful to him for allowing me the freedom I wanted to explore my own ideas and voice my opinions.

I am grateful to my wife Hiromi, who not only had to put up with being married to a graduate student, but also had to adapt to a new culture and language. She was a constant support. My son Christopher has been a great source of pride and delight (and distraction) for the past two years.

I have greatly benefited from the camaraderie of the Somorjai group. I am particularly grateful to Andrew Gellman and Wilfred Tysoe for their constant help and friendship; Michael Quinlan, Eric Garfunkel and Bruce Koel for for their help and guidance during my infancy as a surface scientist; Masahiro Kudo for the XPS and UPS work; and Mark Logan, Francisco Zaera, and the rest of the foosball gang for many hours of enjoyment which helped me keep things in perspective.

The support staff of MMRD saved me many times. Many thanks go to Keith Frank,Wini Heppler, Jim Severns, Hank

Brendel, Dan Colomb, Gloria Pelatowski and the rest of the staff.

I have Richard Smith of Cottonwood High School to thank (or blame) for my interest in chemistry. I took his class simply to fulfill my science requirement and ended up fascinated by chemistry. Prof. Edward Eyring at the University of Utah introduced me to the joys of research and was a constant source of encouragement.

This work was supported by the Division of Material Sciences, Office of Basic Energy Sciences of the U.S. Department of Energy under Contract No. DE-AC03-76Sf00098.

TABLE OF CONTENTS

CHAPTER ONE: INTRODUCTION

Heterogeneous catalysis plays a vital role in the chemical technologies and in many other technologies. Platinum is one of the most versatile heterogeneous metal catalysts [1.1]. Two of the most important uses of platinum are as a petroleum reforming catalyst [1.2 - 1.3] and as a catalyst for the carbon monoxide oxidation reaction [1.4 - 1.5].

In the reforming reaction, straight chain aliphatic hydrocarbons are converted to aromatics and branched hydrocarbons over a platinum catalyst in an excess of hydrogen. The reason this reaction is important can be seen from Fig. 1.1 where the octane number is plotted as a function of the number of carbon atoms in n-alkanes, methylalkanes, dimethylalkanes, naphthenes, aromatics, and olefins. The straight chain hydrocarbons have a low octane number and, in order to increase the octane number, the hydrocarbon must be "reformed" to branched hydrocarbons, aromatics and olefins. Thermodynamic values for the n-hexane conversion reactions are shown in Table 1.1.

The first noble metal reforming catalyst was the "platforming" catalyst developed at Universal Oil Products [1.6]. This catalyst was a highly dispersed platinum supported on alumina, an acidic support. The major function of the platinum in this catalyst is hydrogenation and dehydrogenation, while the acidic sites on the support function as isomerization and hydrocracking sites [1.7]. As

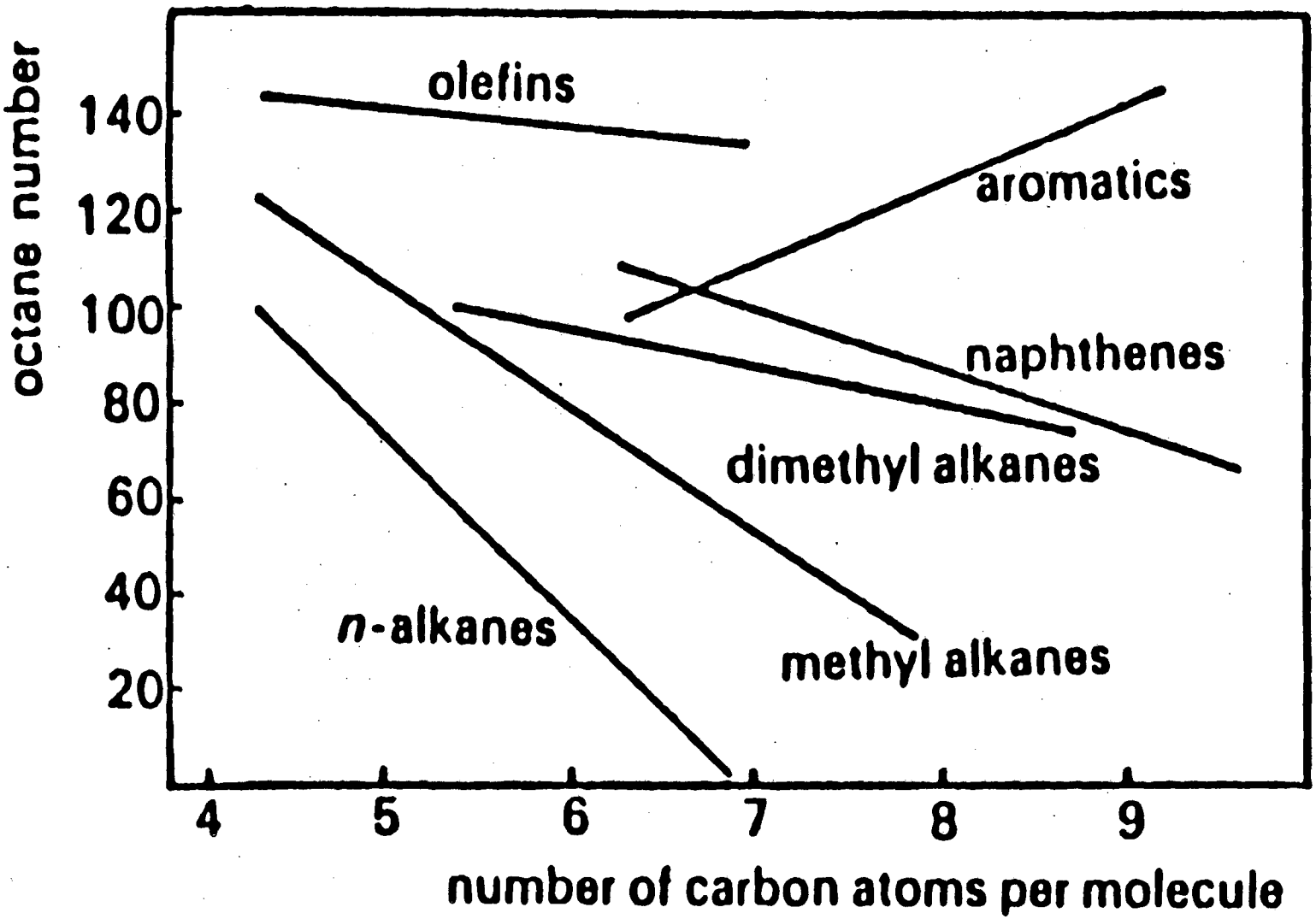

XBL 846-2627

FIG. 1.1

A plot showing the octane number as a function of the carbon number for various hydrocarbons.

TABLE 1.1

REACTION	ΔH°	ΔS°	ΔG°_{570K}
n-hexane + H_2 ---> n-pentane + CH_4	-12.93	4.11	-15.27
n-hexane + H_2 ---> n-butane + ethane	-10.09	5.29	-13.10
n-hexane + H_2 ---> 2 propane	- 9.68	5.36	-12.74
n-hexane ---> methylcyclopentane + H_2	14.46	20.0	3.06
n-hexane ---> benzene + $4H_2$	59.78	96.73	4.64
n-hexane ---> cyclohexane + H_2	10.53	10.04	4.81
n-hexane ---> trans-2-hexene + H_2	27.40	30.16	10.21
n-hexane ---> 2-methylpentane	- 1.70	- 1.50	- 0.84
n-hexane ---> 3-methylpentane	- 1.06	- 1.68	- 0.10

(ΔH° and ΔG° in units of kcal/mole, and ΔS° inunits of cal/mol deg)

will be shown in Chapter 5 however, all of the reforming reactions can occur on the metal surface.

Today, platinum alloys are used in the reforming reaction. These alloys have a greater resistance to poisoning and a more favorable selectivity. The most important of these platinum alloy reforming catalysts is the Pt-Re catalyst [1.8]. Other alloys which have been studied are Pt-Sn [1.9 - 1.11], Pt-Ge [1.12], Pt-Ir [1.13-1.16], Pt-Au [1.17 - 1.23] and Pt-Cu [1.24 - 1.26]. The last two systems are particularly interesting since they contain a 1B metal which is inactive in the reforming reaction. The surface properties and catalytic behavior of these two alloys will be discussed in detail in this thesis.

Most of the studies referenced above were carried out over supported platinum alloys. Several factors make interpretation of the results obtained using supported alloy catalysts difficult : 1) the catalytic activity of the support; 2) modification of the alloy by the support; 3) undefined crystallographic orientation and distribution of the alloy crystallite surfaces; and 4) an undefined alloy surface composition.

A. Surface Segregation

In catalytic studies over supported alloy catalysts the surface composition of the alloys is generally assumed to be the same as that of the bulk due to the difficulty in measuring this quantity. This, however, is a dangerous assumption. Gibbs predicted over one hundred years ago that the composition at the surface of an equilibrium mixture is not necessarily the same as that of the bulk [1.27]. This phenomenon of surface segregation in solid mixtures has been the subject of a great deal of research [1.28 - 1.40].

The major factors effecting the composition of the alloy surface are: 1) the relative surface free energies of the components; and 2) the relative size of the components. If the heat of mixing of the alloy is not too exothermic, the free energy of the system will be at a minimum when the surface is enriched by the component with the lowest surface free energy. An estimation of the relative surface free energies can be made by comparing the heats of sublimation of the components. As can be seen from Table 1.2, the heat of sublimation of both gold and copper is much lower than that of platinum. Ignoring any other factors, one would expect the surface of a Cu-Pt alloy to be enriched with copper and the surface of a Au-Pt alloy to be enriched with gold. This is indeed the case [1.37, 1.41]. A large difference in the size of the components results in a stress on the lattice. Surface segregation is one way in which this stress can be relieved. The adsorption of gasses on an alloy surface can

TABLE 1.2

PHYSICAL CONSTANT	Pt	Au	Cu
Atomic Mass [1.57]	195.09	196.967	63.546
Atomic Radius (A) [1.50]	1.39	1.46	1.28
Atomic Volume (ml/mole) [1.50]	9.10	10.2	7.1
Melting Point (K) (IPTS 1968) [1.57]	2045	1337.58	1356.6
Heat of Sublimation (0 K) (kcal/mol) [1.57]	134.90	87.46	80.58
Electronegativity (Pauling's) [1.50]	2.2	2.4	1.9
Crystal Structure [1.50]	fcc	fcc	fcc
Work Function			
Polycrystalline	5.65 [1.51]	5.1 [1.51]	4.65 [1.51]
(111)	5.7 [1.52]	5.31 [1.53]	4.94 [1.54]
(100)	5.84 [1.55]	5.47 [1.53]	4.59 [1.54]

also result in the segregation of one of the components to the surface if the adsorbate forms a stronger bond with one of the components than with the other [1.42]. The extent of segregation can also depend on the crystallographic orientation of the alloy surface. This was shown by the work of Shek and co-workers [1.33] for a $Pt_{0.98}Cu_{0.02}$ alloy. The extent of segregation on the (110) surface was twice that of the (111) surface.

Using modern surface science techniques, it is possible to control the surface composition of the alloys. This was accomplished by evaporating gold or copper onto a single crystal of platinum and subsequently annealing the crystal to form a surface alloy. The composition of the surface alloy could then be determined by titrating the alloy surface with carbon monoxide molecules which will adsorb only on the platinum atoms at room temperature under ultra-high vacuum conditions.

B. Catalysis by Alloys

Interest in the catalytic properties of alloys began appearing in the 1950's. At this time, the prevailing theory of alloys was the "rigid band model" [1.43]. This model describes the conduction band as having one d-band and one s-p band, and that the band structure of an alloy was the average of the components. Chemisorption and catalytic studies (and later, photoelectron spectroscopic studies) showed that this was not the case. In 1969, Sachtler proposed the "individual surface atom model" [1.44] which considered chemisorption to be a localized phenomenon, i.e. a nickel atom at a nickel metal surface and at a nickel-copper alloy surface were essentially the same. This model lead to the "ensemble effect" [1.11] for catalysis. This model completely ignores any electronic modification of the individual atoms in an alloy or at most considers this effect to be secondary. This model is normally used to describe the catalytic behavior of an alloy which is composed of an active metal and an inactive metal. The catalytic behavior of these alloys is thought to be due to the dilution of the active sites in an inactive matrix. This results in an inhibition of reactions which require large "ensembles" of active sites, but allows reactions to occur which require smaller "ensembles" of active sites. The coherent potential approximation (CPA) [1.45] has been used to calculate the electronic structure of several alloys and has shown good agreement with experimental results. This model postulates

that the individual components of the alloy retain most of their individual character. These ideas are reviewed in Ref. 1.46 - 1.48.

The results presented in chapter 5 show that the "ensemble effect" alone is insufficient to describe the catalytic behavior of alloys. It appears that both "ensemble effects" and "electronic effects" (although not as large as those predicted by the "rigid band model") are important in catalysis by alloys. A recent theory by Falikov and Somorjai [1.49] addresses electronic factors in terms of electronic fluctuations. The results of chapter 5 also indicate that a metal that is not an active catalyst by itself may become active when alloyed with an active metal.

C. Objectives of this Investigation

Alloy catalysis has been the object of an extensive amount of research. The results of this research have often been contradictory due to an inability to control and characterize the alloy surface of the supported catalysts used in most of these studies. The object of the research contained in this thesis was to study the catalytic behavior of well-defined Cu-Pt and Au-Pt alloy surfaces for the n-hexane conversion reaction. Problems due to the presence of a support and undefined crystallographic orientation of the alloy surface were eliminated by forming a surface alloy on the surface of single crystals of platinum. Characterization of these surface alloys was performed using surface sensitive

ultra-high vacuum techniques. Catalytic studies were performed using these well-defined alloy surfaces. In order to avoid exposing these samples to the atmosphere, an in situ high pressure isolation cell was utilized.

Chapter 3 describes the surface properties of copper deposited on Pt(111), Pt(553) and Pt(100) surfaces and also the Cu-Pt surface alloys of these orientations based on LEED, AES and CO TDS work. Chapter 4 covers the electronic properties of gold deposited on Pt(111) and Pt(100) and the alloy surfaces based on XPS and UPS work. The results of the characterization presented in chapters 3 and 4 are used to interpret the results of the n-hexane conversion reaction catalyzed by the (111) and (100) crystal faces of gold-platinum and copper-platinum alloys which are presented in chapter 5.

In addition to the n-hexane conversion reaction, the CO oxidation reaction was also studied and is covered in chapter 6. When a platinum surface was modified by the presence of silicon, the CO oxidation rate exhibited temporal oscillations. Combined surface science / high-pressure reactor techniques were used to elucidate the mechanism of these oscillations. A kinetic model based on these findings is also presented.

D. Data on Pt, Au, Cu and Their Alloys

Selected physical constants for platinum, gold and copper are listed in Table 1.2.

The phase diagram for the Au-Pt system is shown in Fig. 1.2. A miscibility gap exists in this alloy. Bulk alloys prepared with a composition within this gap will separate into two phases, a platinum-rich phase and a gold-rich phase. The existence of this gap restricts the range of alloy compositions which can be studied using bulk alloys. Since the surface alloys formed in the work presented here were not in equilibrium, it was possible to study the entire range of surface compositions. It should also be noted that this system forms no ordered bulk structures. No ordered surface structure were observed either. The phase diagram for the Cu-Pt system is shown in Fig. 1.3. This system has an exothermic heat of mixing and forms ordered structures. The α'phase has a $L1_2$ structure isotropic with $AuCu_3$. The α'' region consists of structures isotropic with AuCu and Au_3Cu. Although careful preparation of the surface alloys could result in an ordered structure, the surface alloys were generally disordered.

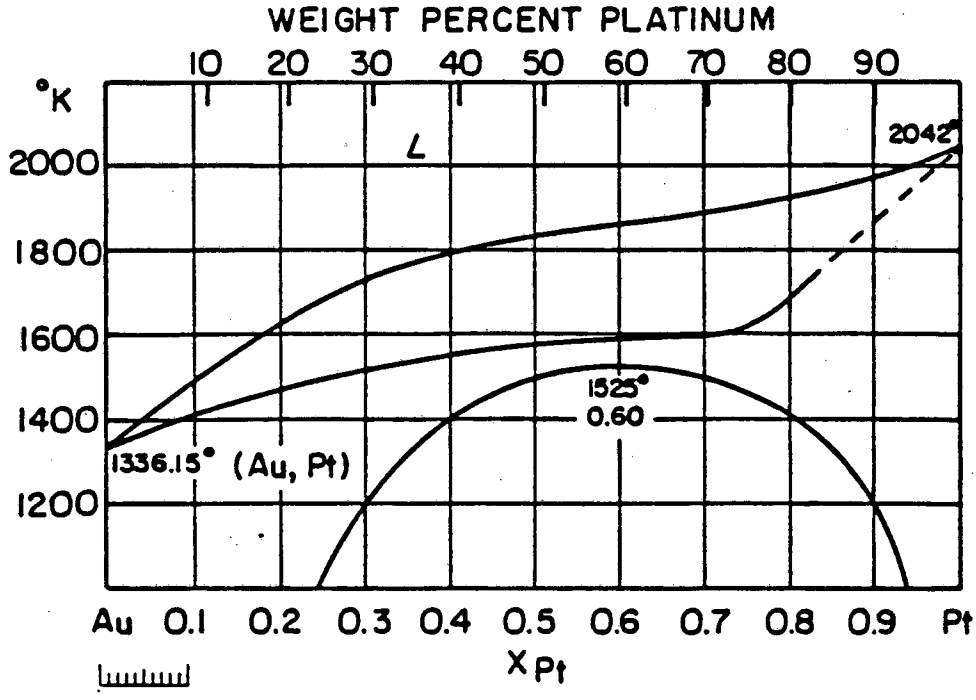

FIG. 1.2

Phase diagram of the Au-Pt system (from Ref. 1.56, Temperatures based on IPTS 1948).

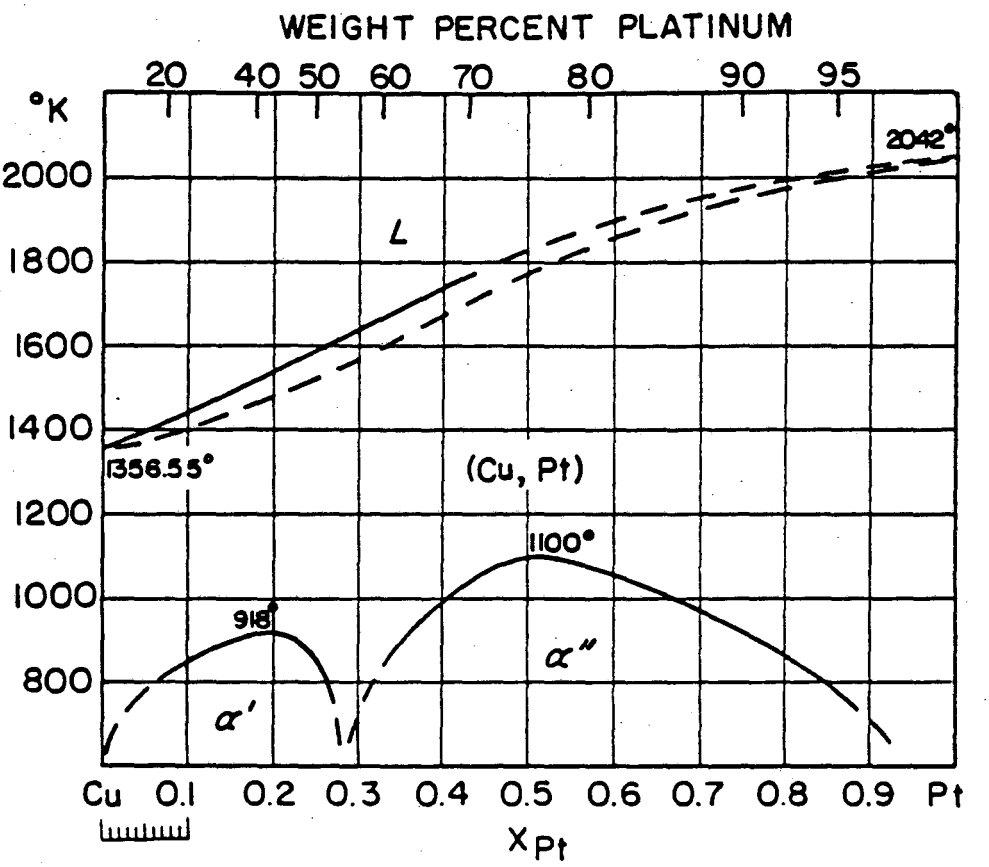

FIG. 1.3

Phase diagram of the Cu-Pt system (from Ref. 1.56, Temperatures based on IPTS 1948).

REFERENCES

1.1) G.A Somorjai, "Chemistry in Two Dimensions", Cornell University Press, London, 1981.

1.2) F.G. Ciapetta and D.N. Wallace, Catal. Rev. 5 (1972) 67.

1.3) J.H. Sinfelt, Progr. Solid State Chem. 10 (1975) 55.

1.4) M. Shelef, Catal. Rev. 11 (1975) 1.

1.5) C.C. Chang and L.L. Hegedus, J. Catal. 57 (1976) 361.

1.6) V. Haensel, U.S. Pat. No. 2,479,109 (1949).

1.7) T. Edmonds, in "Catalysis and Chemical Processes", R. Pearce and W.R. Patterson, eds., Leonard Hill, London 1981.

1.8) H.E. Kluksdahl, U.S. Pat. No. 3,415,737 (1968).

1.9) F.M. Dautzenberg and H.W. Kouwenkoven, German Offenlegungsshrift 2,153.891 (1972).

1.10) F.M. Dautzenberg, German Offenlegungsshrift 2.121.765 (1971).

1.11) F.M. Dautzenberg, J.N. Helle, P. Biloen, and W.H.M. Sachtler, J. Catal. 63 (1980) 119.

1.12) T.P. McCallister and K.R. O'Neal, German Offenlegungsschrift 2.104.765 (1971).

1.13) U.S. Pat. No. 2,848,377.

1.14) U.S. Pat. No. 3,839,194.

1.15) British Pat. No. 1,364,875.

1.16) J.C. Rasser, W.H. Beindorff and J.J.F. Scholten, J. Catal. 59 (1979) 211.

1.17) A. O'Cinneide and F.G. Gault, J. Catal. 37 (1975) 311.

1.18) J.K.A Calrke, A.F. Kane and T. Baird, J. Catal. 64 (1980) 200.

1.19) J.K.A. Clarke, A.C.M. Creaner and T. Baird, Appl. Catal., 9 (1984) 85.

1.20) J.R.H. van Schaik, R.P. Dressing and V. Ponec, J. Catal. 38 (1975) 273.

1.21) P. Biloen, F.M. Dautzenberg and W.H.M. Sachtler, J. Catal. 50 (1977) 77.

1.22) J.W.A. Sachtler, J.P. Biberian and G.A. Somorjai, Surface Sci. 110 (1981) 43.

1.23) J.W.A. Sachtler and G.A. Somorjai, J. Catal. 81 (1983) 77.

1.24) H.C. de Jongste, F.J. Kuijers and V. Ponec, Proceeding of the 6th International Congress on Catalysis, 1976.

1.25) H.C. de Jongste, V. Ponec and F.G. Gault, J. Catal. 63 (1980) 395.

1.26) H.C. de Jongste and V. Ponec, J. Catal. 63 (1980) 389.

1.27) J.W. Gibbs, Trans. Conn. Acad. Sci. 3 (1875/76) 108.

1.28) S.H. Overbury, P.A. Bertrand and G.A. Somorjai, Chem. Rev. 75 (1975) 547.

1.29) F.L. Williams and D. Nason, Surface Sci. 45 (1974) 377.

1.30) W.M.H. Sachtler and R.A. Van Santen, Appl. Surface Sci. 3 (1979) 121.

1.31) R.A. Van Santen and M.A. Boersma, J. Catal. 34 (1974) 13.

1.32) J.J. Burton, C.R. Helms and R.S. Polizzotti, J. Chem. Phys. 65 (1976) 1089.

1.33) M.L. Shek, P.M. Stefan, D.L. Weissman-Wencocur, B.B. Pate, I. Lindau, W.E. Spicer and V.S. Sundram, Surface Sci. 115 (1982) L86.

1.34) R.I. Hedge and A.P.B. Sinha, Surface Sci. 133 (1983) 233.

1.35) R.A. Van Santen and W.M.H. Sachtler, J. Catal. 33 (1974) 202.

1.36) A.D. Van Langeveld and V. Ponec, Appl. Surface Sci. 16 (1983) 405.

1.37) H.H. Brongersma, M.J. Sparnaay and T.M. Buck, Surface Sci. 71 (1978) 657.

1.38) T.S. King and R.G. Donnelly, Surface Sci. 141 (1984) 417.

1.39) G. Kerker, J.L. Morán-López and K.H. Benneman, Phys. Rev. B 15 (1977) 638.

1.40) J.R. Chelikowsky, Surface Sci. 139 (1984) L197.

1.41) J.A. Schwartz, R.S. Polizzotti and J.J. Burton, J. Vacuum Sci. Technol. 14 (1977) 457.

1.42) J.C.M. Harberts, A.F. Bourgonje, J.J. Stephans and V. Ponec, J. Catal. 47 (1977) 92.

1.43) N.F. Mott and H. Jones, "Theories of the Properies of Metals and Alloys", Oxford University Press, London, 1936.

1.44) W.M.H. Sachtler and P Van der Plank, Surface Sci. 18 (1969) 62.

1.45) P. Soven, Phys. Rev. 156 (1979) 809.

1.46) J.K.A. Clarke and A.C.M. Creaner, I&EC Prod. Res. Dev. 20 (1981) 574.

1.47) R. Burch, Acc. Chem. Res. 15 (1982) 24.

1.48) V. Ponec, Catal. Rev.-Sci. Eng. 11 (1975) 41.

1.49) L.M. Falicov and G.A. Somorjai, Submitted to The Prod. Nat'l Acad. Sci.

1.50) Sargent-Welch Scientific Company, "Table of Periodic Properties of the Elements", 1968.

1.51) D.E. Eastman, Phys. Rev. Sect. B 2 (1970) 1.

1.52) J.E. Demuth, Chem. Phys. Lett., 45 (1977) 12.

1.53) H.C. Potter and J.M. Blakeley, J. Vac. Sci. Technol., 12 (1975) 635.

1.54) P.O. Gartland, Phys. Norv., 6 (1972) 201.

1.55) B.E. Nieuwenhuys and W.M.H. Sachtler, Surface Sci. 34 (1973) 317.

1.56) "Selected Values of the Thermodynamic Properties of Binary Alloys", Prepared by R. Hultgren, P.D. Desai, D.T. Hawkins, M. Gleiser and K.K. Kelley, American Society for Metals, Metals Park, Ohio, 1973.

1.57) "CRC Handbook of Chemistry and Physics, 64th Edition", R.C. Weast, M.J. Astle and W.H. Beyer, eds., CRC Press, Inc., Boca Raton, Florida, 1983.

CHAPTER TWO: EXPERIMENTAL METHODS

A. SYSTEM OVERVIEW

The experiments contained in this thesis was carried out using three separate ultra-high vacuum (UHV) chambers. Most of the work in chapter III was done using an ion pumped system equipped with Low energy electron diffraction (LEED), Auger electron spectroscopy (AES) using the LEED optics as a retarding field analyzer (RFA), a quadrapole mass spectrometer, and a ion sputtering gun. The photoelectron spectroscopy work discussed in chapter IV were carried out on an oil diffusion pumped UHV system equipped with a double pass cylindrical mirror analyzer (CMA), an X-ray source (Mg K_α), a He I light source, AES, LEED, mass spectrometer, and a Knudsen-type evaporation source used for gold deposition.

The bulk of the work, however, was carried out using the chamber shown schematically in Fig. 2.1.

1. System pumping

The main chamber was pumped by both an ion pump and a liquid nitrogen trapped "6 inch" oil diffusion pump, the evaporation chamber (to be discussed later) was differentially pumped with a liquid nitrogen trapped "2 inch" oil diffusion pump. The chamber was also equipped with a titanium sublimation pump. A base pressure of 5×10^{-10} torr was achieved after baking out the system. A typical working pressure, however, was 1×10^{-9} torr.

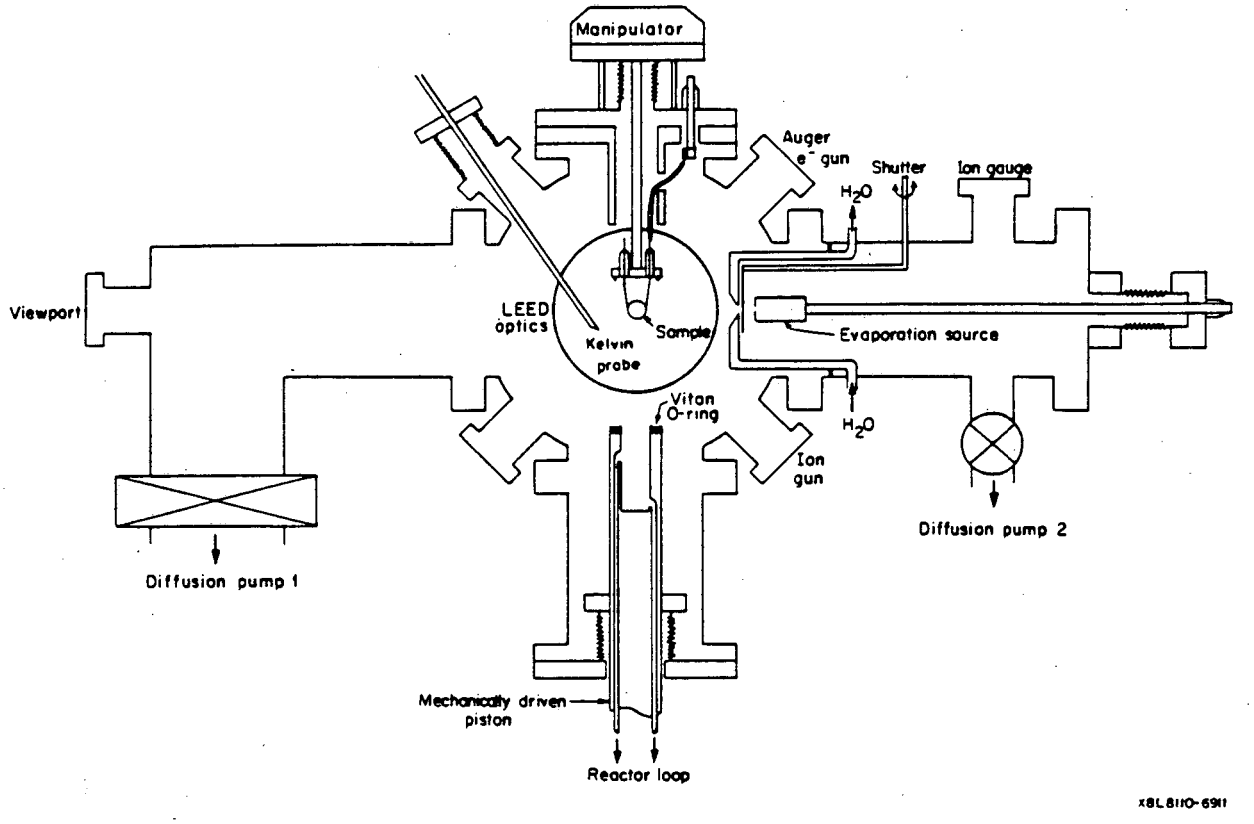

FIG. 2.1

Diagram of the ultra-high vacuum chamber and sample isolation cell.

2. Sample holder

The sample holder was a Varian manipulator which had been modified to incorporate a high-pressure isolation cell. The manipulator allowed vertical movement of several inches, displacement from the vertical of ca. 10 degrees, and limited lateral movement. Four feedthroughs were attached to the crystal holder. Two of these feedthroughs were used to allow current to be passed through the sample in order to heat it. The other two feedthroughs were for thermocouples; one chromel and the other alumel. These feedthroughs were connected to corresponding feedthroughs on the manipulator flange and the connecting wires were insulted with glass sleeving to prevent shorts to ground. These connecting wires were long enough to allow 360 degree rotation of the sample, but short enough to avoid interfering with analysis of the sample. The sample was spot welded to two 1.5 cm long gold wires and mechanically attached to the copper feedthroughs with copper barrel connectors. This arrangement permitted heating of the sample to 1400 K and careful spot welding of the sample resulted in uniform heating. Because of the large mass to which the sample was connected, it took a considerable length of time to cool the sample to room temperature after heating. It was therefore necessary to cool the sample by connecting 0.5 " copper rods to the electrical feedthroughs and placing the rods in liquid nitrogen.

3. Reactor loop

The reactor loop consisted of two parts: a) the main loop; and b) the high-pressure cell. A schematic of the reactor loop is shown in Fig. 2.2. Gasses were introduced into the loop from the gas manifold (GM) and gas pressures were measured using a Wallace and Tiernan pressure gauge (WT) with a internal volume of ca. 20 ml. Gasses could be leaked into the main chamber for mass spectrometric analysis through a leak valve which connected the loop and main chamber. When the reactor was used in a stirred batch mode, the gasses were circulated by a metal bellows pump (Metal Bellows Corp. MB-21). The reaction gasses were analyzed using a Hewlett-Packard 5720A gas chromatograph which was equipped with a flame ionization detector. A 2 ' long 1/8 " stainless steel column packed with 0.19 % picric acid on 80/100 Carbopack C was used to separate the hydrocarbon products (with the exception of benzene, for which a 4 ' long 1/8 " column packed with 10 % squalene on 60/80 Chromosorb W was used). Samples of the reaction mixture were obtained and injected into the gas chromatograph by means of a Carle microvolume six-port sampling valve. The sampling and peak integration were controlled by a Spectraphysics minigrator.

The high-pressure cell allowed high pressure reactions to be carried out over a sample characterized in UHV without exposing it to the atmosphere. In order to isolate the sample, the lower part of the cell was mechanically raised to position it against the sample holder. The seal was made

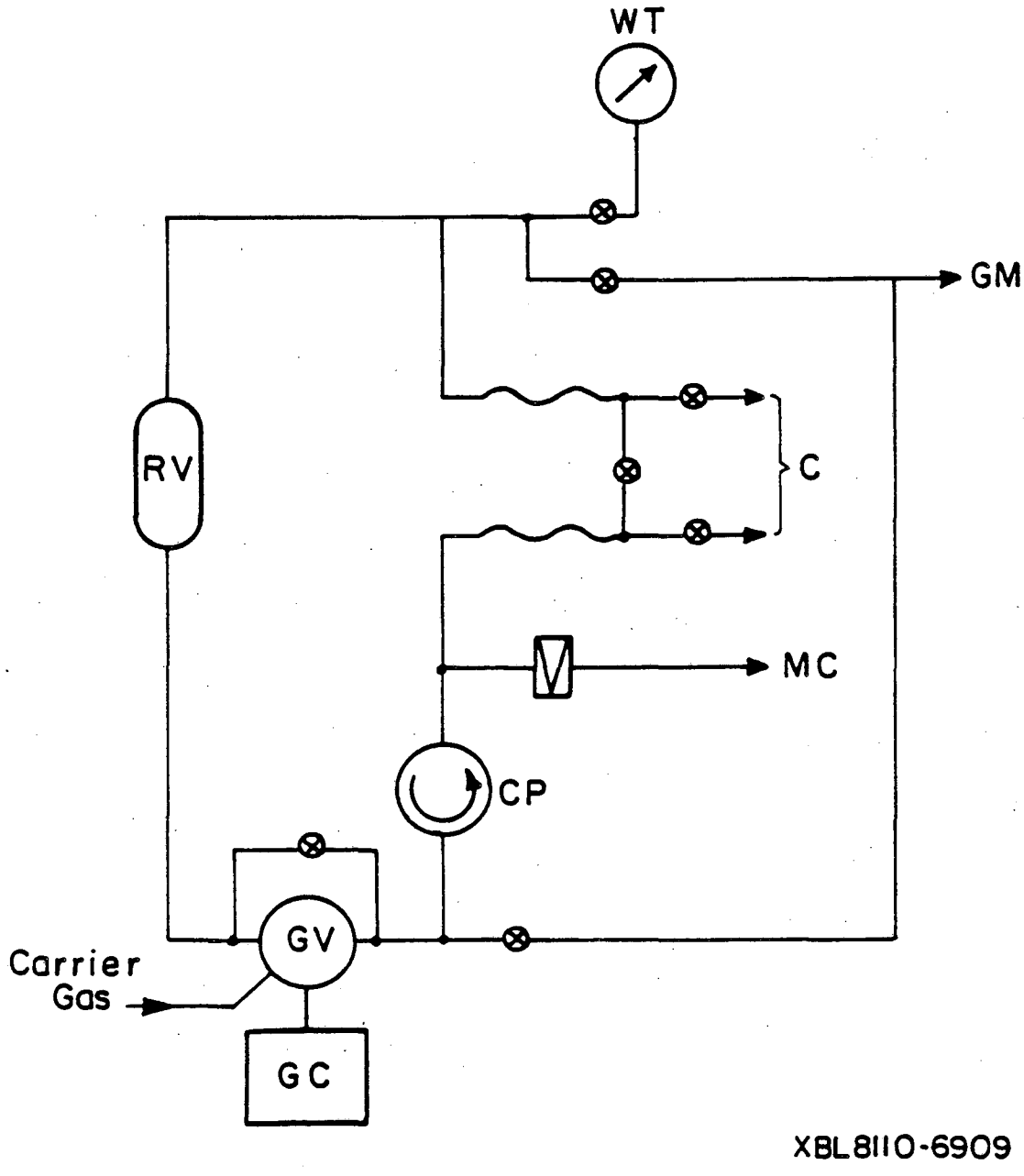

FIG. 2.2

Diagram of the reactor loop.
WT - pressure gauge, C - isolation cell, MC - main chamber,
CP - circulation pump, GV - sampling valve, GM - gas manifold

between a knife-edge on the sample holder and a Viton O-ring in the lower part of the cell. The pressure inside the cell could be raised to 1 atm without the pressure in the main chamber exceeding the 10^{-9} torr range.

After a reaction, the reactor loop was first pumped out to 100 microns using a liquid nitrogen trapped mechanical pump and then pumped down to 10 microns with a sorption pump. The cell could then be opened to UHV without the pressure in the main chamber exceeding 5×10^{-7} torr. The main chamber pressure returned to the 10^{-9} range in a matter of minutes. The post-reaction sample could then be analyzed.

4. Gas manifold

Gasses were introduced into the reactor loop and the main chamber through the gas manifold. The manifold was connected to the main chamber via a leak valve and a right angle valve. Cylinders of argon, oxygen, carbon monoxide and hydrogen were connected to the manifold through molecular sieve traps to dry and purify the gasses. A glass ampule containing n-hexane was also connected to the manifold and was isolated with a viton sealed valve. Pumping of the manifold was achieved with a mechanical pump and two molecular sieve sorption pumps. Pressures inside the manifold could be monitored with a thermal conductivity gauge or the Wallace and Tiernan gauge.

5. The system was also equipped with :

a) 4-grid LEED optics (also used in the retarding field mode as an energy analyzer for AES) (discussed in section II.C.1,2);

b) a cathode ray tube gun was used as an electron gun for AES;

c) a UTI-100C mass spectrometer used in thermal desorption experiments (Sec. II.C.3), for the analysis of residual gasses in the chamber and for leak testing the system;

d) a nude ion gauge for determining the pressure inside the chamber;

e) a Kelvin probe (Delta-Phi Electronics) used for determining work functions (Sec.II.C.5);

f) two variable leak valves for introducing gasses into the chamber, one connected to the gas manifold and the other connected to the reactor loop;

g) a Knudsen-cell type evaporation source used to evaporate gold or copper onto the sample (Sec. II.D.1).

h) a sputtering gun used for argon ion bombardment used to clean the sample surface.

6. Materials

Hydrogen, nitrogen, argon, oxygen, and carbon monoxide gasses were obtained through Lawrence Berkeley Laboratory and were passed through molecular sieve traps before use. The n-hexane was repeatedly freeze-pumped in liquid nitrogen before use. A list of the materials used together with their source and purities is shown in table 2.1.

TABLE 2.1

REAGENT	SOURCE	PURITY	IMPURITY
O_2	Matheson/LBL	>99.9	CO
H_2	Matheson/LBL	>99.99	CH_4
CO	Matheson/LBL	>99.5	$Fe(CO)_5$
Ar	Matheson/LBL		
n-hexane	Phillips	>99.95	methylcyclopentane, benzene

B. CRYSTAL PREPARATION AND CLEANING

A single crystal boule was first checked for imperfections by taking a Laue photograph of several regions of the boule. Once it had been determined that the boule was indeed a single crystal, the rod was fixed onto an aluminum mount with Ductseal and fitted into the goniometer (Phillips Electronics #API-107) for orientation. The oriented rod was then fixed into position with a mixture of Duco cement and copper powder.

The goniometer was then fitted to the track of a Electrodischarge machine (South Bend #1000) and cut with a 0.015 inch Tungsten-copper electrode (EDM Supplies, Inc.). The cut crystal was then mounted in Koldmount (Vernon-Bensoff, Co.) for polishing. The crystal was first polished with 600 grit Wet-or-Dry abrasive paper (MMM) lubricated with kerosene. The crystal was then further polished on a polishing wheel covered with nylon cloth (Buehler #40-7068) using 6 micron diamond paste (Buehler #40-6162) for ~ 2 hours followed by 1 micron diamond paste for another couple of hours. Following polishing, the crystal was cleaned by ultrasound (LECO #820-107) in Liqui-Nox (Alconox, Inc.) for 5 minutes.

The crystal orientation was again checked by Laue, refaced using 600 grit paper lubricated with kerosene, and then turned over to grind the back face parallel to the front face. The entire polishing procedure described above was then repeated.

The polished crystal was then etched briefly in warm Aqua Regia.

Typical impurities, as determined by Auger spectroscopy, were carbon, sulphur, calcium, oxygen and silicon. The crystal was cleaned in the following manner. If silicon or calcium were present, the crystal was initially cleaned by Argon ion bombardment in 5×10^{-5} torr Ar and $\sim 1 \times 10^{-8}$ torr of oxygen while heating the crystal at 900 K. The purpose of the oxygen was to shift the equilibrium of the silicon and calcium towards the surface by forming an oxide. This sputtering was continued until the calcium and silicon were removed from the surface. The crystal was then heated to 1100 K in 2×10^{-7} torr of oxygen for 15 minutes to remove surface carbon. If, during this procedure, impurities segregated from the bulk, this cleaning cycle was repeated. A new crystal could take up to a week to clean.

The crystal was cleaned each day before experiments by Ar ion bombardment in 5×10^{-5} torr of Ar with the crystal at room temperature. The ion bombardment was followed by heating the crystal in 2×10^{-7} torr of oxygen for 15 minutes. This treatment was generally sufficient to clean the surface of the crystal.

Crystal faces of (111), (553), (100) and (13,1,1) orientation were employed in the experiments. These surfaces are shown in Fig. 2.3 . The (111) surface is hexagonally close-packed, the most densely packed surface. The (553) surface is a stepped surface with terraces five atoms wide of

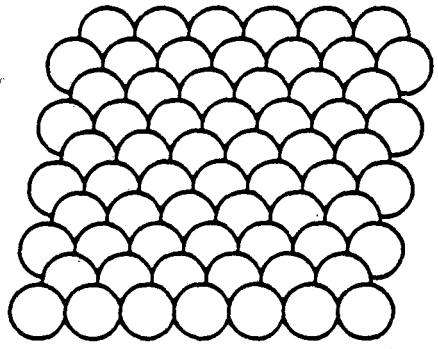

fcc (111)

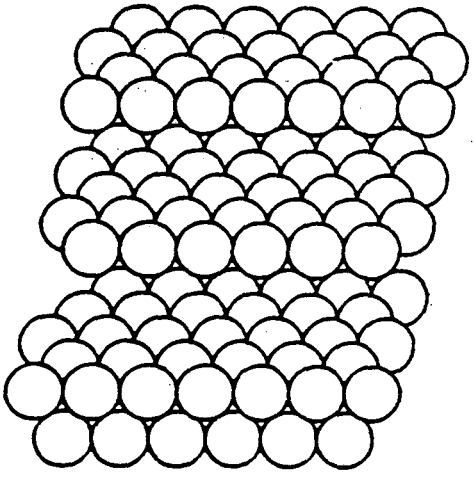

fcc (553)

XBL 8111-12652

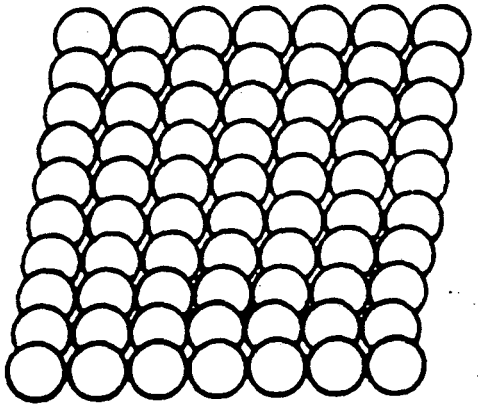

fcc (100)

FIG. 2.3

Surface structure of the Pt(111), Pt(553) and Pt(100) crystal faces.

(111) orientation and monatomic steps. The (100) surface is a more open surface than the (111) surface and has a square geometry. Under UHV conditions, the clean Pt(100) surface reconstructs [2.1 - 2.2] forming a hexagonal overlayer. Adsorption of various gasses removes this reconstruction [2.3 - 2.5]. The (13,1,1) surface is a stepped surface with terraces of (100) orientation 12 atoms wide and monatomic steps. This surface also reconstructs.

C. SURFACE ANALYSIS

1. Auger electron spectroscopy (AES)

AES was used extensively in this work to monitor the cleanliness of the crystal surface and determine coverages of depositted metal overlayers and alloy compositions. A schematic of the experimental set-up is shown in Fig. 2.4. 2000 eV electrons from a cathode ray tube gun are focussed onto the sample (since the energy of an Auger electron is independent of the excitation energy, the energy spread of this excitation electron beam is not important). This results in the ejection of core electrons from the sample. An electron from a higher level can fill this core hole. This process can be followed by one of two processes: a) the energy produced can be transmitted to another electron by a radiationless process (Fig. 2.5a), creating an electron with a characteristic kinetic energy :

$$E(X_0,Y_1,Z_2) = E(X_0) - E(Y_1) - E(Z_2,Y_1) - e\cdot\phi_{sp}$$

where $E(X_0)$ is the binding energy of the primary core electron, $E(Y_1)$ is the binding energy of the electron which fills the core hole, $E(Z_2,Y_1)$ is the binding energy of the ejected electron moving in a field of increased charge, and ϕ_{sp} is the work function of the energy analyzer; or b) the emission of an X-ray (Fig. 2.5b).

The Auger electron energies were analyzed by using the LEED optics as a retarding field analyzer. This was achieved by grounding the first and fourth grids and ramping the retarding voltage on the second and third grids. An

Retarding Field Analyzer for Auger Electron Spectroscopy

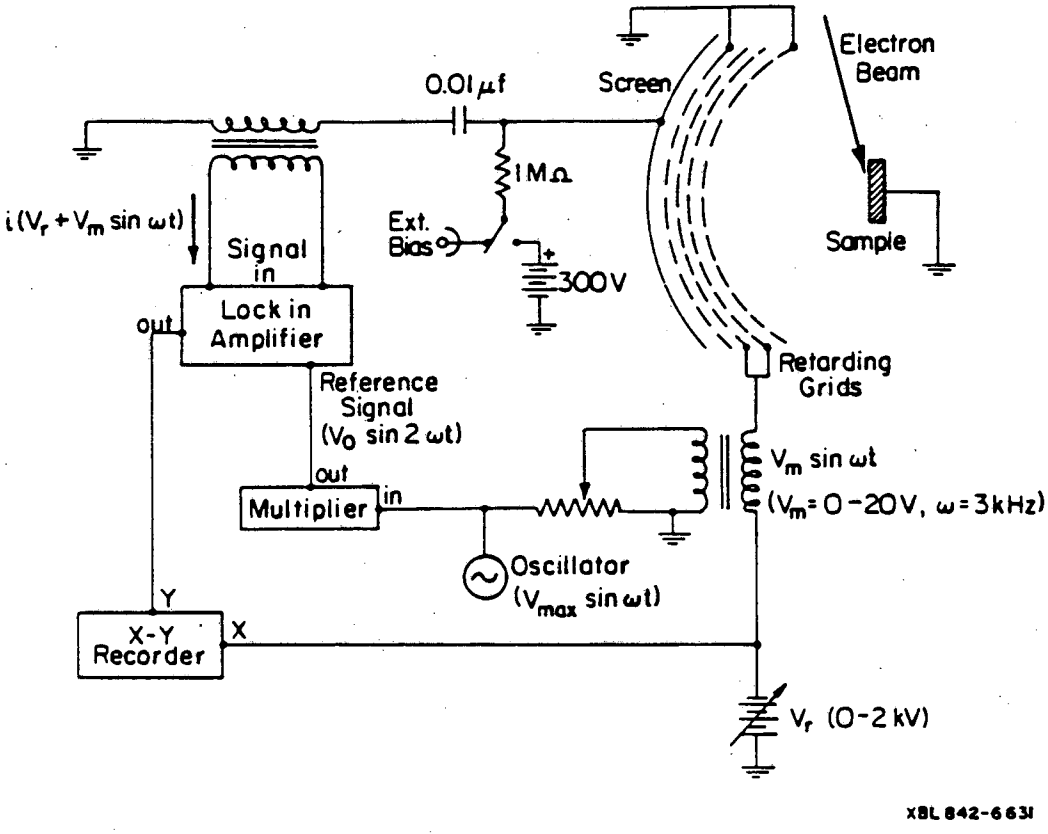

FIG. 2.4

A schematic of the retarding field analyzer (RFA) used for Auger spectroscopy.

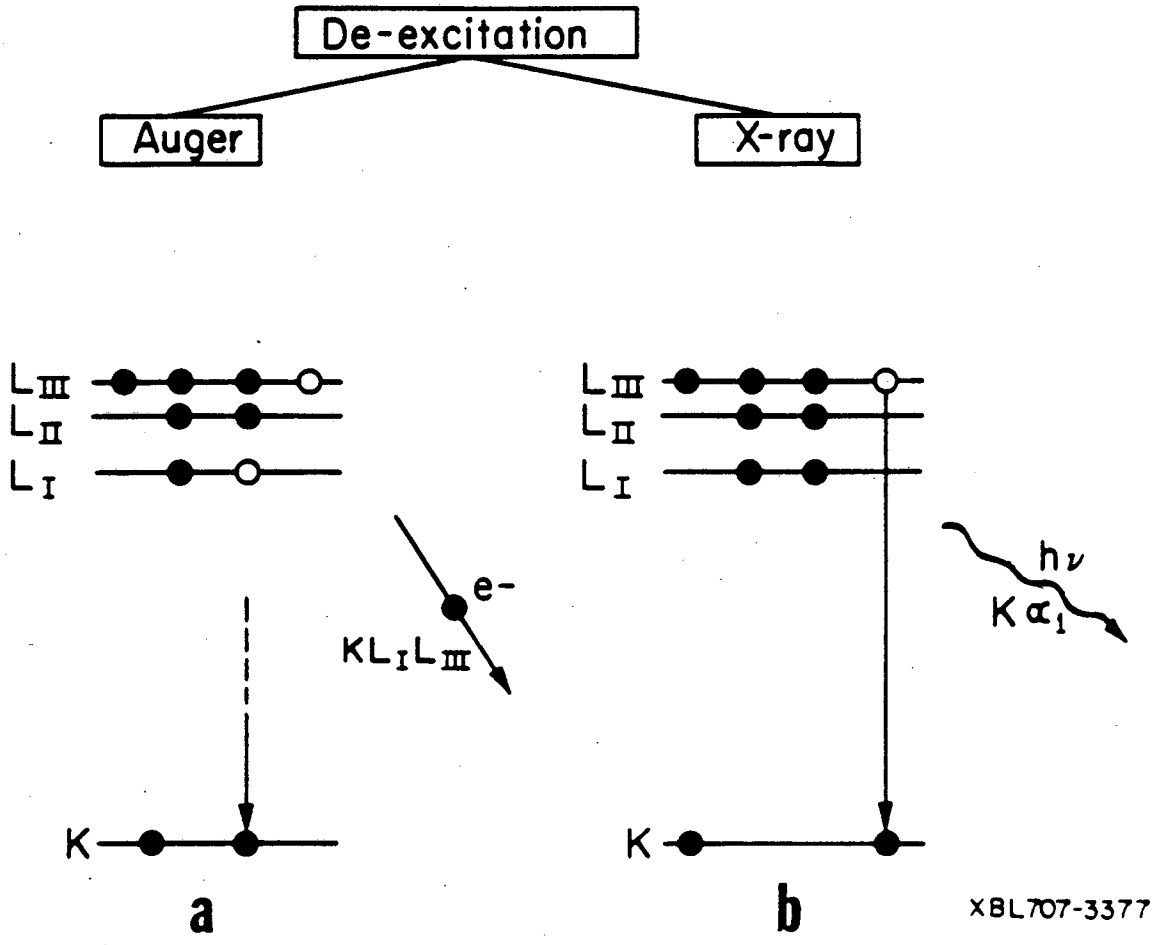

FIG. 2.5

Energy level diagrams showing two mechanisms for de-excitation of an excited ion: a) the emission of an Auger electron; and b) X-ray fluorescence.

modulation voltage of the form :

$$V_m = V_m \sin(wt)$$

was superimposed on the retarding voltage. The LEED screen was baised at 300 V to collect the current passing through the grids. The amplitude of this current with frequency w is:

$$A(w) = V_m i'(V_r) + V_m^3 i'''(V_r)/8 + ...$$

where $i'(V_r)$ is proportional to $N(E_r)$, the number of electrons with energy E_r.

Due to the high background of secondary electrons it was necessary to use the derivative of $N(E_r)$. This was achieved by following the current with a frequency of 2w :

$$A(2w) = V_m^2 i''(V_r)/4 + V_m^4 i''''(V_r)/48 + ...$$

If V_m is not too large, the amplitude of the current with a frequency of 2w is proportional to the derivative of $N(E_r)$. Typically, a modulation voltage of ~7 Volts peak-to-peak was used. A modulation voltage of down to 2 volts was used, however, if higher resolution was needed.

In the determination of coverages and surface concentrations, Auger peaks as close to 100 eV were utilized because of their high surface sensitivity. As can be seen from Fig. 2.6 , the mean free path of a 100 eV electron through a solid is ~ 6 Å, or 2 - 3 atomic layers.

2. Low energy electron diffraction (LEED)

Low energy electron diffraction was used to determine the structure of the topmost layers of the single crystal surface. Like X-ray diffraction, elastically scattered electrons can constructively or destructively interfere with

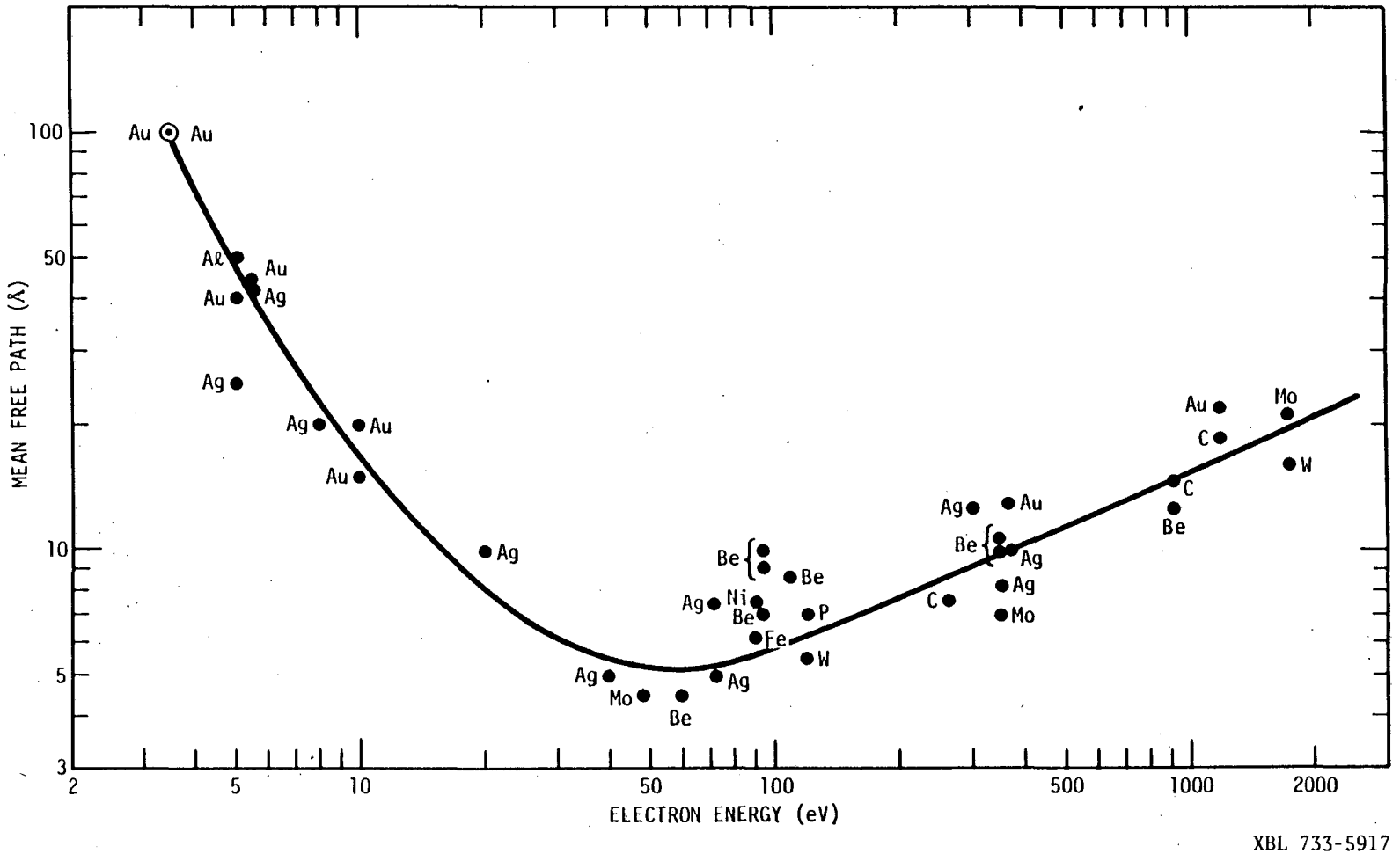

XBL 733-5917

FIG. 2.6

The mean free path of electrons in metallic solids as a function of their energy.

one another if the wavelength of the electrons is close to the lattice spacing of the crystal [2.6]. From the de Broglie relation :

$$\lambda = h/mv = (150/E)^{1/2}$$

where h is Planck's constant, m is the mass of the electron, v is the velocity of the electron, and E is the energy of the electron measured in eV, electron with energies in the range of 50 to 250 eV have wavelengths of 1.73 Å to .775 Å, which is close to the interatomic spacings of most solids and will result in diffraction from an ordered surface. Since electrons interact much more strongly with the solid than do photons, LEED is sensitive to the structure at the surface of a solid.

The experimental set-up is shown in Fig. 2.7. Electrons of a given energy were produced from an indirectly heated cathode inside a Wehnelt cylinder and then passed through a drift tube which was grounded, as were the crystal and the first grid of the 4-grid LEED optics. This produced a relatively field free region between the optics and the sample. Inelasically scattered electrons were filtered out by the second and third grids of the LEED optics which were held at a potential just below that of the primary electron beam. The elastically scattered electrons which passed through the third grid were accelerated toward a phosphor covered screen which was held at a positive potential of several KV. The electrons produced bright spots on the screen which could be photographed for later analysis.

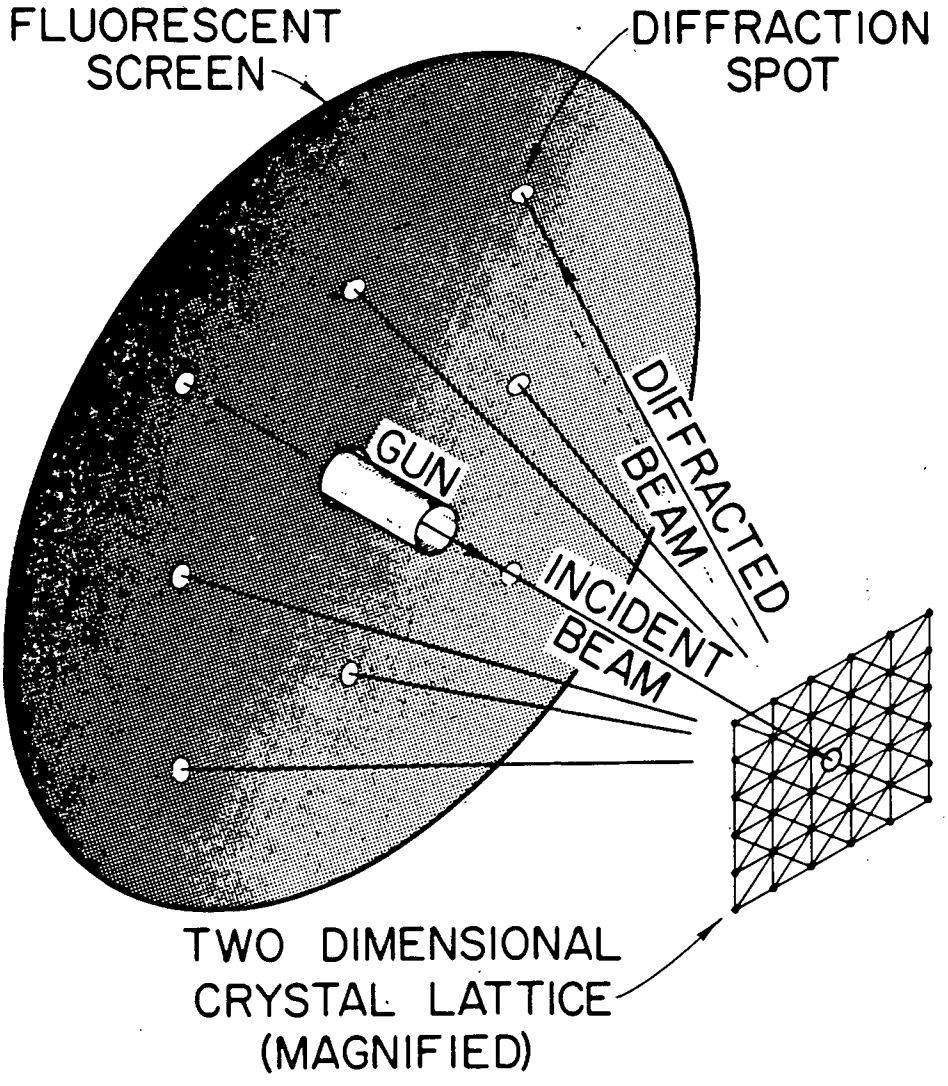

$$\underset{\sim}{k}' = \underset{\sim}{k} + \underset{\sim}{G}$$

FIG. 2.7

Set up for low energy electron diffraction (LEED) experiments.

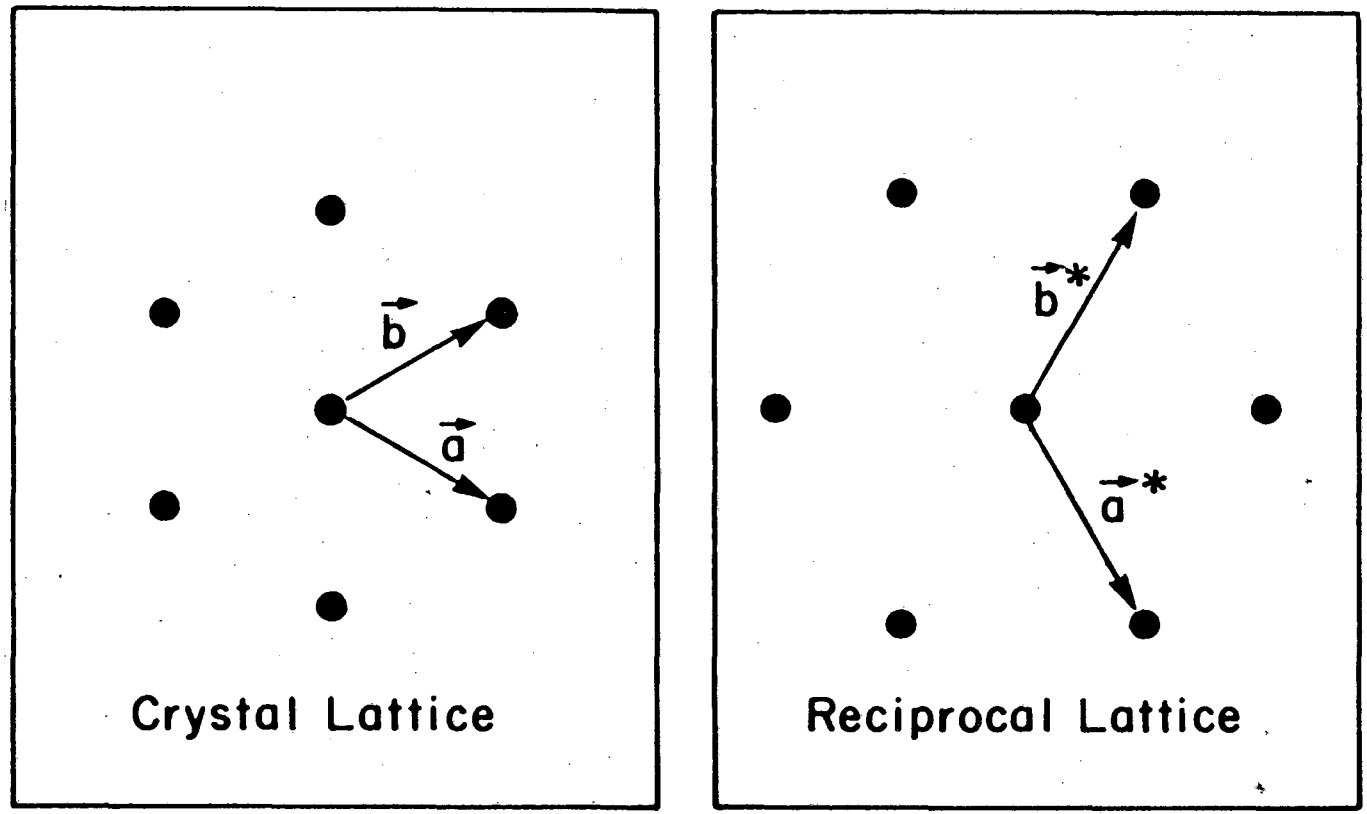

FIG. 2.8

Real space vectors ($\vec{a}$, $\vec{b}$) and reciprocal space vectors ($\vec{a}^*$, $\vec{b}^*$) of a 2-dimensional hexagonal lattice.

XBL 787-9590

Using LEED in this fashion allows the determination of the 2-dimensional geometry of the surface. No information about the bond lengths perpendicular to the surface or the registry of an overlayer super-lattice with the substrate lattice can be obtained. In order to determine these values, a detailed study of the spot intensity variation with electron energy must be made. This procedure is very computer-time intensive due to the multiple scattering which occurs in electron diffraction and was not applied to any of the systems discussed herein. Reviews of this method of analysis are discussed elsewhere [2.7].

The pattern which appears on the LEED screen is a representation of the crystal surface lattice in reciprocal space. This pattern in reciprocal space has translational periodicity, and can be defined by the translation vector :

$$\vec{T}^* = h\vec{a}^* + k\vec{b}^* \quad .$$

The real space lattice also has translational periodicity and can be defined by the translation vector :

$$\vec{T} = n\vec{a} + m\vec{b} \quad .$$

These translation vectors are related to one another by :

$$\vec{a}^* = \frac{\vec{b} \times \vec{c}}{\vec{a} \cdot \vec{b} \times \vec{c}}$$

$$\vec{b}^* = \frac{\vec{c} \times \vec{a}}{\vec{a} \cdot \vec{b} \times \vec{c}}$$

where c is the surface normal. A hexagonal lattice in real space and in reciprocal space is shown in Fig. 2.8.

When a species is adsorbed on the surface, new spots may appear due to the formation of an ordered super-lattice. The

relationship of the mesh of the super-lattice to the mesh of the substrate in reciprocal space is :

$$\vec{a}^{*\prime} = m^{*}_{11}\vec{a}^{*} + m^{*}_{12}\vec{b}^{*}$$
$$\vec{b}^{*\prime} = m^{*}_{21}\vec{a}^{*} + m^{*}_{22}\vec{b}^{*}$$

where $\vec{a}^{*\prime}$ and $\vec{b}^{*\prime}$ are the primitive vectors of the superlattice in reciprocal space.

These equations can be written :

$$\begin{bmatrix}\vec{a}^{*\prime}\\ \vec{b}^{*\prime}\end{bmatrix} = \mathbf{M}^{*} \begin{bmatrix}\vec{a}^{*}\\ \vec{b}^{*}\end{bmatrix}$$

where

$$\mathbf{M}^{*} = \begin{bmatrix} m^{*}_{11} & m^{*}_{12}\\ m^{*}_{21} & m^{*}_{22}\end{bmatrix} .$$

The relationship between the super-lattice and the substrate lattice in real space is:

$$\begin{bmatrix}\vec{a}'\\ \vec{b}'\end{bmatrix} = \mathbf{M} \begin{bmatrix}\vec{a}\\ \vec{b}\end{bmatrix}$$

where

$$\mathbf{M} = \begin{bmatrix} m_{11} & m_{12}\\ m_{21} & m_{22}\end{bmatrix} .$$

$\mathbf{M}^{*}$ is the inverse transposed matrix of $\mathbf{M}$, i.e. $\mathbf{M}^{*} = \bar{\mathbf{M}}^{-1}$. Thus the coefficients of the two matrices are related as follows :

$$m_{11} = (\det \mathbf{M}^*)^{-1} m^*_{22}$$
$$m_{12} = -(\det \mathbf{M}^*)^{-1} m^*_{21}$$
$$m_{21} = -(\det \mathbf{M}^*)^{-1} m^*_{12}$$
$$m_{22} = (\det \mathbf{M}^*)^{-1} m^*_{11} \quad .$$

$\mathbf{M}^*$ can be obtained from the pattern on the LEED screen and $\mathbf{M}$ can then be calculated, thus determining the mesh of the super-lattice with respect to the mesh of the substrate. No information however, is obtained about the registry of the overlayer mesh with that of the substrate and so this must be inferred based on other evidence.

3. Thermal desorption spectroscopy (TDS)

The thermal desorption of carbon monoxide was used as a probe of the effect of alloying platinum with gold or copper on the electronic or binding properties of platinum. Also, since carbon monoxide does not adsorb on gold or copper at room temperature, carbon monoxide TDS was used to titrate the platinum at the alloy surfaces.

The experiment consisted of exposing the crystal to a pressure of gas for some time period. Gas exposures are usually expressed in Langmuirs (L), where 1 L = 10^{-6} torr·s. After evacuating the chamber, the crystal was heated linearly and the desorbing molecules monitored using the mass spectrometer. The rate of desorption can be expressed as follows [2.8] :

$$dn/dt = (V/AkT_g)[(dP/dT)\beta + (S/V)P]$$

where V is the volume of the chamber, A is the surface area of the substrate, k is Boltzmann's constant, T_g is the gas

phase temperature, β is the heating rate (= dT/dt), S is the pumping speed of the system, and P is the pressure inside the chamber minus the base pressure. If the pumping speed to volume ratio is large and the heating rate is low, then the rate of desorption is proportional to the pressure (or the mass spectrometer signal).

The simplest desorption process is a first order desorption when there is no temperature or coverage dependence for the desorption energy, E_d, or for the pre-exponential factor, ν. For this case, the rate of desorption can be expressed as follows :

$$dn/dT = -(\nu/\beta)\ \theta\ \exp\{-E_d/RT\}$$

$$\text{where } T = T + \beta t\ .$$

The desorption peak reaches a maximum for $d[dn/dT]/dT = 0$. Solving for this condition :

$$E_d/RT_m^2 = (\nu/\beta)\exp\{-E_d/RT_m\}$$

and using the approximation $E_d/RT_m \cong \ln(\nu/\beta)$ and solving for the energy of desorption :

$$E_d = RT_m \{ \ln[\nu T_m/\beta] - \ln[\ln(\nu/\beta)] \}\ .$$

In order to solve for E_d, a value for ν must be assumed. From the activated complex theory [2.9],

$$\nu = K\ (F^{\ddagger}/F_A)\ kT/h$$

where K is the transmission coefficient, $F^{\ddagger}$ and F_A are the partition functions of the transition state and the adsorbed molecule, respectively, k and h are Boltzmann's and Planck's constants, and T is the temperature. Based on this equation, values for ν are usually in the range of 10^{13} to 10^{15} s^{-1}.

The dependence of the peak position and peak width (FWHM) is shown in Fig. 2.9. These plots were obtained from a computer simulated TDS experiment in which an iterative method was employed. In Fig. 2.9a, $\nu = 10^{15}$ s^{-1}, the heating rate is 30 K/s, and the initial coverage is 0.5 monolayers. As the desorption energy increases the peak shifts to higher temperatures and the peak width increases. In Fig. 2.9b, E_D is 30 Kcal/mol, the heating rate is 30 K/s, and the initial coverage is 0.5 monolayers. As the pre-exponential factor increases, the desorption peak shifts to lower temperatures and the peak narrows. For a given peak shift, there is a stronger dependence of the peak width on the pre-exponential factor. Also, a shift from 400 K to 500 K requires and increase of ~ 7 Kcal/mol. The pre-exponential factor must be decreased by 5 orders of magnitude to obtain the same shift.

For a first order desorption in which the desorption energy and pre-exponential are independent of coverage, the peak position is independent of initial coverage. Fig. 2.10 shows the TDS of CO from Pt(111) for various CO exposures. The peak shifts to lower temperature as the coverage increases. One explanation for this is a coverage dependent desorption energy [2.10 - 2.11]. As the CO molecules are packed more tightly together, the molecules repel one another resulting in a lower desorption energy.

Work by Hollins [2.12] indicates that CO grows in islands on the Pt(111) surface. This would argue against the increase in lateral repulsion as the CO coverage is

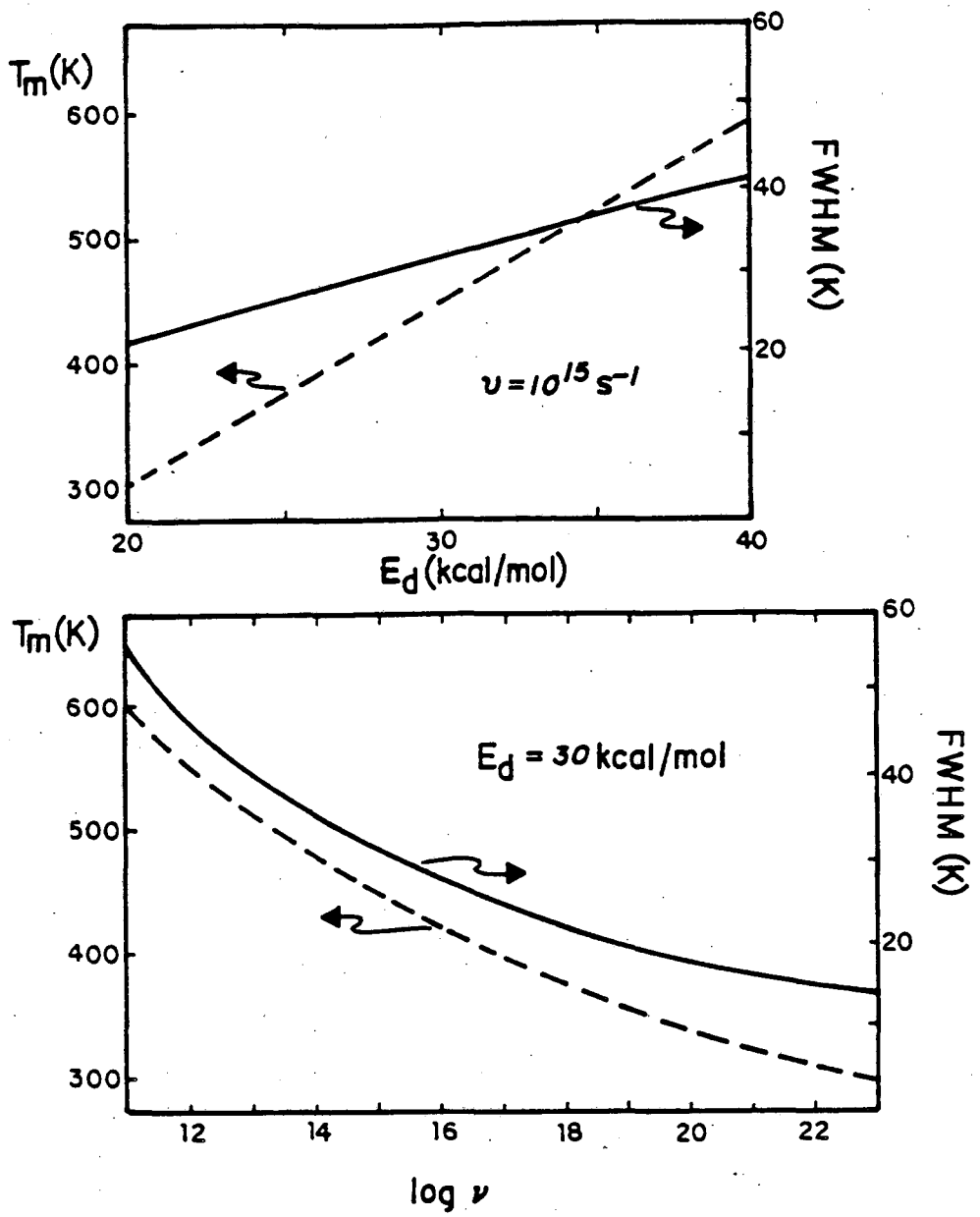

FIG. 2.9

The dependence of the thermal desorption peak position and width as a function of the desorption energy (E_d) and pre-exponential factor for first order desorption. Heating rate = 30 K/s, initial coverage = 0.5 monolayers.

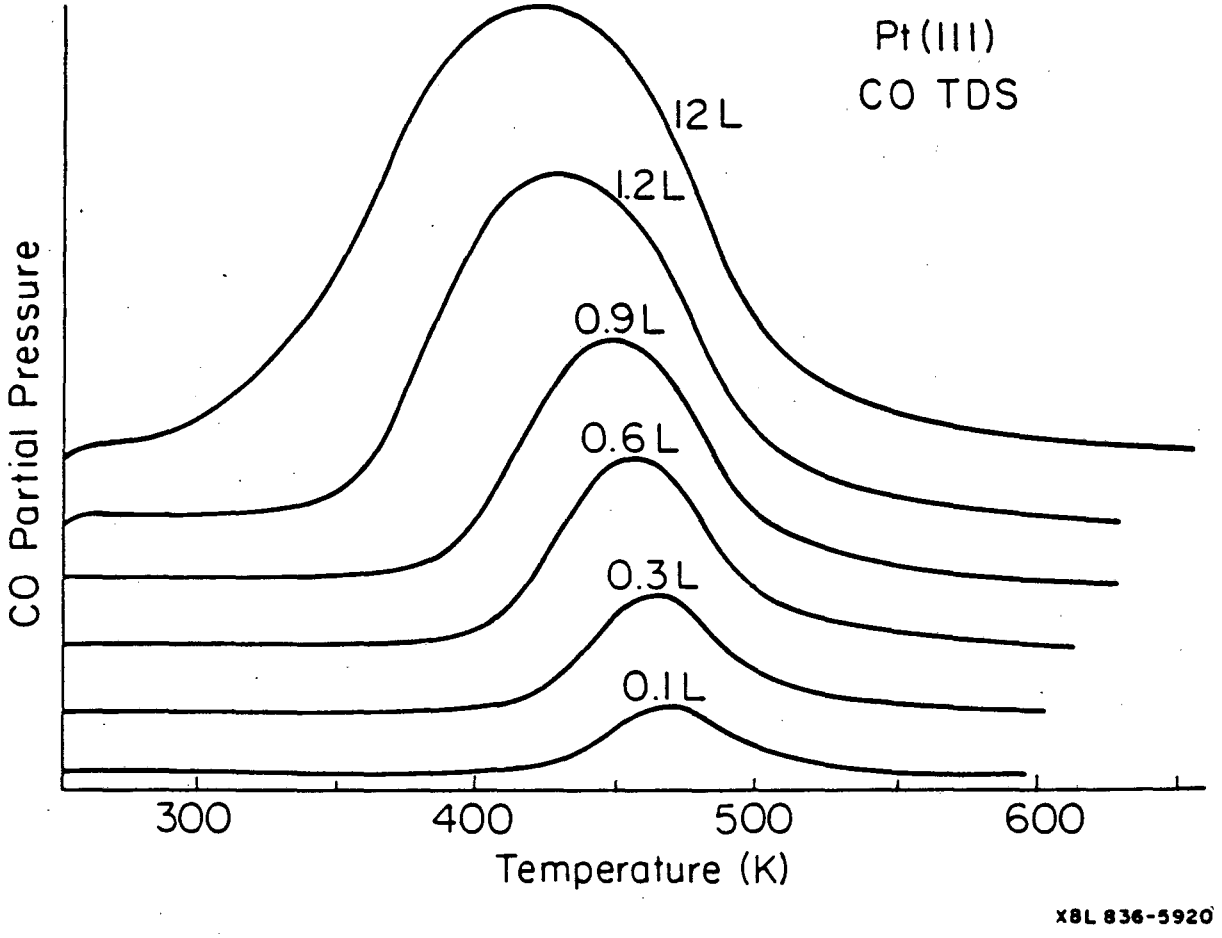

FIG. 2.10

Thermal desorption spectra of CO from a Pt(111) surface after various CO exposures.

increased. Another model which explains the coverage dependent behavior of the TDS of CO from Pt(111) is the precursor state model [2.13 - 2.14]. In this model a molecule is assumed to go through a precursor state before desorbing.

According to this model, the rate of desorption is :

$$dn/dt = \nu \theta F \exp\{-E_d/RT\}$$

where $F = (1 - f_a) - (f_a f_m/(1 - f_m))\ [\ 1 + K\ \theta/(1 - \theta)\ ]^{-1}$ and f_a is the probability that a precursor molecule over an open site will re-adsorb, f_d is the probability that a precursor molecule over an open site will desorb, f_m is the probability that a precursor molecule over an open site will hop to another site. $K = f_d'/(1 - f_m)$, where f_d' is the probability that a precursor molecule over a filled site will desorb, and f_m' is the probability that a precursor molecule over a filled site will hop to another site.

Calculated thermal desorption curves for E_d = 30 Kcal/mol, $\nu = 10^{15}\ s^{-1}$, f_a = 0.3, f_d = 0.1, and f_d' = 0.4 are shown in Fig. 2.11 for initial coverages of 0.5 ML down to 0.05 ML. The desorption maximum of the peaks shifts to higher temperatures as the initial coverage decreases.

Experimental factors which may effect the thermal desorption spectra are uneven heating of the crystal and poor pumping speed. Fig. 2.12 shows a calculated TDS curves for first order desorption from a uniformly heated surface and a surface with a 50 K temperature difference across the surface. The effect of the uneven heating of the surface was

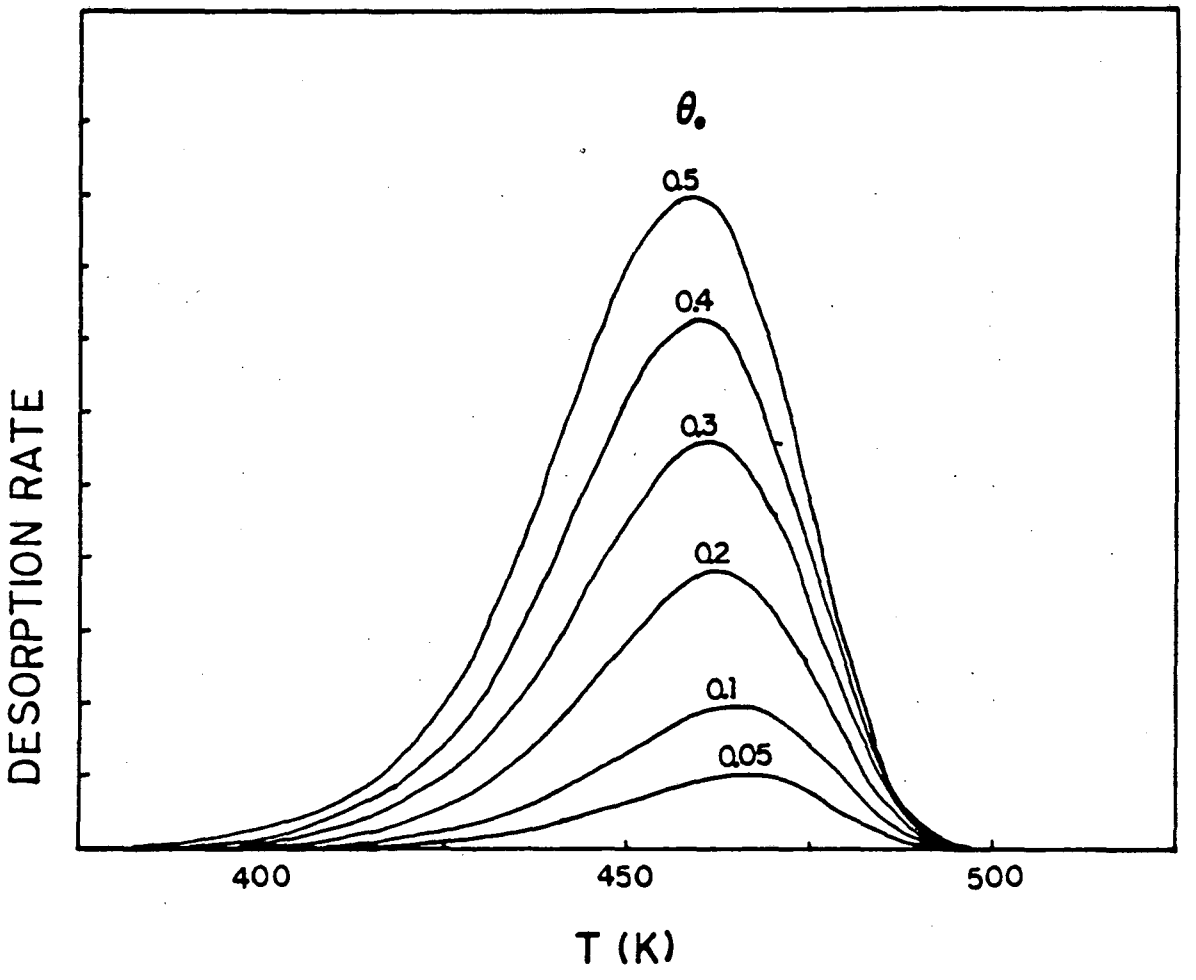

FIG. 2.11

Calculated thermal desorption spectra showing the effect of a precursor state in first-order desorption kinetics. (see text for parameters)

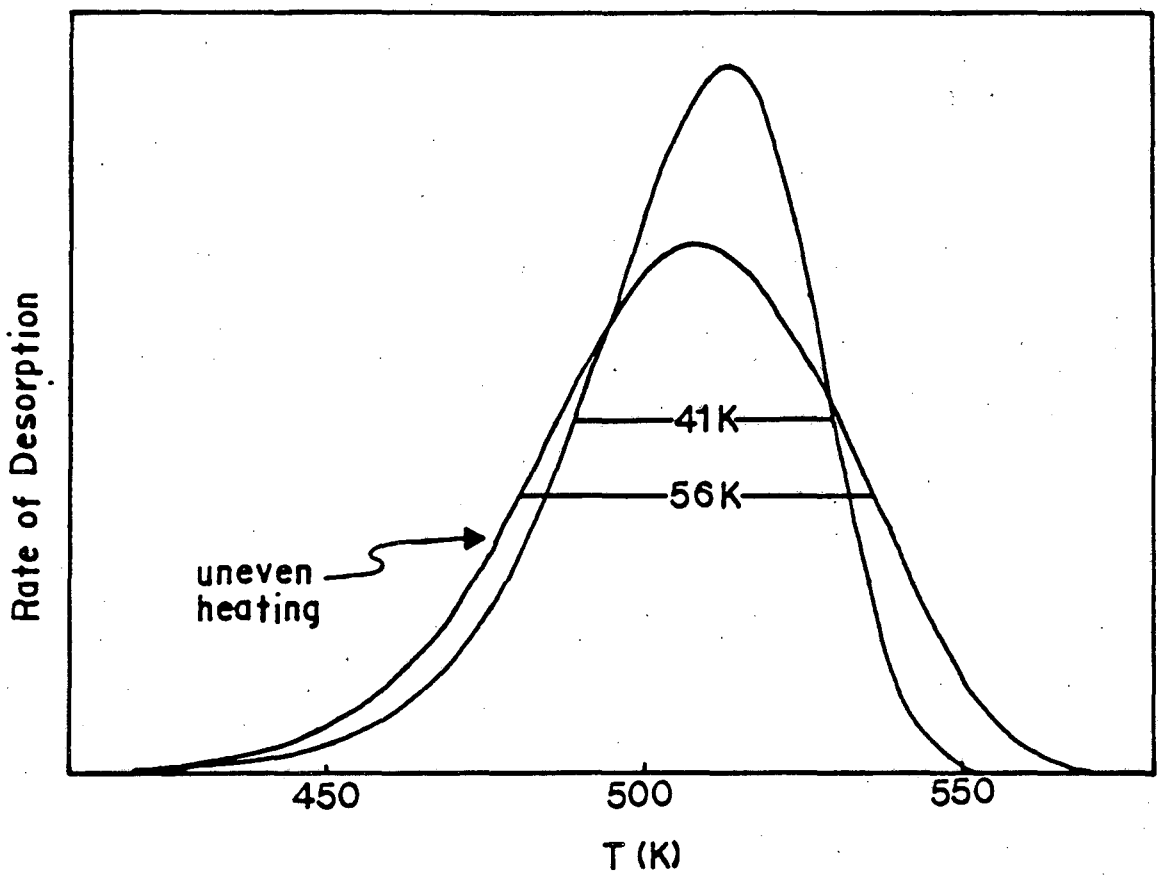

FIG. 2.12

Calculated thermal desorption spectra showing an ideal curve (FWHM = 41 K) and the effect of uneven sample heating (FWHM = 56 K). (see text for parameters)

to broaden the peak. This broadening can lead to grossly erroneous results when determining the kinetic parameters using the method of Chan and Weinberg [2.15]. The input kinetic parameters were E_d = 30 kcal/mole and ν = 10^{13} s^{-1}. Calculating these parameters for the position and width of the broadened peak gives E_d = 21 kcal/mole and ν = 1.5 X 10^9 s^{-1}.

As was mentioned previously, the pressure inside the chamber during a TDS experiment will be proportional to the desorption rate only if the pumping speed to volume ratio is high and the heating rate is low. The TDS curves in Fig. 2.13 were calculated using the same kinetic parameters used in the previous example, a heating rate of 30 K/s, an ambient temperature of 300 K, a system volume of 50 l, and a surface area of 1 cm^2. The pressure is shown as a function of sample temperature for S/V = 0, 1 and 10. The kinetic parameters calculated from the peak width and position for S/V =1 are E_d = 23 kcal/mole and ν = 4.4 X 10^9 s^{-1}, again a large degree of error.

4. Photoelectron spectroscopies

Photoelectron spectroscopy was used to probe the electronic structure of the gold-platinum system. The experimental set-up is shown in Fig. 2.14. In X-ray photoelectron spectroscopy (XPS), X-ray radiation was used for the light source. X-rays were produced by bombarding a Mg target with electrons with a energy of about 10 keV. The

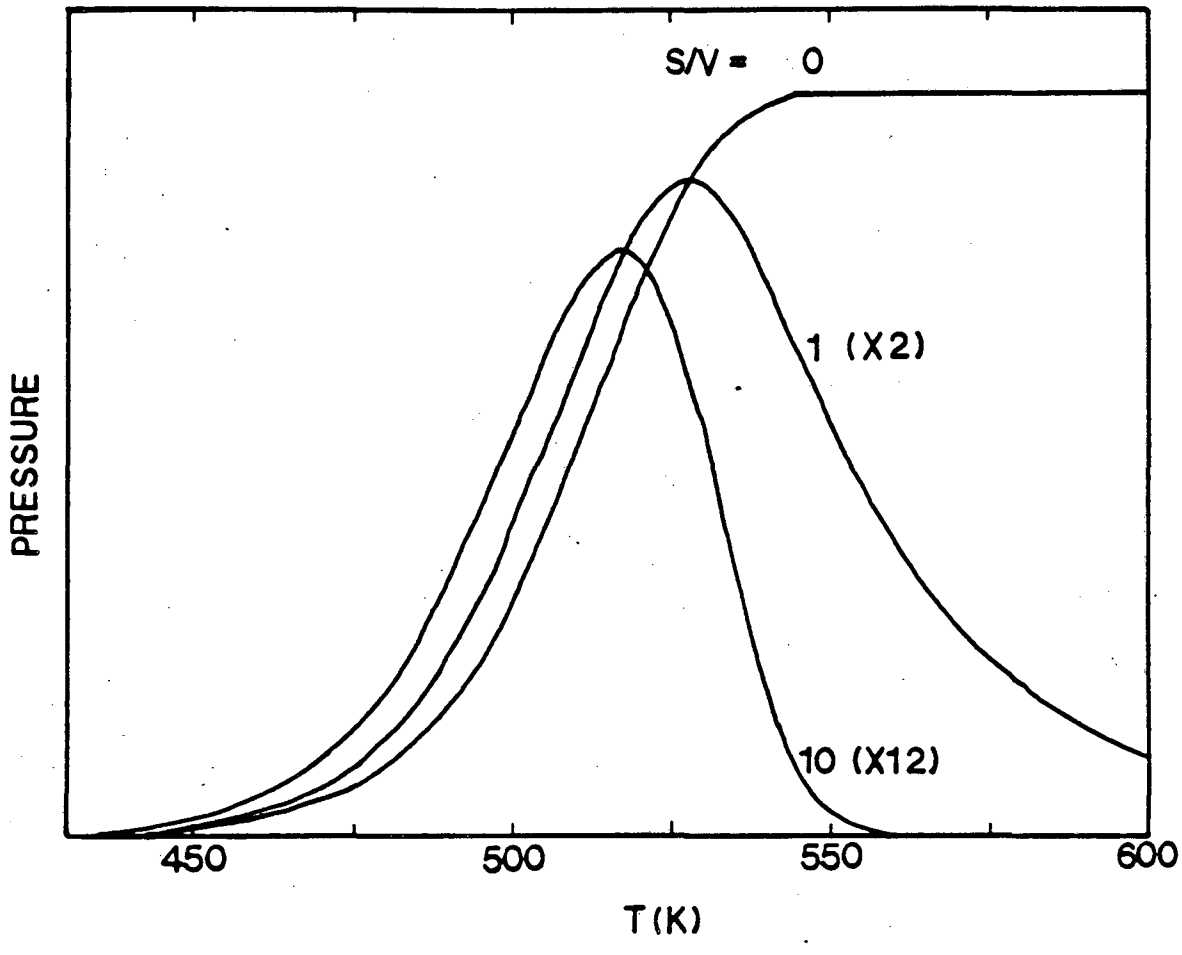

FIG. 2.13

Calculated thermal desorption spectra showing the pressure as a function of sample temperature. Results are shown for a pumping speed to volume ratio of 0, 1 and 10. (see text for parameters)

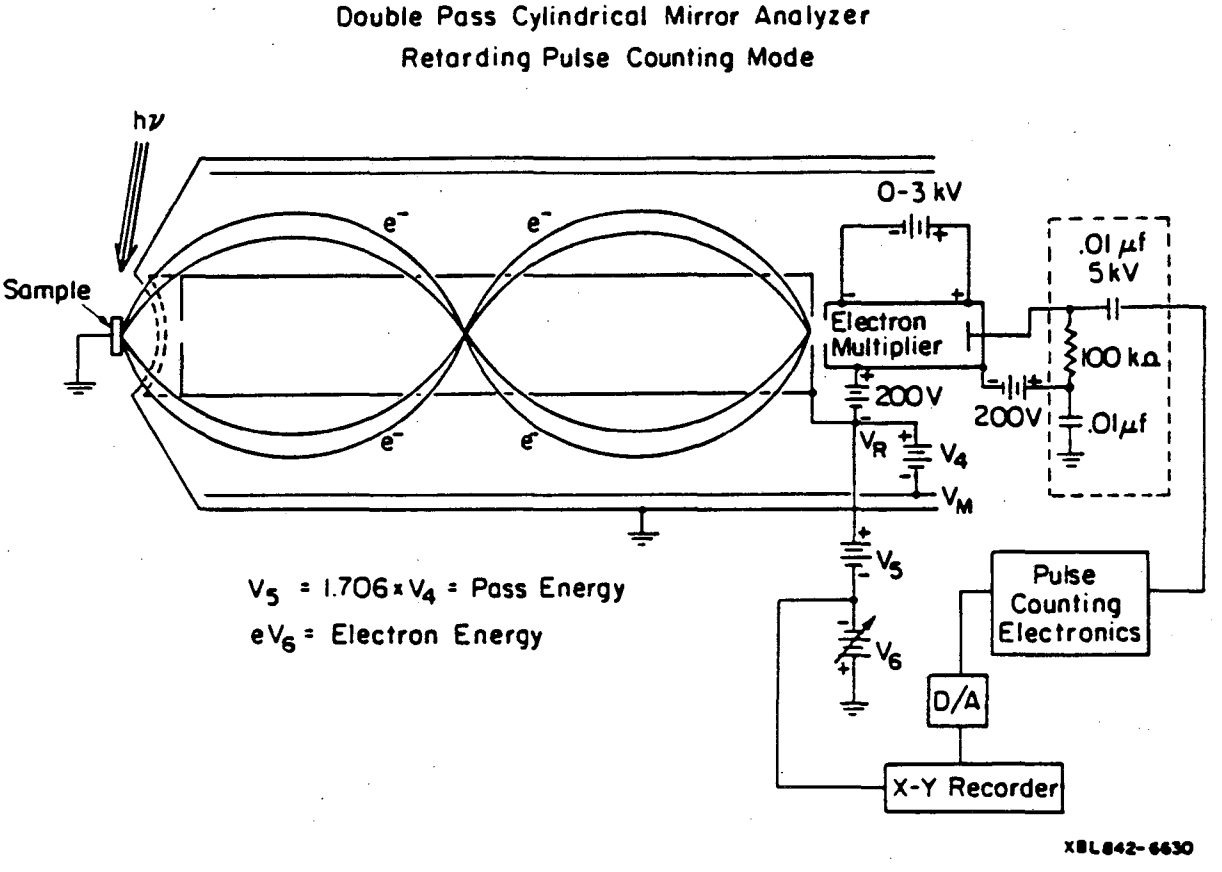

FIG. 2.14

Schematic of the double pass cylindrical mirror analyzer used in ultraviolet and X-ray photoelectron spectroscopies.

energy of the photons produced was 1253.6 eV and was used to probe core electrons. In ultra-violet spectroscopy (UPS) the He I resonance line from a He discharge lamp was used as the photon source. This line has an energy of 21.2 eV and was used to probe the valence electrons. The light source was directed toward the sample and the electrons which were ejected from the sample were collected and analyzed using a double pass cylindrical mirror analyzer (CMA) [2.16 -2.17]. The relation between the photon energy and the kinetic energy of the ejected electrons is :

$$E_{kin} = h\nu - E_b - e\phi_{sp}$$

where E_{kin} is the kinetic energy of the ejected electron, hv is the energy of the photon, E_b is the binding energy of the ejected electron, and ϕ_{sp} is the work function of the spectrometer.

In addition to the main peaks whose energy is directly dependent on the binding energy of the electron, other peaks may be present. For example, since the Mg k_α source is not purely monochromatic, satellite peaks which are shifted by 8.4 eV and 10.2 eV toward higher energy are present [2.18].

5. Kelvin probe

The work function, ϕ, of a solid is defined as the energy necessary to remove an electron from the Fermi level to just outside the surface. Another definition commonly used is the energy necessary to remove an electron from the Fermi level to the vacuum level and the origin of the energy

scale is defined to be $-e\phi_o$, where ϕ_o is the electrostatic potential just outside the surface. These quantities are related to the chemical potential $\bar{\mu}$ of the electrons in the solid by :

$$e\phi = e\phi_o - \bar{\mu} \quad .$$

If two electrical conductors are brought into contact with each other, current flows until the Fermi levels of the two line up. A potential difference is created just outside the surfaces of the two solids. This potential is :

$$V_{ab} = \phi_b - \phi_a \quad .$$

One method of measuring the work function of a solid is the Kelvin method [2.19], also known as the vibrating capacitor method. A schematic of the experimental set-up is shown in Fig. 2.15. The sample and reference are separated by a small distance ($\sim$ 1 mm) forming a capacitor. The charge on the capacitor is :

$$Q = C\ V_{ab} \quad .$$

The reference is connected to a piezoelectric and vibrates with a frequency w. This periodic variance of the distance between the sample and the reference results in a periodic change in the capacitance, thus producing an alternating current :

$$i(t) = V_{ab}\ (dC/dt) = V_{ab}\ w\Delta C\ \cos(wt) \quad .$$

This current flows through a high impedance electrometer amplifier, through a filter and the periodic signal, the amplitude of which is proportional to V_{ab}, is read by the lock-in amplifier. A bias potential is applied until the

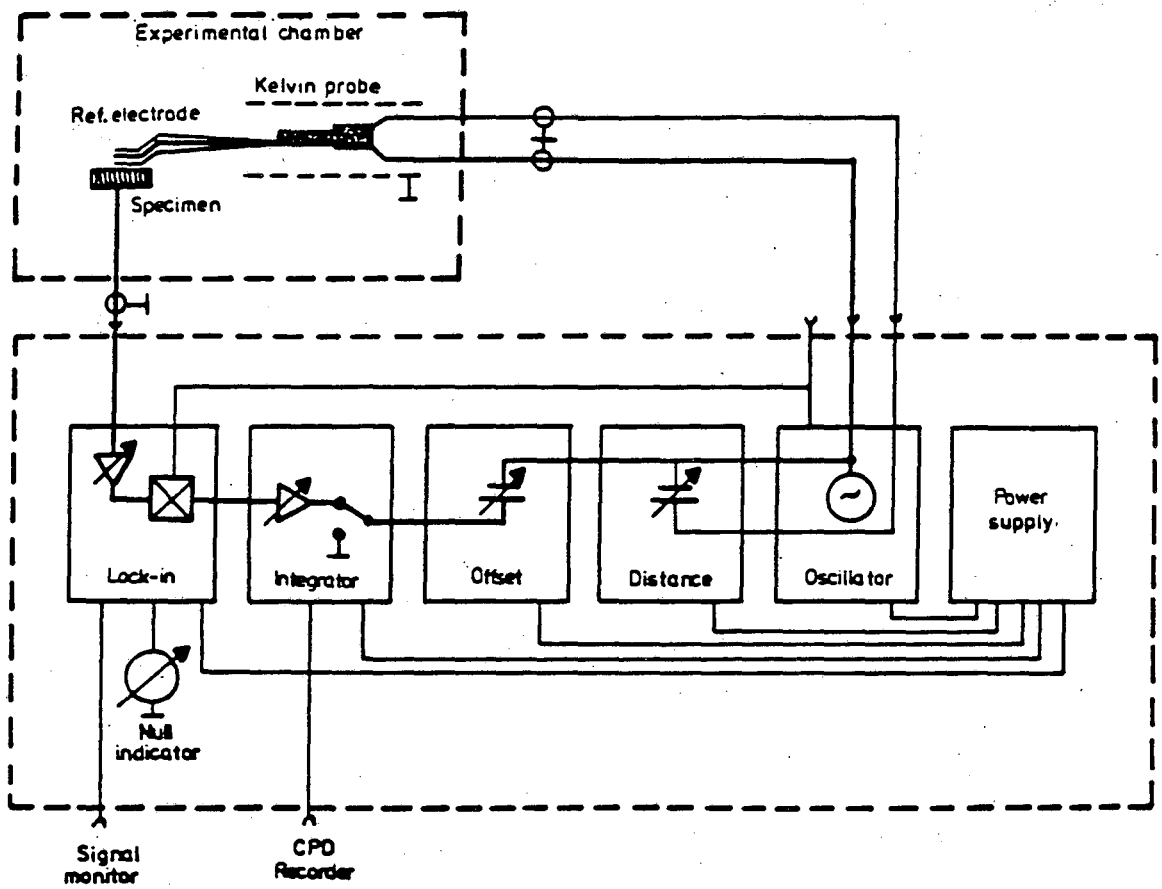

FIG. 2.15

Schematic of the Kelvin probe set-up used in measuring work functions.

signal is nulled. This bias is equal to the difference between the work function of the sample and the work function of the reference.

This method of measuring the work function is convenient because the work function can be monitored continuously while gasses are being adsorbed onto the surface or while a reaction is occurring at the surface. A plot of the work function with time can be obtained by plotting the bias potential as a function of time.

D. METAL DEPOSITION AND ALLOY FORMATION

Epitaxial layers of gold or copper on platinum surfaces were formed by evaporation of gold or copper from the evaporation source shown in Fig. 2.16. It consisted of a high-density alumina tube which was sealed at one end and a alumina plug with a small aperture in the center was inserted into the other end. The tube was wrapped with 0.020 in. diameter tungsten wire. Another alumina tube was placed around this tube in order to decrease the amount of heat lost. This source was mounted on 0.25 in. diameter copper rods which were connected to feedthroughs on a 2 3/4 in. flange. A machined bellows made the positioning of the source possible. The entire assembly was mounted inside a differentially pumped chamber which was also water cooled. This evaporation chamber was connected to the main chamber through a 2 mm shuttered aperture. It was possible to operate the evaporation source with less than a 10^{-9} torr pressure increase in the main chamber and to interrupt the metal deposition at any time.

Deposition rates as high as several monolayers/min were possible, however, more controllable rates of ~ .1 ML/min. were generally used. The flux was very stable and no variation was found in the deposition rates over periods of several weeks.

Several types of growth mechanisms for a metal deposited onto another metal substrate are possible. A Volmer-Weber type of growth mechanism [2.20] consists of the formation of

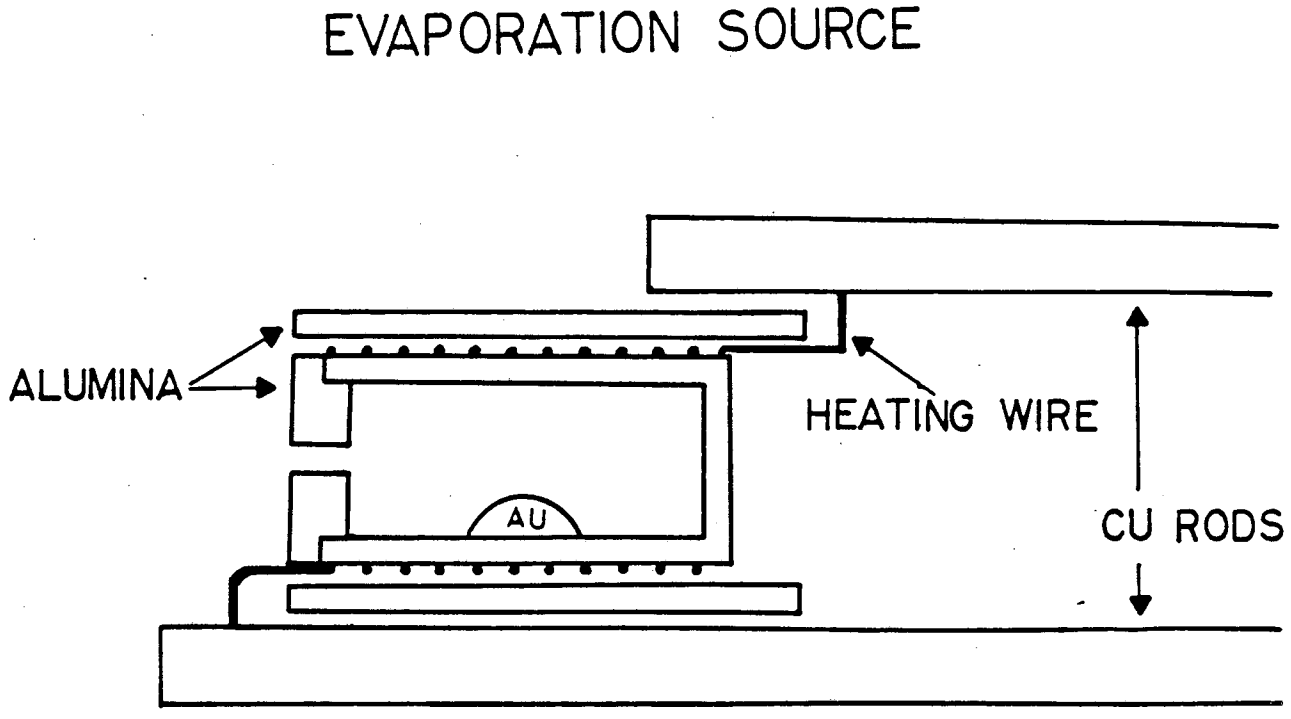

FIG. 2.16

Diagram of the evaporation source used for metal deposition. This source was inside the evaporation chamber showed in Fig. 2.1.

3-dimensional crystallites. This type of growth mechanism is most likely when the surface free energy of the deposited metal is higher than that of the substrate metal. This is the growth mechanism for platinum deposited onto a Au(100) substrate [2.21]. A Frank-Van der Merve type of growth mechanism [2.22 - 2.25] is a layer-by-layer growth mechanism in which the substrate is completely covered by a monolayer of the deposited metal before a second layer begins, and the second layer is completed before the third begins, and so on. This type of mechanism is most likely when the substrate metal has a higher surface free energy than the deposited metal. This mechanism was seen for both copper and gold deposited onto Pt(111) and Pt(100) substrates [2.26 - 2.29]. A third type of growth mechanism is the Stranski-Krastanov type [2.30] which is a hybrid of the other two mechanisms. The growth begins by forming a complete monolayer after which 3-dimensional crystallites begin to grow.

The intensity of the Auger signal of the substrate and the adsorbate can be approximated as :

$$I_j = \sum_i X_{j,i}\, I_{j,1} \exp\{(1-i)/z\}$$

where $X_{j,i}$ is the fraction of j in the ith layer from the surface, $I_{j,1}$ is the intensity of the topmost layer of pure j, and z is the attenuation factor. This model ignores the backscattering factor which may be important for some systems [2.31]. Fig. 2.17 shows the change in the Auger signal intensities as a function of deposition time for a (a) Volmer-Weber type growth mechanism, (b) a Frank-Van der Merve

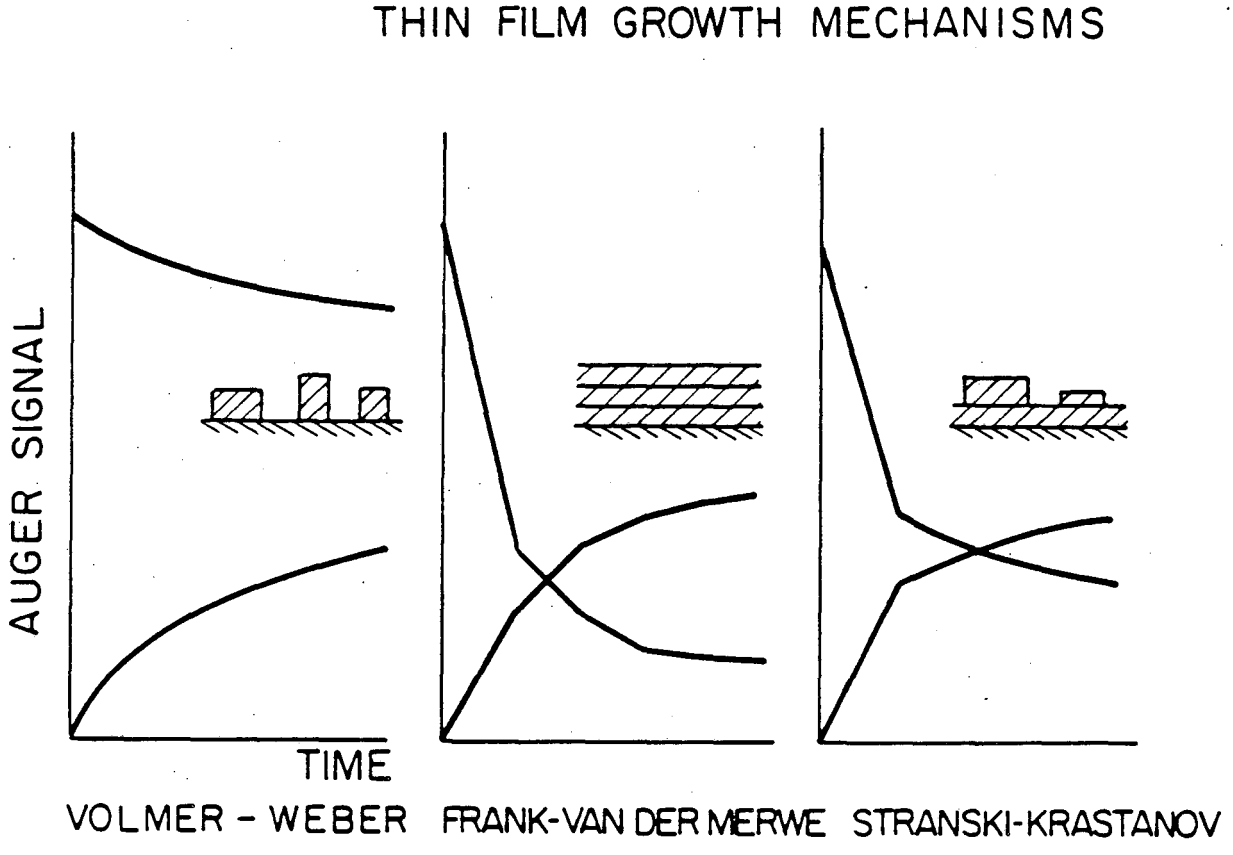

FIG. 2.17

The behavior of the substrate and adsorbate Auger signals as a function of deposition time for Volmer-Weber, Frank-Van der Merve and Stranski-Krastinov type growth mechanisms.

type growth mechanism, and (c) a Stranski-Krastanov type growth mechanism. The Volmer-Weber type mechanism shows slow smooth changes in the Auger intensities as the adsorbate coverage increases. A distribution of crystallite sizes and shapes results in the smooth change and since areas of the substrate remain uncovered, the signal changes slowly. For Frank-Van der Merve type growth, The signals change rapidly and linearly with increasing adsorbate coverage. At the completion of a monolayer, the slope changes and a new linear section begins. When layer-by-layer growth is present, the deposition source can be calibrated from the breaks in the curves. This must be done with caution, however, and other techniques, e.g. TDS, should be used to confirm the completion of a monolayer. The Stranski-Krastanov type mechanism shows first a linear, rapid change in signal with adsorbate coverage and then a change to a slower, smooth change after the completion of a monolayer. It is difficult to experimentally distinguish between a Frank-Van der Merve and Stranski-Krastanov type growth mechanism due to the error normally present in the data.

Surface alloys were formed by first depositing several monolayers of gold or copper onto the platinum surface and then annealing the crystal to allow the deposited metal to diffuse into the platinum. Surface concentrations were determined by carbon monoxide titration. Since carbon monoxide does not adsorb on gold or copper at room temperature, the areas under the CO TDS curves were used to

determine the amount of platinum on the surface of the alloys. Because the CO/Pt ratio may vary with the alloy composition, a knowledge of the alloy surface structure is important. Saturation of CO on a clean Pt(111) surface is 0.5 monolayers [2.32], i.e. a CO/Pt = 0.5. An alloy surface consisting of 75 % Cu and 25 % Pt is made up of completely isolated Pt atoms. The ratio of CO to Pt must therefore be 1. Considerations of this type must be made in order to obtain meaningful surface alloy concentrations. Since the escape depth of Auger electrons is several monolayers, AES cannot give an accurate measure of the surface concentrations in the alloys.

In preparing alloy surfaces prior to the high pressure reactions, 2-3 monolayers of gold were deposited and ~10 monolayers of copper were deposited prior to annealing. The larger amount of copper was needed to saturate the near surface region of the alloy which slowed down the diffusion process. Following the annealing process, the alloy surface was characterized as described above.

If a random distribution of the gold or copper at the alloy surface is assumed, the distribution of sites on the alloy surface can be calculated as follows :

Four-fold sites ((100) surfaces) -

Fraction containing 4 Pt atoms = $(1 - X)^4$

Fraction containing 3 Pt atoms = $4X(1 - X)^3$

Fraction containing 2 Pt atoms = $6X^2(1 - X)^2$

Fraction containing 1 Pt atom = $4X^3(1 - X)$

Fraction containing 0 Pt atoms = X^4

Three-fold sites ((111) surfaces)-

Fraction containing 3 Pt atoms = $(1 - X)^3$

Fraction containing 2 Pt atoms = $3X(1 - X)^2$

Fraction containing 1 Pt atom = $3X^2(1-X)$

Fraction containing 0 Pt atoms = X^3

Two-fold sites ((111) and (100) surfaces)-

Fraction containing 2 Pt atoms = $(1 - X)^2$

Fraction containing 1 Pt atom = $2X(1 - X)$

Fraction containing 0 Pt atoms = X^2

where X = the surface atom fraction of Cu or Au.

A plot of these distribution is shown if Fig. 2.18 - 2.20. Although the Cu-Pt system probably has some degree of short-range order, using a random distribution will show the same trends when interpreting the high pressure reaction results.

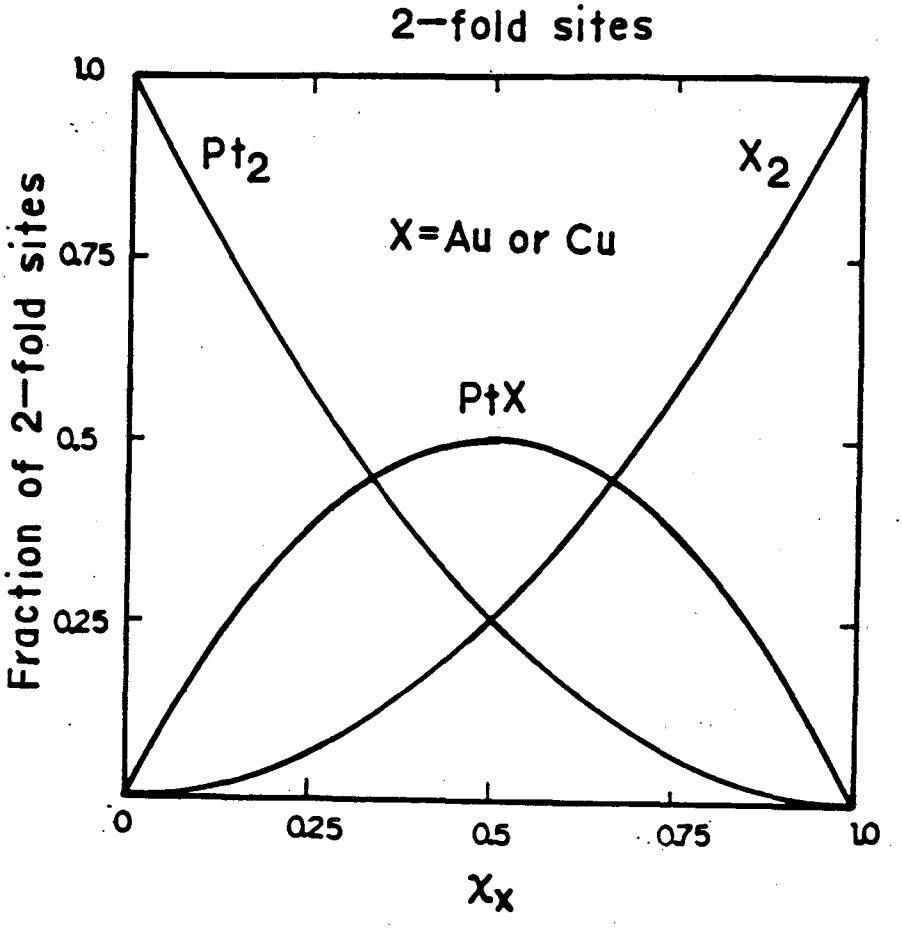

FIG. 2.18

Fraction of 2-fold sites containing 2, 1 and 0 platinum atoms as a function of the IB metal surface atom fraction. Distributions are for a random alloy surface.

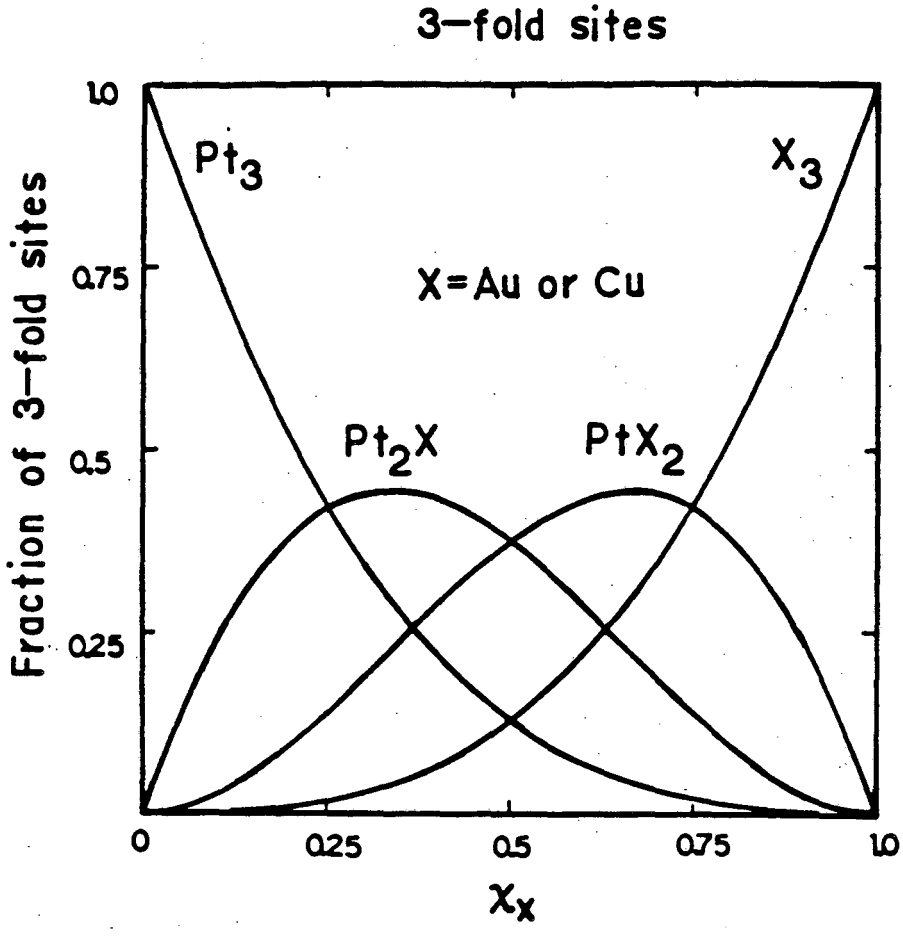

FIG. 2.19

Fraction of 3-fold sites containing 3, 2, 1 and 0 platinum atoms as a function of the IB metal surface atom fraction. Distributions are for a random alloy surface.

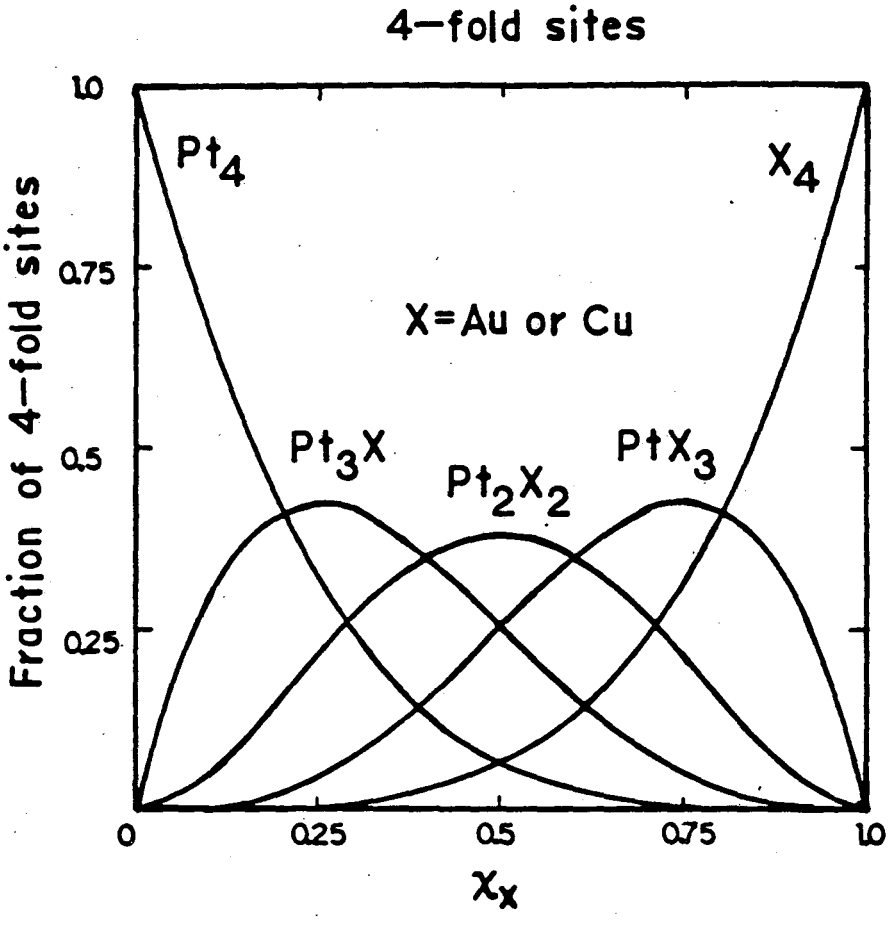

FIG. 2.20

Fraction of 4-fold sites containing 4, 3, 2, 1 and 0 platinum atoms as a function of the IB metal surface atom fraction. Distributions are for a random alloy surface.

E. HIGH PRESSURE REACTIONS

Before any high pressure reaction was carried out, the catalyst surface was thoroughly cleaned, modified and characterized under UHV conditions, as described in the previous sections. After this preparation, the sample was enclosed in the high-pressure cell described in the system overview section (II.A).

1. The n-hexane conversion reaction

a. Reaction procedure

After the high-pressure cell was closed, ~ 20 torr of n-hexane was introduced into the the reactor loop. The valves to the high-pressure cell were then opened, allowing the n-hexane into the cell. The pressure of the n-hexane (which dropped due to the increase in volume) was increased to 20 torr, after which 200 torr of hydrogen was introduced into the reactor loop. The gasses in the loop were circulated by means of a metal bellows pump (Metal Bellows Corp. model MB-21) for a 20 minute period to insure mixing of the hydrogen and hydrocarbon. After mixing and prior to heating the catalyst, a sample of the reaction mixture was fed into the gas chromatograph in order to determine the hydrocarbon impurity concentrations. The major impurity was methylcyclopentane which was present at a concentration of ca. 500 ppm. The catalyst was heated resistively to 570 K in the circulating gasses and samples of the reaction mixture were taken every 20 minutes and analyzed by gas chromatography. After two hours of reaction, the crystal was

cooled and the reactor loop was pumped out, first by mechanical pump and then by sorption pump. Following the evacuation of the reactor loop (10 - 20 minutes), the high-pressure cell was isolated and opened to UHV. The catalyst surface was then analyzed with UHV techniques.

b. Rate calculations

The flame ionization detector of the gas chromatograph was calibrated using a standard mixture of 200 ppm methane in nitrogen. A plot of the FID signal as a function of the standard mixture pressure is shown in Fig. 2.21. The slope of this line is 10.75 counts per torr of the standard mixture. With a reactor volume of 165 ml, a gas temperature of 300 K, a catalyst surface area of A with an atomic density of d, and a FID signal proportional to the number of carbons in the molecule (N_C), the turnover number (TN) of a given product is :

$$4.94 \times 10^{13} \text{ (counts/AdN}_C\text{)}.$$

A typical accumulation curve (TN versus time) for methylcyclopentane formation (□), hydrogenolysis (○), and isomerization (△) is shown in Fig. 2.22. The slope of the curves decreased with increasing time due to the poisoning of a carbonaceous layer which built up on the surface. In order to obtain initial rates of reaction, this process was modeled in the following way.

The rate of the reaction (d(TN)/dt) was assumed to be proportional to the fraction of the surface not covered by

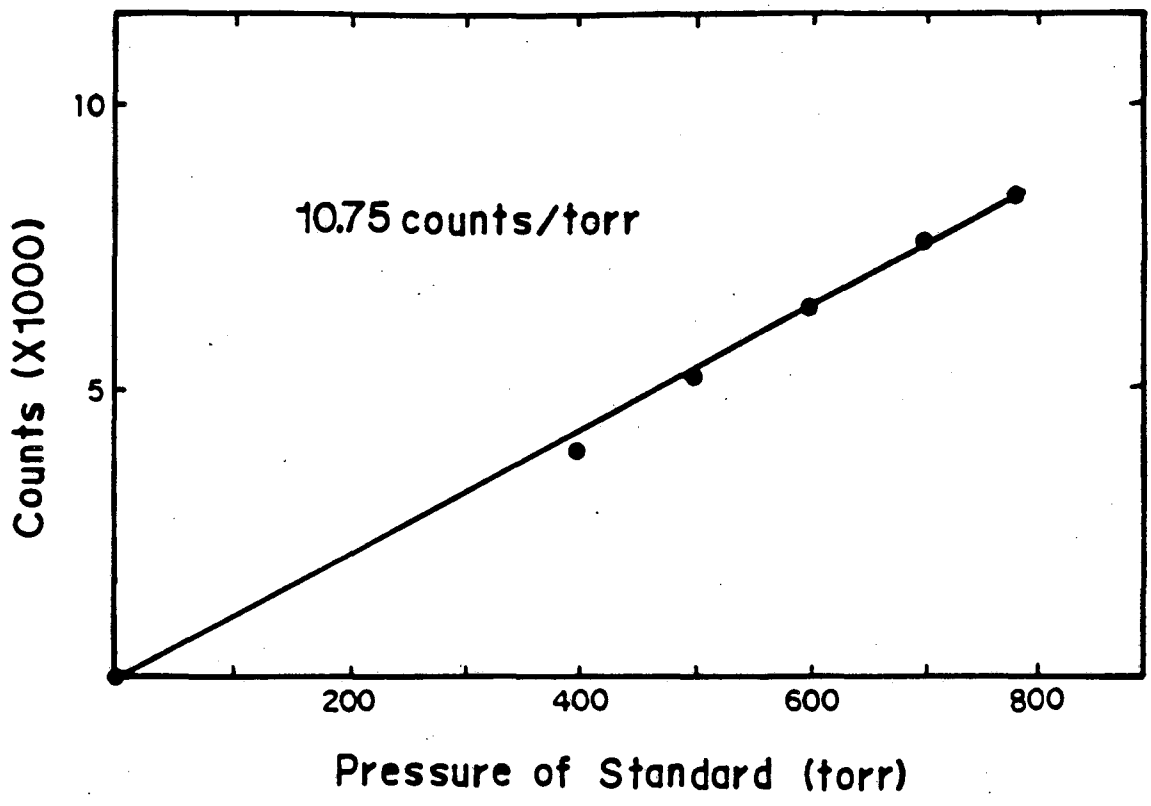

FIG. 2.21

Plot of the number of counts from the flame ionization detector as a function of the pressure of a 100 ppm CH_4 in N_2 standard mixture.

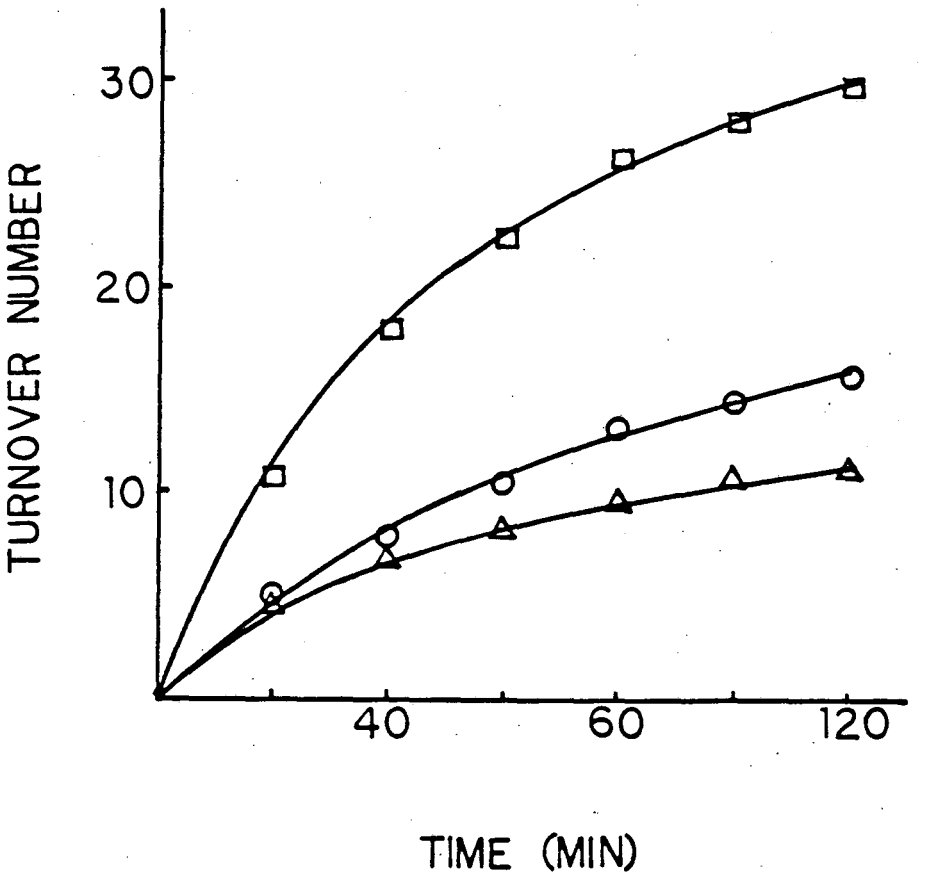

FIG. 2.22

Example of an accumulation curve for methylcyclopentane formation (□), hydrogenolysis (○), and isomerization (△). Solid lines are a fit of the data to the model discussed in the text.

the carbonaceous deposit which poisoned the surface (θ_{Pt}) :

$$d(TN)/dt = k_1\theta_{Pt}.$$

The rate of poisoning ($-d(\theta_{Pt})/dt$) was also assumed to be proportional to θ_{Pt} :

$$d(\theta_{Pt}) = -k_2\theta_{Pt}.$$

The TN as a function of time is :

$$TN(t) = (k_1/k_2)(1 - e^{-k_2t}),$$

which can be approximated by :

$$TN(t) \cong (k_1/k_2)(k_2t/(k_2t + 1)).$$

This equation can be linearized and fit to the data by a least square analysis. The fit obtained was excellent as shown in accumulation curves in Fig. 2.22 where the solid lines are the fit to the data.

The effect of changing the order of the reactions was also tested. Varying the order from 1 to 6 resulted in no more than 5 % difference in the calculated initial rates. The constants k_1 and k_2 however, differed considerably. Because of this, no interpretations were based on the individual values of these constants.

Setting $a = k_2$ and $b = (k_1/k_2)$, the initial rate of reaction is :

$$d(TN(t=0))/dt = ab,$$

and the turnover number at time t is :

$$TN(t) = b/(1 + (1/at)).$$

Although the crystal faces were always well defined, the structure and impurities levels of the crystal edges were not known. In order to remove the contribution of the crystal

edges reactions were carried out over crystals whose faces were completely covered by an inactive material. Data obtained from these reactions was always subtracted from the data obtained for the reactions carried out over clean and alloy surfaces.

c. Fitting of rates to site distributions

As was mentioned in section II. D., the results of the n-hexane conversion reactions over the alloy surfaces were fit to a distribution of sites based on a randomly distributed alloy surface. In doing this, the rate of a reaction was assumed to equal :

$$R = \sum_j R_{i,j} f_{i,j}$$

where i is the number of atoms per site (i = 3 for the (111) surface and i = 4 for the (100) surface), j is the number of Pt atoms in the i-fold site, $R_{i,j}$ is the rate of reaction at a i-fold site which contains j Pt atoms, and $f_{i,j}$ is the fraction of i-fold sites on the surface which contain j Pt atoms.

The values of $R_{i,j}$ were determined by fitting the experimentally obtained reaction rates as a function of surface alloy composition to the calculated site distributions discussed in section II. D. This subject is discussed in more detail in Chapter IV.

2. CO oxidation reaction

In order to keep the CO and oxygen concentrations constant during the course of the reaction, the reaction was carried out in a flow through mode. Reaction gasses were passed through molecular sieve traps before being introduced into the reactor through the gas manifold (refer to Fig. 2.2). This filtering was especially important to remove iron carbonyls from the CO. The reactant gasses were then passed over the catalyst and then vented out through the fume hood in the laboratory. Flow rates and concentrations were controlled by adjusting needle valves which were connected to the gas lines between the gas regulators and the gas manifold. Flow rates were determined by measuring the flow rate of the exhaust with a bubble flow meter while the catalyst was not being heated. Typical flow rates were 200 ml/min with the CO concentration ranging between 1 and 30 %. The catalyst was heated resistively and temperatures between 400 K and 800 K were studied.

Because the reaction is very exothermic (~70 kcal/mole), it was convenient to follow the rate of the reaction by monitoring the temperature of the catalyst. The validity of this procedure was check by leaking the reaction mixture from the reactor into the UHV chamber through a leak valve and following the concentrations of CO, O_2, and CO_2 using the mass spectrometer inside the chamber as a function of time. When the catalyst temperature increased the CO_2 concentration increased and the CO and O_2 concentrations

decreased. The converse was true when there was a drop in catalyst temperature. The changes in gas concentrations were much more gradual than the temperature changes due to the mixing of gasses in the volume between the catalyst and the leak valve. The change in temperature, therefore, gave a much better indication of the rate.

There was an induction period of several days between the time a clean platinum crystal was subjected to reaction conditions and the observation of oscillations in the reaction rate. Because of this, the crystal was left in the reactor for several weeks at a time while data was being taken after which the reactor was pumped out and the isolation cell opened to UHV conditions for analysis.

REFERENCES

2.1) M.A. Van Hove, R. J. Koestner, P.C. Stair, J.P. Biberian and G.A. Somorjai, Surface Sci. 103 (1981) 189.

2.2) M.A. Van Hove, R. J. Koestner, P.C. Stair, J.P. Biberian and G.A. Somorjai, Surface Sci. 103 (1981) 218.

2.3) A.E. Morgan and G.A. Somorjai, Surface Sci. 12 (1968) 405.

2.4) R.J. Behm, P.A. Thiel, P.R. Norton and G. Ertl, J. Chem. Phys. 78 (1983) 7437.

2.5) R.J. Behm, P.A. Thiel, P.R. Norton and G. Ertl, J. Chem. Phys. 78 (1983) 7448.

2.6) G. Ertl and J. Küppers, "Low energy Electrons and Surface Chemistry", Verlag-Chemie, Weinhein, 1974.

2.7) M.A. Van Hove and S.Y. Tong, "Surface Crystalllography by LEED", Springer-Verlag, Berlin 1979.

2.8) M.W. Roberts and C.S. McKee, "Chemistry of the Metal-Gas Interface", Oxford University Press, Oxford 1978.

2.9) H. Eyring, J. Walter and G.E. Kimball, "Quantum Chemistry", John Wiley & Sons, Inc., New York 1944.

2.10) G.Ertl, M. Neumann and K.M. Streit, Surface Sci. 64 (19977) 393.

2.11) R.W. McCabe and C.D. Schmidt, Surface Sci. 65 (1977) 189.

2.12) D. Hollins, Surface Sci. 107 (1981) 75.

2.13) M. Alnot and A. Cassuto, Surface Sci. 112 (1981) 325.

2.14) A. Cassuto and D.A. King, Surface Sci. 102 (1981) 388.

2.15) C.M. Chan, R. Aris and W.H. Weinberg, Appl. Surface Sci. 1 (1978) 360.

2.16) "Handbook of X-Ray and Ultraviolet Photoelectron Spectroscopy", D. Briggs, ed., Heyden 1978.

2.17) T.A. Carlson, "Photoelectron and Auger Spectroscopy", Plenum Press, New York 1975.

2.18) C.D. Wagner, W.H. Riggs. L.E. Davis, J.F. Moulder and G.E. Muilenberg, "Handbook of X-Ray Photoelectron Spectroscopy", Perkin Elmer Corp., Minnesota 1978.

2.19) P.P. Craig and V. Radeka, Rev. Sci. Instr. 41 (1970) 258.

2.20) M.Volmer and A. Weber, Z. Phys. Chem. 119 (1926) 277.

2.21) J.W.A. Sachtler, M.A. Van Hove, J.P. Biberian and G.A. Somorjai, Surface Sci. 110 (1981) 19.

2.22) T.E. Gallon, Surface Sci. 17 (1969) 486.

2.23) D.C. Jackson, T.E. Gallon and A. Chambers, Surface Sci. 36 (1973) 381.

2.24) M.P. Seah, Surface Sci. 32 (1972) 703.

2.25) F.C. Frank and J.H. Van der Merve, Proc. R. Soc. A198 (1949) 205.

2.26) P.W. Davies, M. Quinlan and G.A. Somorjai, Surface Sci. 121 (1982) 290.

2.27) R. Yeates and G.A. Somorjai, Surface Sci. 134 (1983) 729.

2.28) J.W.A. Sachtler and G.A. Somorjai, J. Catal. 81 (1983) 77.

2.29) M.T. Paffett, C.T. Campbell, T.N. Taylor and S. Srinivasan, Surface Sci. 154 (1985) 284.

2.30) I.N. Stranski and L. Krastanov, Sitzungsker. Akad. Wiss. Wien, Math-Naturwiss., K1 IIb, 146 (1938) 797.

2.31) M.L. Tarng and G.K. Wehner, Proc. Physical Electronic Conf., Albuquerque, N.M. 1972.

2.32) P.R. Norton, J.A. Davies and T.E. Jackman, Surface Sci. 122 (1982) L593.

CHAPTER THREE : CHARACTERIZATION OF Cu/Pt SURFACES

A. INTRODUCTION

Studies of the deposition and growth of one transition metal on the ordered surface of another transition metal are important to understand the nature of epitaxy and the mechanism of metal crystal growth. Investigations of how alloys form by the diffusion of one of the constituents into the other from the surface reveal the mechanism of the initial stages of alloying. The copper-platinum system is a good choice for both of these studies. The interatomic distance of the metals is similar (copper is 8 % smaller than platinum). Their heat of mixing is exothermic (-10 kcal/mole) and they form several ordered alloy structures (Pt_3Cu, PtCu, and $PtCu_3$).

The catalytic properties of a transition metal surface can also be drastically altered by the addition of another metal which may not itself catalyze the reaction of interest. The catalytic properties of Cu/Pt alloys supported on silica in the hydrocarbon conversion reaction have been studied [3.1 - 3.3]. These investigations showed an increased selectivity for cracking for the alloys compared to pure platinum, a rather surprising result since copper itself does not exhibit activity for cracking. Because of the poor characterization of the alloy surface, interpretation of these results is difficult. Impurities such as oxygen, which would have a profound effect on the reaction [3.4], could not be detected if present. Since copper tends to segregate to the surface

of Cu/Pt alloys [3.5], the bulk compositions reported are not representative of the composition of the catalytic surface. Also, ordering and structure of the alloy surface can effect the selectivity of the catalyst, again impossible to detect using supported alloys. In chapter 5, the catalytic properties of well characterized Cu/Pt and Au/Pt single crystal surfaces in the n-hexane conversion reaction will be discussed.

In order to better understand the novel selectivity and activity of the Cu/Pt system, the surface properties of the alloy need to be better characterized. In this chapter, the results of experiments directed toward understanding the composition, structure, and chemisorption characteristics of this alloy surface are reported. The atomically flat, hexagonally closest packed Pt(111) surface, the stepped Pt(553) surface and the square lattice of the Pt(100) surface were studied. Copper was deposited by evaporation onto the crystal surface. Surface alloys were formed by heating the sample to temperatures at or above 550 K, allowing the copper to diffuse into the platinum substrate. Surface structure was studied using low energy electron diffraction (LEED), surface composition was determined using Auger electron spectroscopy (AES) and thermal desorption spectroscopy (TDS) of carbon monoxide was used to probe the changes in bonding characteristics of the platinum at the alloy surface.

B. RESULTS

1.Growth of Copper Layers on Platinum Surfaces

AES has been used to determine the growth mechanism of one metal deposited on a single crystal substrate of another metal [3.6]. In this procedure, the Auger signal of both the substrate and the adsorbate are plotted versus the deposition time of the adsorbate. If a constant sticking coefficient is assumed for the adsorbate, the time of deposition from a constant flux source is proportional to the coverage of the adsorbate. The abscissa can the be labeled in units of deposited metal monolayers. In Fig. 3.1 the Auger signal, normalized to the peak-to-peak height of the pure platinum ($N_5N_6N_6$) Auger transition at 150 eV (Pt-150 V), is plotted versus copper coverage on the Pt(111) surface. The Pt-150 V signal dropped off sharply and linearly with copper coverage, with a change in the slope at a coverage assigned to one monolayer of copper. Another change in the slope was observed after an equal period of deposition indicating the completion of a second monolayer of copper. At low copper coverages the signal of copper ($M_{2,3}M_4V$) Auger transition at 105 eV (Cu-105 V) was buried in the background of the platinum Auger spectrum. Once the Cu-105 V signal was resolved, however, the growth of the signal was linear with coverage with breaks at the same coverages as the breaks which occurred in the Pt-150 V signal versus copper coverage plot. This behavior is indicative of a layer-by-layer growth mechanism [3.6] in which one monolayer of copper was formed

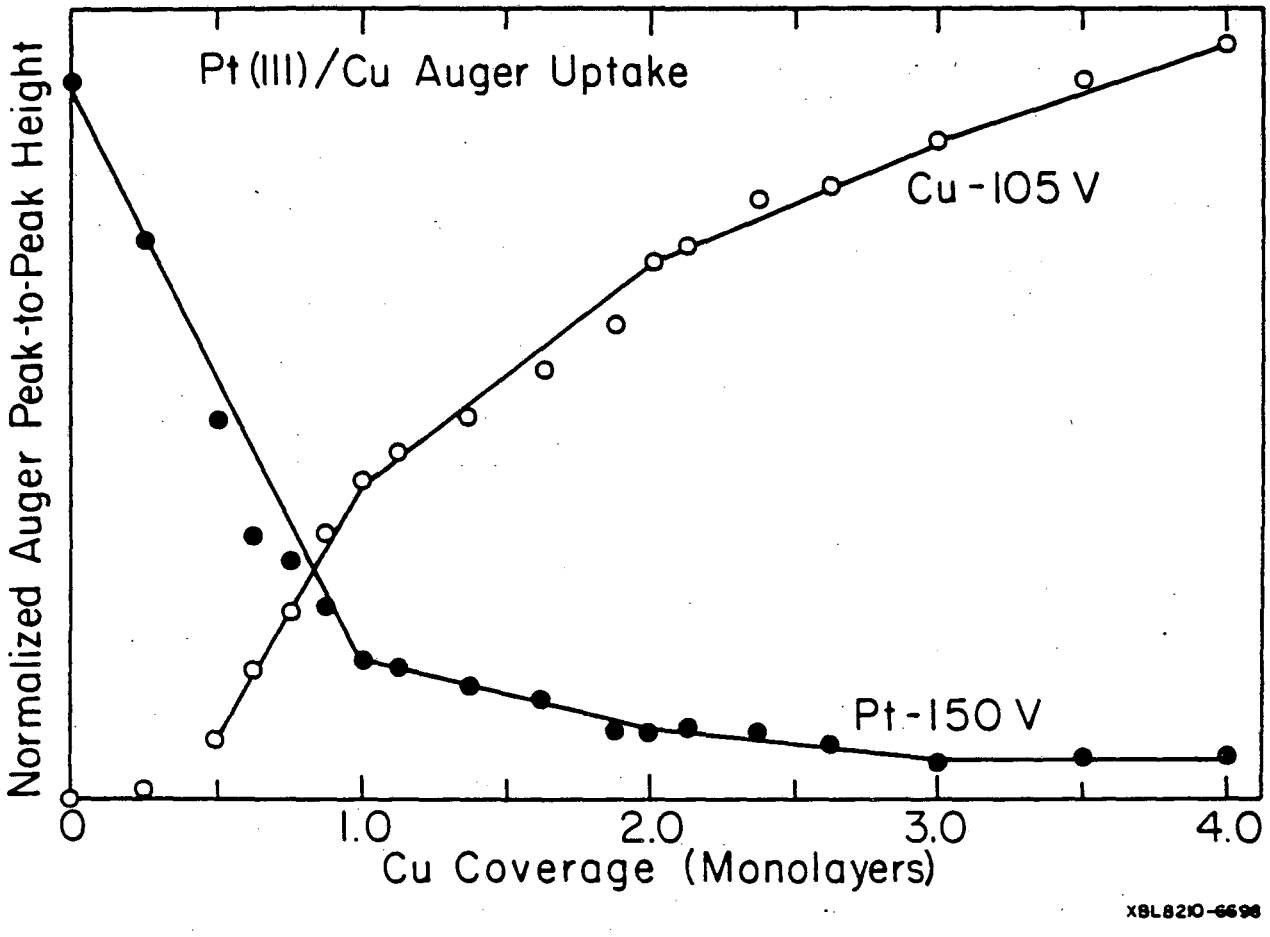

FIG. 3.1

Plot of the Auger peak-to-peak intensity of the Pt-150 V peak and the Cu-105 V peak versus copper coverage for copper deposited on the Pt(111) surface.

before a second began and the growth continued layer-by-layer.

The clean Pt(111) single crystal surface showed the expected hexagonal LEED pattern. As copper was deposited neither the spot positions nor their sharpness changed and no new spots appeared up to one monolayer copper coverage. Relative diffraction spot intensities changed somewhat but no attempt was made to analyze this behavior. After more than one monolayer of copper had been deposited, the diffraction spots began to lose their intensity and sharpness. After four monolayers had been deposited a (12 X 12) coincidence pattern was observed after slight annealing at 450 K. The diffraction pattern of this surface and the (1 X 1) surface is shown schematically in Fig. 3.2. Results of Paffett [3.7] show that this close-packed copper overlayer can be formed by the second copper layer if the platinum substrate is heated to 450 K during copper deposition. This type of pattern has been observed for silver deposited on a Cu(111) substrate [3.7]. Upon heating the platinum crystal which had several monolayers of copper deposited on it to 500 K, the diffraction spots lost intensity and sharpness. On occasion, however, a (2 X 2) pattern was observed for a surface which was ~75 % copper.

The thermal desorption spectra of carbon monoxide from the Pt(111) surface with several different coverages of copper are shown in Fig. 3.3. The sample was exposed to CO to obtain a saturation coverage of CO (12 L) at 250 K. At

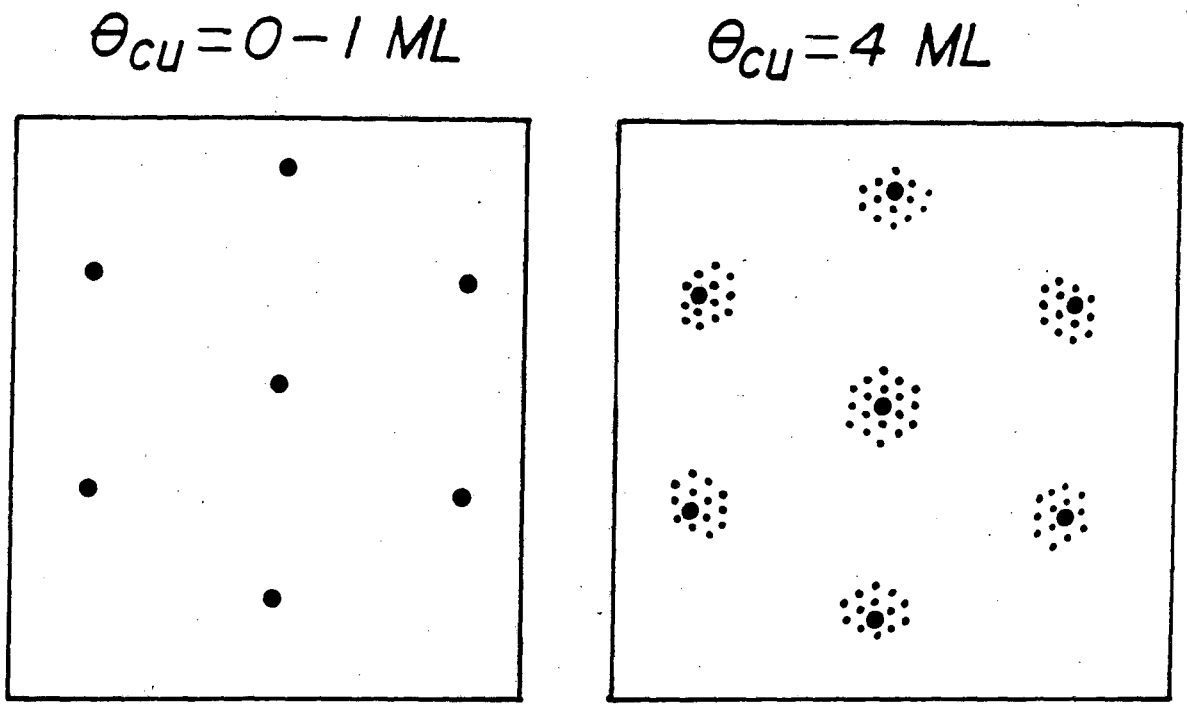

FIG. 3.2

Diagram of the LEED patterns for the (1 X 1) and (12 X 12) coincidence structures obtained for Cu deposited on a Pt(111) surface.

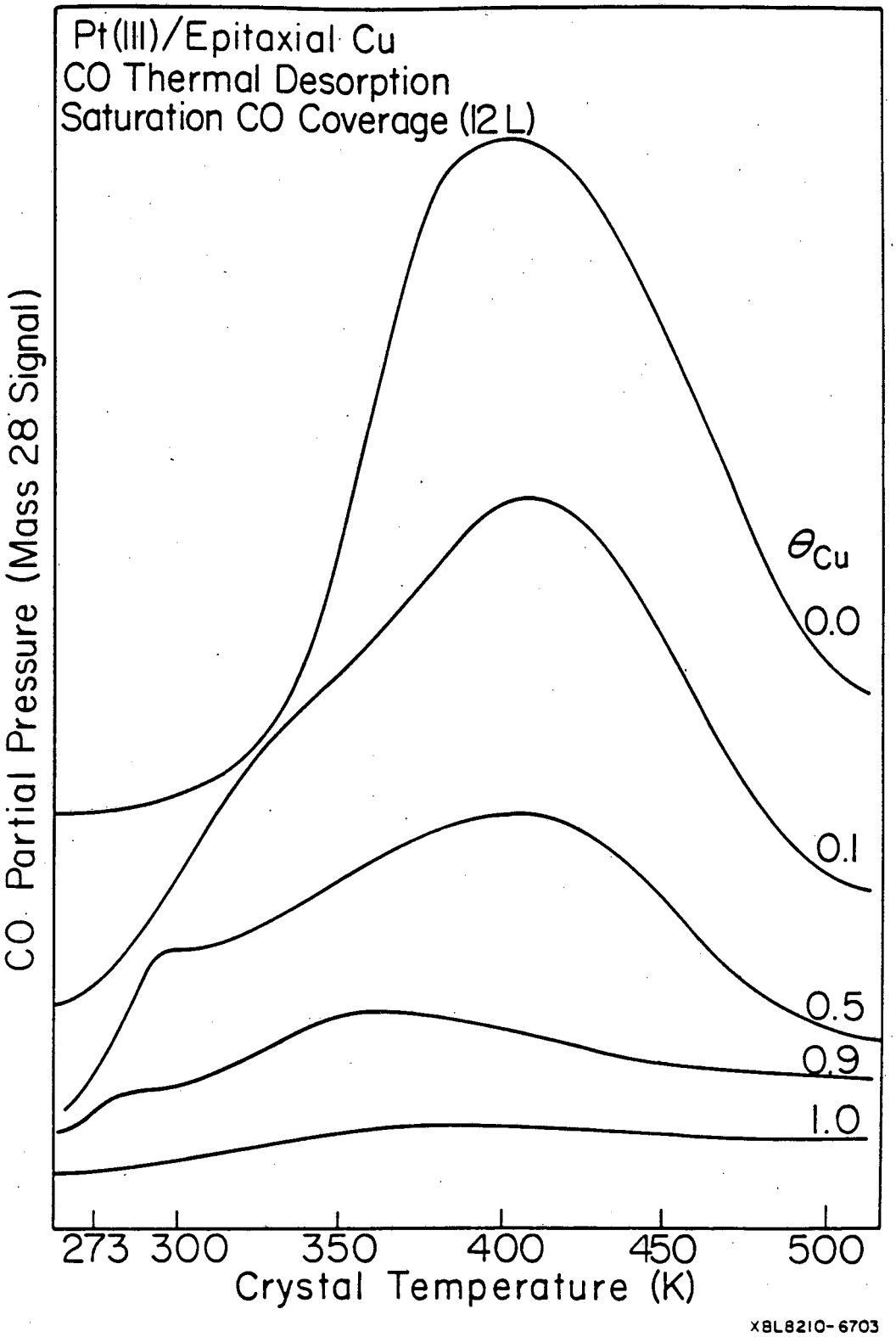

FIG. 3.3

CO thermal desorption spectra for the Pt(111) surface covered with varying amounts of copper, after a saturation exposure of 12 L CO.

this temperature, the CO adsorbed only on the platinum sites. The TDS was therefore representative of desorption from the platinum surface atoms. Fig. 3.4 shows a plot of the area under these curves, which was proportional to the amount of CO desorbed, versus the copper coverage. The amount of CO desorbed fell of linearly with copper coverage and leveled off at a copper coverage corresponding to the first break in the plot of the Auger signal versus copper coverage, which confirmed the assignment of one monolayer of copper to this coverage. The residual CO desorption at this and higher coverages was due to the desorption of CO from the platinum crystal edges (which were not masked or exposed to the copper flux) and from the tantalum support wires. The position (temperature) of the desorption peaks remained constant until high copper coverages. In addition to the main desorption peak, a low temperature shoulder appeared. The saturation coverage of CO on the Pt(111) surface at 250 K is 0.5 monolayers [3.9]. Since one complete monolayer of copper was required to block all CO adsorption sites, two copper atoms were required to block one CO adsorption site on the platinum surface.

The growth of copper on the Pt(553) surface, which is a stepped surface with terraces of (111) orientation, was somewhat different than the copper growth on the (111) surface of platinum. The Auger signal versus copper coverage plot for the surface is shown in Fig. 3.5. As was the case with the Pt(111) surface, the Pt-150 V signal dropped off

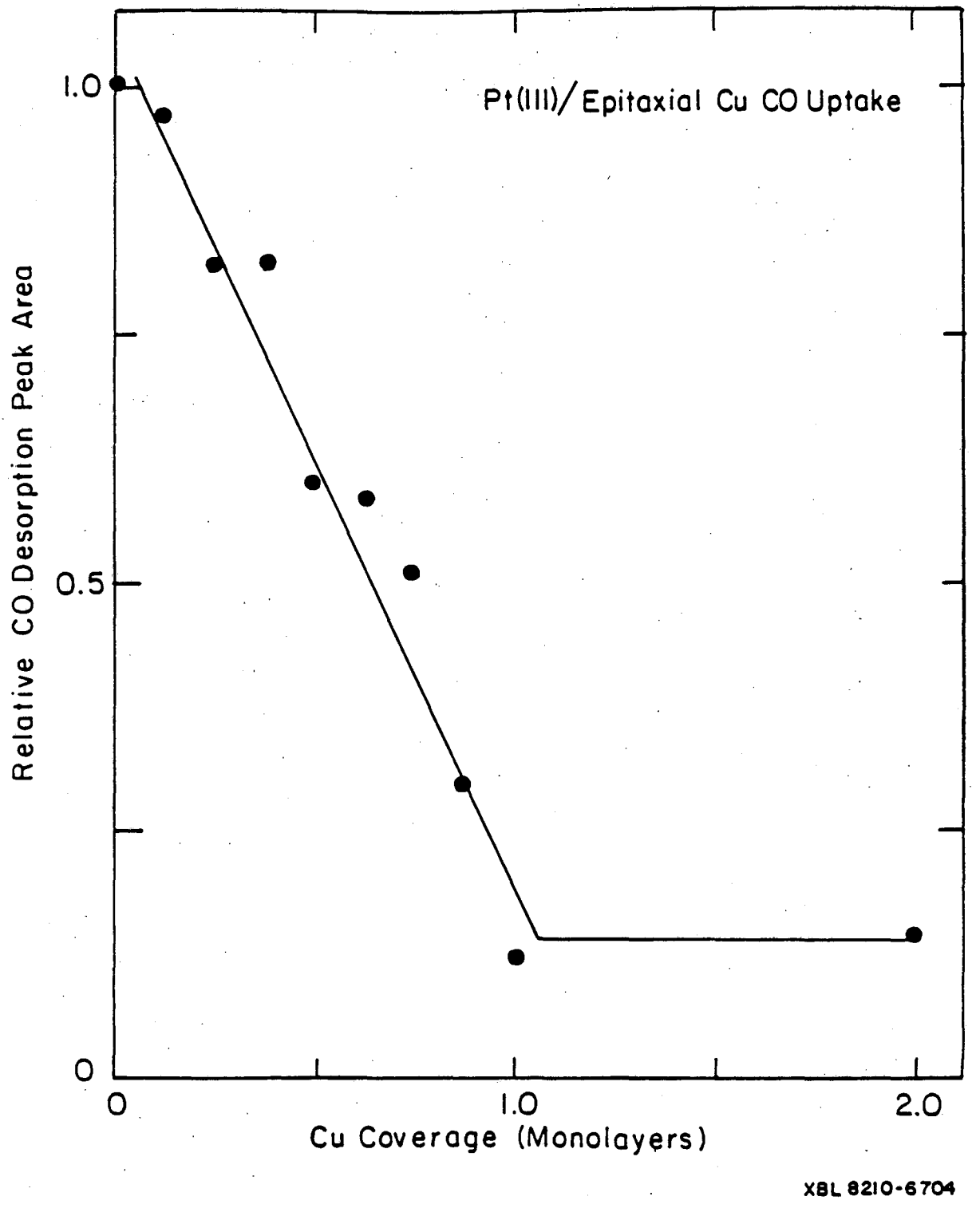

FIG. 3.4

Plot of the relative CO desorption yield from a Pt(111) surface with varying coverages of copper after a saturation exposure of CO, versus the copper coverage.

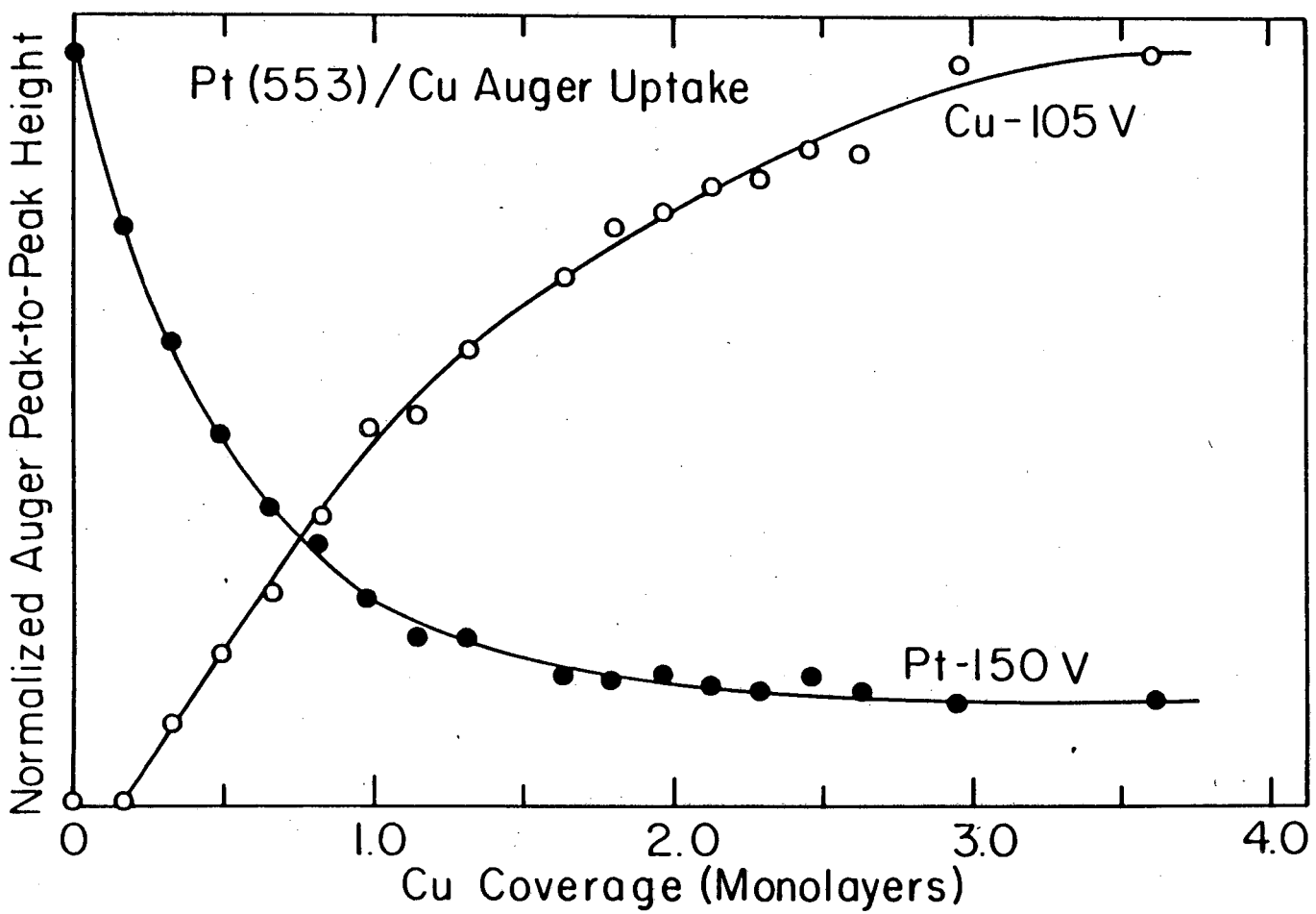

FIG. 3.5

Plot of the Auger peak-to-peak intensity of the Pt-150 V peak and the Cu-105 V peak versus copper coverage for copper deposited on the Pt(553) surface.

rapidly with copper coverage. Unlike the Pt(111) surface, however, the signal was not linear with copper coverage and there were no obvious breaks in the curve. It would seem from this behavior that the copper almost formed a complete monolayer, but before completion of that monolayer, a second began.

The thermal desorption spectra of carbon monoxide from the Pt(553) surface with various copper coverages (Fig. 3.6) showed a decrease in the CO desorption yield with increasing copper coverage. In Fig. 3.7 it can be seen that again the CO desorption yield decreased linearly with the copper coverage until coverages near one monolayer were reached. At near monolayer coverage the curve is rounded, again indicating that a second layer began to form before the first was completed. Closer inspection of Fig. 3.6 reveals a cause for this behavior. In the TDS of CO from the clean Pt(553) surface there was a peak around 400 K and a high temperature shoulder. The main desorption peak was due to desorption from the terrace sites and the high temperature shoulder was due to desorption from the step sites. As copper was deposited onto the surface the desorption of CO from the terrace sites was attenuated, whereas the desorption from the step sites remained unchanged. This trend continued until high copper coverages. This site selectivity of adsorbing copper atoms on the stepped surface was responsible for the growth mechanism observed. This behavior is illustrated more clearly in Fig. 3.8 where the TDS of CO from the clean

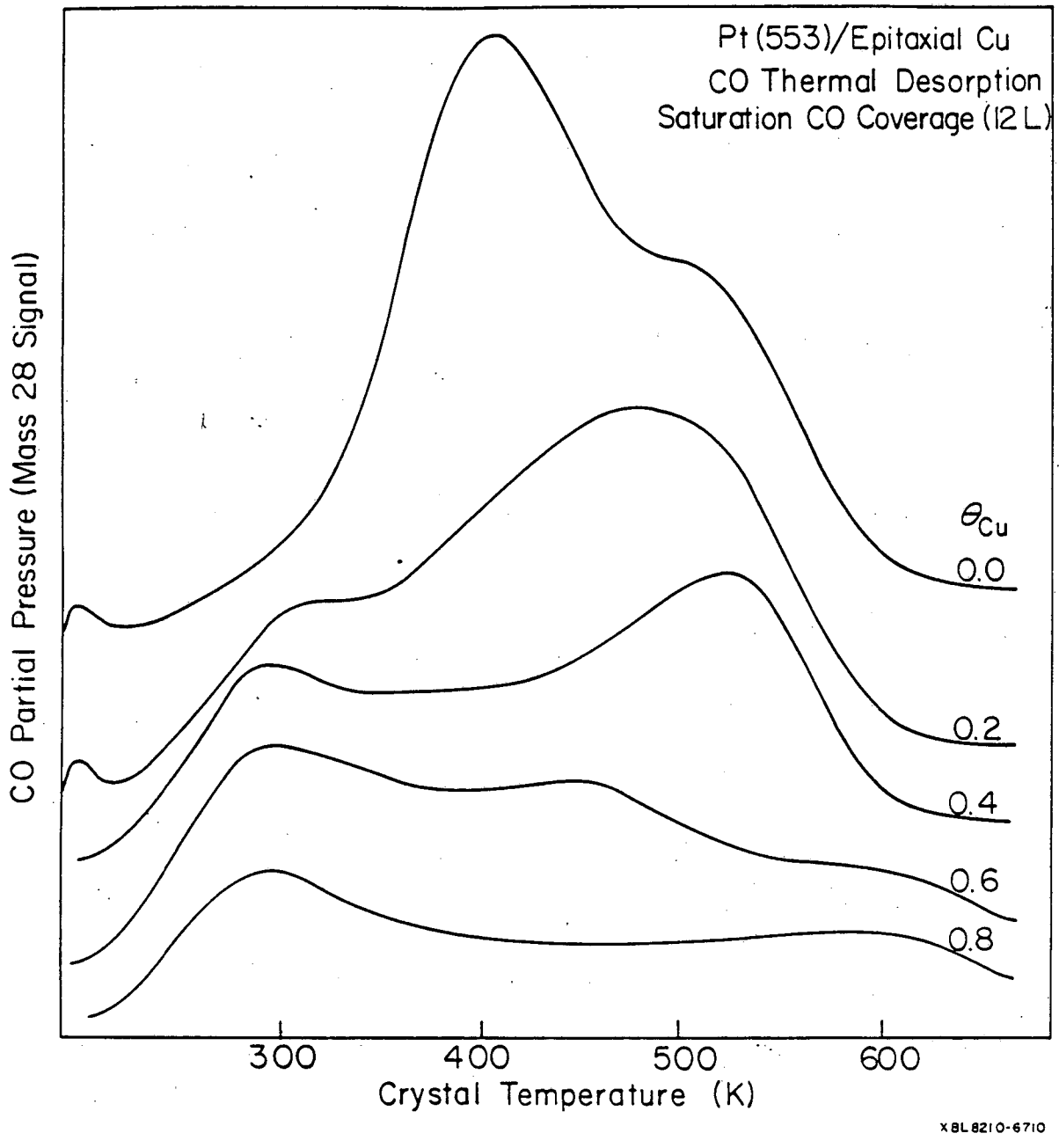

FIG. 3.6

CO thermal desorption spectra for the Pt(553) surface covered with varying amounts of copper, after a saturation exposure of 12 L CO.

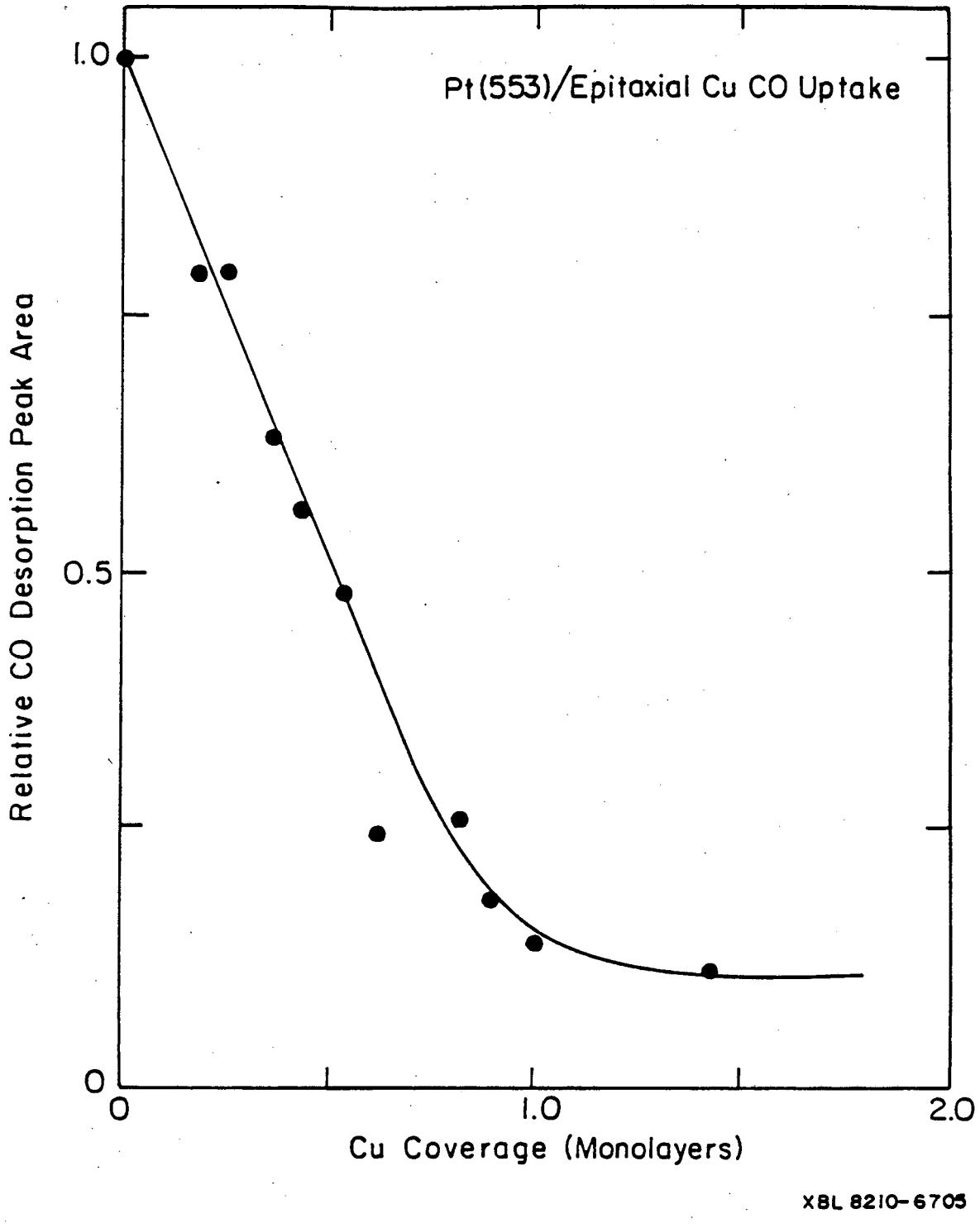

FIG. 3.7

Plot of the relative CO desorption yield from a Pt(553) surface with varying coverages of copper after a saturation exposure of CO, versus the copper coverage.

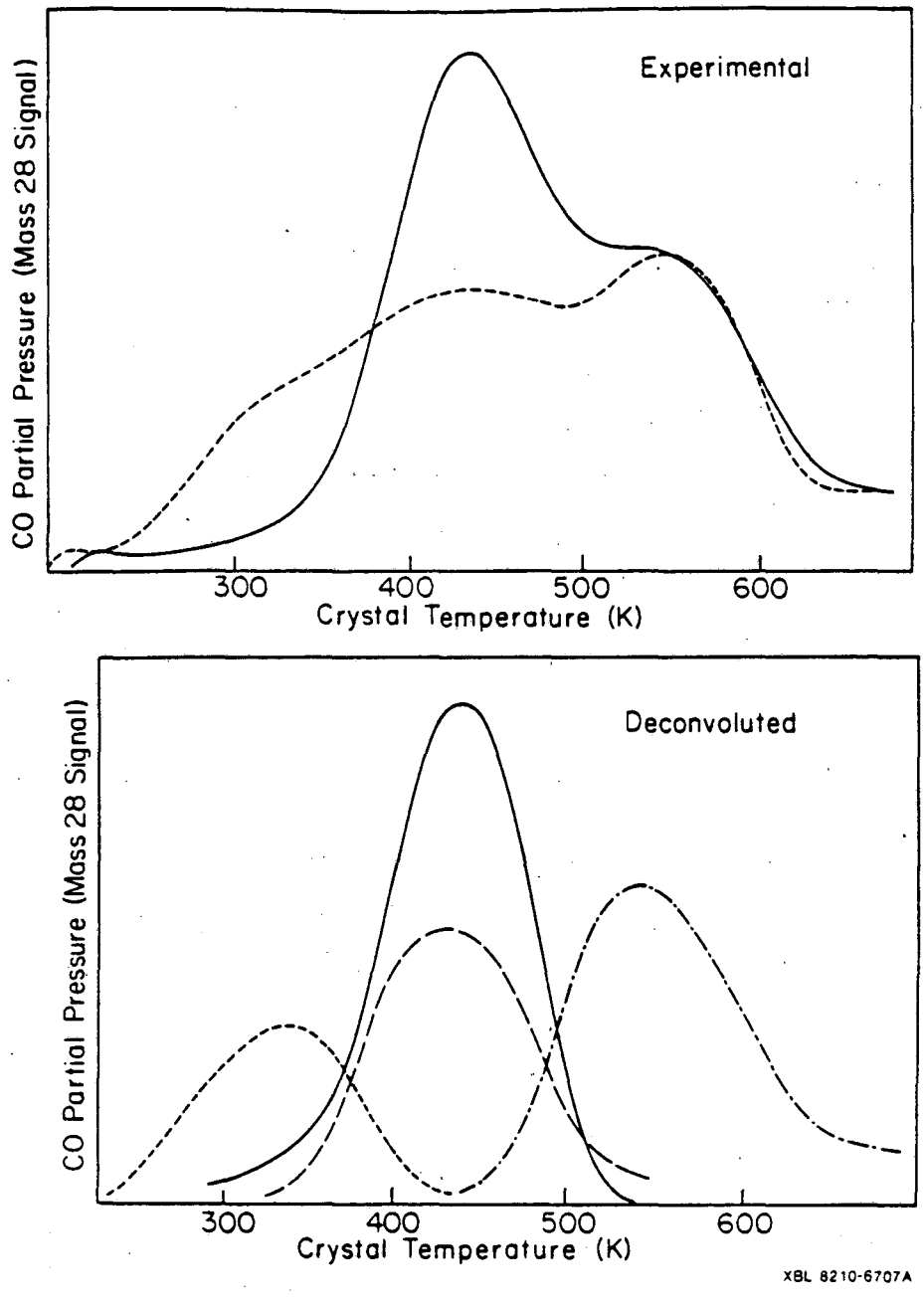

FIG. 3.8

Upper: CO thermal desorption from a clean Pt(553) surface (———) and a Pt(553) surface covered with 0.2 ML Cu (— — —). Lower: Same spectra deconvoluted into desorption from step sites (—·—·— with and without Cu), desorption from terrace sites (——— without Cu and— — with Cu) and desorption from sites neighboring a Cu atom (-----).

Pt(553) and the TDS of CO from the Pt(553) surface covered by 0.2 ML of copper are shown. The lower figure shows deconvoluted spectra. The TDS of CO from the clean Pt(553) surface was deconvoluted into two peaks, the lower temperature peak was due to desorption from the terrace sites and the other peak was due to desorption from the step sites. The TDS of CO from the Pt(553) surface covered with 0.2 ML of Cu was deconvoluted into three peaks, the two higher temperature peaks matching the deconvoluted spectrum of desorption from the Pt(553) surface, and a new, low temperature peak. The area under the high temperature peak was the same for both the clean and Cu covered surfaces, the desorption from the terrace sites was attenuated for the copper covered surface. The new, low temperature peak appeared in approximately the same position as the low temperature shoulder in the TDS of CO from the Cu covered Pt(111) surfaces and was due to desorption from Pt sites which neighbored a Cu atom.

The clean Pt(100) surface reconstructs, forming a hexagonal overlayer [3.10]. For copper coverages up to 0.5 ML the reconstruction remained. At copper coverages greater than this, the LEED spots corresponding to the reconstruction began to fade and were nearly gone by a copper coverage of 0.5 monolayers. By a copper coverage of 1 monolayer, a sharp pattern corresponding to a (1 X 1) surface structure was observed.

Fig. 3.9 shows the Auger signal of platinum and copper as a function of copper coverage on the Pt(100) surface. A modulation voltage of 6.4 volts peak-to-peak was used which resulted in poor resolution of the Cu-105 V peak at coverages below 0.5 monolayers. The Pt-237 V peak, however, linearly with increasing copper coverage and showed a change in slope at the completion of each monolayer of copper. The break in the Pt-237 V curve at a copper coverage of 0.5 monolayers corresponds to the removal of the reconstruction. This assignment of one monolayer was again checked by titrating the surface with CO. After the Cu-105 V peak was resolved, it increased linearly with increasing copper coverage with breaks in the curve at points which corresponded the the breaks in the Pt-237 V curve.

2. Diffusion of Surface Copper into the Pt(111) Substrate

When copper was deposited onto the platinum substrate and subsequently heated, the copper diffused into the platinum bulk. The extent of diffusion was monitored by following the Pt-105 V Auger signal with time with the platinum crystal held at a constant temperature. A direct proportionality of the Auger signal to the fraction of the surface with platinum atoms exposed was assumed. The change in the amount of copper at the surface with time was calculated from this data. The diffusion was studied at temperatures between 520 K and 580 K and was modeled as

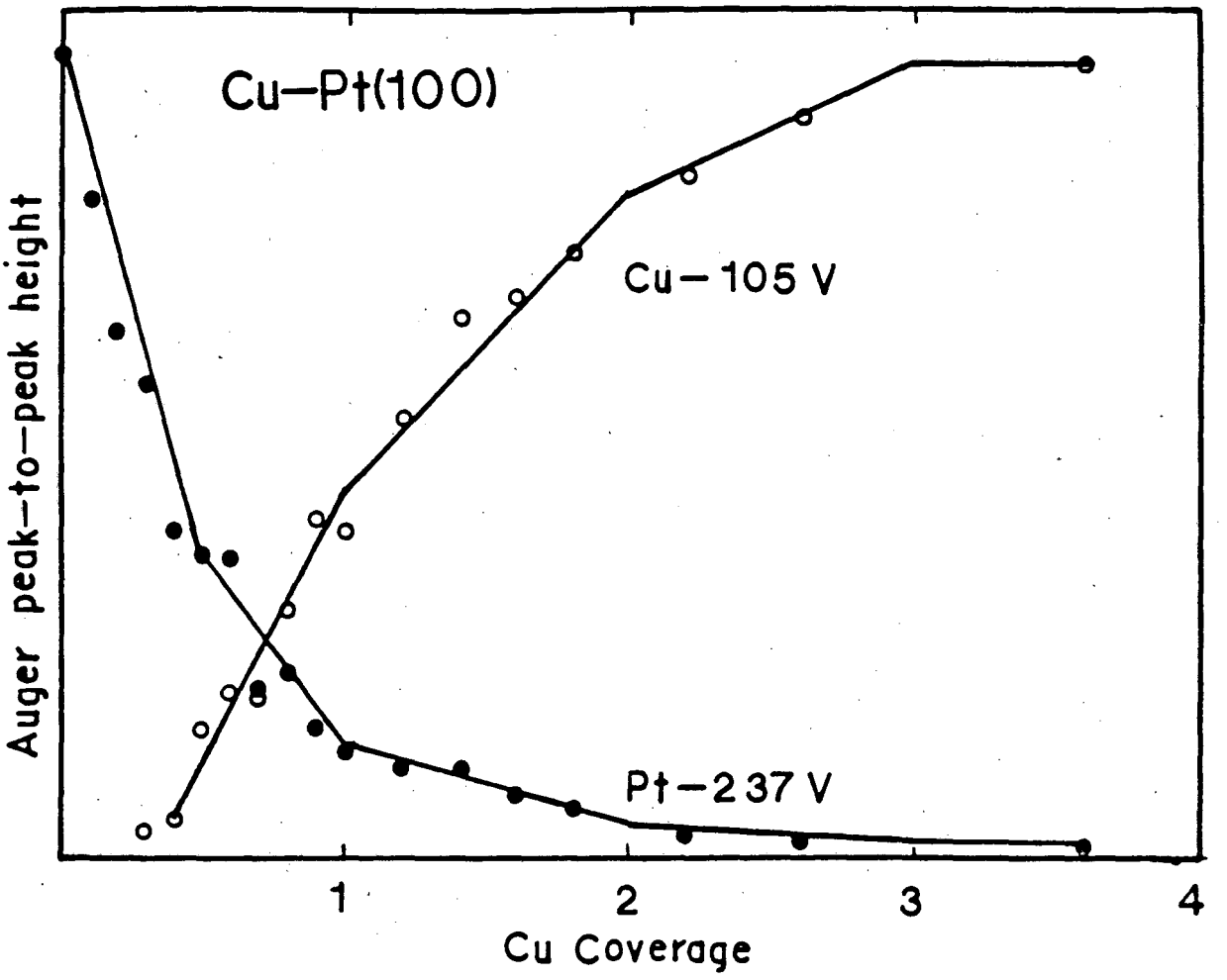

FIG. 3.9

Plot of the Auger peak-to-peak intensity of the Pt-237 V peak and the Cu-105 V peak versus copper coverage for copper deposited on the Pt(100) surface.

described by Schouten for the dissolution of carbon into nickel [3.11]. This model has also been successfully used to obtain the activation energy for the diffusion of rubidium into silver [3.12]. Briefly, the model utilized a constant plane source solution to Fick's second law for diffusion in one dimension. Integration of this solution with respect to time gave the total amount of copper diffused into the bulk and can be equated to the amount of copper depleted from the surface. It was found that :

$$\Delta\theta_{Cu} = -mt^{-1/2}$$

where m is a constant proportional to the square root of the diffusion coefficient, i.e. $D^{1/2}$. If Arrhenius type behavior is assumed, the activation energy for this process can be determined from the slope of the plot of ln(m) versus T^{-1}. Such a plot is shown in Fig. 3.10. A linear fit was obtained with an activation energy of 120 kJ/mole. This value falls between values for copper surface diffusion [3.13] and bulk diffusion for copper in a Cu/Pt alloy [3.14].

3. Cu/Pt Alloy Surfaces

TDS of CO from Cu/Pt(111) alloy surfaces are shown in Fig. 3.11. Two monolayers of copper were deposited onto the Pt(111) surface and then exposed to 12 L of CO. No desorption was seen since CO does not adsorb on copper at 250 K and 10^{-8} torr. The crystal was heated to 600 K during this thermal desorption. This temperature rise resulted in the

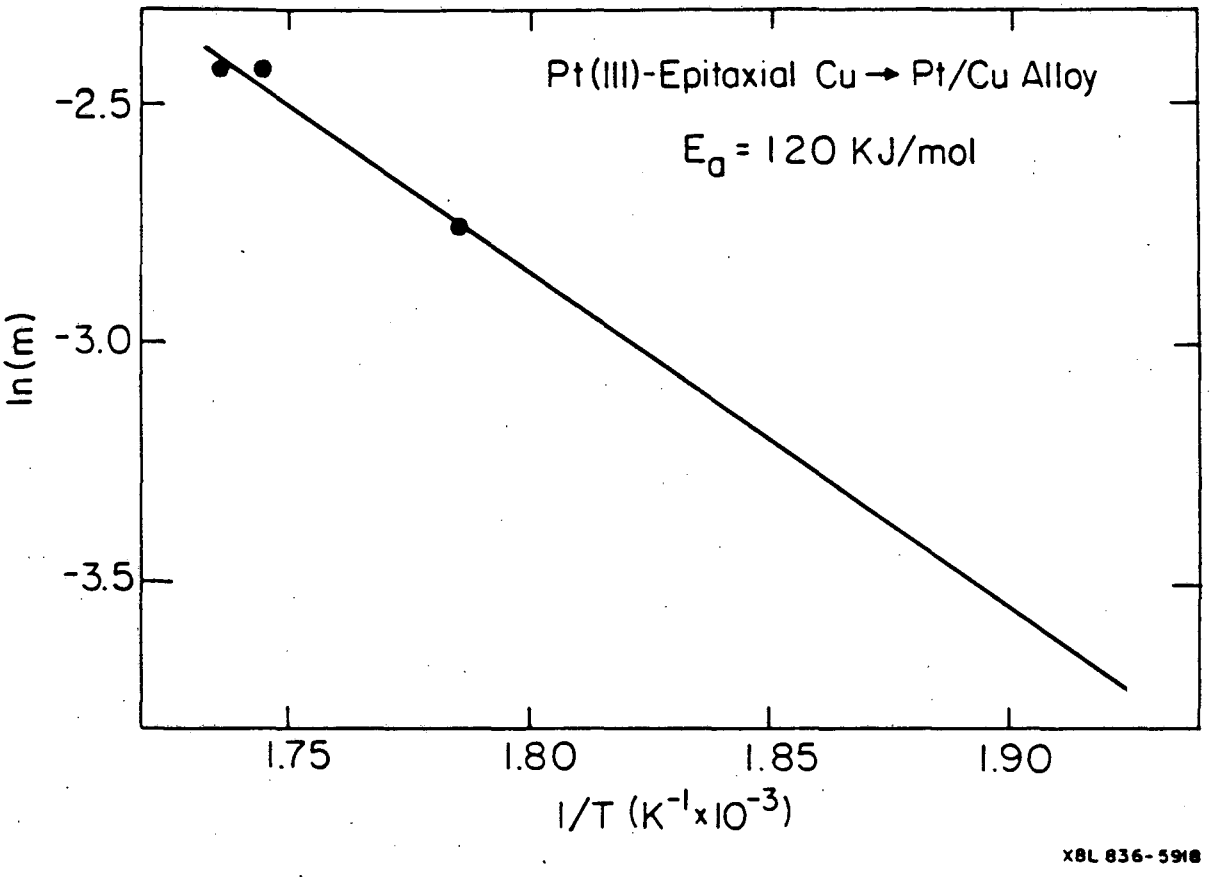

FIG. 3.10

Arrhenius plot for an estimation of the activation energy for surface-to-bulk diffusion of Cu on a Pt(111) surface.

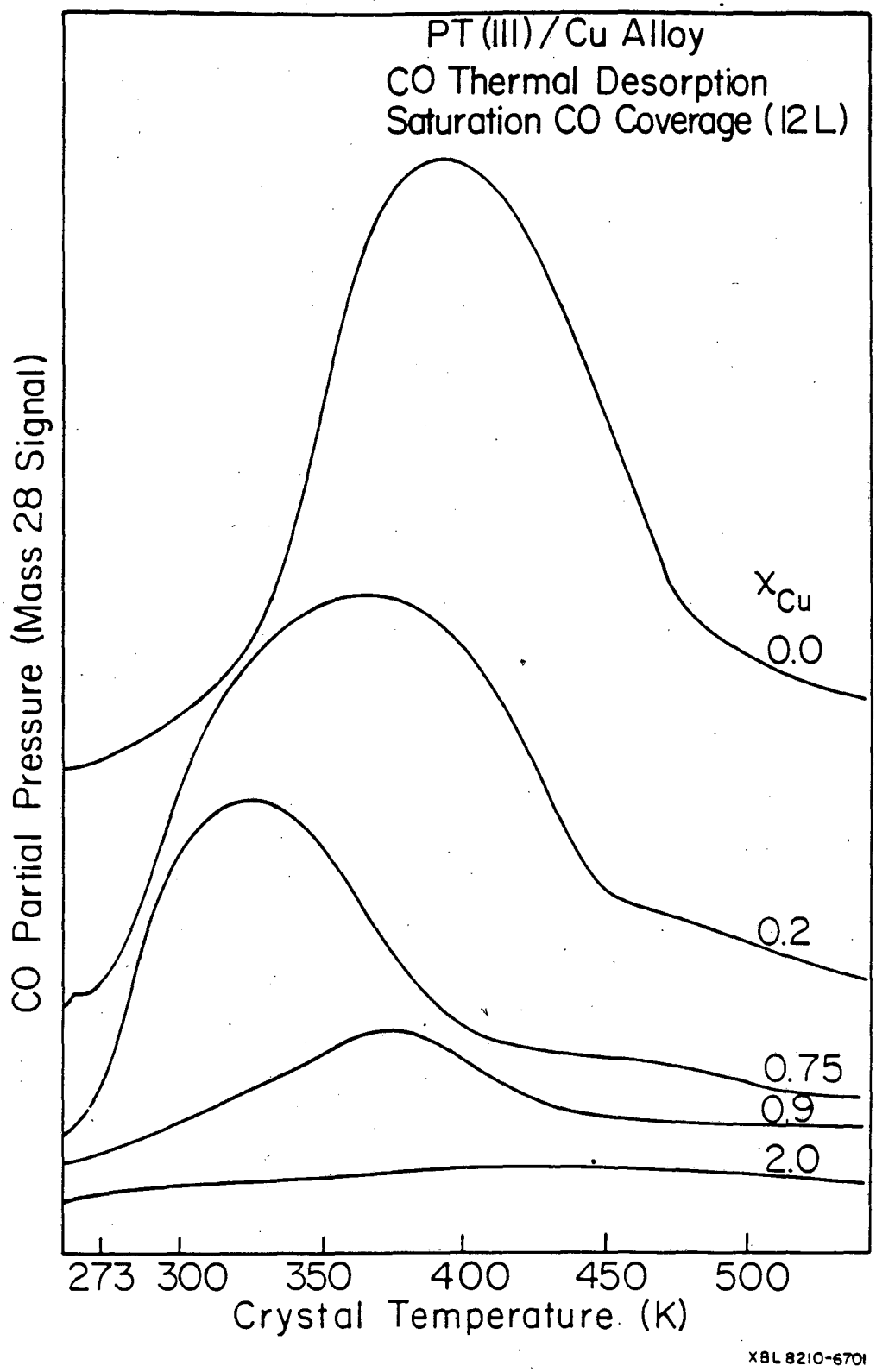

FIG. 3.11

CO thermal desorption spectra from Cu-Pt(111) alloy surfaces of varying composition after a saturation exposure of 12 L CO.

diffusion of some of the copper into the platinum bulk. This alloy surface was again exposed to 12 L of CO and the TDS showed a small broad peak. The shape and position of the desorption peak changed noticeably with each successive heat treatment until a surface composition of X_{Cu} = 0.85 was reached. (Surface composition was determined from the CO desorption yield from the CO saturated alloy surface relative to the yield from the CO saturated pore platinum surface. This point will be considered further in the discussion section.) This surface was relatively stable. The temperature at which the CO desorption rate from this alloy surface reached a maximum was shifted down ~100 K from the temperature of maximum CO desorption rate from a pure Pt(111) surface. The fraction of copper in the surface alloy could further be reduced by flashing the crystal to increasingly higher temperatures. Using the standard Redhead formula [3.15] and assuming a pre-exponential factor of 10^{13} s^{-1}, the temperature at which the rate of desorption reached a maximum could be used to calculate an energy of desorption. The energy of desorption of CO from the alloy surfaces is plotted versus the surface copper concentration in Fig. 3.12. The energy of desorption decreased smoothly with increasing copper concentration at the surface. In all cases only one desorption peak was observed with no shoulders present.

Usually, the repulsive interaction between adsorbed CO molecules results in a shift to higher temperature of the desorption peak as the CO coverage is decreased. This effect

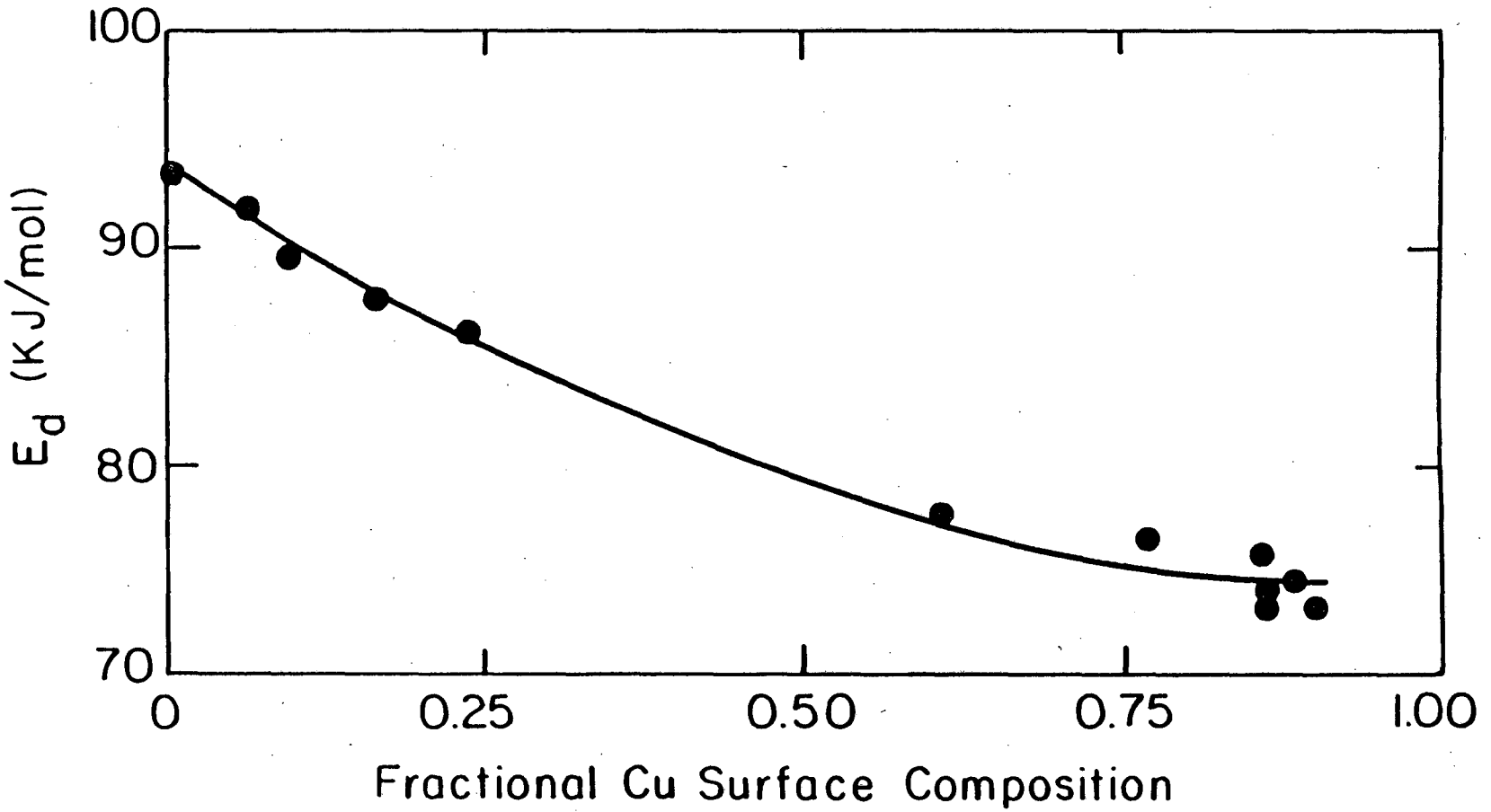

XBL836-5919

FIG. 3.12

Surface alloy composition dependence of the desorption energy of CO from Cu-Pt(111) alloy surfaces (saturation coverage of CO).

can be seen in Fig. 3.13, where a series of TDS of CO from a Pt(111) surface after various CO exposures is shown. Fig. 3.14 shows a similar series of TDS of CO from an alloy surface containing 76 % copper. The behavior observed for the alloy surfaces was the same as that for the pure platinum surface. In Fig. 3.15 the calculated energies of desorption of CO is plotted versus the amount of CO desorbed relative to the amount of CO desorbed from a CO saturated pure Pt(111) surface. The energy of desorption decreased with increasing CO coverage for all the surfaces. Extrapolation to an initial CO coverage of zero gives the CO desorption energy without any contribution from the CO intermolecular repulsions, i.e., a desorption energy which is dependent on only the Pt-CO bond strength. The energy of desorption from the alloy surface containing 76 % copper at an initial CO coverage of zero is 24 kJ/mole lower that the energy of desorption of CO from the pure platinum surface.

LEED results of the Cu-Pt(111) alloy surfaces showed the presence of a (2 X 2) surface structure at high copper concentrations. Ordering of these surface alloys was very difficult since energy added to the system to promote ordering also resulted in the diffusion of copper into the bulk due to the large concentration gradient at the surface. Generally, the LEED patterns for the Cu-Pt(111) surfaces indicated a (1 X 1) surface structure. The diffraction spots were broader and the background was more intense than the LEED pattern of the clean Pt(111) surface. The diffraction

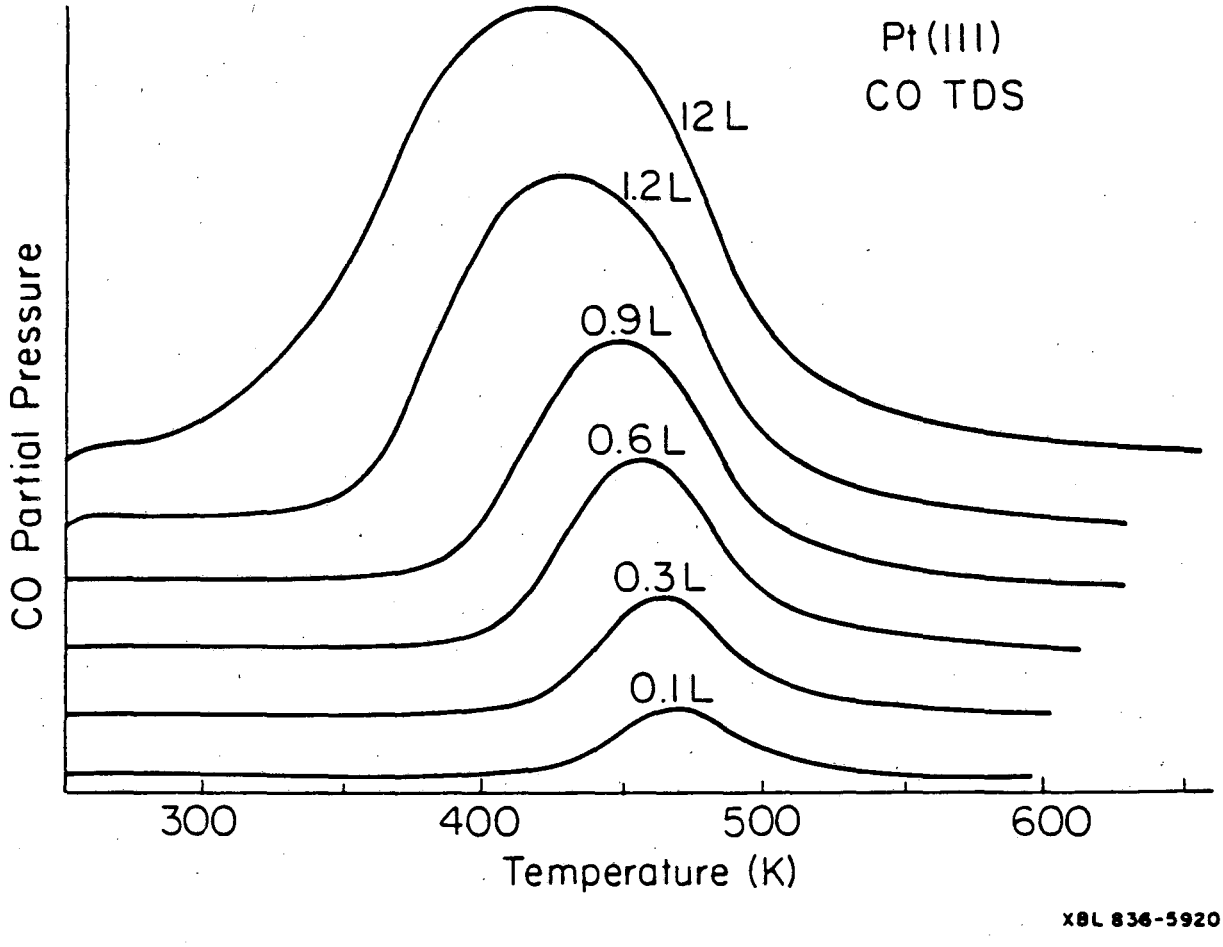

FIG. 3.13

CO thermal desorption spectra from a Pt(111) surface after various exposures of CO.

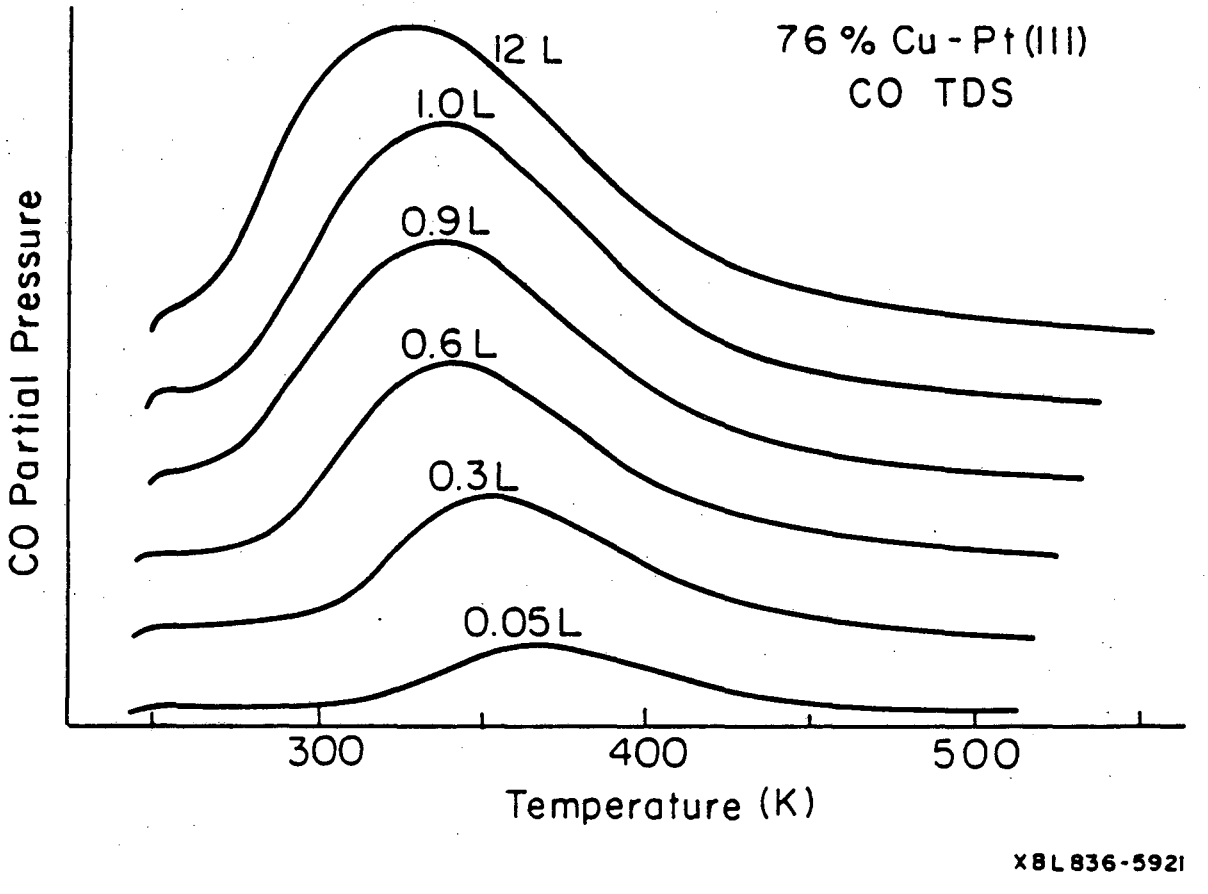

FIG. 3.14

CO thermal desorption spectra from a Cu-Pt(111) alloy surface with a copper atom fraction of 0.76 after various exposures of CO.

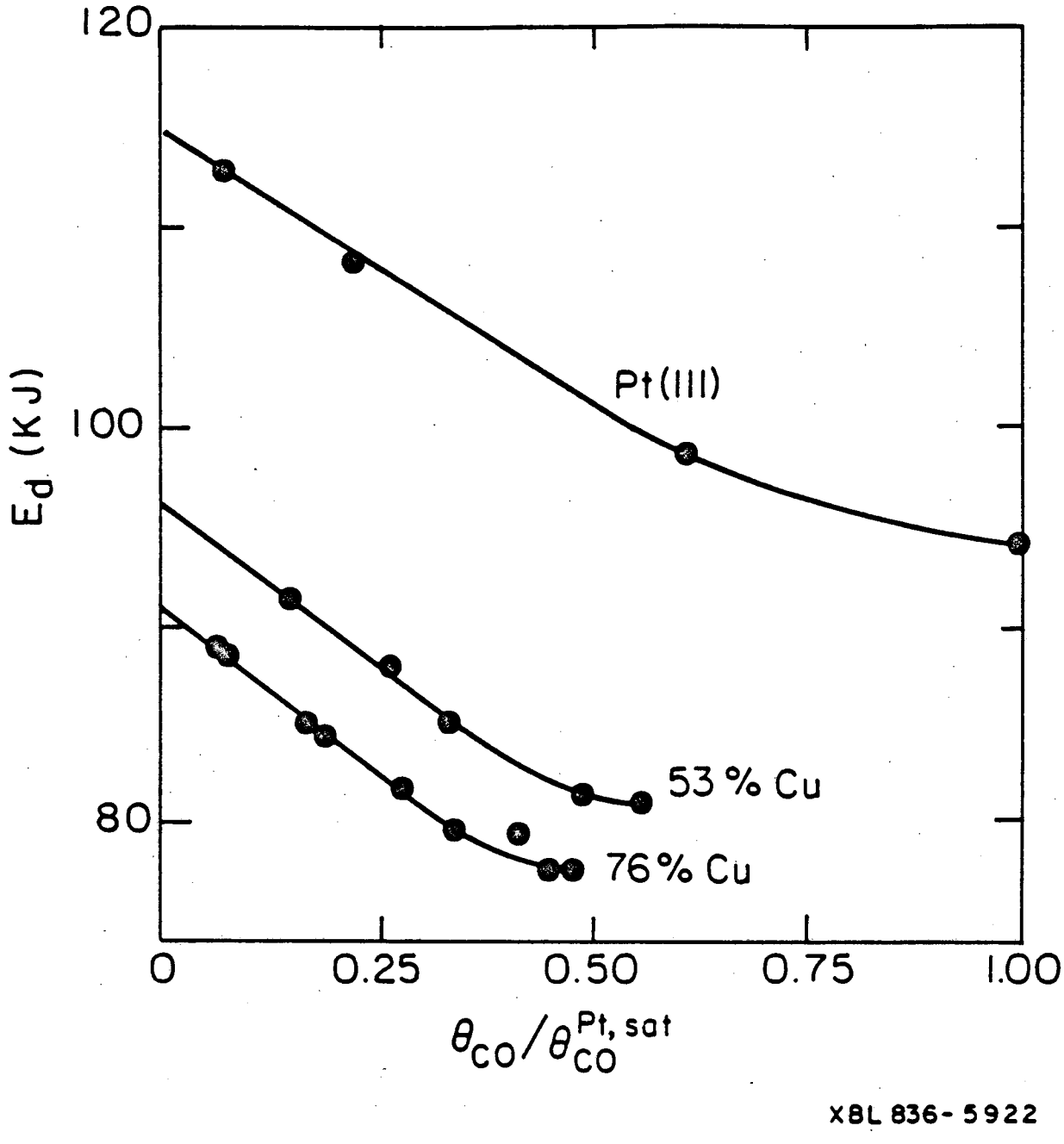

FIG. 3.15

A plot of the desorption energy of CO from a Pt(111) surface and two Cu-Pt(111) alloy surfaces versus the relative CO desorption yield.

spots sharpened and the background intensity decreased as the crystal was annealed.

The thermal desorption spectra of CO from the Cu-Pt(553) alloy surfaces are shown in Fig. 3.16. For high copper concentrations the only peak observed was the low temperature peak which was at the same temperature as the TDS peak for the (111) surface at high copper concentrations. As more copper was diffused into the platinum bulk, however, peaks at 410 K and 510 K began to appear and the intensity of the peak at 300 K decreased. By a copper concentration of 0.3 the peak at 300 K was nearly gone.

Thermal desorption spectra of CO from the Cu-Pt(100) alloy surfaces are shown in Fig. 3.17. The desorption peak for the clean Pt(100) surface had a maximum at 480 K which corresponds to a desorption energy of 117 kJ/mole. For the alloy surfaces with a high copper concentration the desorption maximum shifted down to 400 K, from which a desorption energy of 97 kJ/mole was calculated. This 20 kJ/mole decrease in the desorption energy of CO from the alloy surface with a high concentration of copper relative to the clean platinum surface was the same shift that was observed for the Cu-Pt(111) surfaces with a high concentration of copper.

As the copper was diffused into the platinum bulk a new peak at 360 K appeared, a desorption energy of 112 kJ/mole. In contrast to the (111) surfaces where only one desorption peak was observed at all concentrations, there were clearly

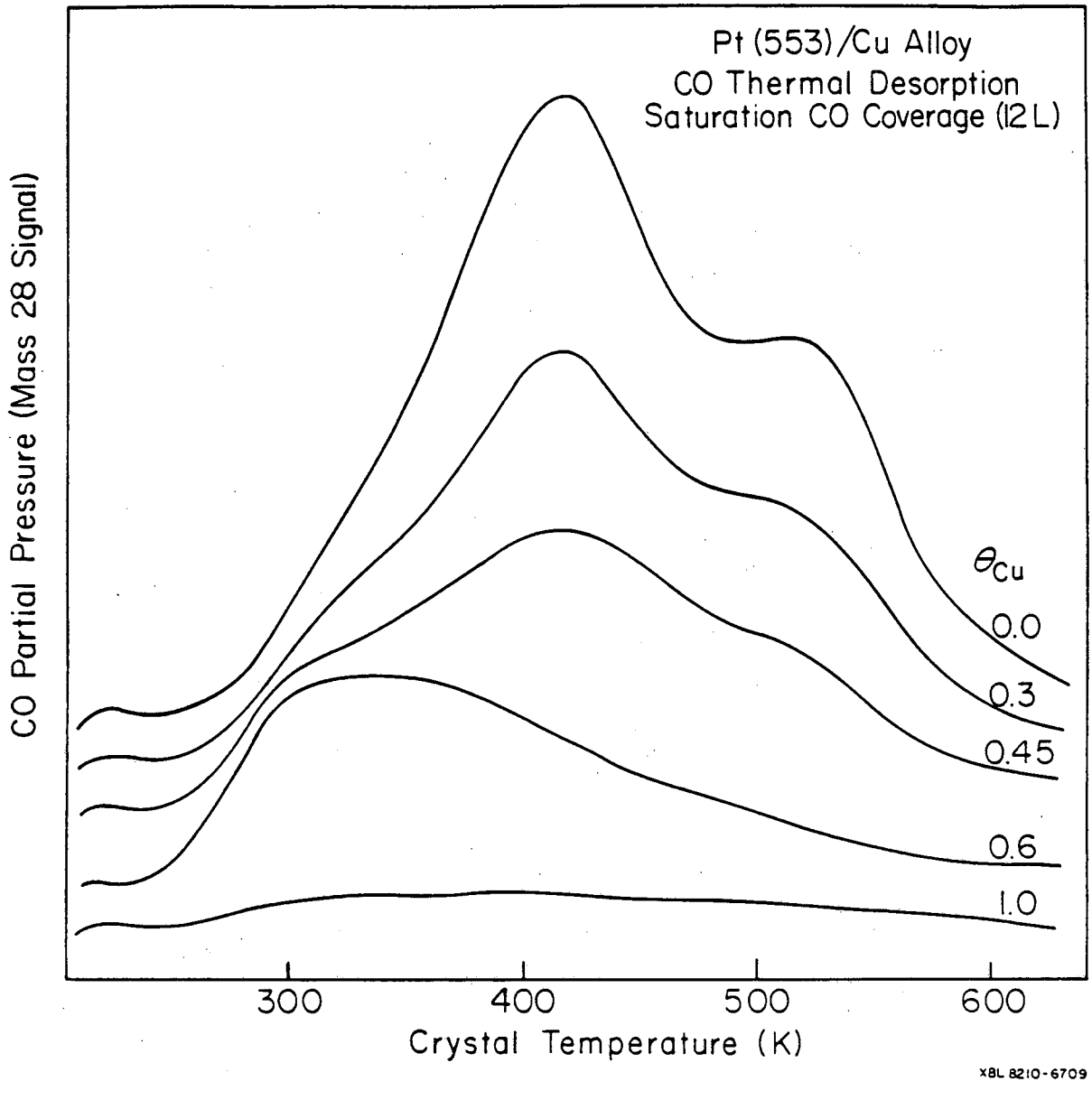

FIG. 3.16

CO thermal desorption spectra from Cu-Pt(553) alloy surfaces of varying composition after a saturation exposure of 12 L CO.

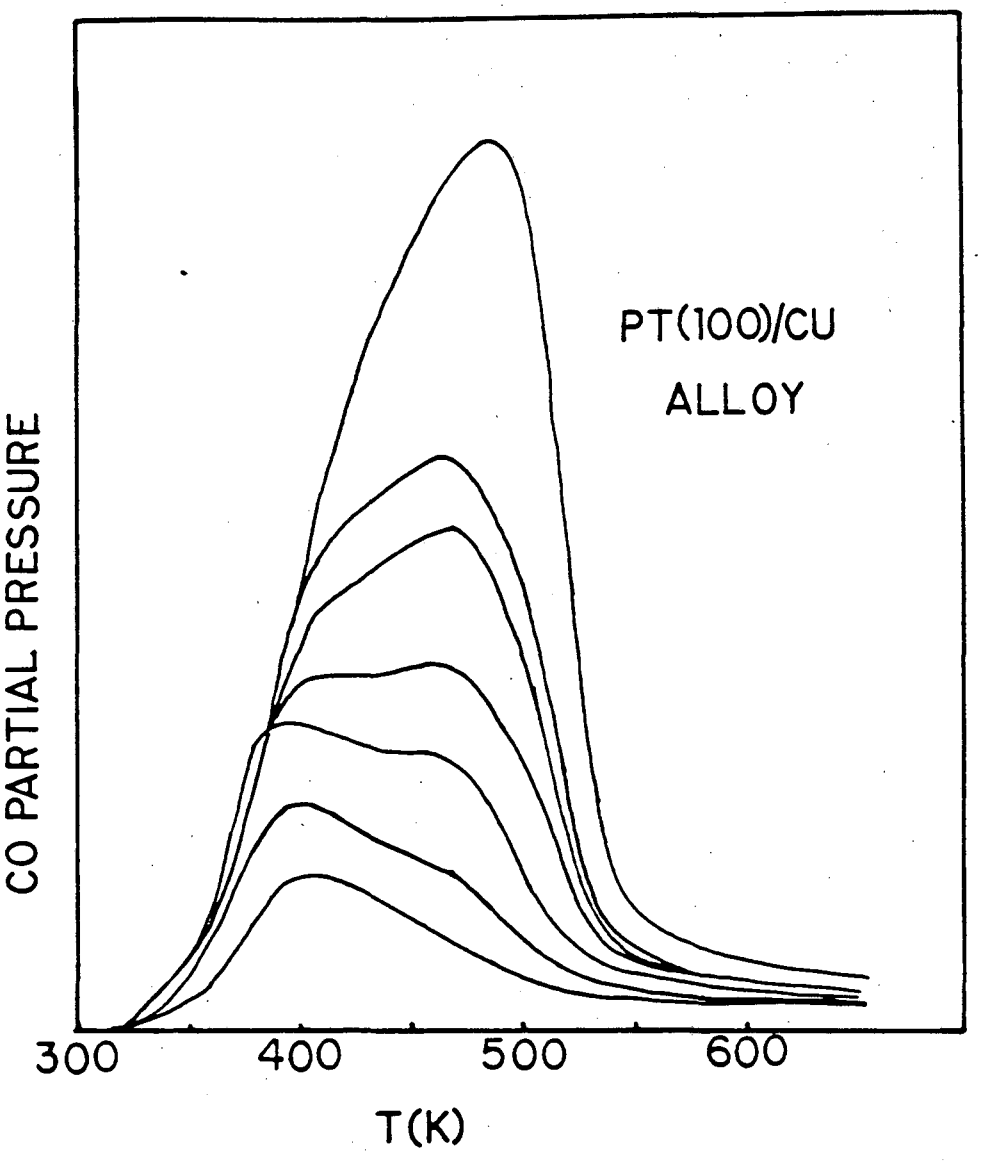

FIG. 3.17

CO thermal desorption spectra from Cu-Pt(100) alloy surfaces of varying composition after a saturation exposure of 12 L CO.

two desorption peaks present for the (100) surface over a wide range of concentrations. Also, as the copper concentration was decreased, the desorption peaks shifted to higher temperatures, similar to the behavior observed for the (111) alloy surfaces.

LEED results showed an ordered structure for the Cu-Pt(100) surface at high copper concentration which corresponded to a (2 X 2) surface structure. As was the case for the Cu-Pt(111) surfaces, the (100) alloy surfaces displayed a LEED pattern which corresponded to a (1 X 1) surface structure and the diffraction spots were broadened, but sharpened when the crystal was annealed. The diffraction pattern for the reconstructed surface began to appear at low copper concentrations and become more intense as a the copper concentration was decreased.

C. DISCUSSION

Copper growth on Pt(111) was seen to proceed by a layer-by-layer type growth mechanism. This was partly due to the lower surface free energy of copper, but also was the result of a relatively strong interaction between the copper and platinum. This favorable interaction would be expected since the bulk alloy has an exothermic heat of mixing [3.16]. The LEED results showed that copper, which has a bulk lattice constant that is 8 % smaller than platinum's, took on the platinum lattice spacing for the first few monolayers of copper, also indicating a strong interaction between the two metals. The sharpness of the LEED spots and low background intensity for copper coverages up to one monolayer of copper suggest that the copper grew in islands. If this was not the case and the copper atoms were randomly distributed across the platinum surface, the TDS of CO would have shown an increase in the temperature of the desorption peak with increasing copper coverage due to a separation of the CO molecules, which would have resulted in a decrease in the lateral repulsions between the adsorbed CO molecules. This increase in the temperature of the desorption peak was not observed. The position of the desorption peak remained constant until near monolayer coverages of copper. The new feature which did appear when copper was deposited was a low temperature shoulder. This was probably due to desorption of CO from the edges of the copper islands. It may also indicate some alloy formation, although this would be a minor

contribution since the rate of diffusion was negligible at 250 K, the temperature at which the copper was deposited. The TDS also showed a linear decrease in the CO desorption yield with increasing copper coverage and that two copper atoms were required to block one CO molecule, a behavior which requires island formation. The growth of copper on the Pt(100) surface appeared to be analogous to the growth of copper on the Pt(111) surface, although it was not studied in as much detail.

The Pt(553) surface is a stepped surface with terraces of (111) orientation, five atoms wide and steps of monotonic height. The behavior of copper of the terraces would be expected to be similar to that described for the Pt(111) surface and any differences in the behavior of the copper atoms on the surface as a whole to be induced by the steps. As was seen, the plot of the Auger signal versus copper coverage for this surface indicated that the growth mechanism was not layer-by-layer. The sharp decrease in the Pt-150 V signal with increasing copper coverage and the linear decrease in the desorption yield of CO to near monolayer coverages of copper suggest that the first monolayer was nearly completed before a second began. The TDS of CO from the Pt(553) surface shows that copper preferentially adsorbed at sites away from the step site where CO adsorbed. Since it would be energetically favorable for the copper atoms to increase their coordination with the platinum, it seems reasonable that the copper growth began at the bottom of the

steps and moved out onto the terraces. The energetically least favorable site would be at the top of a step where the coordination with the platinum atoms is low. The energy of adsorption of copper at the top of a step appears to be close to the energy of adsorption of copper on the top of the first layer of copper. Thus, the second monolayer began to form before the first was complete. These results would suggest that the CO which desorbed from the step and gave a high temperature shoulder in the TDS was adsorbed at the top of the step and that the presence of a copper atom at the bottom of the step had little effect on the bonding of that CO molecule to the platinum.

The low temperature shoulder in the TDS of CO was much more pronounced for the Pt(553) with sub-monolayer copper coverages than for the Pt(111) with sub-monolayer copper coverages and the desorption yield was nearly constant over a broad range of copper coverages. This behavior can be rationalized in the following way. The copper was preferentially adsorbed at the bottom of the platinum steps creating long, thin islands of copper. The desorption of CO from the edges of these islands gave the low temperature shoulder in the TDS. As more copper was deposited, it added to the edge of the copper islands already formed, and resulted in a nearly constant concentration of copper island edge sites.

The TDS of CO from the alloy surfaces showed a significant decrease in the temperature of the desorption

peaks. This shift of the CO desorption peak is indicative of a decrease in the the energy of desorption of CO from the platinum at the surface of the Cu/Pt alloys brought about by a copper induced electronic change in the platinum. UPS studies carried out by Shek et al. [3.17] on Cu/Pt alloys indicated an electronic modification of the constituents of the alloy. Using 150 eV radiation from a synchrotron, an energy at which platinum has a Cooper minimum, they were able to selectively study the electronic structure of copper in the alloy. An example of the spectra obtained in this study is shown in Fig. 3.18. The increase in the photoelectron emission between E_F and -1.4 eV from the alloy relative to the Cu single crystal surface was attributed to significant Cu3d-Pt5d hybridization. XPS studies have shown that there is little or no charge transferred between the copper and platinum atoms when alloyed [3.18]. This would imply that the weakening of the CO-Pt bond was due to a rehybridization of the platinum orbitals. Infrared spectroscopic studies of CO adsorbed on Cu/Pt alloy surfaces [3.19] showed that a dependence of the C-O stretching frequency on the copper concentration could be correlated with changes in the dipole-dipole interactions of the adsorbed molecules. This would indicate that alloying platinum with copper caused a weakening of the Pt-CO 5σ bond without effecting the back donation into the $2\pi^*$ orbital. High resolution electron energy loss spectroscopy (HREELS) studies would help clarify the nature of the Pt-CO at the alloy surface.

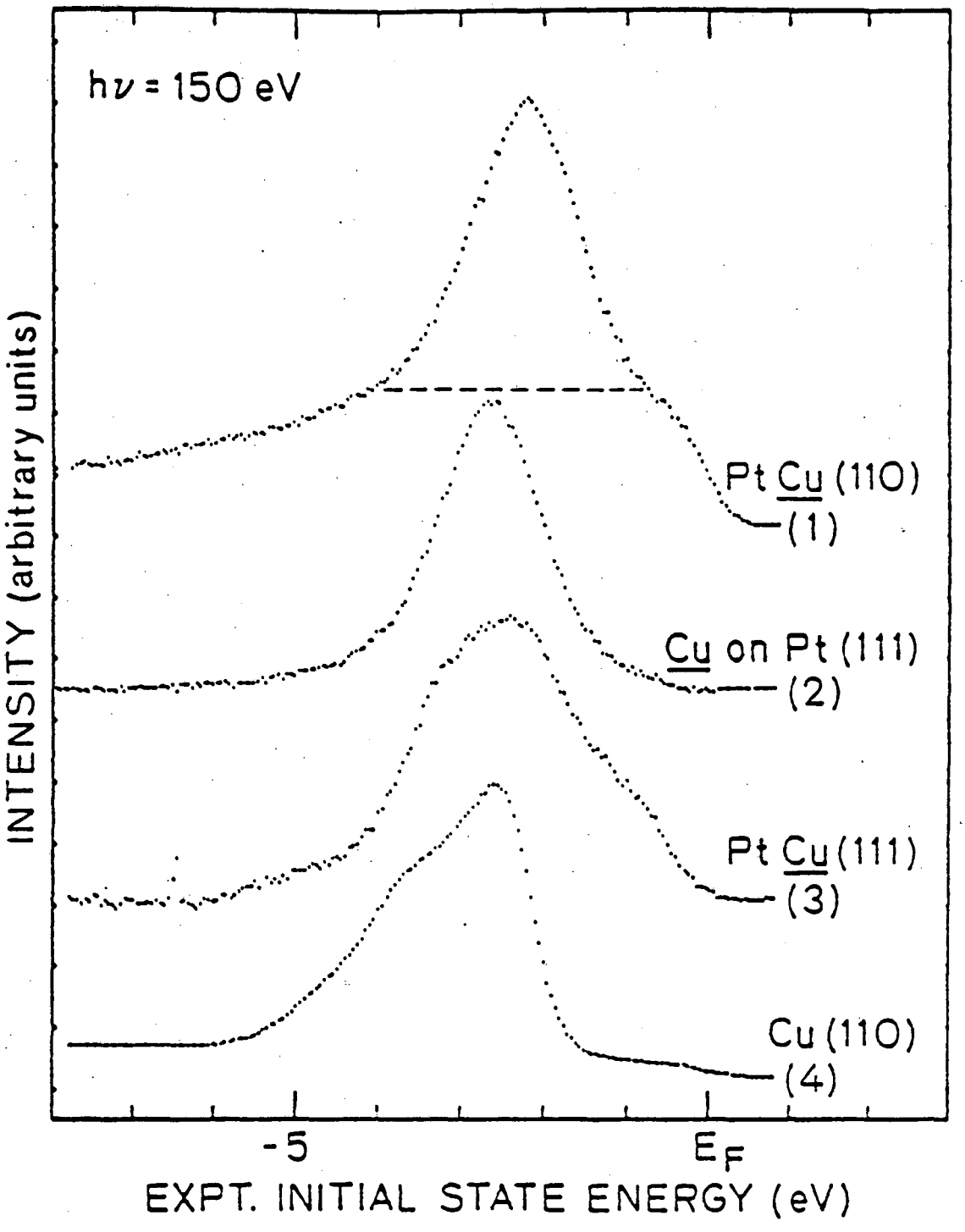

FIG. 3.18

UPS spectra taken at a photon energy of 150 eV. a) Cu-Pt(110) alloy with a copper surface atom fraction of 0.059. b) Difference spectrum between Pt(111) covered with 0.2 ML Cu and pure Pt(111). c) Difference between Cu-Pt(111) alloy with a copper surface atom fraction of 0.077 and pure Pt(111). d) Cu(110) (from Ref. 3.17)

There are several other factors which could possibly result in the observed shift of the CO desorption peak upon alloying platinum with copper. These are : 1) an increase in the pre-exponential factor; 2) CO adsorption on mixed sites; 3) closer packing of the CO molecules on the alloy surface. Several orders of magnitude increase in the pre-exponential factor would be needed to cause the observed 100 K decrease in the position of the CO desorption peak. This could be explained by a decrease in the mobility of the CO adsorbed on the alloy surface and/or an increase in the mobility of the transition state. As has been discussed by Weinberg [3.20], however, the decrease in the temperature of the desorption peak would be accompanied by a narrowing of the desorption peak if the shift was caused by a change in the pre-exponential factor. A decrease in the desorption energy would also result in a narrowing of the TDS peak, but to a lesser degree, as was discussed in chapter 2 section 3.C. This narrowing was not observed, arguing against any significant change in the pre-exponential factor. Mixed adsorption sites have been proposed for several alloy surfaces [3.13]. It has been argued that desorption from a site consisting of two different metal atoms would have a desorption energy somewhere between the desorption energies for the pure component surfaces. If mixed sites were responsible for the decrease in the desorption energy of CO from the alloy surface, two desorption peaks would be present at low copper concentrations. One peak due to desorption

from mixed sites and another due to desorption from pure platinum sites. Two desorption peaks were never observed in the TDS of CO from the (111) alloy surfaces. As can be seen in Fig. 3.12, the energy of desorption decreased smoothly with increasing copper concentration. Another possibility is that the CO molecules were being forced closer together by the copper atoms. This would result in a stronger intermolecular repulsion and a shift of the desorption peak to a lower temperature. In this case extrapolation of the desorption energy to zero coverage would give the same desorption energy for CO from the alloys as from pure platinum. Inspection of Fig. 3.15 shows that this was not the case.

The magnitude of decrease in desorption energy of CO from the Pt(100) when alloyed with copper was the same as that observed for the Pt(111) surface. There were however, generally two peaks present in the thermal desorption spectra of CO from the (100) alloy surfaces.

This electronic effect appears to be a rather short range effect. Copper at the (111) alloy surface was always highly dispersed which resulted in a rather smooth shift in the CO desorption peak to higher temperatures as the copper concentration was decreased. The copper dispersion on the (100) alloy surfaces was not as high which was manifest in the appearance of two CO desorption peaks over a broad range of copper concentrations. The poorest copper dispersion was on the stepped (553) alloy surfaces were shifts in the

desorption peaks were observed for high copper concentrations only.

Bulk Cu/Pt alloys form several ordered structures at temperatures below 1100 K [3.21]. It seems likely that the surfaces of these alloys would also be ordered. Only one ordered structure was observed by LEED. This pattern corresponded to a (2 X 2) structure and was seen for a high concentration of copper at the surface. The structure of Cu_3Pt is essentially fcc with copper at the faces and platinum at the corners. The (111) face of this structure would produce a (2 X 2) LEED pattern having each platinum atom completely surrounded by copper atoms. The (100) face of the Cu_3Pt structure would also produce a (2 X 2) structure, again with the copper atoms completely surrounding the platinum atoms. This was the only ordered alloy surface structure observed by LEED for the (100) alloy surfaces.

In determining the surface concentrations of the alloy with CO thermal desorption yields, the ordering of the alloy surface can be important. CO adsorbs on the clean Pt(111) surface in a one-to-two ratio (one CO molecule per two platinum atoms). On a surface with isolated platinum atoms, however, the CO would be able to adsorb in a one-to-one ratio. The solid line in Fig. 3.19 shows the relationship between the CO desorption yield from an alloy surface saturated with CO and the copper concentration at the surface of the alloy. At copper concentrations $\geq$ 75 % the CO-to-platinum ratio is one. At copper concentrations $\leq$ 25 % the

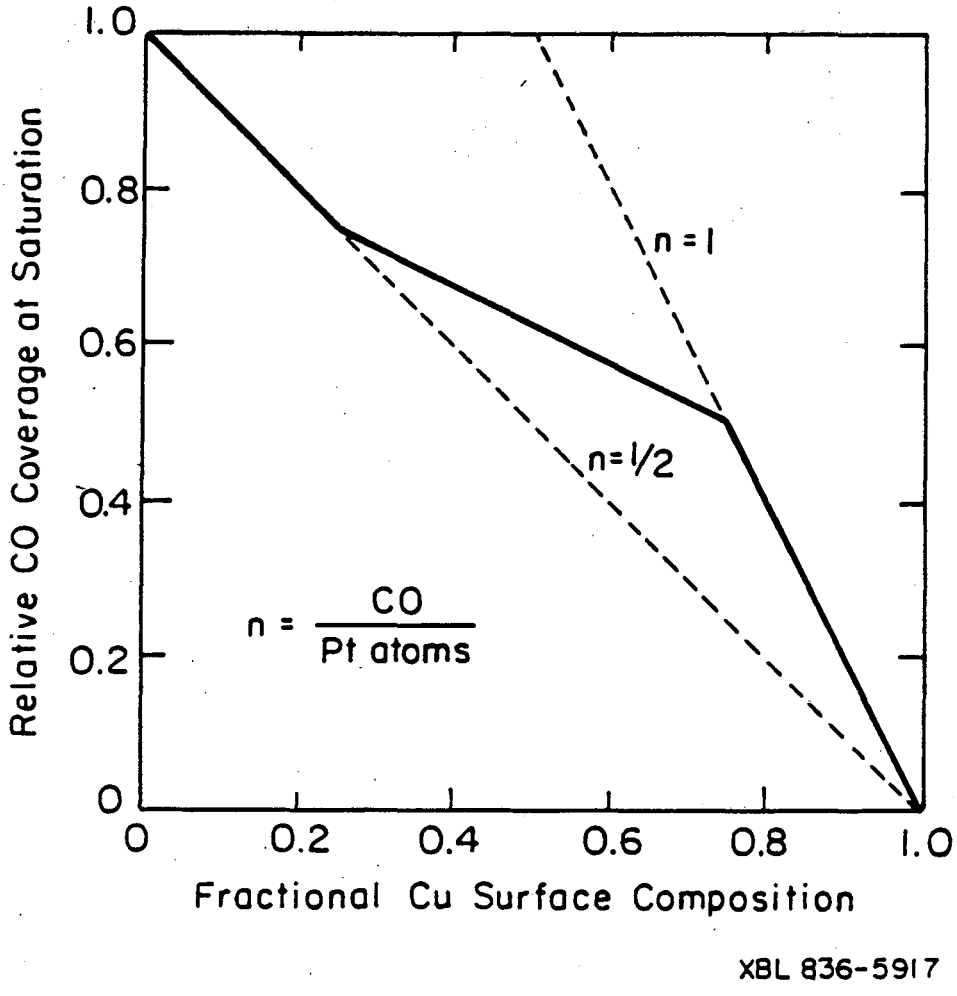

FIG. 3.19

Plot of the desorption yield of CO from a Cu-Pt(111) alloy surface after a saturation exposure of CO versus the copper surface atom fraction.

ratio is 1/2. Until further information is available on the ordering at intermediate concentrations, a linear transition between the conditions at the two extremes will be assumed.

D. CONCLUSIONS

1) Copper grew in (1 X 1) islands via a layer-by-layer mechanism on the Pt(111) and Pt(100) surfaces. On the stepped Pt(553) surface, copper adsorbed preferentially at the bottom of a step. This preferential adsorption resulted in a slight disturbance of the layer-by-layer growth.

2) The activation energy for the diffusion of surface copper into the Pt(111) substrate was found to be 28.7 kcal/mol.

3) Ordered surface alloys with a (2 X 2) structure were observed for the Cu-Pt(111) and Cu-Pt(100) surfaces. These ordered surfaces were difficult to prepare, however, and the alloy surface generally had a (1 X 1) structure.

4) Copper, when alloyed with platinum, modified the electronic structure of platinum. This modification was manifest in a reduction of the CO desorption energy of up to 4.8 kcal/mol.

REFERENCES

3.1) H.C. de Jongste, V. Ponec and F.G. Gault, J. Catal. 63 (1980) 395.

3.2) H.C. de Jongste, F.J. Kuijers, and V. Ponec, Proc. 6th Int. Congress Catal. (1976) 915.

3.3) H.C. de Jongste and V. Ponec, J. Catal. 63 (1980) 385.

3.4) C.E. Smith, J.P Biberian and G.A. Somorjai, J. Catal. 57 (1979) 426.

3.5) H.H. Brongersma, M.J. Sparnaay and T.M. Buck, Surface Sci. 71 (1978) 657.

3.6) G.E. Rhead, J. Vac. Sci. Technol. 13 (1976) 603.

3.7) M.T. Paffett, C.T. Campbell, T.N. Taylor and S. Srinivasan, Surface Sci. 154 (1985) 284.

3.8) E. Bauer, Surface Sci. 7 (1967) 351.

3.9) P.R. Norton, J.A. Davies and T.E. Jackman, Surface Sci. 122 (1982) L593.

3.10) M.A. Van Hove, R.J. Koestner, J.P. Biberian, L.L Kesmodel, I. Bartos and G.A. Somorjai, Surface Sci. 103 (1981) 218.

3.11) F.C. Schouten, E. TeBrake, O.L.J. Grijzeman and G.A. Bootsma, Surface Sci. 74 (1978) 1.

3.12) N.D. Spencer and R.M. Lambert, Surface Sci. 104 (1981) 63.

3.13) K.Y. Yu, D.T. Ling and W.E. Spicer, J. Catal. 44 (1976) 373.

3.14) J. Askill, "Tracer Diffusion Data for Metals, Alloys, and Simple Oxides", IFI/Plenum (1970) 59.

3.15) P. Redhead, Vacuum 12 (1962) 203.

3.16) F. Weibke and H.Matthes, Z. Elekrochem. 47 (1941) 421.

3.17) M.L. Shek, P.M. Stefan, D.L. Wiessman-Wenocur, B.B. Pate, I. Lindau and W.E. Spicer, J. Vac Sci. Technol. 18 (1981) 533.

3.18) G.G. Kleiman, V.S. Sundaron, J.D. Rogers and M.B. de Moraes, Phys. Rev B 23 (1981) 3177.

3.19) F.J.C.M. Toolenaar, D. Reinalda and V.Ponec, J. Catal. 64 (1980) 110.

3.20) C.M. Chan, R. Aris and W.H. Weinberg, Appl. Surface Sci. 1 (1978) 360.

3.21) A. Schneider and U. Esch, Z. Elektrochem. 50 (1944) 290.

CHAPTER FOUR : XPS AND UPS OF THE Au/Pt SYSTEM

A. INTRODUCTION

Materials composed of two metals, such as epitaxial systems and binary alloys, are of great importance in many technologies. Epitaxial systems, composed of one metal deposited on the surface of another metal, have been used as passivation coatings which are resistant to corrosion or radiation damage. Sometimes they exhibit unique magnetic and catalytic behavior not observed for the individual components. Bimetallic catalysts have been shown to have favorable selectivities in many chemical reactions, high specific rates and greater resistance to poisoning than the one component metallic catalyst systems [4.1 - 4.9].

At present, the cause for this beneficial catalytic behavior is not well understood. It is therefore important to study well characterized bimetallic systems. The gold-platinum system was chosen for this study because the catalytic behavior of this system has been investigated in our laboratory (which is discussed in Chapter V and in references [4.10 - 4.12]). It was found that gold deposited on the Pt(111) surface enhances the cyclohexene dehydrogenation rate by a factor of six relative to the pure platinum surface (at a gold coverage of 0.5 monolayers). It was also found that forming a Au-Pt alloy resulted in a selectivity change in isomerization, hydrogenolysis, cyclization, and aromatization reactions [4.13] and that the

behavior of the (111) and (100) alloy surfaces differed. Although these effects have been explained using geometric models (ensemble effects), they are not yet fully understood. Detailed investigations of the electronic structure are also needed to better understand these complicated problems.

In this chapter, surface electronic properties of the epitaxially grown gold thin films on both the Pt(111) and Pt(100) surfaces and their alloys as determined using X-ray photoelectron spectroscopy (XPS) and ultra-violet photoelectron spectroscopy (UPS), in addition to Auger electron spectroscopy (AES) and low energy electron diffraction (LEED) are discussed. Results are presented which show the differences between the epitaxially grown and alloyed surfaces and the effect of the crystallographic orientation of the platinum substrate.

B. RESULTS

1. XPS results on Au/Pt(111) and Au-Pt(111) alloy

Fig. 4.1 shows the XPS spectra obtained from the Pt(111) surface covered with various amounts of Au. It has previously been shown from an intensity analysis of AES spectra that Au growth on both the Pt(111) [4.13] and Pt(100) [4.10] surfaces is layer-by-layer (Frank-van der Merwe type) [4.14]. In this text, this type of surface with epitaxially deposited Au is denoted as Au/Pt(111) and Au/Pt(100). The alloy surfaces will be expressed as Au-Pt(111) and Au-Pt(100) alloys. As is seen in Fig. 4.1, the Au 4f peaks shifted gradually to higher binding energy as the Au coverage was

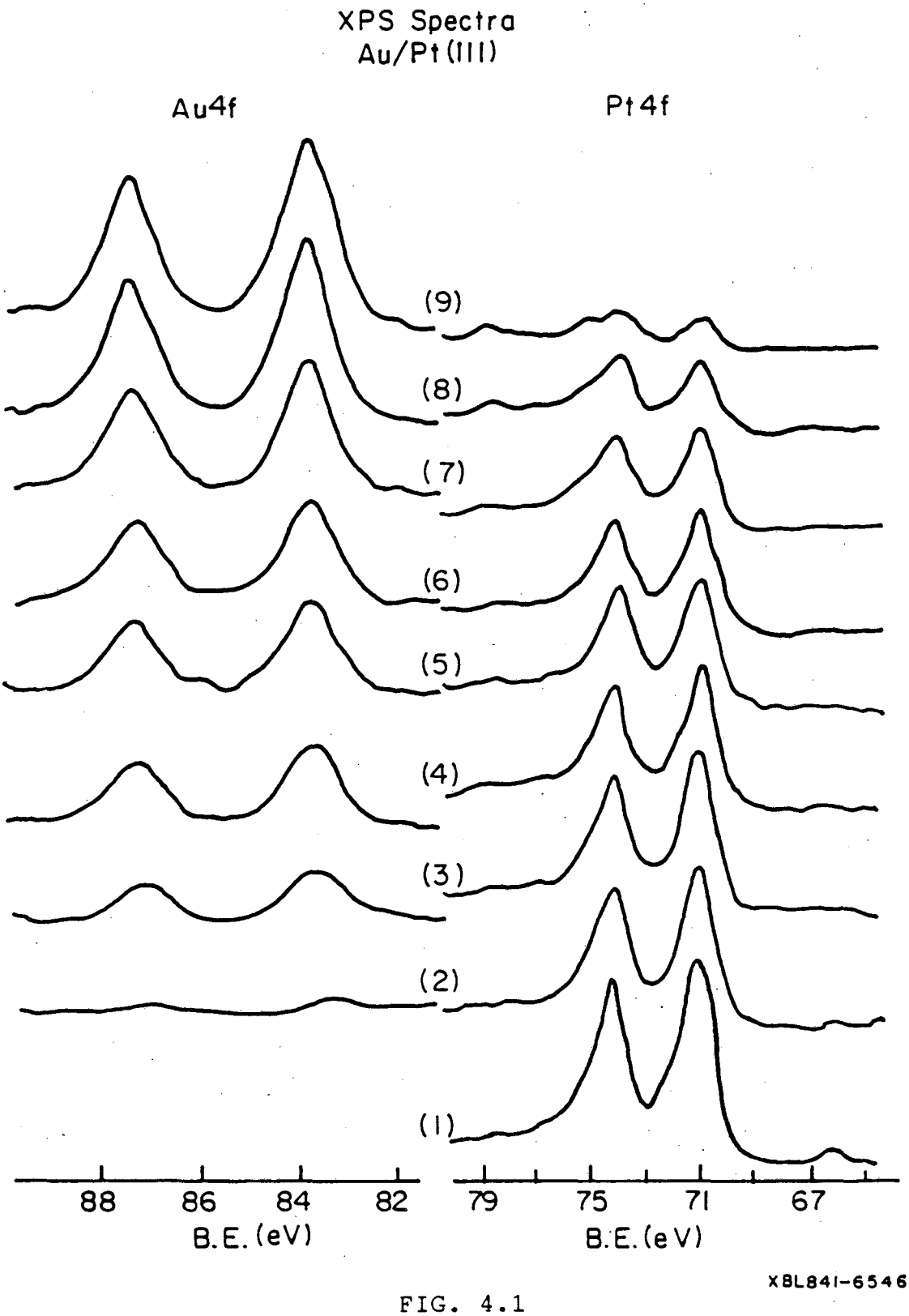

FIG. 4.1

XPS spectra of Au on a Pt(111) surface. Gold coverages : 1) 0 ML; 2) 0.4 ML; 3) 1.3 ML; 4) 1.9 ML; 5) 2.3 ML; 6) 2.5 ML; 7) 3.4 ML; 8) 4.6 ML; 9) 6.1 ML.

increased. The Pt 4f peaks however, did not shift upon Au deposition. The deformed shape of the Pt 4f at the high Au coverage is due to excitation by the satellite x-ray lines (Mg $K_{\alpha 3,4}$) and is not a new chemical state of Pt. The shift of the Au peaks between the coverage of 0.4 and 3.7 monolayers is 0.5 $\pm$ 0.1 eV and at high enough coverages bulk Au values were reached. The shift observed in the Au 4f spectra can be interpreted in terms of the coordination number of each Au atom, which will be discussed later.

In Fig. 4.2, XPS spectra obtained from the Au-Pt(111) alloy surfaces are shown with the average surface gold concentration determined with AES. An annealing temperature from 800 K to 1200 K was used to diffuse the Au atoms into the Pt substrate. This alloying resulted in a shift of the Au 4f peaks of as much as 1.0 eV to lower binding energy. This direction of shift is expected when the Au atoms become more isolated from each other. The higher the annealing temperature, the larger the observed shift. This is because a higher annealing temperature caused more diffusion of Au into the Pt bulk, decreasing the Au-Au coordination. The trend observed for the epitaxial system (Fig. 4.1) was again seen for the the alloy system, i.e. the higher the Au-Au coordination, the higher the binding energy of the Au peaks. When two stages of similar intensity ratios of Au 4f and Pt 4f peaks in Fig. 4.1 and Fig. 4.2 are compared, the shift for the Au-Pt(111) alloy was larger than that for the Au/Pt(111) system. This is most likely the result of island formation

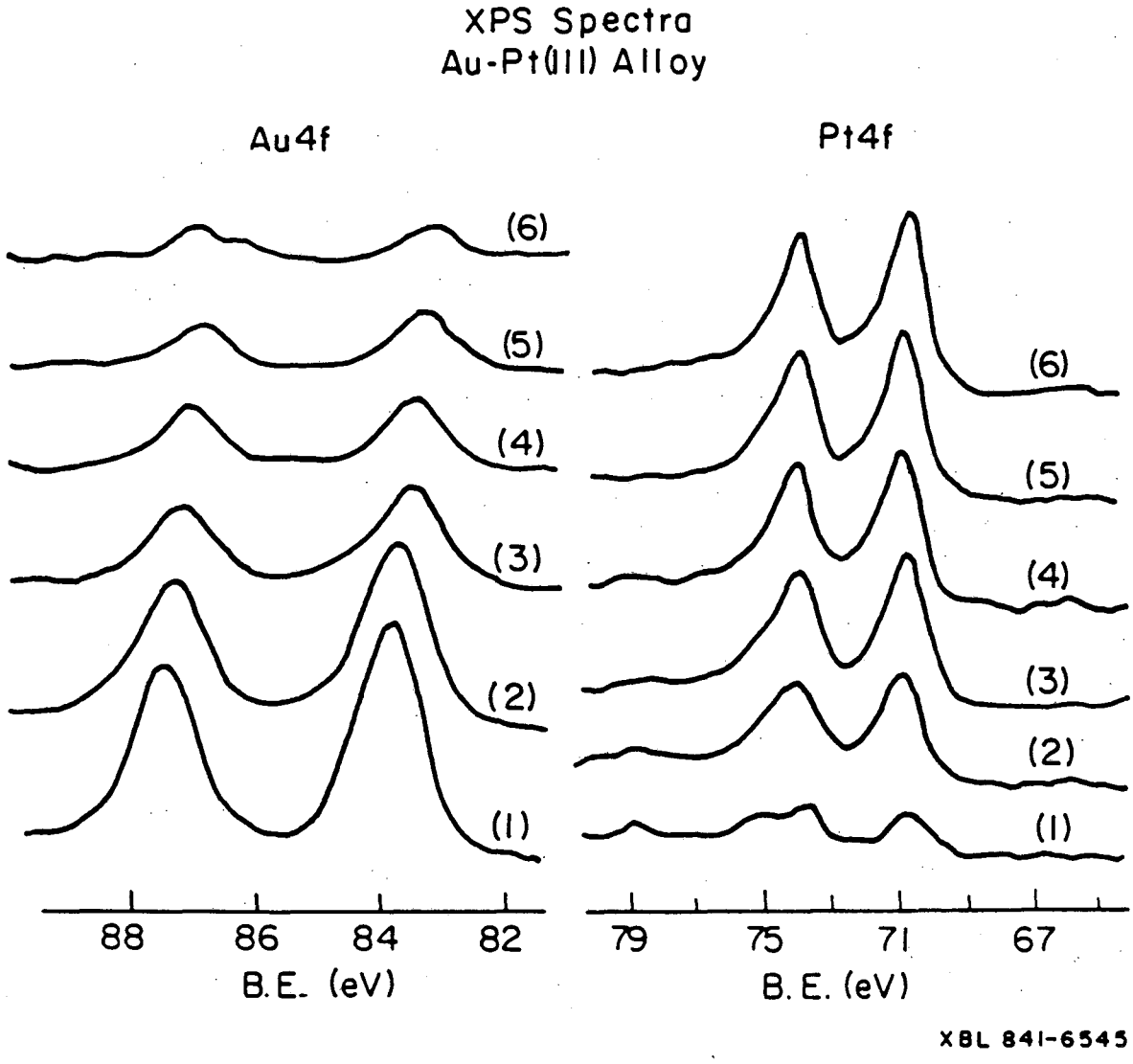

FIG. 4.2

XPS spectra of Au-Pt(111) alloys. Average amount of gold at the surface as determined by AES: 1) 6.1 ML (as deposited); 2) 4.0 ML; 3) 2.2 ML; 4) 1.6 ML; 5) 1.3 ML; 6) 0.7 ML.

of the epitaxial Au and not a result of a change in the interaction between Au and Pt atoms upon alloying. As was observed for the epitaxially grown surface, the Pt 4f peaks did not shift during the course of the alloying.

2. XPS results on Au/Pt(100) and Au-Pt(100) alloy

Fig. 4.3 shows the XPS spectra obtained for the Pt(100) surface which was covered with an epitaxially grown Au layer. As is evident in this figure, the Au 4f peaks shifted about 0.5 eV to higher binding energy at higher Au coverage, and the Pt 4f peaks did not shift. The magnitude and direction of the shift is quite similar to the results obtained for the Au/Pt(111) system.

The change in the XPS spectra upon formation of an alloy on the Pt(100) surface is shown in Fig. 4.4. In this case again, the Au 4f peaks shifted about 1.0 eV toward lower binding energy. The magnitude of the shift was larger for the alloy than the epitaxially grown surface for a given Au/Pt ratio, analogous to the Pt(111) surface. Again, this was most likely due to islanding of the gold in the epitaxial system.

As is seen in Fig. 4.1 to Fig. 4.4, the behavior of the core levels of the Au and Pt for the two crystallographic orientations is similar. The UPS results however, show a clear distinction between the Pt(111) and Pt(100) surfaces.

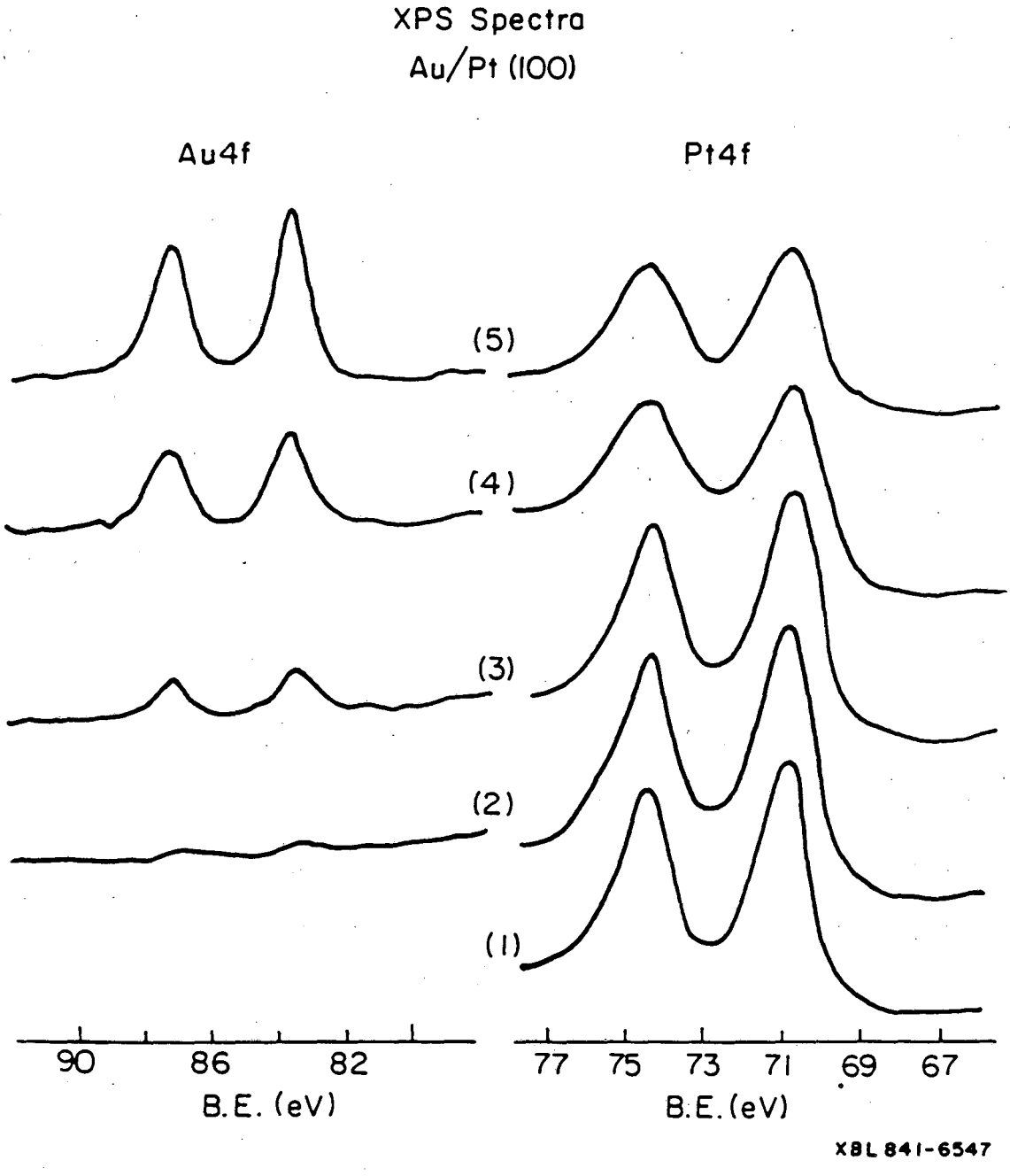

FIG. 4.3

XPS spectra of Au on a Pt(100) surface. Gold coverages : 1) 0 ML; 2) 0.2 ML; 3) 0.8 ML; 4) 1.8 ML; 5) 3.1 ML.

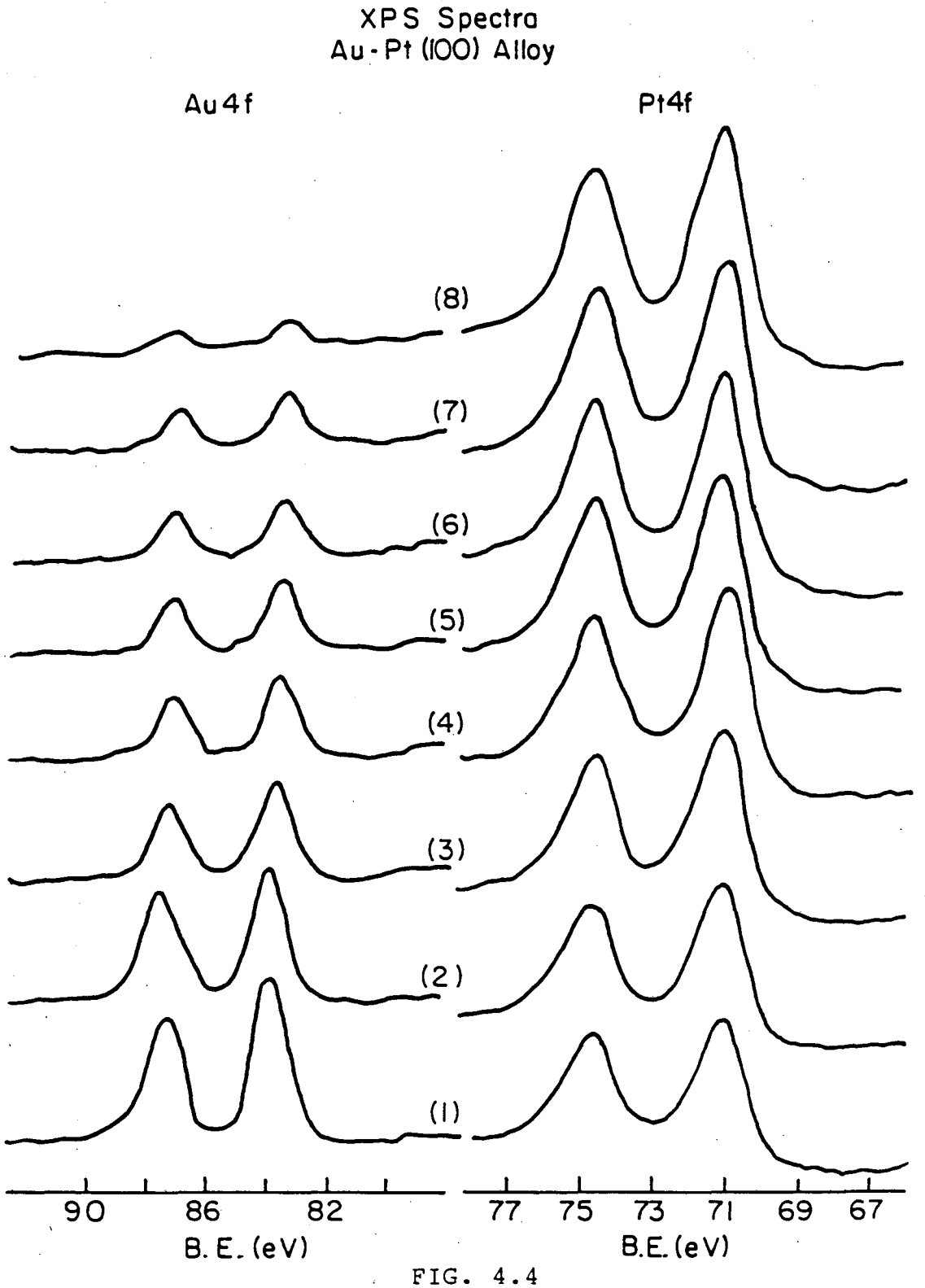

FIG. 4.4

XPS spectra of Au-Pt(100) alloys. Average amount of gold at the surface as determined by AES: 1) 3.1 ML (as deposited); 2) 2.6 ML; 3) 1.9 ML; 4) 1.5 ML; 5) 1.3 ML; 6) 1.1 ML; 7) 1.0 ML; 8) 0.5 ML.

3. UPS results on Au/Pt(111) and Au-Pt(111) alloy

To observe the change in the UPS spectra clearly, difference spectra were made by subtracting the standard spectrum of the clean platinum surface. In the following text, this type of spectra will be referred to as "difference spectra". In addition to this standard type of difference spectra, the difference between spectra obtained for two successive stages (either gold deposition or diffusion of gold into the platinum bulk) were also made. Spectra obtained in this manner will be referred to as "increment spectra".

The change in the UPS spectra upon the epitaxial deposition of Au on the clean Pt(111) surface is shown in Fig. 4.5. After the deposition of a small amount of Au, the strong Pt surface state peak, located at 0.8 eV below the Fermi level, was greatly attenuated. The peak at ~8 eV can be attributed to CO adsorbed on the surface. This peak disappeared at higher Au coverages indicating that CO did not adsorb on the Au atoms, nor did the CO become trapped beneath the Au layers but was displaced by the Au atoms upon deposition. As the Au coverage was increased, new peaks appeared between 4 and 6 eV. The work function, which was derived from the secondary electron emission edge in the UPS spectra, showed a monotonous decrease with Au deposition up to 4 monolayers of Au [4.15].

Fig. 4.6 shows the change in the UPS spectra upon annealing a gold covered Pt(111) sample. The difference

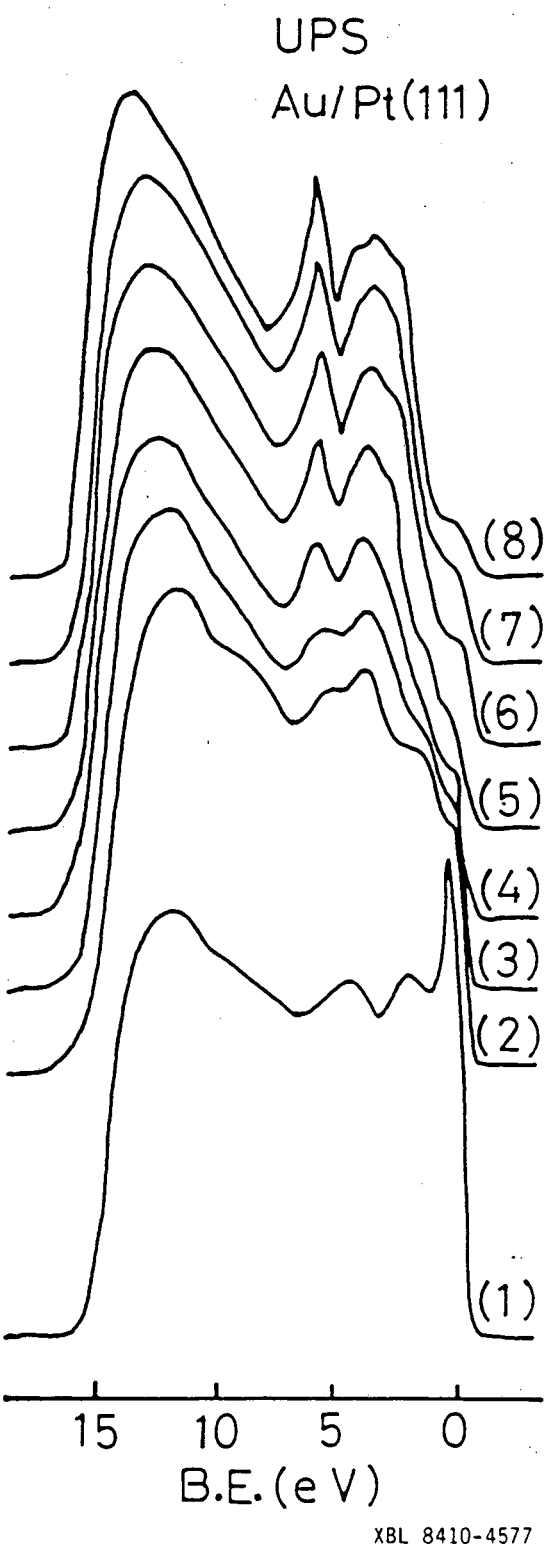

FIG. 4.5

UPS spectra of Au on a Pt(111) surface. Gold coverages : 1) 0 ML; 2) 0.6 ML; 3) 1.1 ML; 4) 1.6 ML; 5) 2.3 ML; 6) 2.9 ML; 7) 3.4 ML; 8) 4.4 ML.

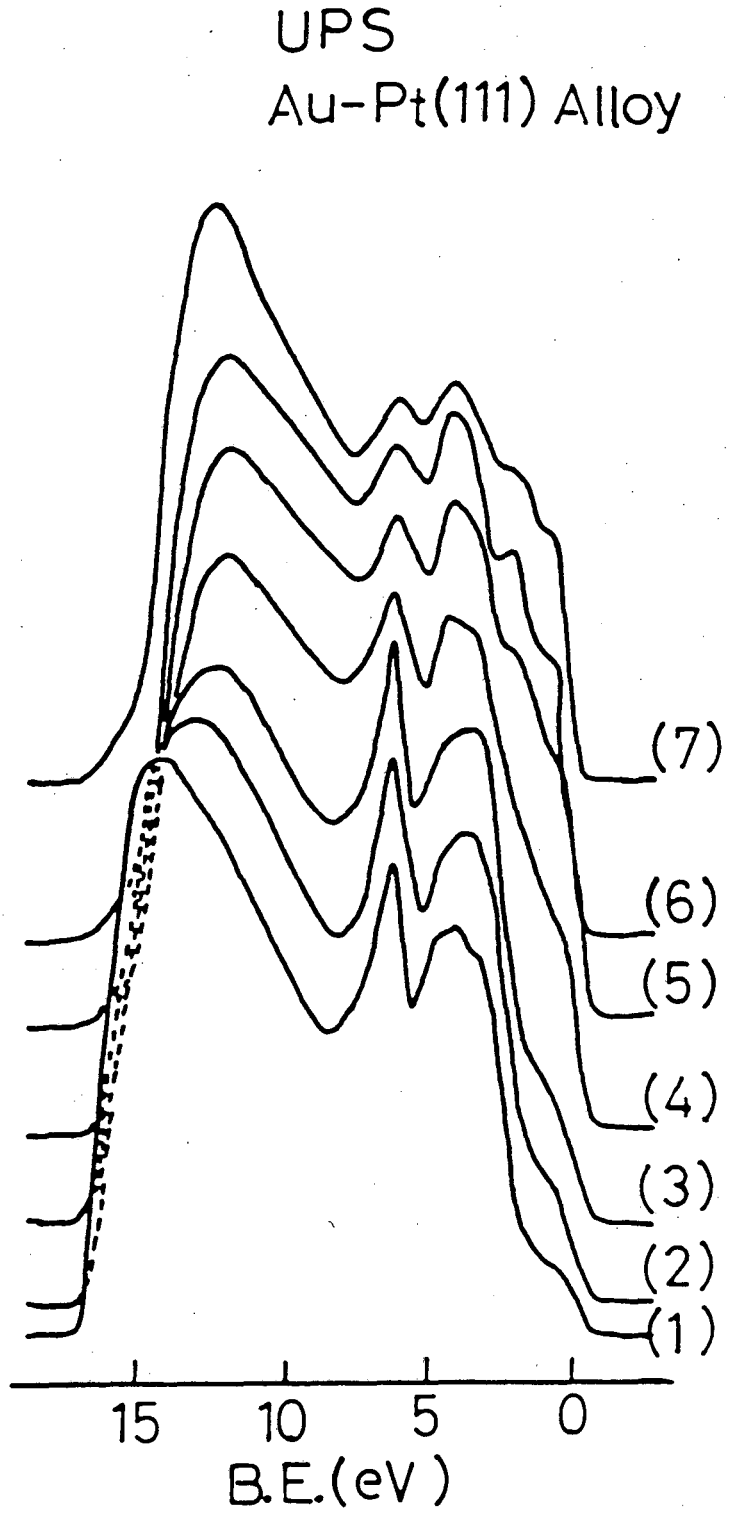

XBL 8410-4578

FIG. 4.6

UPS spectra of Au-Pt(111) alloys. Average amount of gold at the surface as determined by AES: 1) 4.4 ML (as deposited); 2) 3.4 ML; 3) 2.9 ML; 4) 2.3 ML; 5) 1.6 ML; 6) 1.1 ML; 7) 0.6 ML.

spectra, obtained by subtracting the spectrum of clean Pt(111) from each spectrum after Au deposition, are shown in Fig. 4.7 (solid lines). The deep valley around 0.8 eV below the Fermi level is due to the disappearance of the surface state peak of the clean Pt(111) and the peaks which originate from the Au adatoms are located between 1.5 and 8 eV.

Two peaks could be seen upon the deposition of Au. One is located around 6.5 eV and the other at 4.0 eV. The former, which is a bonding-like state [4.16], grew in intensity as the Au coverage was increased. The peak at 4.0 eV, which is assigned to an anti-bonding state [4.16], also grew with increasing Au coverage, but began to show some structure at higher coverages. The relative peak heights also changed with Au coverage, i.e. at higher coverages, the higher binding energy peak became more intense than the lower binding energy peak. A slight shift of less than 0.3 eV to higher binding energy was observed for the peak at 6.5 eV. This small shift is very different than the shift observed for the Au/Pt(100) system, as will be shown.

In order to gain a better understanding of what was occurring at each step of deposition, adjacent difference spectra were subtracted to produce "increment spectra". Looking at these increment spectra (dotted lines) as well as the usual difference spectra carefully, several things can be noted. The spectra for up to 1 monolayer Au coverage show a simple resonance-like feature which consists of two peaks. These two peaks shifted slightly to higher binding energy as

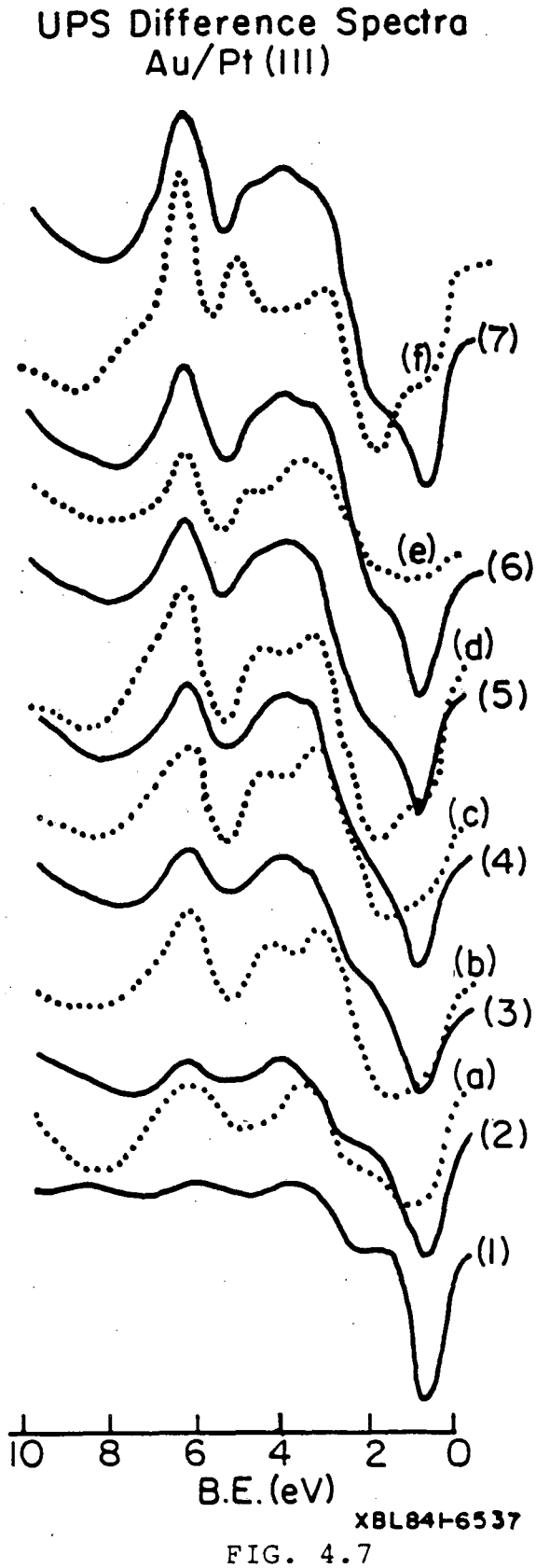

FIG. 4.7

UPS difference spectra of Au on a Pt(111) surface. Gold coverages: 1) 0.6 ML; 2) 1.1 ML; 3) 1.6 ML; 4) 2.3; 5) 2.9 ML; 6) 3.4 ML; 7) 4.4 ML.
Difference spectra (———) Increment spectra (·····)

the Au coverage was increased. This can be explained by a simple coordination number model. On the other hand, for a Au coverage between 1 and 3.4 monolayers, the lower binding energy peak showed some structure unlike the higher binding energy peak which simply increased in intensity. Increment spectra (b) through (e) are very similar to each other, implying that these spectra correspond to the additional Au layers in which the Au-Au interaction has the dominant contribution. These increment spectra have peaks at 6.2, 4.5, and 3.2 eV and also have two shoulders around 7.2 and 2.8 eV. The increment spectra for Au coverages greater than 4 monolayers (f) have three peaks and are different than the previous increment spectra.

When alloys were formed by annealing a Au covered sample, the UPS spectra changed in a complex way, as Fig. 4.8 shows. Inspection of the difference spectra reveals that as alloying proceeded, the higher binding energy peak was attenuated and broadened, though the peak position did not change until stage (5) was reached. The lower binding energy peak showed more structure at the initial stages of annealing and a simple structureless, resonance-like peak at the final stages of annealing. Comparing the increment spectra (shown as dotted lines) (a) to (d) with the increment spectra in Fig. 4.7, it can be seen that the change to this stage is due to the loss of Au into the Pt bulk. After further annealing, the high energy peak broadened and shifted to lower binding energy when compared with the epitaxial system.

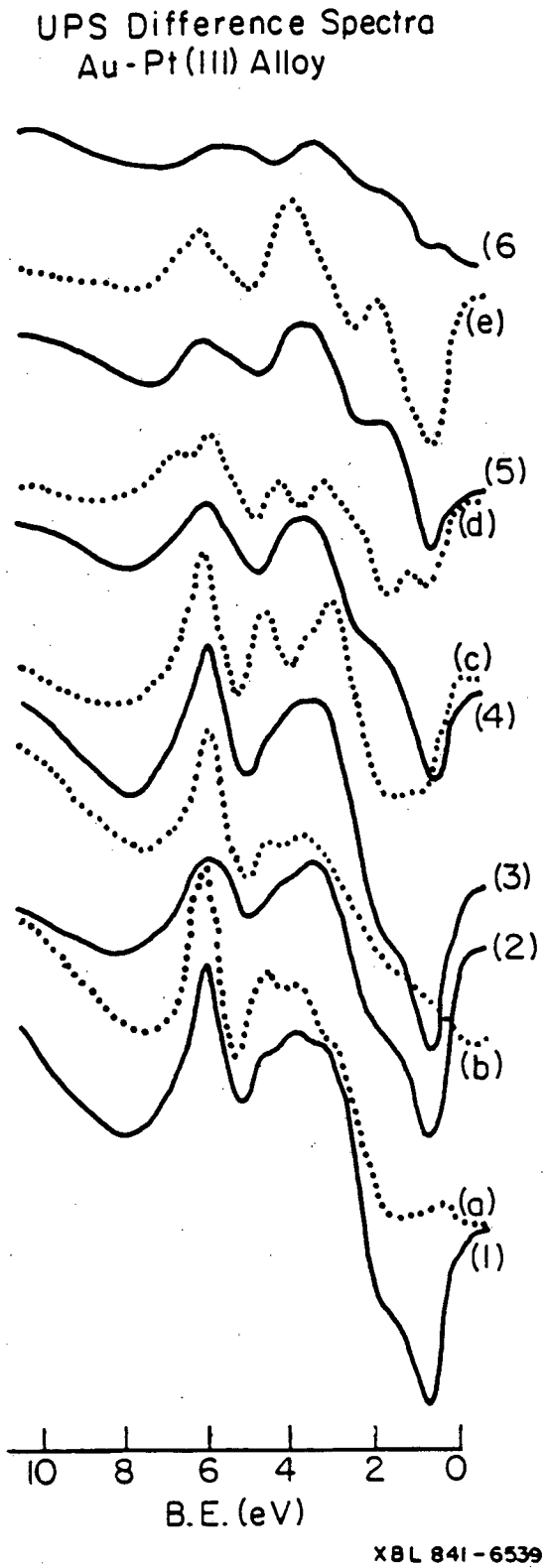

FIG. 4.8

UPS difference spectra of Au-Pt(111) alloys. Average amount of gold at the surface as determined by AES: 1) 4.4 ML (as deposited); 2) 2.8 Ml; 3) 2.6 ML; 4) 1.6 ML; 5) 0.9 ML; 6) 0.7 ML.
Difference spectra (———) Increment spectra (·····)

4. UPS results on Au/Pt(100) and Au-Pt(100) alloy

The UPS difference spectra for the Au deposited on the Pt(100) surface, shown in Fig. 4.9, were different than those obtained for the Pt(111) surface. Both the low and high energy peaks shifted to higher binding energy by as much as 0.8 eV. This shift continued up to ~ 3 monolayers, whereas for the Pt(111) surface the shift was only observed up to 1 monolayer.

The increment spectra for coverages up to 1 monolayer showed two simple, resonance-like peaks which shifted to higher binding energy as the Au coverage was increased. This direction of shift agrees well with the coordination number effect or the edge atom effect [4.17]. For coverages greater than 1 monolayer the spectra were similar to those for the Pt(111) system.

The peak at 1.2 eV below the Fermi level was only observed for the Pt(100) surfaces (both epitaxial and alloy) and only for coverages of less than 2 monolayers. In the spectra from the Au/Pt(111) and Au-Pt(111) alloy, a small tail at a little higher energy was seen for up to several monolayer of Au. A similar tail also appeared in theoretical calculations [4.18] and in other XPS results [4.18]. The small peak observed for the Pt(100) surface is probably not the same as this tail or other peaks observed by Bonzel et al. [4.19], but an interface state [4.20].

The difference and increment spectra for the alloyed Au-Pt surfaces are shown in Fig. 4.10. The difference spectra

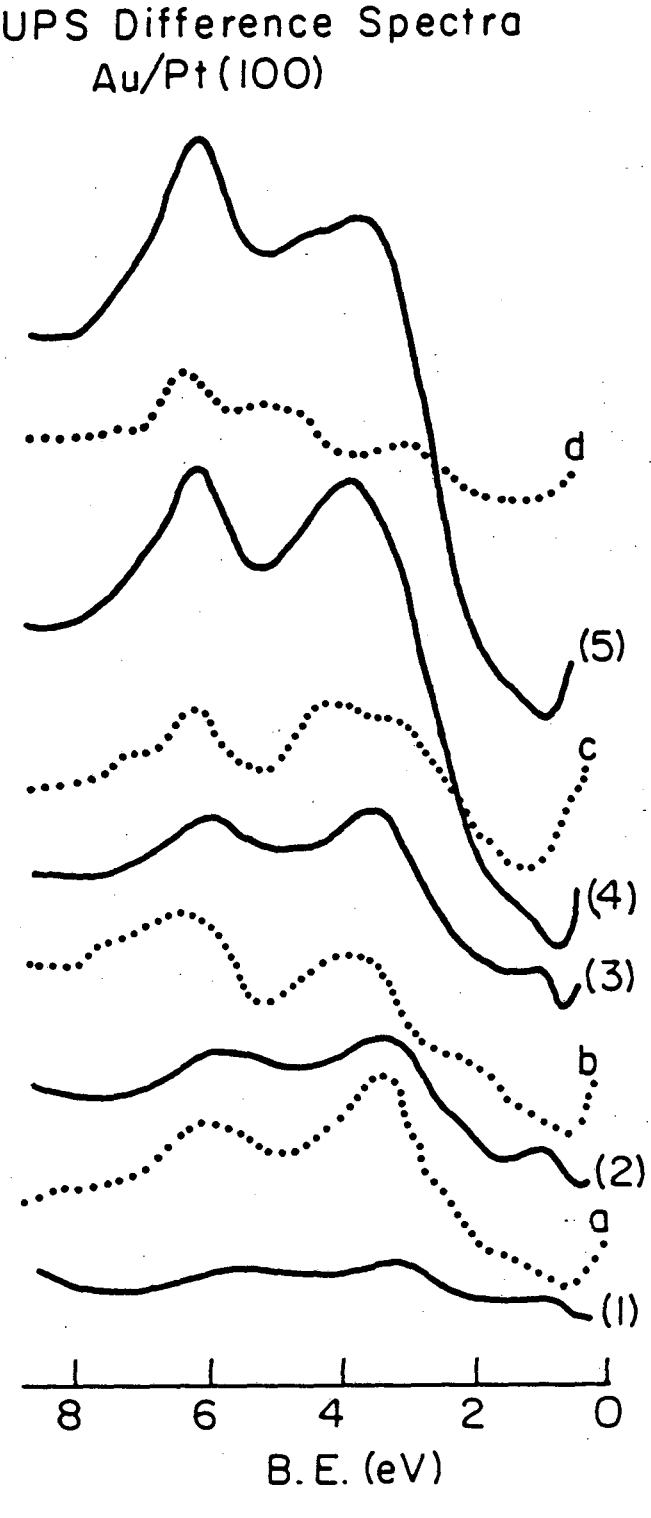

FIG. 4.9

UPS difference spectra of Au on a Pt(100) surface. Gold Coverages: 1) 0.4 ML; 2) 0.6 ML; 3) 1.4; 4) 1.6 ML 5) 2.9 ML; 6) 3.9 ML.
Difference spectra (———) Increment spectra (·····)

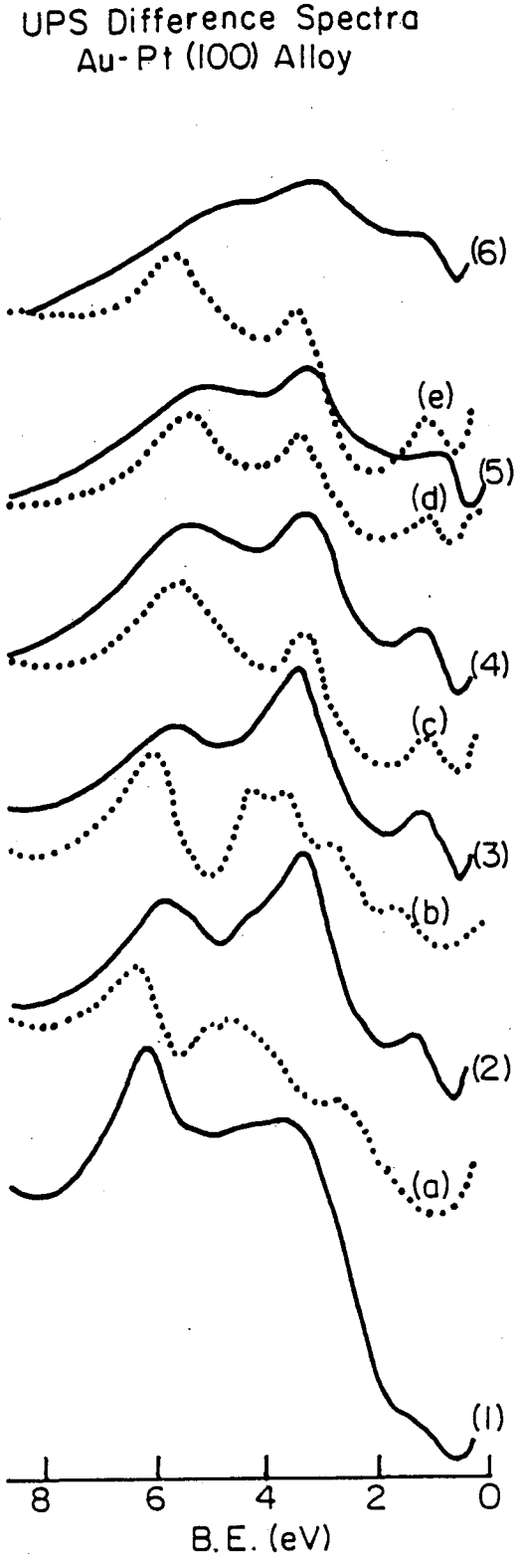

FIG. 4.10

UPS difference spectra of Au-Pt(100) alloys. Average amount of gold at the surface as determined by AES.: 1) 4.1 ML (as deposited); 2) 2.6 ML; 3) 1.8 ML; 4) 1.2; 5) 0.8 ML; 6) 0.4 ML.
Difference spectra (———) Increment spectra (·····)

showed that the high energy peak shifted by more than 1 eV toward lower binding energy upon alloying. This was a much larger shift that that observed for the Au-Pt(111) alloy. The low energy peak lost structure but did not shift upon alloying. The total d-band became narrower and the d-band centroid shifted to lower energy. The magnitude of this shift was much larger than that observed for the Au-Pt alloy.

C. DISCUSSION

There have been several photoemission studies [4.21 - 4.26] of atoms in the surface region. Some of these studies concentrated on the electronic structure of the top layer of atoms of polycrystalline [4.21] or single crystal [4.22 - 4.26] samples and investigated the surface core level shifts (SCS). In these studies, the XPS shifts observed from the surface atoms, including atoms in site and kink sites, were generally interpreted with the well known "coordination number model" [4.17]. It is a general rule that the higher the coordination number of the atom, the higher its core level binding energy. This rule holds except for metals such as Ti and Sc [4.27] where other factors including rehybridization of surface d-band electrons, d-band narrowing and surface states should be taken into account to give a complete explanation of the phenomena.

In the epitaxial systems of Au/Pt(111) and Au/Pt(100), however, this simple and semi-empirical "coordination number model" explains the experimental results quite satisfactorily. That is, the more Au atoms on the surface, the higher their core level binding energy. Alloying gives rise to a core level shift which similar to that of the epitaxial system. The magnitude of the shift was not as great for the epitaxial systems due to island formation. There was no significant charge transfer seen for this system since no shift in the Pt 4f peaks was observed. This conclusion has been reached by other authors [4.28 - 4.29].

This makes it unnecessary to consider charge redistribution in the bulk. In the synchrotron radiation study of the Cu/Pt(111) system, a shift of about 0.2 eV in the Pt 4f peak was observed [4.30]. Therefore, the shift in our study may be too small to be detected by our experimental system.

The work function change of the Pt(100) surface upon Au epitaxial deposition has already been reported by Salmeron et al. [4.17]. A gradual decrease in the work function has also been observed for the Au/Pt(111) system, but in this case no minimum in the work function was observed. Among the factors which can effect the work function, charge transfer between the adatoms and the substrate in most important [4.31]. The minimum in the work function which has been observed for alkali metal adatoms such as K [4.32] and Na [4.33], is due to the repulsive interaction between the adatoms which are charged as a result of charge transfer between the substrate and the adatoms. Therefore, if there is no charge transfer, a minimum would not necessarily be seen. A similar monotonous decrease in the work function of Pt(111) upon Cu deposition has been reported previously [4.30]. No charge transfer was observed for this system either [4.30, 4.34, 4.35], and several possible factors such as polarization and surface dipole changes were suggested to explain this behavior [4.30], although a detailed analysis has not been carried out.

The difference between the Au/Pt(111) and the Au/Pt(100) can clearly be seen in the UPS difference spectra shown in

Fig. 4.7 and Fig. 4.9. The Au $5d_{3/2}$ peak shifted ~0.3 eV for Au deposited on the Pt(111) surface, whereas a shift as large as 0.8 eV was observed for Au deposited on the Pt(100) surface and this shift continued up to several monolayers of Au. These results can be explained in terms of the atomic structure of the two surfaces. A LEED study revealed that on the Pt(111) surface, the Au deposition showed only a (1 X 1) structure up to multilayer coverages. There was a gradual weakening of the hexagonal reconstruction of the Pt(100) surface upon Au deposition and at a coverage of 0.5 monolayers, a (1 X 1) surface structure was observed. This (1 X 1) structure remained unchanged up to 2 monolayers of Au although the lattice constants of Au were decreased by 2-6 %. Au atoms on the Pt(111) surface are more densely packed than on the Pt(100) surface. Therefore, the Au atoms on the Pt(111) surface are more bulk-like than those on the Pt(100) surface, even at submonolayer coverage. This results in a smaller shift of the Au $5d_{3/2}$ peak from the bulk value on the Pt(111) surface than on the Pt(100) surface. Because of the openness of the Pt(100) surface, it requires several monolayers of Au to achieve a bulk-like nature. This agrees well with the experimental results show in Fig. 4.7 and Fig. 4.9.

The resonance-like, simple spectrum shapes obtained for coverages less than 1 monolayer were different than the surface spectrum obtained from a polycrystalline sample [4.21]. It is quite interesting to note that the energy of

this resonance-like spectrum not only depends of the amount of Au, but also on the crystal structure of the substrate, which suggests that the XPS surface level shift should be interpreted in term of the surface crystallographic orientation.

It may also be worthwhile to note that the increment spectra (f) in Fig. 4.7 and (d) in Fig. 4.9 are different from the rest of the spectrum shapes. The LEED analysis [4.13] indicated that Au layers on the Pt substrates were contracted by several percent at lower coverages. However, on the Pt(111) surface these Au surface layers expanded to the bulk Au lattice constants at a coverage between 6 and 10 monolayers. In the case of Au layers on the Pt(100) surface, this contraction continued until higher coverages (20-30 monolayers). Based on these LEED results, these UPS three-peak spectra may be interpreted as bulk Au spectra, although other possibilities such as small amounts of surface contamination cannot be excluded.

Information about the width, shift and spin-orbit splitting of the d electrons of the alloy surfaces can be obtained by UPS. The band width (w) of the valence region can be expressed, from the tight binding theory [4.37], as follows : $w \propto z^{1/2} \times l^{-1/5}$, where z is the coordination number and l is the distance of the nearest neighbors. Upon alloying, z becomes smaller because each Au atom is diluted in the Pt substrate. In the case of Pt(100), the contribution from the change in l was small, therefore a

total d-band narrowing was observed. For the Au-Pt(111), on the other hand, the change in l was large enough to compensate for the change in z, which resulted in no explicit d-band narrowing. This occurred since there is a much stronger dependence of w on l than on z. Although direct information on the nearest neighbor distance for these surfaces is not available, it can be assumed that the degree of expansion in the Au-Pt(111) is smaller than for the Au-Pt(100) since the Au-Pt(100) alloy is only expanded slightly compared with pure Pt(100) [4.13].

Generally, spin-orbit splitting becomes smaller when atoms are more isolated from each other. In the case of Au-Pt(100), this general tendency was observed explicitly, though no clear change was observed for the Au-Pt(111). Smaller spin-orbit splitting leads to d-band narrowing and a shift of the d-band centroid to lower binding energy. This trend was observed for the systems studied here and for most alloys, i.e. Cu-Al [4.35], Cu-Ag [4.36], Ag-Al [4.35], Al-Au [4.35], and In-Au [4.37] (an exception is Cu-Pt [4.30, 4.38, 4.39]).

D. SUMMARY

The major results obtained in this study are summarized as follows:

(1) The XPS results showed that on both the Pt(111) and Pt(100) surfaces the Au 4f peaks shifted to higher binding energy as Au was deposited. The magnitude of the shift was ~0.5 eV between coverages of submonolayer and several monolayers. The Pt 4f peaks were not observed to shift.

(2) Upon alloying, the Au 4f peaks shifted about 1.0 eV to lower binding energy for both the Au-Pt(111) and Au-Pt(100) and the Pt 4f peaks did not shift.

(3) The UPS results were different for the Pt(111) and the Pt(100) surfaces. Only a small shift to higher binding energy was observed for the Au/Pt(111), and a shift of up to 0.8 eV to higher binding energy was observed for the Au/Pt(100). This shift continued up to several monolayers of Au.

(4) The UPS spectra of the Au-Pt(100) alloys showed that only the higher binding energy peak shifted 1.0 eV to lower binding energy as the alloying proceeded. The spin-orbit splitting of the two d peaks decreased and the total d-band width became narrower and shifted to lower binding energy. This behavior was quite different from the small change observed for the Au-Pt(111) alloy system.

(5) A peak was observed at a binding energy of 1.0 eV below the Fermi level for the Au/Pt(100) and the Au-Pt(100) alloy surfaces and not for the Au/Pt(111) nor the Au-Pt(111)

alloy surfaces. This peak was assigned to an interface state.

(6) The work function of both the Pt(111) and Pt(100) surfaces decreased monotonicly upon Au deposition. Conversely, alloying resulted in an increase in the work function.

REFERENCES

4.1) F.M. Dautzenberg, J.N. Helle, P. Biloen and W.H.M. Sachtler, J. Catal. 63 (1980) 119.

4.2) B. Spurlock and R.L. Jacobson, U.S. Pat. No. 3,507,781 (1970).

4.3) J.H. Sinfelt, U.S. Pat. No. 3,835,034 (1974).

4.4) C. Betizeav, G. Leclercq, R. Maurel, C. Bolivar, H. Charcosset, R. Frety and L. Tournayan, J. Catal. 45 (1976) 179.

4.5) P. Biloen, J.N. Helle, H. Verbeek, F.M. Dautzenberg and W.H.M. Sachtler, J. Catal. 63 (1980) 112.

4.6) J.R.H. Van Schaik, R.P. Dressing and V. Ponec, J. Catal. 38 (1975) 273.

4.7) A. O'Cinneide and F.G. Gault, J. Catal., 37 (1975) 311.

4.8) V. Ponec and W.H.M. Sachtler, J. Catal. 24 (1972) 250.

4.9) J.H. Sinfelt, J.L. Carter and J.C. Yates, J. Catal. 24 (1972) 283.

4.10) J.W.A. Sachtler, M.A. Van Hove, J.P. Biberian and G.A. Somorjai, Phys. Rev. Lett. 45 (1980) 1601.

4.11) J.W.A. Sachtler, M.A. Van Hove, J.P. Biberian and G.A. Somorjai, Surface Sci. 110 (1981) 19.

4.12) J.W.A. Sachtler, J.P. Biberian and G.A. Somorjai, Surface Sci. 110 (1981) 43.

4.13) J.W.A. Sachtler, Ph.D. Thesis, Ch. 5.

4.14) F.C. Frank and J.H. Van der Merve, Proc. R. Soc. A198 (1949) 205.

4.15) C. Binns and C. Norris, Surface Sci. 115 (1982) 395.

4.16) N.J. Shevchik, J. Phys. F 5 (1975) 1860.

4.17) M. Salmerón, S. Ferrer, M. Jazzar and G.A. Somorjai, Phys. Rev. B 28 (1983) 1158.

4.18) N.V. Smith, G.K. Wertheim, S. Hüfner and M.M. Traum, Phys. Rev. B 10 (1974) 3197.

4.19) H.P. Bonzel, C.R. Helms and S. Kelemen, Phys. Rev. Lett., 35 (1975) 1237.

4.20) Ding-Sheng Wang, A.J. Freemann and H. Krakauer, Phys. Rev. B 29 (1984) 1665.

4.21) P.H. Citrin and G.K. Wertheim, Phys. Rev. Lett. 41 (1978) 1425.

4.22) T.M. Duc, C. Guillot. Y. Lassailly. J. Lecante, Y. Jugnet and J.C. Vedrine, Phys. Rev. Lett. 43 (1979) 789.

4.23) P. Heimann, J.Hermanson and H. Miosga, Phys. Rev Lett. 43 (1979) 1957.

4.24) P. Heimann, J.F. Van der Veen and D.E. Eastman, Solid State Commun. 38 (1981) 595.

4.25) J.F. Van der Veen, F.J. Himpsel and D.E. Eastman, Phys. Rev. Lett. 44 (1980) 189.

4.26) J.F. Van der Veen, D.E. Eastman, A.M. Bradshaw and S. Holloway, Solid State Commun. 39 (1981) 1301.

4.27) P.J. Feibelman and D.R. Hammann, Solid State Commun. 31 (1979) 413.

4.28) J.J. Stephan, V. Ponec and W.M.H. Sachtler, Surface Sci. 47 (1975) 403.

4.29) J.R. Anderson, K. Foger and R.J. Breakspere, J. Catal. 57 (1979) 458.

4.30) M.L. Shek, Ph.D. Thesis, Stanford University (1982) Chapter 4.

4.31) G. Ertl and J. Küppers, "Low Energy Electrons and Surface Chemistry", Verlag-Chemie, Weinheim (1974) p.115.

4.32) M. Kudo, E.L. Garfunkel and G.A. Somorjai, submitted to Surface Sci.

4.33) R.L. Gerlach and T.N. Rhodin, Surface Sci. 19 (1970) 403.

4.34) G.G. Kleiman, V.S. Sundaram, C.L. Barreto and J.D. Roers, Solid State Commun. 32 (1979) 919.

4.35) G.G. Kleiman, V.S. Sunaram. J.D. Rogers and M.B. de Moraes, Phys. Rev. B 23 (1981) 3177.

4.36) D.A. Shirley, Phys. Rev. B 5 (1972) 4709.

4.37) N.E. Christensen and B.O. Seraphin, Phys. Rev. B 4 (1971) 332.

4.38) J.C. Fuggle, L.M. Watson, D.J. Fabian and P.R. Norris, Solid State Commun. 13 (1973) 507.

4.39) N.J. Shevchik and A. Goldmann, J. Electron Spectrosc. and Relat. Phenom. 5 (1974) 631.

CHAPTER FIVE : THE CONVERSION OF n-HEXANE OVER GOLD-PLATINUM AND COPPER-PLATINUM ALLOY SURFACES

A. INTRODUCTION

Alloys have become important catalysts in many chemical processes due to their superior properties over single component catalysts. These properties include increased reaction selectivity and greater resistance to deactivation. One group of alloys which has been studied quite extensively is the group VIII - IB alloys [5.1 - 5.3]. The literature, however, is full of seemingly conflicting results. There are two factors which are probably responsible for this confusion: 1) the difficulty of characterizing surface of the supported alloy catalysts on the atomic scale; and 2) surface structure sensitivity of the reactions studied.

This chapter deals with the n-hexane conversion reaction catalyzed by the Au-Pt(111), Cu-Pt(111), Au-Pt(100) and Cu-Pt(100) alloy surfaces. Catalytic studies, using single crystal catalysts, coupled with surface science techniques, have proven extremely useful in understanding the nature of the working catalyst [5.4 - 5.7]. This method of catalytic research allows 1) a detailed characterization of the surface using the surface sensitive surface science techniques discussed in chapters II and III; 2) the study of surface structure sensitivity through the use of single crystal catalysts; and 3) the study of the catalytic properties of the metal alone without the contribution or modification of a

support. There have, however, been very few high-pressure catalytic studies using single crystal alloy catalysts. One explanation for the catalytic behavior of alloys is the ensemble effect [5.8 - 5.11]. Since this argument is based on the structure of the alloy surface, it is imperative that alloys with well defined surface structure be studied. The catalytic reforming of hydrocarbons is an important industrial reaction which is dependent on platinum alloy catalysts [5.11 - 5.15]. The n-hexane conversion reaction was chosen as a model for the reforming reaction because it can undergo all of the reactions important in catalytic reforming, i.e. isomerization, cyclization, aromatization and hydrogenolysis.

The behavior of the alloy catalysts has been found to be structure sensitive and the effects of alloying platinum with copper and with gold on the selectivity and activity to be drastically different.

B. RESULTS

The catalytic conversion of n-hexane was studied over the (100) surface of gold-platinum alloys and the (111) and (100) surfaces of copper-platinum alloys. Studies of the n-hexane conversion reaction over the (111) surface of gold-platinum alloys have been carried out in our laboratory previously [5.16] and will be included in this discussion. In Fig. 5.1 and Fig. 5.2, the initial rates (rates per surface atom i.e. platinum and gold or copper) of isomerization (formation of 2- and 3-methylpentane), cyclization (formation of methylcyclopentane), aromatization (formation of benzene), and hydrogenolysis (formation of molecules containing 5 carbons or less) are shown as a function of surface alloy composition. Let us first consider the results obtained for the (111) alloy surfaces shown in Fig. 5.1. The rate of cyclization decreased with a positive deviation from the linear as gold was added to the surface, but was strongly inhibited by the addition of copper. The behavior of the aromatization and hydrogenolysis reactions was very similar for both the Au-Pt and Cu-Pt (111) alloy surfaces. These two reactions were greatly inhibited by the addition of the "inactive" metal. The most striking result was the high degree of enhancement for isomerization upon the addition of gold to the Pt(111) surface, with a doubling of the initial rate at a gold atom fraction of 0.25. In contrast to this behavior, the isomerization rate on the Cu-

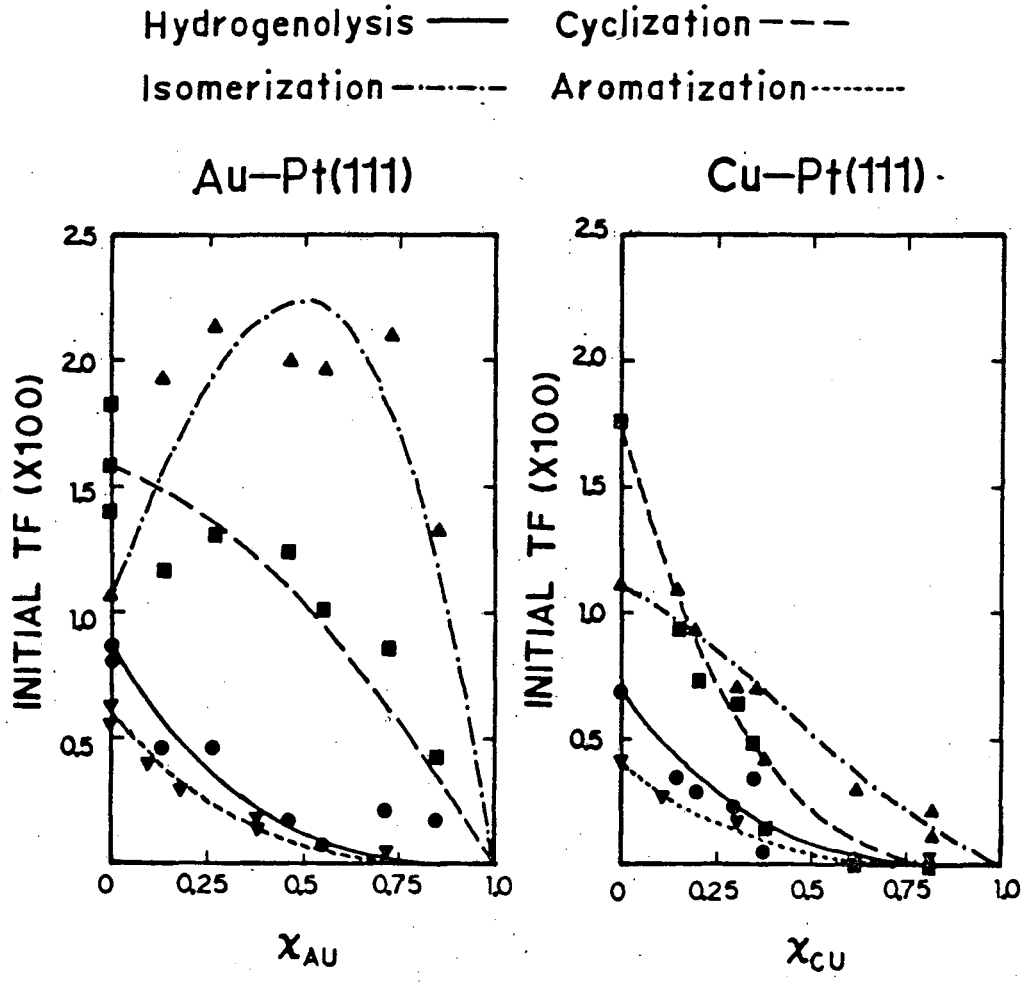

FIG. 5.1

Initial turnover frequencies of the n-hexane conversion reaction over Au-Pt(111) and Cu-Pt(111) alloy surfaces as a function of the IB metal surface atom fraction. Turnover frequencies are expressed as molecules produced per surface atom (platinum and IB metal) per second.

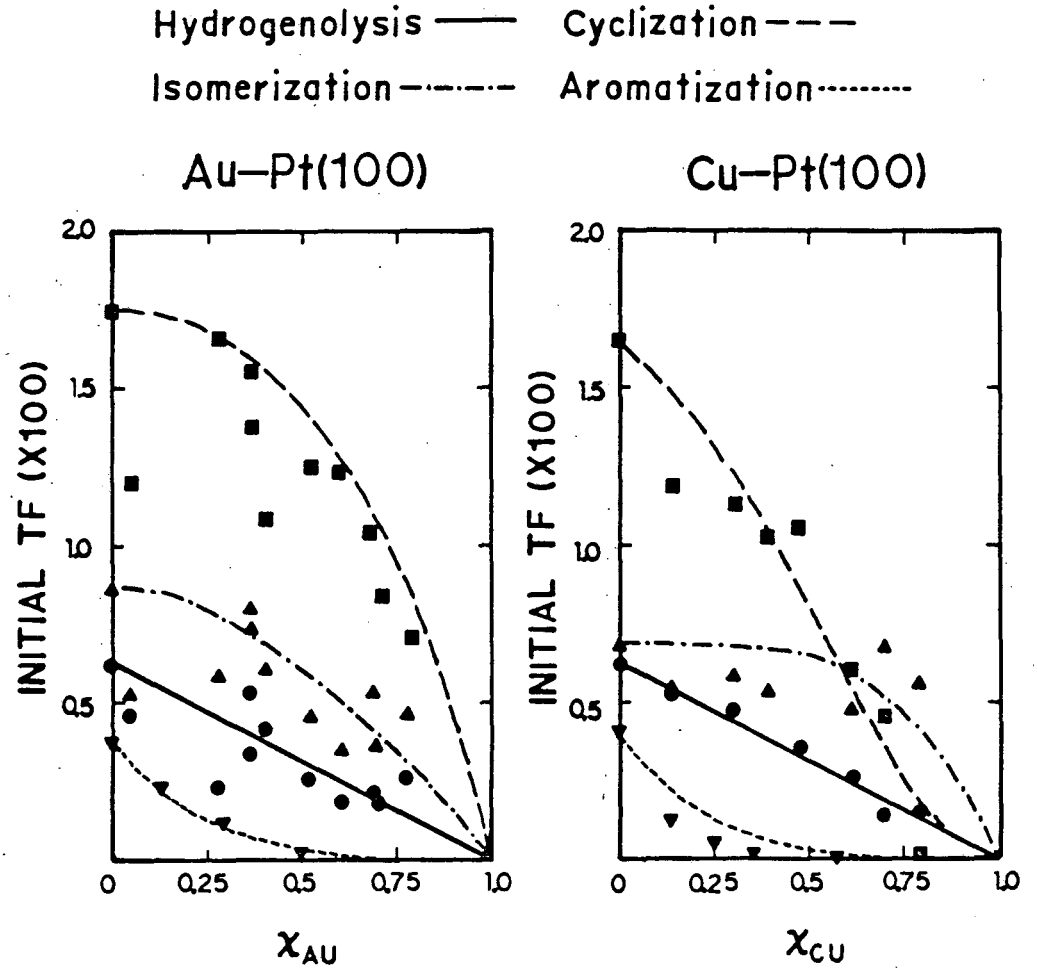

FIG. 5.2

Initial turnover frequencies of the n-hexane conversion reaction over Au-Pt(100) and Cu-Pt(100) alloy surfaces as a function of the IB metal surface atom fraction. Turnover frequencies are expressed as molecules produced per surface atom (platinum and IB metal) per second.

Pt(111) surface dropped off nearly linearly with increasing copper atom fraction.

The behavior of the initial rates per surface atom on the Au-Pt(100) and Cu-Pt(100) is shown in Fig. 5.2. The cyclization rates fell off nearly linearly on both alloy surfaces. The Au-Pt(100) surface displayed a larger deviation from the linear than did the Cu-Pt(100) surface. The isomerization rates on both the Au-Pt(100) and the Cu-Pt(100) surfaces showed a positive deviation from the linear with the effect more pronounced on the Cu-Pt(100) surfaces. Neither of these surfaces showed the great enhancement for isomerization that was observed for the Au-Pt(111) surface. The rates of hydrogenolysis for the (100) alloy surfaces did not reflect the inhibition which was observed for the (111) alloy surfaces. On the (100) alloy surfaces the hydrogenolysis rate fell off linearly with increasing "inactive" metal atom fraction. The rates of aromatization on the (100) alloy surfaces showed the same inhibition as was observed for the (111) alloy surfaces.

The dependence of the selectivity of the reaction on the alloy surface composition is shown in Fig. 5.3 and 5.4. By looking at the selectivity, the relative rates of the reaction can be compared regardless of the overall activity of the catalyst. The selectivity for the (111) alloy surfaces is shown in Fig. 5.3. As can be seen, the selectivity behavior for the (111) surfaces of the Cu-Pt and Au-Pt alloys was nearly identical, in contrast to the

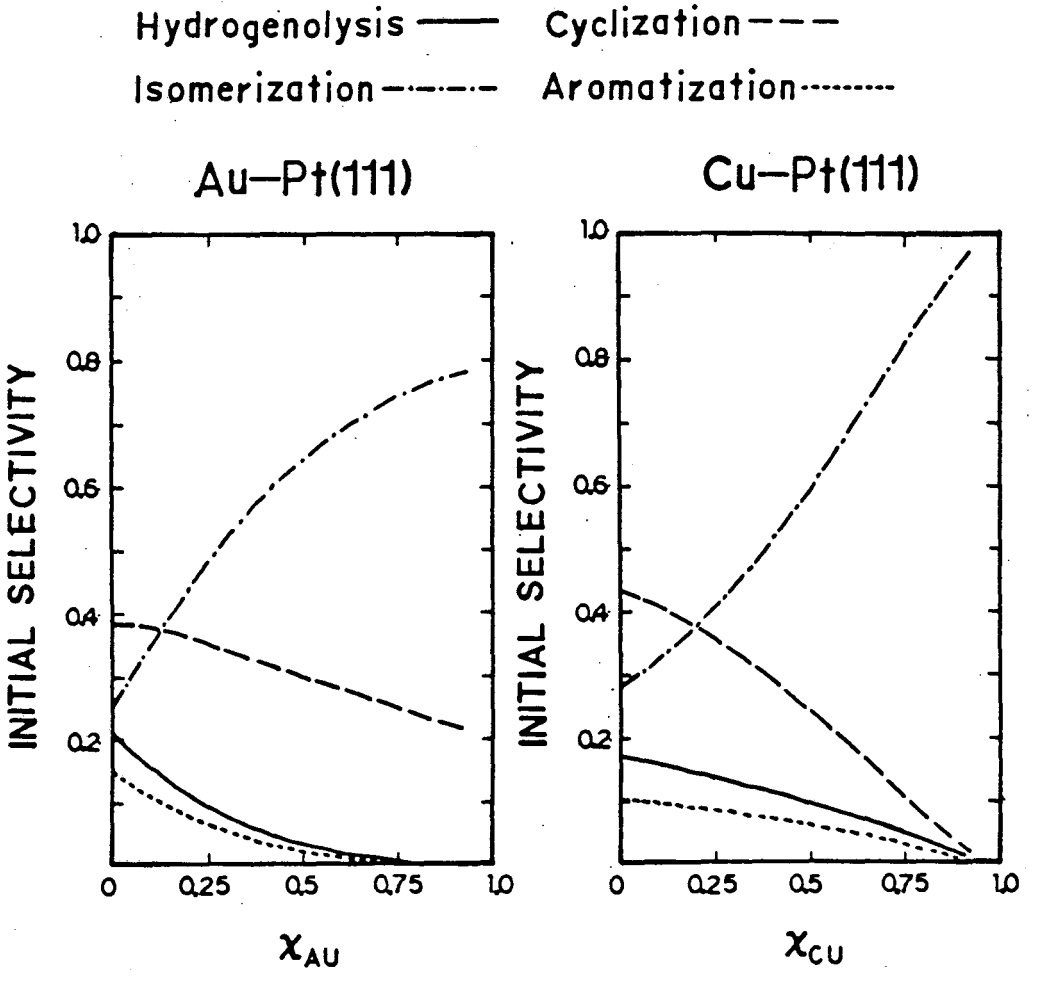

FIG. 5.3

Initial selectivities of the n-hexane conversion reaction over Au-Pt(111) and Cu-Pt(111) alloy surfaces as a function of the IB metal surface atom fraction.

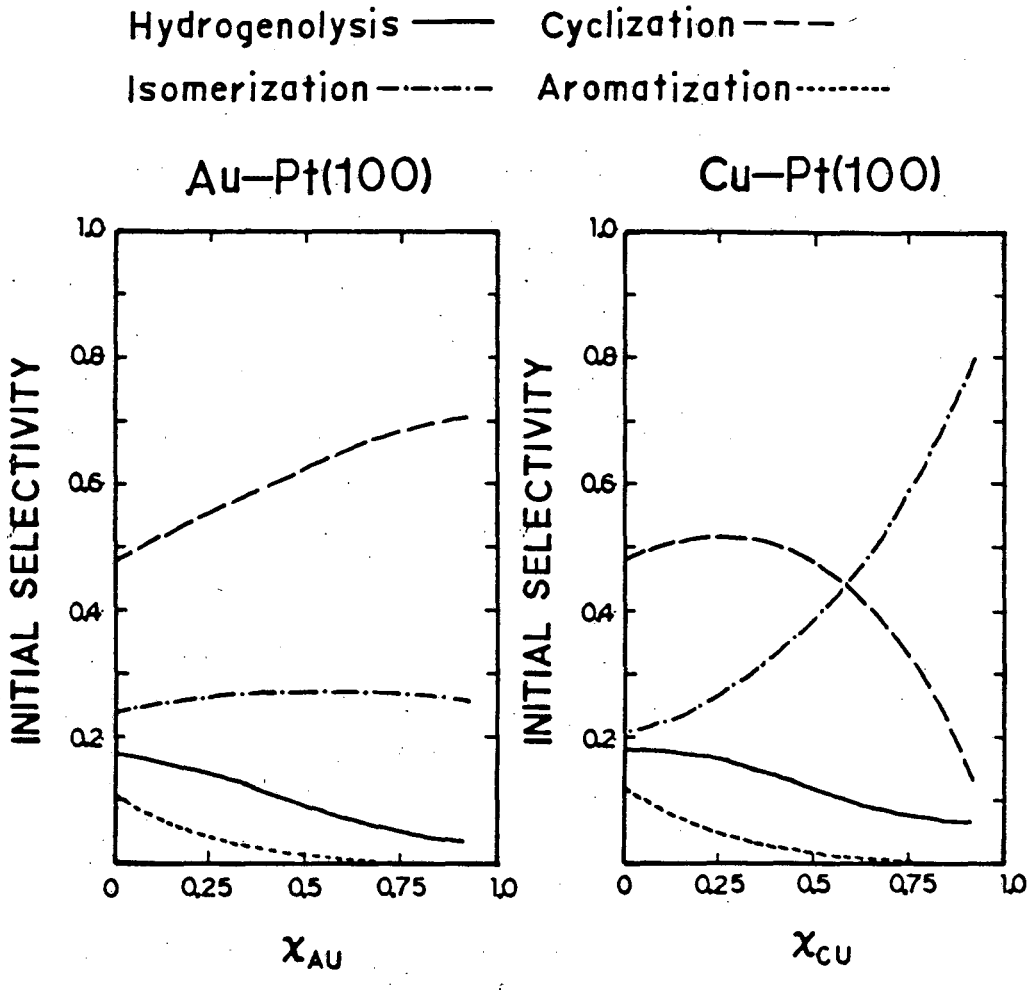

FIG. 5.4

Initial selectivities of the n-hexane conversion reaction over Au-Pt(100) and Cu-Pt(100) alloy surfaces as a function of the IB metal surface atom fraction.

differences observed for the initial rates themselves. On both the alloys, the selectivity for isomerization increased dramatically with increasing IB metal atom fraction at the expense of the cyclization, hydrogenolysis, and aromatization selectivities.

The (100) alloy surfaces displayed the same trends in selectivity at low IB metal atom fraction. As the IB metal atom fraction was increased, however, the selectivity for isomerization on the Au-Pt alloy leveled off, but continued to increase on the Cu-Pt alloy. Also, the selectivity for cyclization continued to increase on the Au-Pt alloy with increasing gold atom fraction, while on the Cu-Pt alloy, increasing the copper atom fraction resulted in a sharp decrease in the cyclization selectivity. The trend in the selectivity for hydrogenolysis and aromatization was to decrease with increasing IB metal atom fraction.

In Fig. 5.5, the total initial rate of n-hexane conversion over the (111) alloy surfaces is shown as a function of the IB metal atom fraction. The Au-Pt alloys showed a positive deviation from the linear (an enhancement in the rate per platinum atom) while the Cu-Pt alloys showed a negative deviation from a linear decrease (an inhibition of the rate per platinum atom). The total initial rates for the (100) alloy surfaces, shown in Fig. 5.6, decreased nearly linearly with increasing IB metal atom fraction.

In order to see the effect alloying had on the rate of poisoning of the catalyst (due to a carbonaceous deposit),

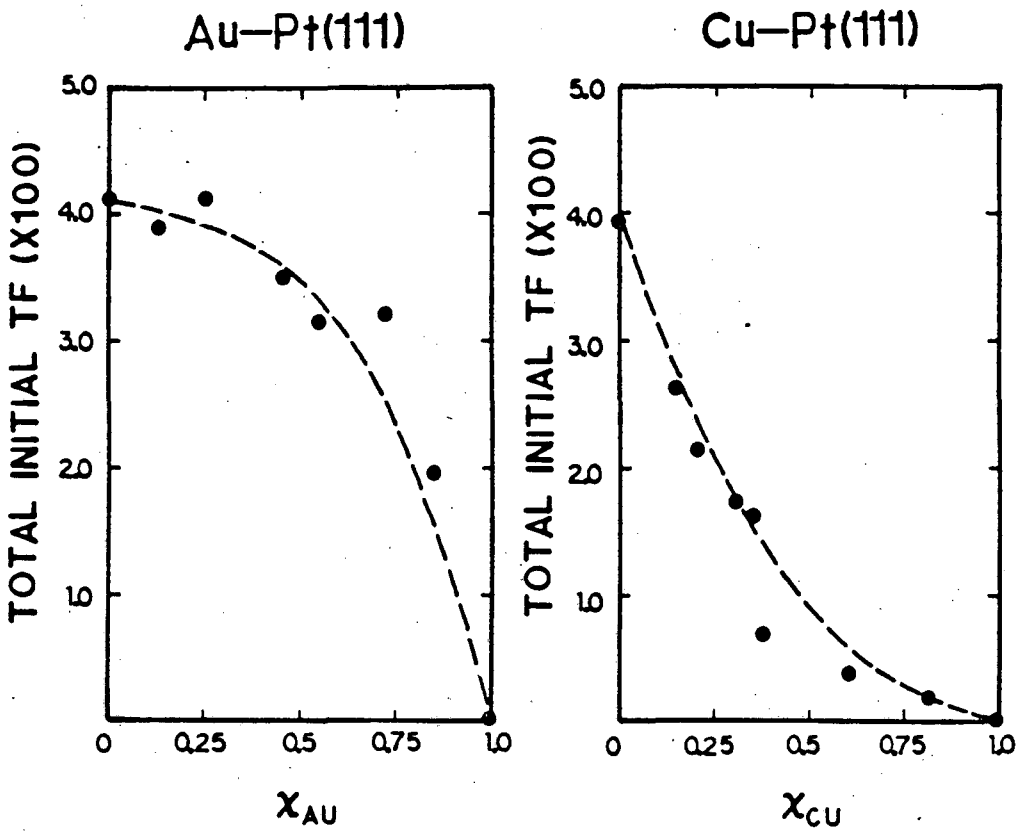

FIG. 5.5

Total initial turnover frequency of the n-hexane conversion reaction over Au-Pt(111) and Cu-Pt(111) alloy surfaces as a function of the IB metal surface atom fraction.

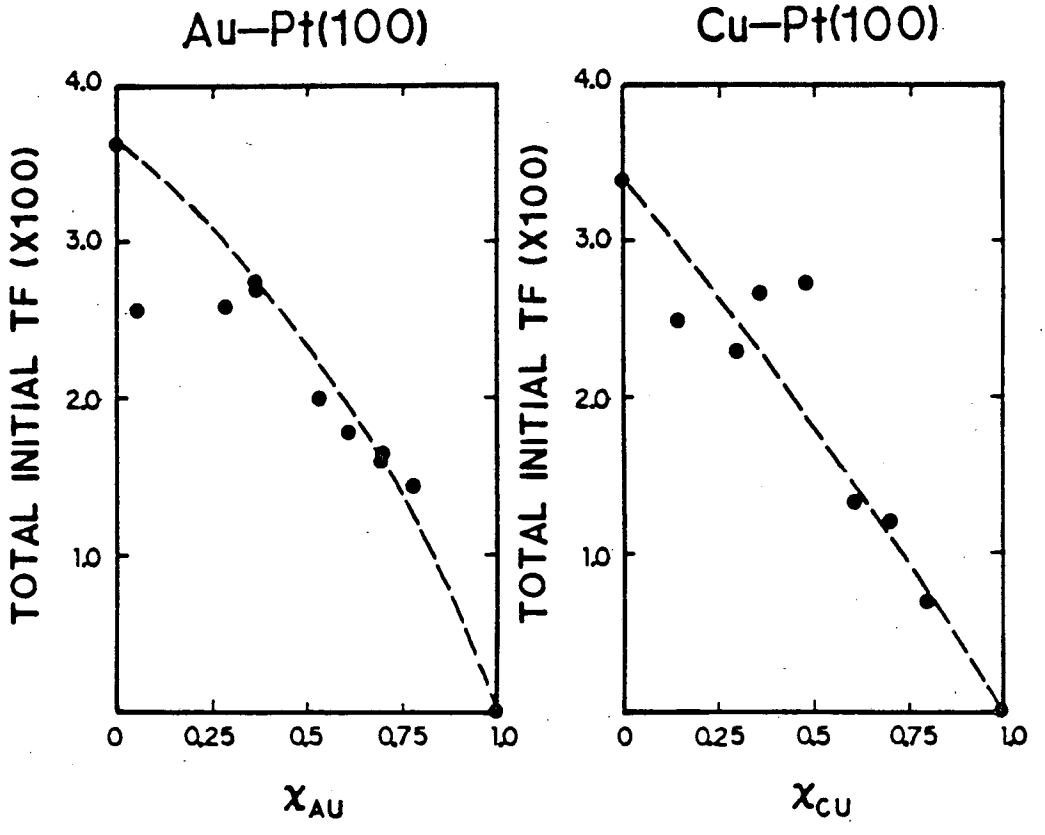

FIG. 5.6

Total initial turnover frequency of the n-hexane conversion reaction over Au-Pt(100) and Cu-Pt(100) alloy surfaces as a function of the IB metal surface atom fraction.

the total turnover number of the n-hexane conversion reaction is plotted versus the IB metal atom fraction for the (111) and (100) alloy surfaces in Fig. 5.7 and Fig. 5.8 respectively. The major effect seen here is the large enhancement on the Au-Pt(111) alloy surface. The behavior of the other alloy surfaces was nearly the same as that seen for the initial rates.

The initial selectivities for the hydrogenolysis products over the Pt(111) and Pt(100) surfaces are shown in Fig. 5.9. Alloying the platinum with gold and copper resulted in a slight decrease in the selectivity for methane and an increase in the C_3 selectivity.

The ratio of 2-methylpentane to 3-methylpentane as a function of copper atom fraction for the (100) and (111) alloy surfaces is shown in Fig. 5.10. The ratio showed a tendency to decrease at higher copper atom fractions.

The trans-2-hexene production was also monitored. Its concentration had nearly reached a maximum by the time the first sample was taken. No information, therefore, about the initial rate of dehydrogenation was available. The maximum turnover number of trans-2-hexene achieved during a reaction is plotted in Fig. 5.11 as a function of copper atom fraction for the (100) and (111) surfaces of the Cu-Pt alloys. The maximum turnover went through a maximum at 0.5 copper atom fraction on the (100) alloy surface and at about 0.65 copper atom fraction on the (111) alloy surface. No correlation was

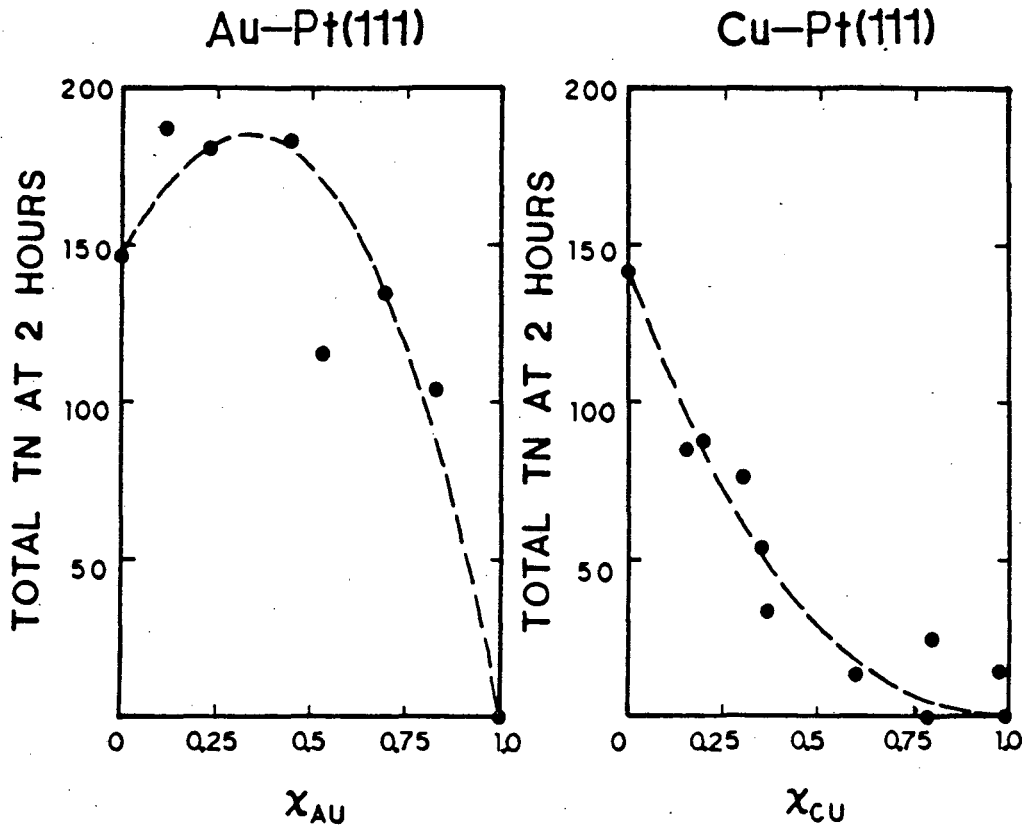

FIG. 5.7

Total turnover number at 2 hours of the n-hexane conversion reaction over Au-Pt(111) and Cu-Pt(111) alloy surfaces as a function of the IB metal surface atom fraction.

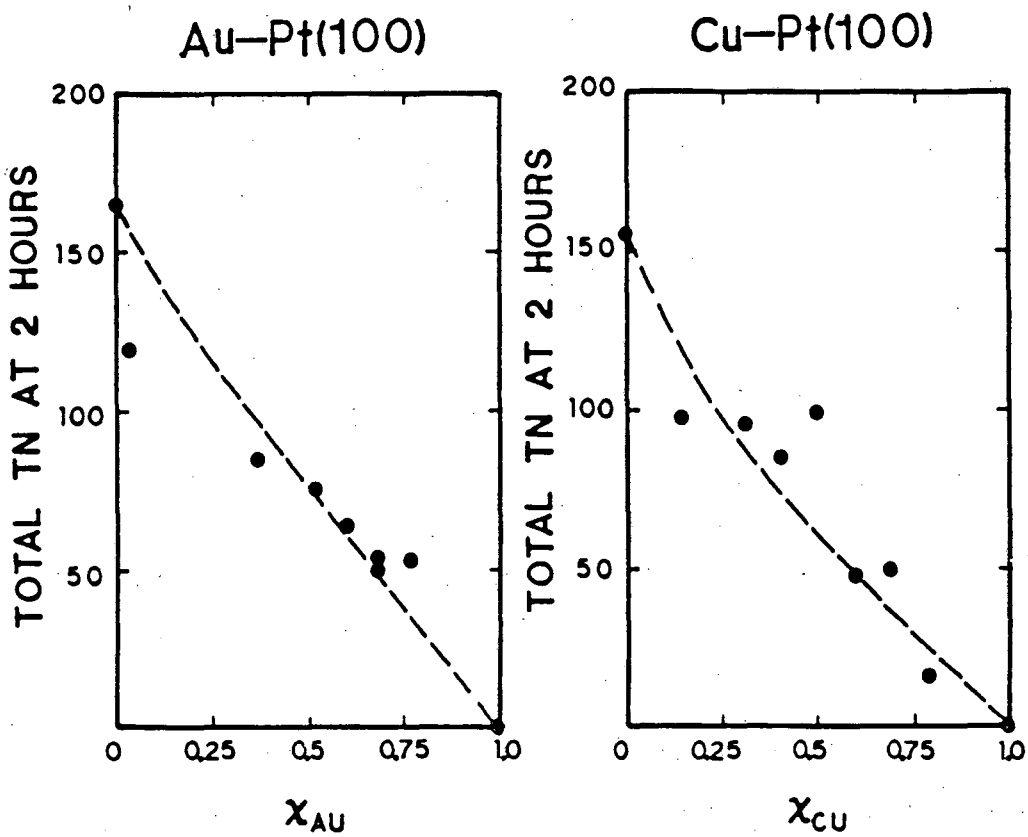

FIG. 5.8

Total turnover number at 2 hours of the n-hexane conversion reaction over Au-Pt(100) and Cu-Pt(100) alloy surfaces as a function of the IB metal surface atom fraction.

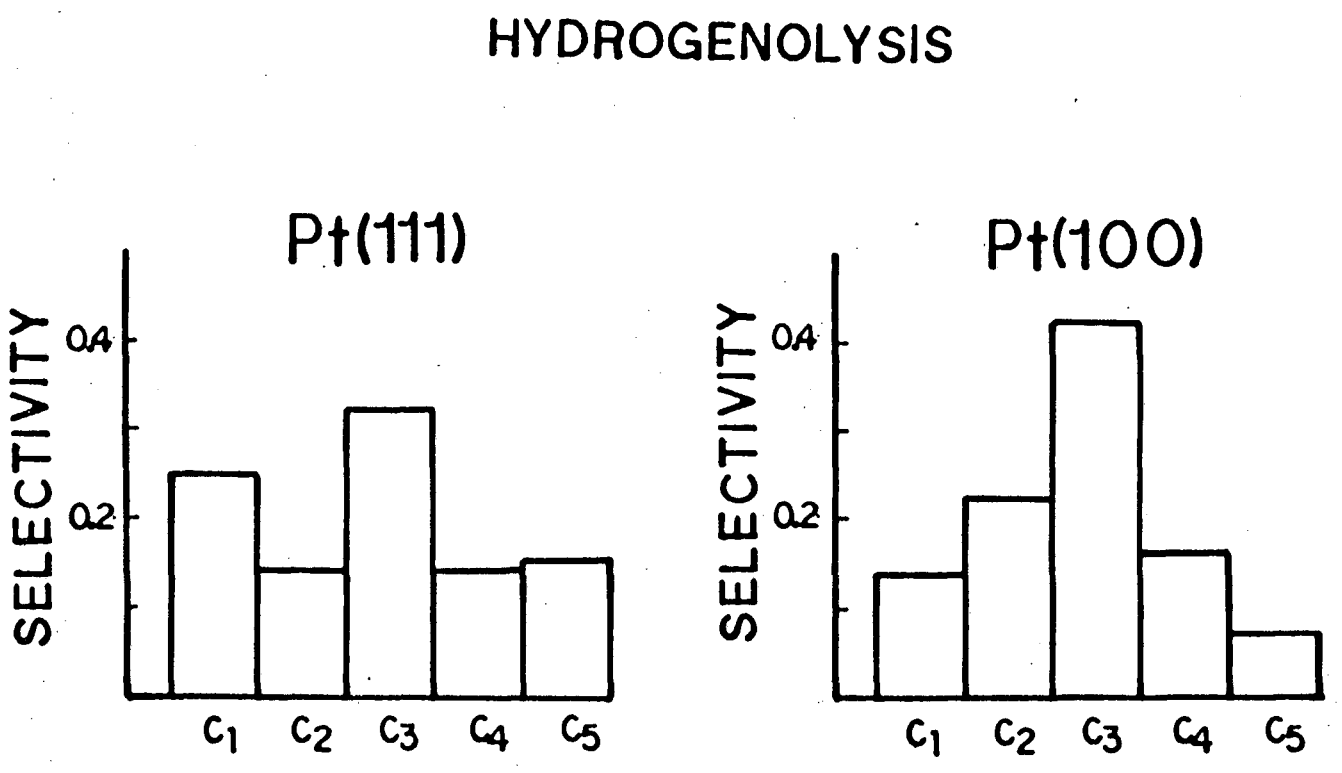

FIG. 5.9

Initial hydrogenolysis product distribution for the Pt(111) and Pt(100) surfaces.

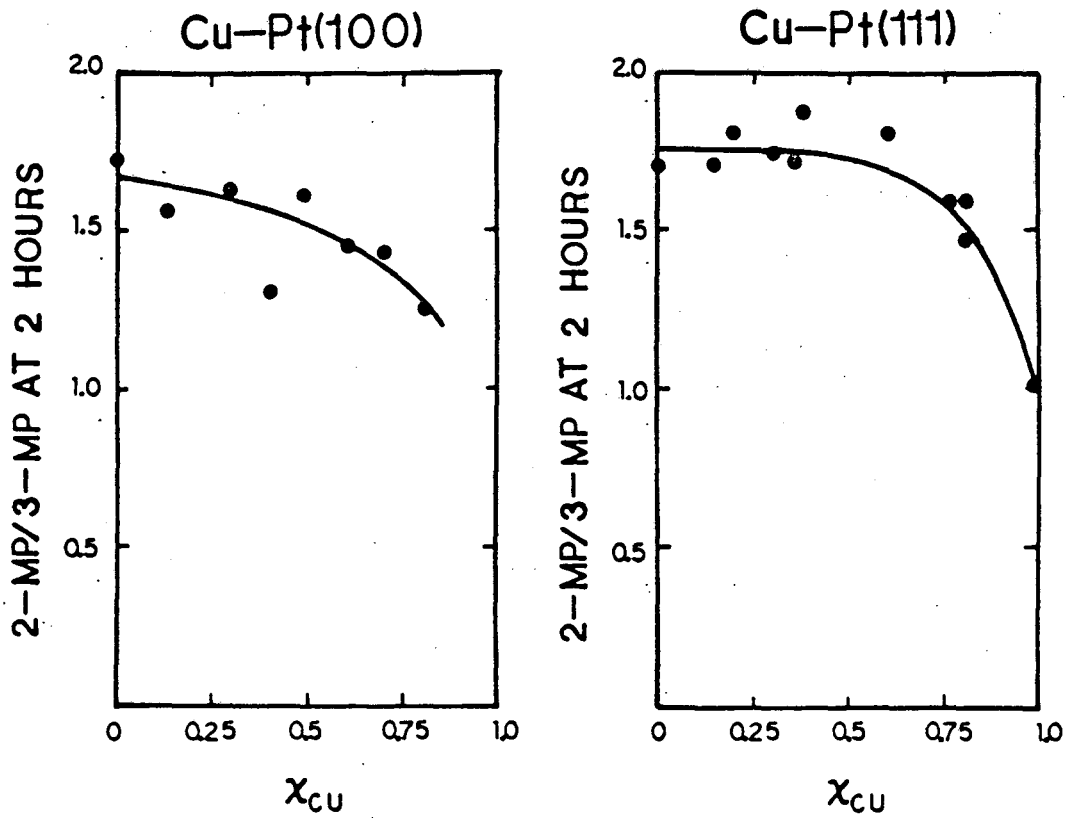

FIG. 5.10

The ratio of 2-methylpentane to 3-methylpentane at 2 hours as a function of the copper surface atom fraction for the Cu-Pt(100) and Cu-Pt(111) alloy surfaces.

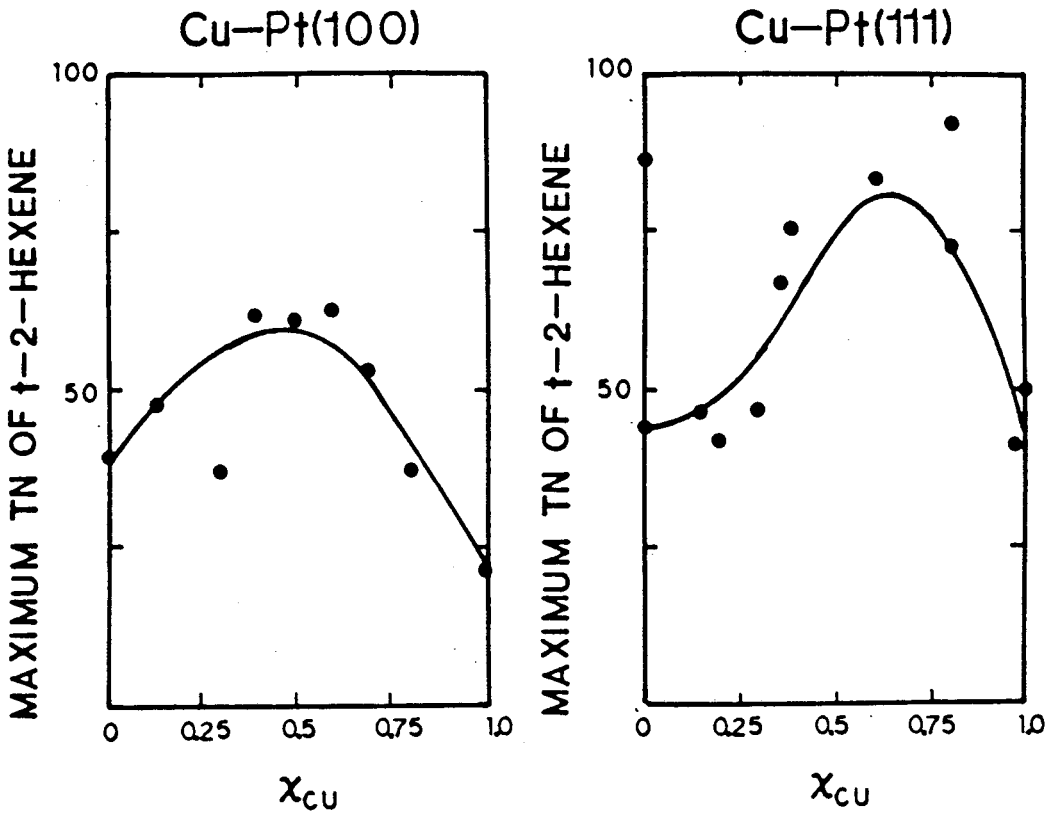

FIG. 5.11

Maximum turnover number of trans-2-hexene observed during the n-hexane conversion reaction as a function of copper surface atom fraction for the Cu-Pt(100) and Cu-Pt(111) alloy surfaces.

found between the rate of dehydrogenation and the rate of the other reaction studied here [5.16].

C. DISCUSSION

1. Activity of alloy sites

In order to understand the effect alloying platinum with gold or copper has on the local activity and selectivity of platinum, the data shown in Fig. 5.1, 5.2 and 5.5 - 5.8 were fit to the site distributions shown in Fig. 5.12 and Fig. 5.13. The 3-fold site was considered for the (111) alloy surfaces and the 4-fold site for the (100) alloy surfaces. It must be stressed here that this model simply provides a means to quantify the trends observed and does not necessarily define exactly what is happening on the surface during the reaction. The solid lines drawn through the data points in these figures are the result of the fit. The rates of hydrogenolysis, cyclization, isomerization and aromatization on the (111) alloy surfaces at 3-fold sites containing 3, 2 and 1 platinum atoms obtained by the fit are shown in Table 5.1. The rates of these reactions for the (100) alloy surfaces at 4-fold sites containing 4, 3, 2 and 1 platinum atoms obtained by the fit are shown in Table 5.2. A site which contained only copper or gold atoms was assumed to be inactive in all cases. To make interpretation of the data easier, the rates per platinum atom at the various sites relative to the rate at a site containing only platinum atoms are shown in Table 5.3 for the (111) alloy surfaces and in Table 5.4 for the (100) alloy surfaces. In Tables 5.3 and 5.4, values greater the 1.0 are indicative of an activity

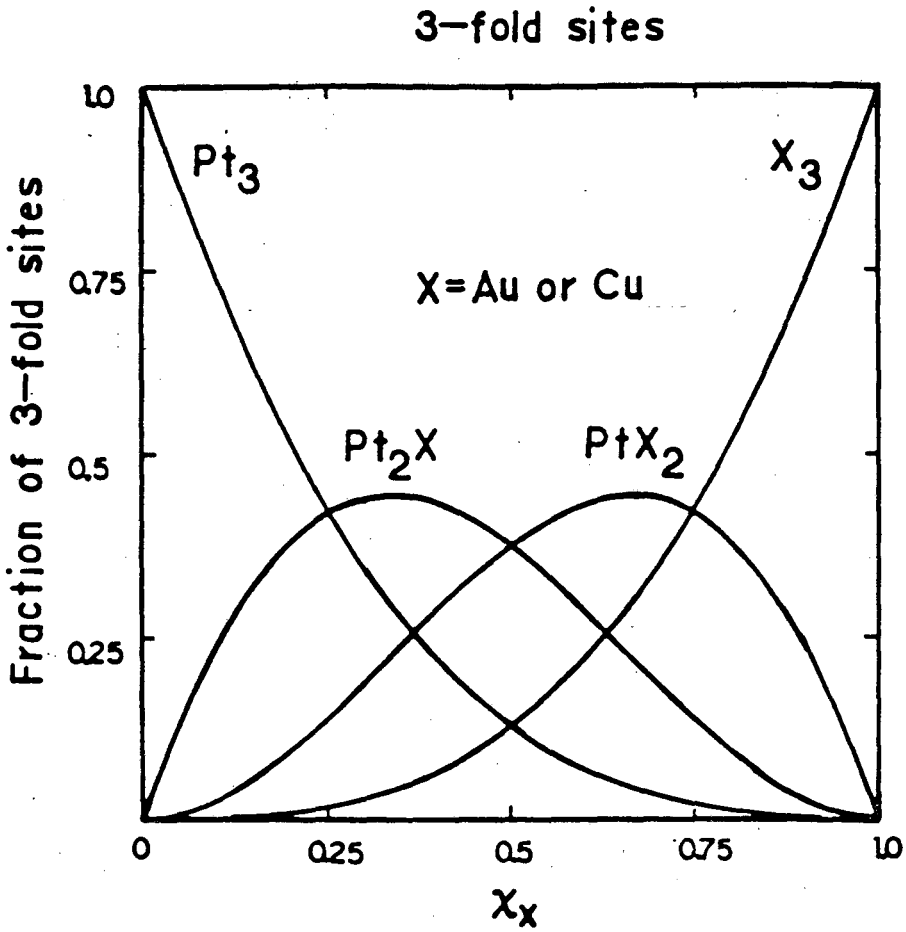

FIG. 5.12

Fraction of 3-fold sites containing 3, 2, 1 and 0 platinum atoms as a function of the IB metal surface atom fraction. Distributions are for a random alloy surface.

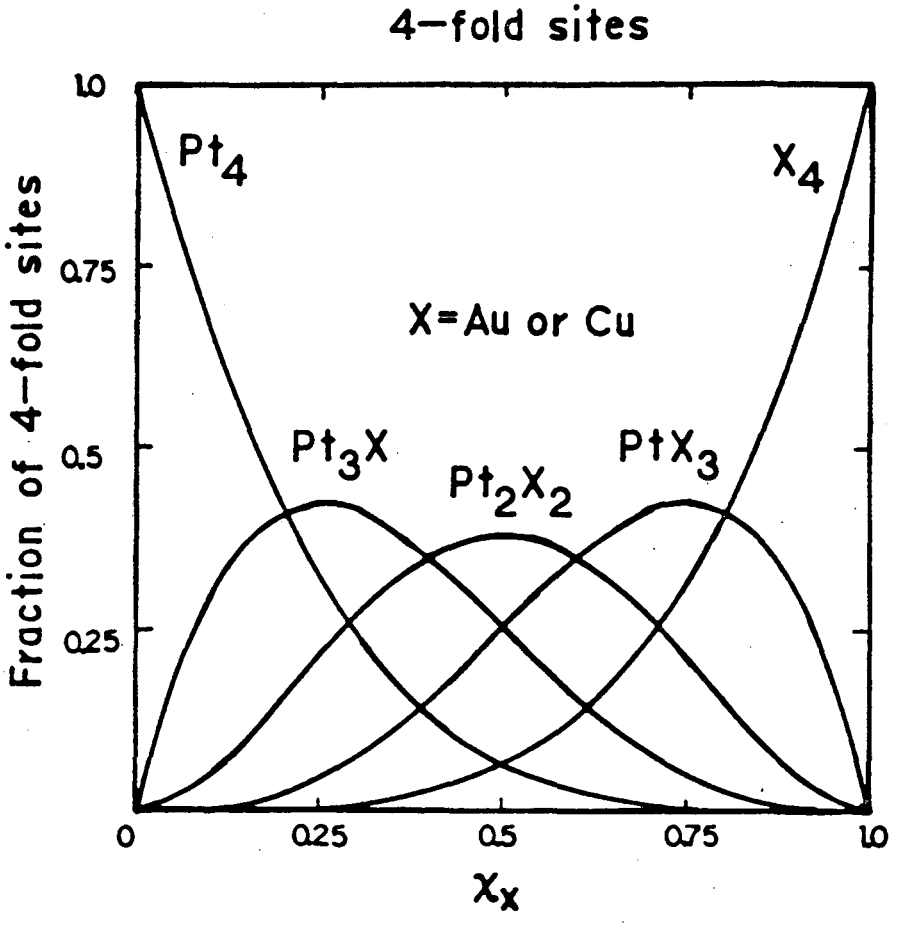

FIG. 5.13

Fraction of 4-fold sites containing 4, 3, 2, 1 and 0 platinum atoms as a function of the IB metal surface atom fraction. Distributions are for a random alloy surface.

TABLE 5.1

(111) ALLOY SURFACES

ALLOY	REACTION	Initial rate (X100) at a 3-fold site containing : 3 Pt atoms	2 Pt atoms	1 Pt atom
	Hydrogenolysis			
Au-Pt		8.68	0.0	0.0
Cu-Pt		6.83	0.0	0.0
	Cyclization			
Au-Pt		15.81	13.75	8.5
Cu-Pt		17.5	0.0	0.0
	Isomerization			
Au-Pt		10.39	24.0	32.0
Cu-Pt		11.25	8.45	1.89
	Aromatization			
Au-Pt		6.1	0.0	0.0
Cu-Pt		4.28	0.0	0.0
	Total rate			
Au-Pt		40.98	37.75	40.5
Cu-Pt		39.86	8.45	1.89

TABLE 5.2

(100) ALLOY SURFACES

ALLOY	REACTION	Initial rate (X100) at a 4-fold site containing : 4 Pt atoms	3 Pt atoms	2 Pt atoms	1 Pt atom
	Hydrogenolysis				
Au-Pt		6.2	4.65	3.1	1.55
Cu-Pt		6.2	4.65	3.1	1.55
	Cyclization				
Au-Pt		17.5	17.5	15.0	11.2
Cu-Pt		16.4	14.0	9.0	0.0
	Isomerization				
Au-Pt		8.7	8.7	6.0	4.0
Cu-Pt		6.8	6.8	6.8	6.8
	Aromatization				
Au-Pt		3.9	0.0	0.0	0.0
Cu-Pt		4.1	0.0	0.0	0.0
	Total rate				
Au-Pt		36.3	32.4	22.9	17.1
Cu-Pt		33.5	27.0	17.8	8.8

TABLE 5.3

(111) ALLOY SURFACES

ALLOY	REACTION	Relative initial rate per Pt atom at a 3-fold site containing : 3 Pt atoms	2 Pt atoms	1 Pt atom
	Hydrogenolysis			
Au-Pt		1.0	0.0	0.0
Cu-Pt		1.0	0.0	0.0
	Cyclization			
Au-Pt		1.0	1.3	1.62
Cu-Pt		1.0	0.0	0.0
	Isomerization			
Au-Pt		1.0	3.64	9.24
Cu-Pt		1.0	1.12	0.51
	Aromatization			
Au-Pt		1.0	0.0	0.0
Cu-Pt		1.0	0.0	0.0
	Total rate			
Au-Pt		1.0	1.16	2.49
Cu-Pt		1.0	0.32	0.15
	$(1 - X)^3$	1.0	0.0	0.0
	$(1 - X)^2$	1.0	0.5	0.0
	$(1 - X)$	1.0	1.0	1.0

TABLE 5.4

(100) ALLOY SURFACES

ALLOY	REACTION	Relative initial rate per Pt atom at a 4-fold site containing : 4 Pt atoms	3 Pt atoms	2 Pt atoms	1 Pt atom
	Hydrogenolysis				
Au-Pt		1.0	1.0	1.0	1.0
Cu-Pt		1.0	1.0	1.0	1.0
	Cyclization				
Au-Pt		1.0	1.31	1.72	2.56
Cu-Pt		1.0	1.13	1.10	0.0
	Isomerization				
Au-Pt		1.0	1.33	1.38	1.84
Cu-Pt		1.0	1.33	2.0	4.0
	Aromatization				
Au-Pt		1.0	0.0	0.0	0.0
Cu-Pt		1.0	0.0	0.0	0.0
	Total rate				
Au-Pt		1.0	1.19	1.26	1.88
Cu-Pt		1.0	1.08	1.20	0.88
	$(1 - X)^4$	1.0	0.0	0.0	0.0
	$(1 - X)^2$	1.0	0.67	0.33	0.0
	$(1 - X)$	1.0	1.0	1.0	1.0

greater than that obtained for the pure platinum surface, values less than 1.0 indicate an inhibition, and values equal to 1.0 indicate an activity which depends only on the number of platinum atoms on the surface, independent of their geometry.

To illustrate this point, Fig. 5.14 shows the behavior of the relative rate as a function of the atom fraction of the IB metal when a reaction on the (111) alloy surface requires 3 platinum atom, 2 platinum atoms or 1 platinum atoms. When a reaction requires 3 platinum atoms, the rate falls off as the third power of the platinum atom fraction, and linearly if only 1 platinum atom is required. If a reaction required a site containing 3 platinum atoms, a fit of the rates to the distribution of sites would give relative rates per platinum atom of 1.0, 0.0 and 0.0 for sites containing 3, 2 and 1 platinum atoms respectively. The result of a fit of these three examples is shown at the bottom of Table 5.3. It can be seen from these examples that any value greater than 1.0 for the relative rate per platinum atom indicates a rate which is enhanced over the rate at a pure platinum site. Fig. 5.15 illustrates this point for the 4-fold site fit of the rates on the (100) alloy surfaces. The rate of a reaction which required 4 platinum atoms would decrease as the forth power of the platinum atom fraction. A reaction which required only a single platinum atom would decrease linearly with increasing IB metal atom fraction as was the case for the (111) surface. The relative

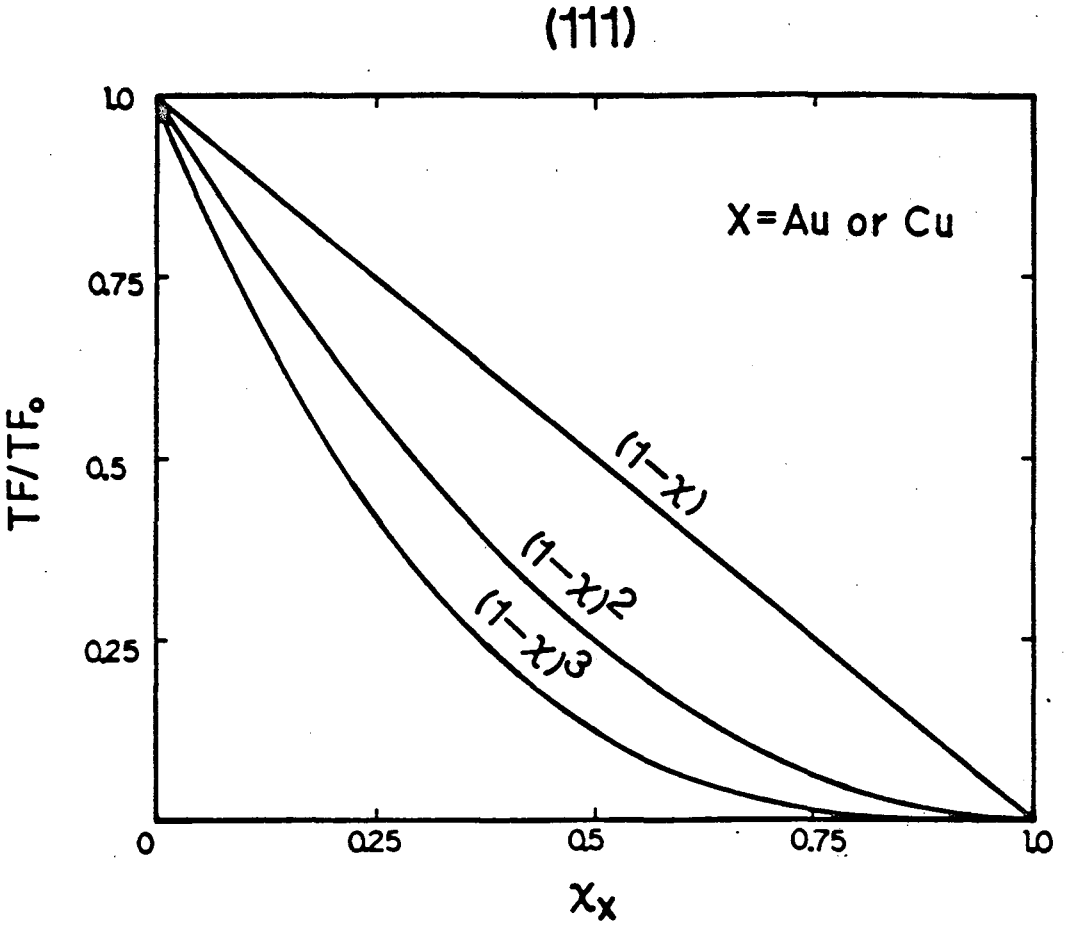

FIG. 5.14

Dependence of the initial turnover frequency relative to the initial turnover frequency of a pure Pt(111) surface as a function of IB metal surface atom fraction for a reaction which requires ensembles of one [$(1 - X)$], two [$(1 - X)^2$] and three [$(1 - X)^3$] platinum atoms.

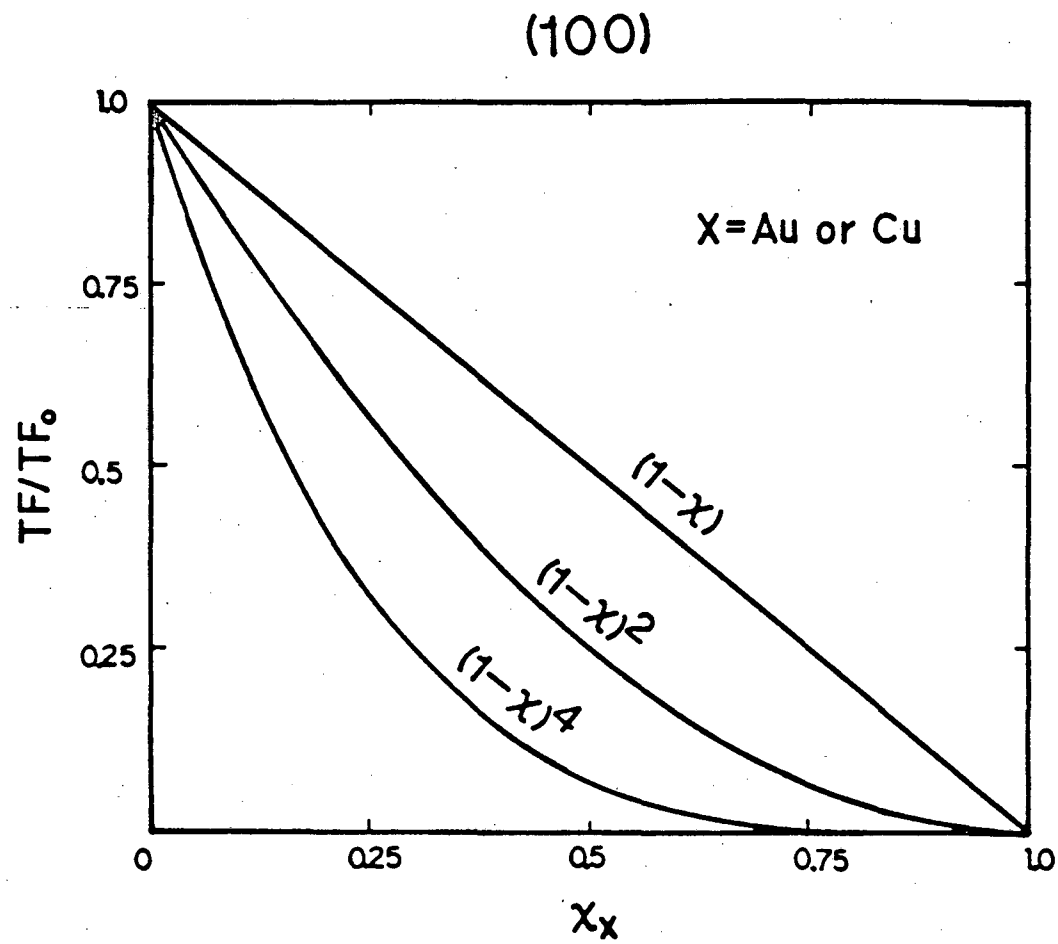

FIG. 5.15

Dependence of the initial turnover frequency relative to the initial turnover frequency of a pure Pt(100) surface as a function of IB metal surface atom fraction for a reaction which requires ensembles of one [$(1 - X)$], two [$(1 - X)^2$] and four [$(1 - X)^4$] platinum atoms.

rates per platinum atom for sites containing 4, 3, 2 and 1 platinum atoms which would be obtained by fitting these examples to the 4-fold site distributions are shown at the bottom of Table 5.4.

The values obtained for the relative rates per platinum atom for the various 3-fold sites on the (111) alloy surfaces indicate that the hydrogenolysis reaction required three platinum atoms. Replacing one platinum atom in a 3-fold site with a gold or copper atom resulted in the poisoning of that of that site for the hydrogenolysis reaction. A 3-fold site which contained 1 or 2 gold atoms had a greater activity for cyclization per platinum atom than a site which contained 3 platinum atoms. Copper, on the hand, poisoned the site for cyclization. The greatest effect was seen for isomerization on the Au-Pt(111) surfaces where the per platinum atom rate at a 3-fold site containing 2 gold atoms and 1 platinum atom was nine times greater than that for the pure platinum site. The effect of the addition of copper was quite different. A site containing 2 copper atoms was only half as active (per platinum atom) as the pure platinum site. The aromatization reaction was poisoned by the addition of 1 gold or copper atom to a 3-fold site. The overall rate showed an enhanced rate per platinum atom for the Au-Pt alloy. A 3-fold site which contained 2 gold atoms was 2.5 times as active as a pure platinum site. The addition of copper, however, resulted in an overall inhibition in the rate per platinum.

A site which contained 2 copper atoms showed very little overall activity.

The values obtained for the rates of various 4-fold sites on the (100) alloy surfaces indicate that hydrogenolysis required only a single platinum atom whereas on the (111) surface it required 3 platinum atoms. The cyclization reaction was slightly enhanced by the addition of gold. The addition of copper resulted in little enhancement, and a site which contained 3 copper atoms was inactive for cyclization. The isomerization reaction was enhanced only slightly by the addition of gold to the (100) surface, in contrast to the striking enhancement observed for the Au-Pt(111) system. The addition of copper resulted in a larger enhancement on this surface than the addition of gold, the reverse of the findings for the (111) alloy surfaces. The aromatization reaction rate was strongly inhibited by the addition of gold or copper, with the site being poisoned by the addition of 1 copper or gold atom. This result is similar to the behavior found for the (111) alloy surfaces. The overall rate showed a slight enhancement for the Au-Pt system and a very slight inhibition for the Cu-Pt system. The magnitude of both effects was smaller then those on the (111) alloy surfaces.

The initial rates <u>per platinum atom</u> determined from the fit of the experimental data to the site distributions as a function of the IB metal atom fraction are shown for the hydrogenolysis and cyclization reactions in Fig. 5.16 and for

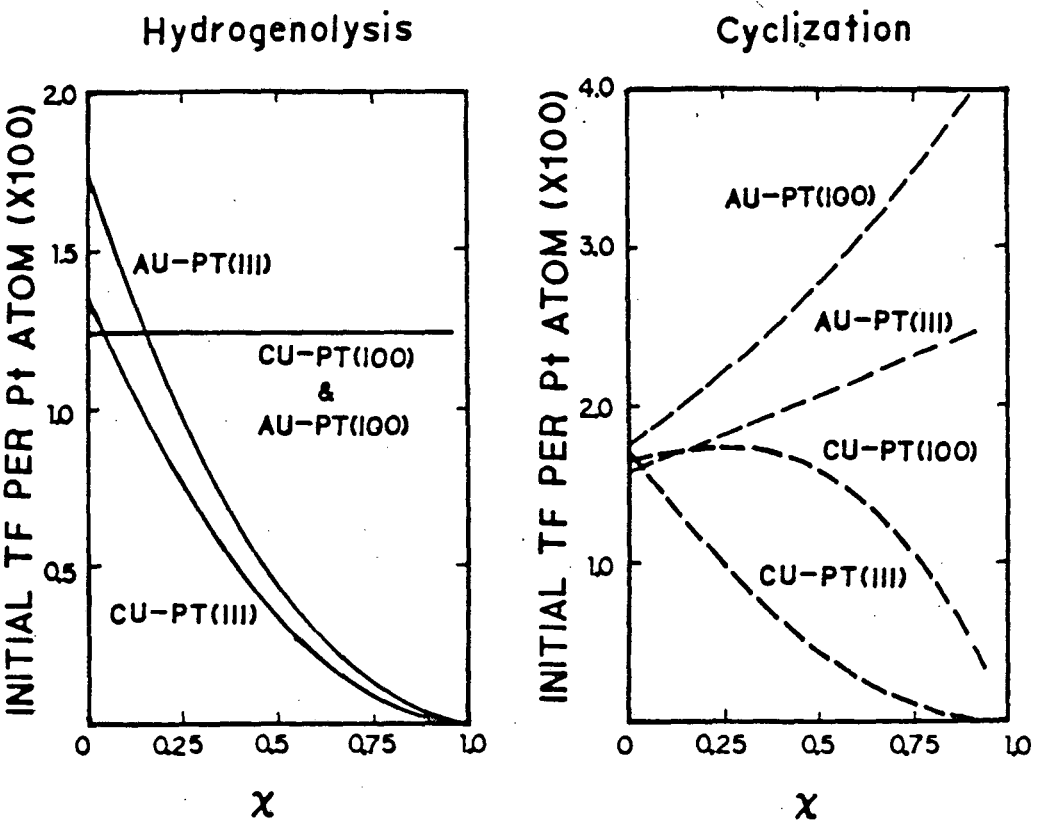

FIG. 5.16

Initial turnover frequencies per platinum atom of hydrogenolysis and cyclization as a function of IB metal surface atom fraction.

the isomerization and aromatization reactions in Fig. 5.17. These figures give another perspective of the trends discussed above.

2. Mechanistic implications

As the preceding discussion clearly indicates, the effect alloying platinum with an "inactive" IB metal has on the activity and selectivity of the n-hexane conversion reaction is strongly dependent on the crystallographic orientation of the alloy surface and on the IB metal itself. It is not surprising then that studies of the n-hexane conversion reaction over supported Pt-IB metal alloys would yield conflicting results. The most widely used explanation the catalytic behavior of these alloys is the "ensemble effect" [5.8 - 5.11]. It is believed that a particular reaction requires a specific number of platinum atoms on which to occur and that this number, or "ensemble size", is varies from reaction to reaction. By alloying the platinum surface with an inactive metal, the platinum is diluted and the average ensemble size decreased. Thus, the alloying blocks reactions which require relatively large ensemble while allowing reactions which require smaller ensembles to occur. This argument completely ignores any participation of the "inactive" metal atoms in the reaction and any electronic changes induced in the platinum by the presence of the "inactive" metal.

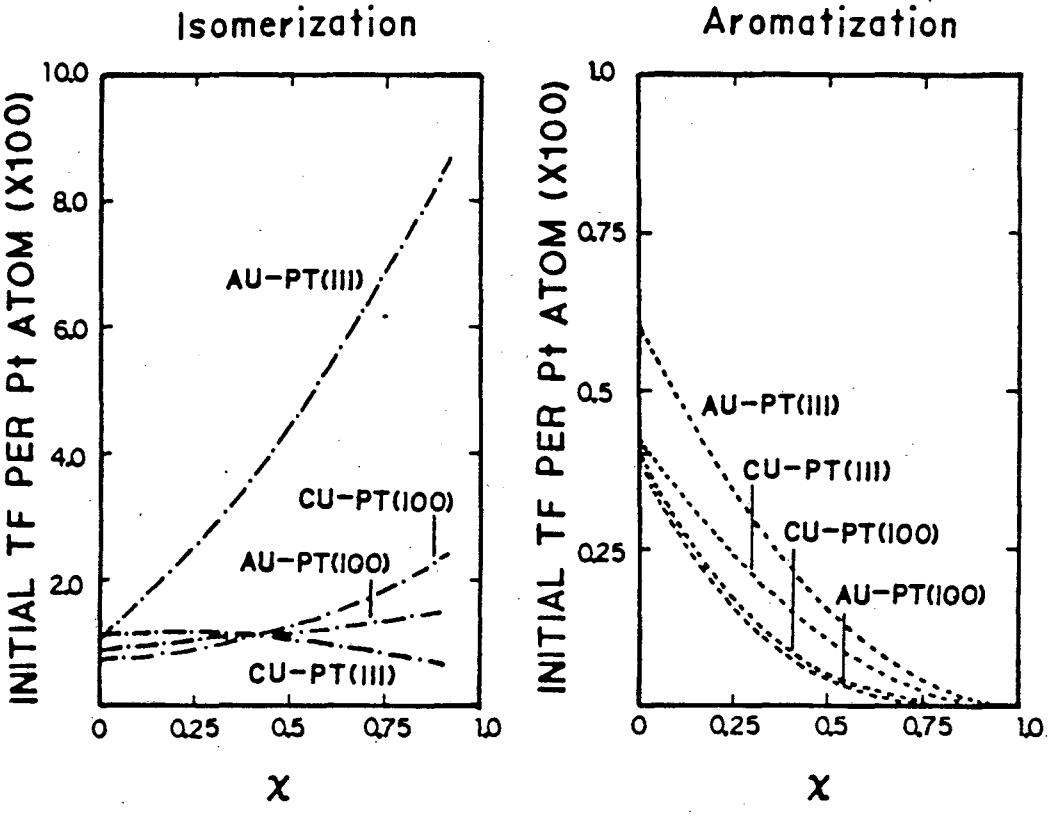

FIG. 5.17

Initial turnover frequencies per platinum atom of isomerization and aromatization as a function of IB metal surface atom fraction.

Several mechanisms have been proposed for each of the products of the platinum catalyzed n-hexane conversion reaction. Since the reactions presented in this report were all carried out at a temperature of 570 K and a total pressure of 220 torr with a n-hexane/hydrogen ration of 1/10, no kinetic data besides the individual rates at a given surface composition are available. The results, however, can be discussed in terms of the mechanisms which have been proposed by other authors.

a) Hydrogenolysis

The most widely accepted intermediate for hydrogenolysis reaction of longer chain hydrocarbons is a 1,1,3 or 1,3,3 tri-adsorbed species [5.1, 5.17 - 5.18]. Evidence presented by Leclercq et. al. [5.18] indicates that C-C bonds contiguous to the multiple carbon-metal (C-M) bonds are broken with a higher probability than C-C bonds next to a single C-M bond. These authors point out that 1,4 and 1,5 bound species may also play a role in C-C bond breaking.

The hydrogenolysis of n-hexane clearly requires three platinum atoms to occur on the (111) alloy surfaces. This result would indicate that the 1,1,3 tri-adsorbed intermediate exists at a 3-fold site on the (111) surface and that even if it forms on a single platinum atom, no C-C bonds are broken. It may be that the intermediate is adsorbed at a 3-fold site on the alloy surface, but the weaker bonding of the IB metal results in no C-C bond breaking. The linear decrease in the initial hydrogenolysis rate for the (100)

alloy surfaces, however, indicates that hydrogenolysis can occur on a single platinum atom on the (100) surface. On this surface, a 1,4 diadsorbed species species may become important [5.19]. Davis and co-workers reported a 1,3 diadsorbed species which formed on a single platinum at over the Pt(100) surface in the isomerization reaction of C_4 hydrocarbons [5.20]. This intermediate did not form on a single platinum atom of the Pt(111) surface. Since the (100) surface is a more open surface than the (111) surface, second layer atoms may also be involved in the formation of this intermediate. These trends are seen clearly in Fig. 5.16. The ability of this intermediate to form on a single atom of the Pt(100) surface and not on the Pt(111) surface is due to the difference in the d-orbital geometries. The Pt(100) surface has one d-orbital lobe protruding perpendicular to the surface and four lobes at 45 degrees to the surface. This geometry apparently favors the formation of the 1,3 diadsorbed species and the subsequent breaking of a carbon-carbon bond.

Results reported by Clarke, Kane and Baird (CKB) [5.19] and by van Schaik, Dressing and Ponec (SDP) [5.21] for the hydrogenolysis of n-hexane over silica-supported Au-Pt alloys show a strong inhibition similar to the Au-Pt(111) alloy surfaces. The results of de Jongste, Kuijers and Ponec (JKP) [5.22] for a silica-supported Cu-Pt alloy showed an increase in the hydrogenolysis selectivity, which is in conflict with the results reported here.

b) Cyclization

The intermediate for the cyclization reaction is generally believed to be a 1,1,5 tri-adsorbed species [5.23 - 5.24] which can be bound to one or more platinum atoms. The 5-member ring is formed by the formation a bond between the carbon atoms bound to the metal.

The rate of cyclization on the Au-Pt(111) alloy surfaces decreases nearly linearly with increasing gold atom fraction showing only a slight enhancement. This result indicates that only one platinum atom is needed for the cyclization reaction. In contrast to this, cyclization on the Cu-Pt(111) surfaces shows a poisoning of the reaction when one copper atom is included in a 3-fold site. These results can only be explained by the differing effects the IB metal has on the platinum in the alloy. As shown in chapter III, copper modifies the electronic structure of platinum. The results presented in chapter IV showed no change in the electronic structure of platinum in the Au-Pt alloys. This result has also been shown by the thermal desorption of CO for the Au-Pt alloys [5.16]. The strong inhibition of the cyclization reaction over the Cu-Pt alloy surfaces is due to the electronic modification of platinum [5.25] by the presence of the copper. This electronic effect is also manifest on the (100) alloy surfaces. Fig. 5.16 clearly shows that the cyclization rate per platinum atom is inhibited by copper and promoted by gold.

c) Isomerization

There are two classes of mechanisms which are thought to occur for isomerization. The bond shift mechanism is believed to involve a 1,1,3 tri-adsorbed intermediate [5.17, 5.26] or a σ-alkyl adsorbed radical intermediate. The cyclic mechanism involves the same intermediate as the cyclization reaction. In this mechanism, the ring closure is followed by ring opening. Three types of ring opening have been proposed by Gault and his co-workers : a nonselective ring opening, which results in a 1:2:2 ratio of 3-MP:2-MP:n-hexane; a selective ring opening where the ring is not opened at the carbon bound to the methyl group, which results in a 1:2 ratio of 3-MP:2-MP; and a partly selective ring opening where the ring can be opened at the carbon bound to the methyl group but with a lower probability than at the other C-C bonds.

O'Cinneide and Gault [5.27] claim that the isomerization of n-hexane over an alumina supported 15 % Pt-85 % Au alloy proceeds exclusively via the non-selective ring opening mechanism. They observed an increase in the cyclization selectivity and a decrease on the isomerization selectivity compared to the pure platinum catalyst. These results are similar to the results reported here for the Au-Pt(100) alloy surfaces (Fig. 5.4).

The isomerization selectivity over the Au-Pt(111) and Cu-Pt(111) alloy surfaces increased dramatically with increasing IB metal atom fraction (Fig. 5.3). The

isomerization selectivity also showed a sharp increase on the Cu-Pt(100) alloy surfaces with increasing copper atom fraction (Fig. 5.4). CKB reported that on a silica supported 10 % Pt- 90 % Au alloy, isomerization was the exclusive product and that only 3-MP was produced. CKB suggest that the 3-MP was produced via a bond shift mechanism although they report no specifics. SDP also reported a large enhancement of the isomerization selectivity at high gold concentrations over silica supported Au-Pt alloy catalysts and that there was a large increase in the amount of 3-MP produced relative to the amount of 2-MP produced. Their explanation is that isomerization proceeds via a carbonium ion-like bond shift mechanism [5.28]. It is not clear why this mechanism produced 3-MP with a higher selectivity than 2-MP. The production of 2-MP and 3-MP over the Cu-Pt(111) and Cu-Pt(100) alloy surfaces also showed an enhancement of the 3-MP production relative to the 2-MP production at higher copper atom fractions (Fig. 5.10).

Another interesting point about the Au-Pt(111) alloy surfaces is the overall enhancement of the initial rate upon the addition of gold to the platinum, with a 3-fold site that contained only one platinum atom having a total rate per platinum atom 2.5 times that of a pure platinum 3-fold site (see Table 5.3). The conclusion which must be reached from these results is that a <u>new bimetallic site has been created for the isomerization reaction</u>. Although the large absolute enhancement for isomerization observed for the Au-Pt(111)

system was not observed for the Cu-Pt(111) system due to the electronic effect, there was a large relative enhancement in the isomerization rate as indicated by the increased isomerization selectivity (Fig. 5.3). The electronic changes in the platinum induced by the presence of the copper on the (100) alloy surfaces seemed to favor this new isomerization mechanism since the rate per platinum atom in a 4-fold site which contained only one platinum atom was 4 times as active as a pure platinum site. It is not clear at this point what the exact nature of this new mechanism is nor why it was not observed for the Au-Pt(100) surface. More detailed mechanistic work is needed to elucidate this point.

d) Aromatization

The rate of aromatization was strongly inhibited by the addition of gold or copper to both the (111) and (100) surface. This behavior was unique to the aromatization reaction indicating a mechanism different from those discussed above. Although several authors have proposed a ring enlargement mechanism in which the MCP ring is opened and then closed again to form a six-member ring [5.29 - 5.30], other work on single crystal platinum surfaces [5.31] clearly shows that this mechanism is not important on platinum surfaces. Details of the aromatization reaction are not known, however is is clear that 3 or more platinum atoms are required for the reaction to proceed and that the direct 1,6 ring closure is important.

D. CONCLUSIONS

1) Hydrogenolysis requires 3 platinum atoms on the Pt(111) surface and only 1 platinum atom on the Pt(100) surface.

2) Cyclization can occur over a single platinum atom.

3) A new mechanism for isomerization becomes important on the Au-Pt(111), Cu-Pt(111) and Cu-Pt(100) alloy surfaces. The absolute enhancement was greatest for the Au-Pt(111) alloy surfaces, less for the Cu-Pt(100) alloy surfaces and even less for the Cu-Pt(111) alloy surfaces. The behavior of the isomerization selectivity showed the same trend on all three alloy surfaces.

4) The electronic changes in platinum induced by the presence of copper poison the cyclization reaction. These effects are more pronounced on the (111) alloy surfaces than on the (100) alloy surfaces.

5) Aromatization required at least 3 platinum atoms to occur. The ring enlargement mechanism was not important.

REFERENCES

5.1) J.K.A. Clarke and A.C.M. Creaner, I&EC Prod. Res. Dev. 20 (1981) 574 and references therein.

5.2) R. Burch, Acc. Chem. Res. 15 (1982) 24 and references therein.

5.3) V. Ponec, Catal. Rev.-Sci. Eng. 11 (1975) 41 and references therein.

5.4) S.M. Davis, F. Zaera and G.A. Somorjai, J. Catal. 85 (1984) 206.

5.5) F. Zaera and G.A. Somorjai, J. Amer. Chem. Soc., in press.

5.6) M. Asscher and G.A. Somorjai, Surface Sci. 143 (1984) L389.

5.7) G.A. Somorjai and S.M. Davis, Platinum Met. Rev. 17 (1983) 54.

5.8) J.J Burton and J.E. Hyman, J. Catal. 37 (1975) 106.

5.9) J.A. Dalmon and G.A. Martin J.Catal. 66 (1980) 214.

5.10) W.M.H. Sachtler and R.A. van Santen, in "Advances in Catalysis", eds. D.D. Eley, H. Pines and P.B. Weisz, Vol. 26, Academic Press, New York (1977) p. 69.

5.11) F.M. Dautzenberg, J.N. Helle, P. Bioen and W.M.H. Sachtler, J. Catal. 63 (1980) 119.

5.12) R.L. Jacobsen, H.E. Kleksdahl, C.S. McCoy and R.W. Davis, Proc. Am. Pet. Inst. (1969) 504.

5.13) U.S. Pat. No. 2,848,377

5.14) U.S. Pat. No. 3,415,737.

5.15) J.C. Rasser, W.H. Beindorff and J.J. Scholten, J. Catal. 59 (1979) 211.

5.16) J.W.A. Sachtler and G.A. Somorjai, J. Catal. 81 (1983) 77.

5.17) J.R. Anderson and N.R. Avery, J. Catal. 5 (1966) 446.

5.18) G. Leclercq, L. Leclercq and R. Maurel, J. Catal. 50 (1977) 87.

5.19) J.K.A. Clarke, A.K. Kane and T. Baird, J. Catal. 64 (1980) 200.

5.20) S.M. Davis, F. Zaera and G.A. Somorjai, J. Amer. Cham. Soc. 104 (1982) 7453.

5.21) J.R.H. van Schaik, R.P. Dressing and V. Ponec, J. Catal. 38 (1978) 273.

5.22) H.C. de Jongste, F.J. Kuijers and V. Ponec, Proc. 6th Int. Congress Catal (1976).

5.23) F.G. Gault, V. Amir-Ebranimi, F. Garin, P. Paraure and F. Weisang, Bull. Soc. Chim. Belg. 88 (1979) 475.

5.24) F. Garin and F.G. Gault, J. Am. Chem. Soc. 97 (1975) 4466.

5.25) R. Yeates and G.A. Somorjai, Surface Sci. 134 (1983) 729.

5.26) F.G. Gault, J.J. Rooney and C. Kemball, J. Catal. 1 (1962) 255.

5.27) A. O'Cinneide and F.G. Gault, J. Catal. 37 (1975) 311.

5.28) M.A. McKervey, J.J. Rooney and N.G. Samman, J. Catal. 30 (1973) 330.

5.29) J.K.A. Clarke and J.J. Rooney, Adv. Catal. 25 (1976) 125.

5.30) P. Parayre, V. Amir-Ebrahimi and F.G. Gault, J. Chem. Soc. Faraday Trans. 1, 76 (1980) 1723.

5.31) F. Zaera, Ph.D. Thesis, Univerity of CA, Berkeley (1984).

CHAPTER SIX : THE OSCILLATORY BEHAVIOR OF THE CO OXIDATION REACTION OVER SILICON CONTAMINATED PLATINUM SURFACES

A. INTRODUCTION

Oscillatory reactions have a long and distinguished history in chemical sciences [6.1]. One such reaction which has been studied in great detail is the catalyzed oxidation of carbon monoxide by oxygen to form carbon dioxide. Temporal oscillations in the reaction rate have been observed over platinum, palladium, and iridium catalysts [6.2 - 6.3]. This behavior was first reported by Hugo 1970 using a supported platinum catalyst [6.4]. Since then, this reaction has been studied over a variety of platinum surfaces including wires, foils, deposited films and single crystals [6.5 - 6.16], and the temporal oscillations have been shown to be a surface mediated phenomenon rather than the result of mass transfer effects [6.16].

The research carried out to date on this reaction over well characterized single crystal surfaces focused on the oscillatory behavior at low pressure [6.11 - 6.13], in which the surface was exposed to a flowing mixture of carbon monoxide and oxygen at a total pressure of ~ 5×10^{-4} torr. Low energy electron diffraction observations and work function measurements showed that, over the Pt(100) surface, the oscillations are associated with a surface phase transition from the hexagonal (hex) structure ((5 X 20) structure) to the square (1 X 1) and c(2 X 2) structures. It was found that a maximum in the rate coincides with the

presence of the hex phase and a high coverage of atomic oxygen while the minimum rate is observed coincidentally with the (1 X 1)/c(2 X 2) phase and a high concentration of adsorbed carbon monoxide.

The most detailed kinetic modeling of the reaction at atmospheric pressure has been done by Sales, Turner, and Maple (STM) in conjunction with their experimental studies [6.17]. This model includes the formation of an oxide in the near-surface region of the catalyst. In the two branches of the CO oxidation reaction, the surface is alternately oxidized and reduced, thus changing the surface oxide coverage. This model, however, does not include an autocatalytic step, necessary to drive the transition between the two branches, unless the creation of reaction sites during the reduction of the surface is considered to be the autocatalytic step.

The work presented in this chapter combines surface science techniques, available in ultra high vacuum, with an in situ high pressure cell. Such surface science techniques were not available to STM in their high pressure reaction studies. Platinum single crystals with (111), (100), and (13,1,1) orientations have been used to determine if surface structure is important in this oscillatory reaction. Since the (100) surface reconstructs and the (111) surface does not, we were able to study the role reconstruction plays in the oscillations observed at high pressure.

The results obtained by Cox et al. [6.11] for the reaction at low pressure were reproduced in this work. It appears that their surface reconstruction model explains the oscillatory behavior in the low pressure regime. At atmospheric pressure, however, oscillations were observed over both the (111) and the (100) platinum surfaces. Also, the surfaces examined after sustained oscillations were heavily oxidized and silicon impurities had segregated from the bulk to the surface. These results indicate that the mechanism at low pressure is different from that at high pressure.

A model is presented which is based on the kinetic equations of STM which also takes into account the non-isothermal behavior of the reaction. The introduction of a temperature that depends on the reaction rate into the model provides a mechanism for the transition between the two reaction branches, similar to the non-autocatalytic non-isothermal systems discussed by Gray and Scott [6.18] and Uppal, Ray, and Poore [6.19].

B. RESULTS

1. Oscillatory Behavior

a. Low pressure experiment

The experiment reported by Cox et al [6.11] was repeated in order to compare the results which they obtained at low pressure with our results at atmospheric pressure. The work

function of a clean, annealed Pt(100) crystal surface was monitored continuously during exposure to 4 X 10^{-4} torr of O_2 and 1 X 10^{-4} torr of CO at a temperature of 425 K. Oscillations in the work function of the platinum surface were as large as 300 mV. The work function results are shown in Fig. 6.1. These oscillations were similar to those reported by Cox et. al. The work function of the Pt(100) surface was also monitored without heating the crystal and while heating the crystal in UHV. Under these conditions, no changes in the work function were observed.

b. High pressure experiments

When the clean, annealed Pt(100) surface was exposed to a mixture of O_2 and CO at atmospheric pressure no oscillations were observed in the composition range 1 - 30 % CO and the temperature range of 300 - 1000 K. In addition, oscillations were never observed using either clean, annealed Pt(13,1,1) or clean, annealed Pt(111) surfaces. However, when any of the crystals were sputtered for 20 min. at 1000 eV, small erratic oscillations with a magnitude of about 2 degrees and a period ranging from 1 to 60 seconds were observed, although not reproducibly.

When a clean, annealed crystal was left in the high pressure cell for several days, without cleaning, oscillatory behavior in the reaction developed. This behavior was observed on all three Pt(111), Pt(100), and Pt(13,1,1) surfaces. These results are summarized in Table 6.1.

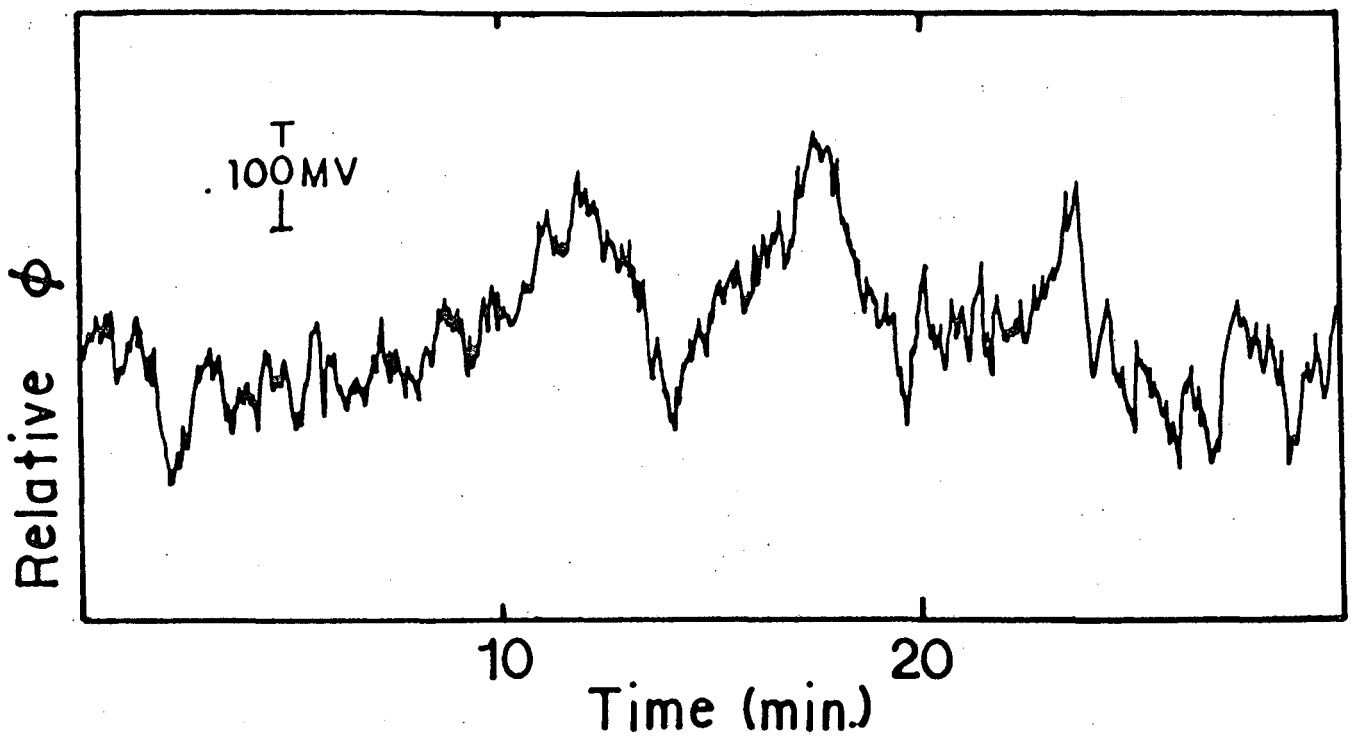

FIG. 6.1

Relative work function of a Pt(100) surface as a function of time. The platinum crystal was heated to 425 K in 4 X 10^{-4} torr of O_2 and 1 X 10^{-4} torr of CO.

TABLE 6.1

	Pt(111)	Pt(13,1,1)	Pt(100)
10^{-4} torr Clean Annealed	No Oscillations	No Oscillations	OSCILLATIONS
1 Atm Clean Annealed	No Oscillations	No Oscillations	No Oscillations
1 Atm "dirty"	OSCILLATIONS	OSCILLATIONS	OSCILLATIONS
Atm Clean Sputtered	?	Small Erratic Oscillations	?

The typical oscillatory behavior obtained on the various crystal surfaces and under a variety of conditions is shown in Fig. 6.2. Since the reaction was very exothermic (70 kcal/mole), the reaction rate was monitored by following the temperature of the platinum crystal. This procedure was tested by leaking the product gasses into the chamber through a leak valve and following the gas composition with the mass spectrometer. A good agreement was found. Since the temperature response time was much faster and following the crystal temperature was proceduraly simple, the rate will be plotted as crystal temperature in what follows.

In general, as the temperature of the catalyst was increased, the period and magnitude of the oscillations decreased; the magnitude increased as the carbon monoxide concentration was increased. This behavior is the similar to that reported by other authors [6.17]. Fig. 6.3 shows a plot of temperature versus carbon monoxide concentration. The region between the two curves gives the conditions under which oscillations were obtained on a Pt(13,1,1) crystal surface. The shape of this oscillatory region is similar to that reported by Turner et. al. [6.17]. This oscillatory region was not stable. After one week of reaction the region had changed, presumably due to changes at the crystal surface. This behavior was not studied, however.

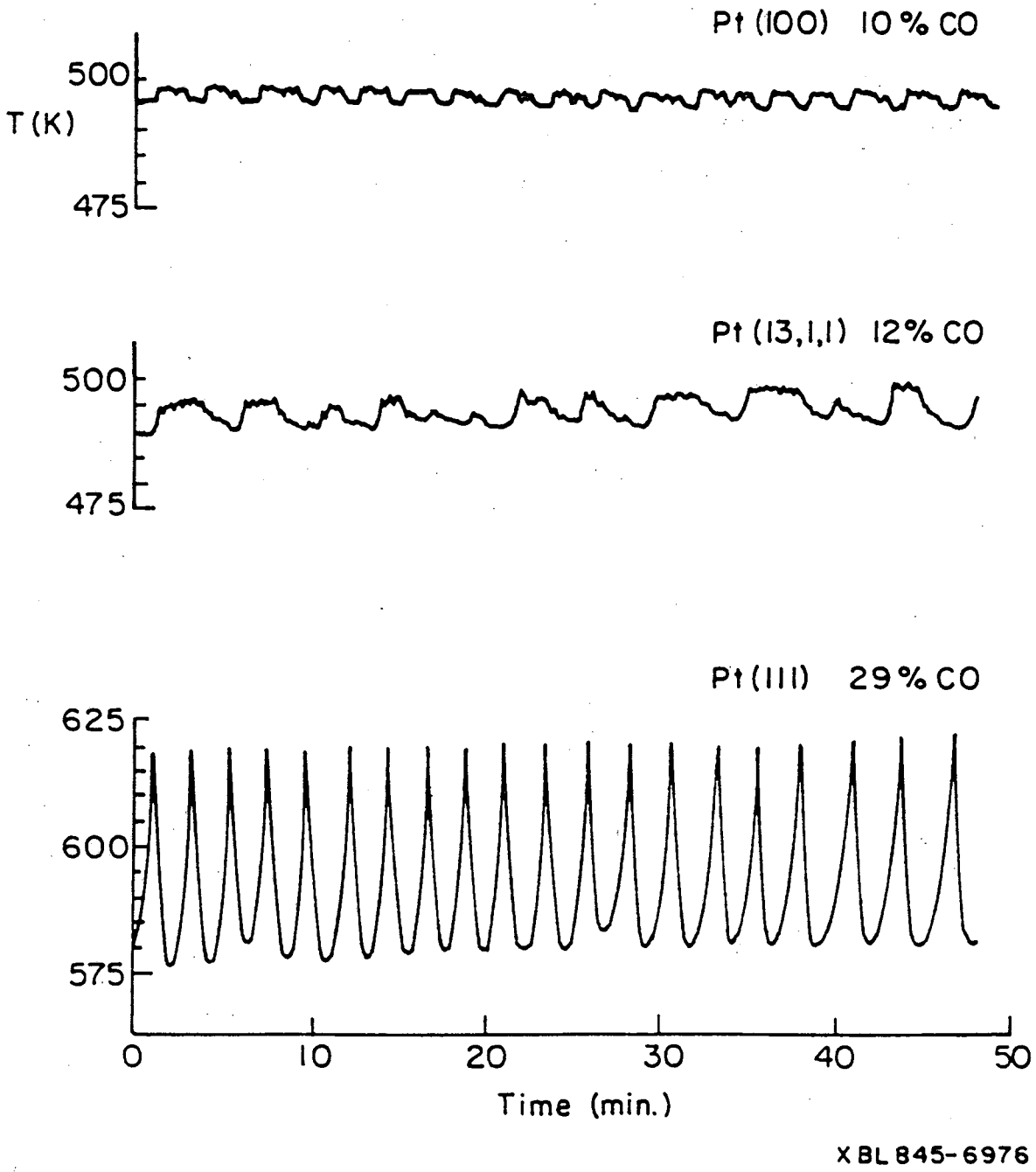

FIG. 6.2

Typical oscillations obtained on three platinum crystal surfaces under various conditions. Sample temperature is plotted versus time.

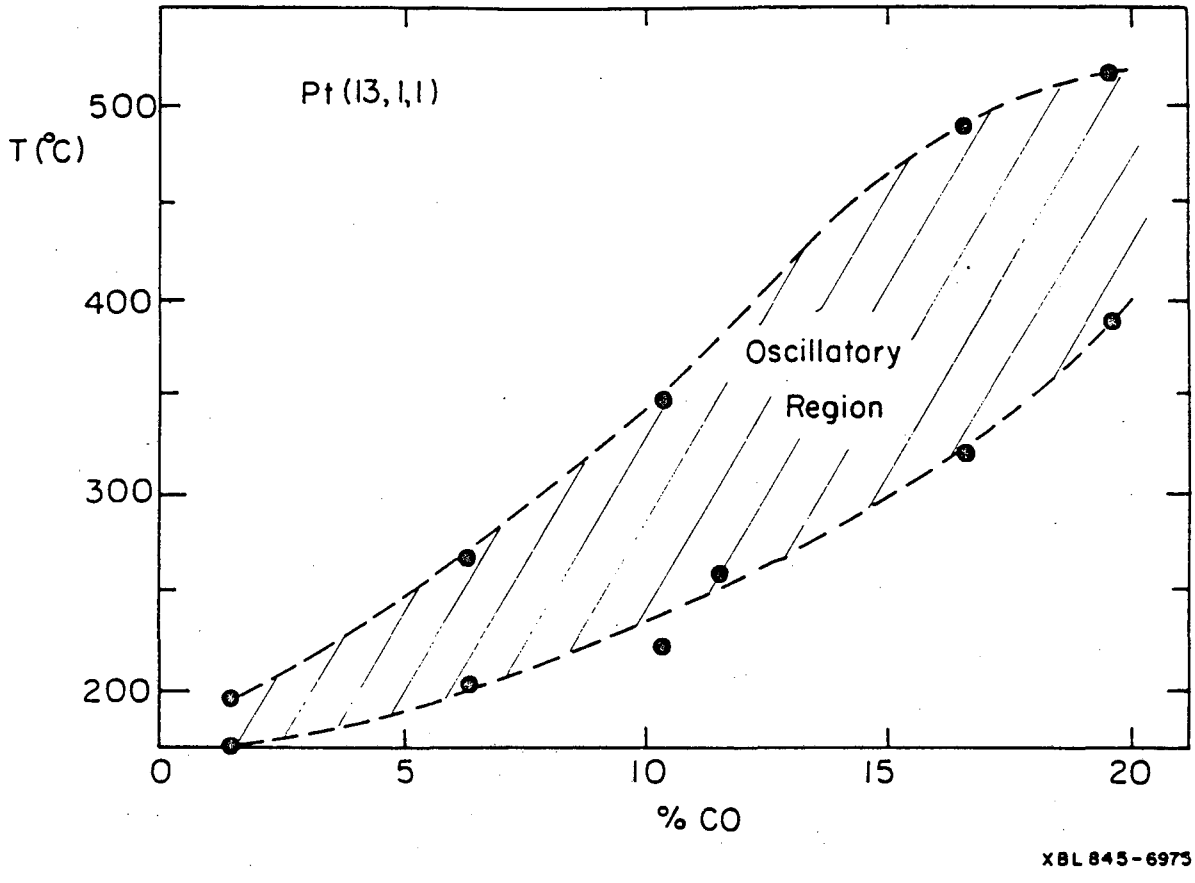

FIG. 6.3

A plot of sample temperature versus carbon monoxide concentration showing the conditions for which oscillatory behavior was observed over a Pt(13,1,1) crystal surface.

2. Surface Analysis

An Auger spectrum of the Pt(111) surface after the oscillating reaction is shown in Fig. 6.4. The platinum peaks were greatly attenuated relative to those for clean platinum. The peak at 81 eV was due to heavily oxidized silicon [6.20] and a large oxygen peak at 512 eV was present. This Auger spectrum was typical of the spectra obtained for all surfaces examined after oscillations had been observed, although calcium and sulfur were also present on some of the platinum surfaces. Because of the presence of several species on the surface, it is difficult to quantitatively determine the amount of silicon and oxygen present. Based on standard Auger spectra, however, it is clear that there must be sub-surface oxygen present, in addition to surface oxygen, to give an oxygen Auger peak of the magnitude observed and the amount of silicon (in the form of SiO_2) present was 1/4 to 1/2 of a monolayer.

The LEED pattern of the Pt(111) surface after oscillations had been observed is shown in Fig. 6.5. This is a slightly misfit $(\sqrt{3} \times \sqrt{3})$-R30° surface structure. A $(\sqrt{3} \times \sqrt{3})$-R30° structure has been reported for PtO_2 formed on platinum by high oxygen exposure at elevated temperatures [6.21]. The LEED of the Pt(100) surface after oscillations showed a diffuse (1 X 1) surface structure which was relatively faint.

Because the copper support rods were heavily oxidized after the reaction, an accurate oxygen thermal desorption

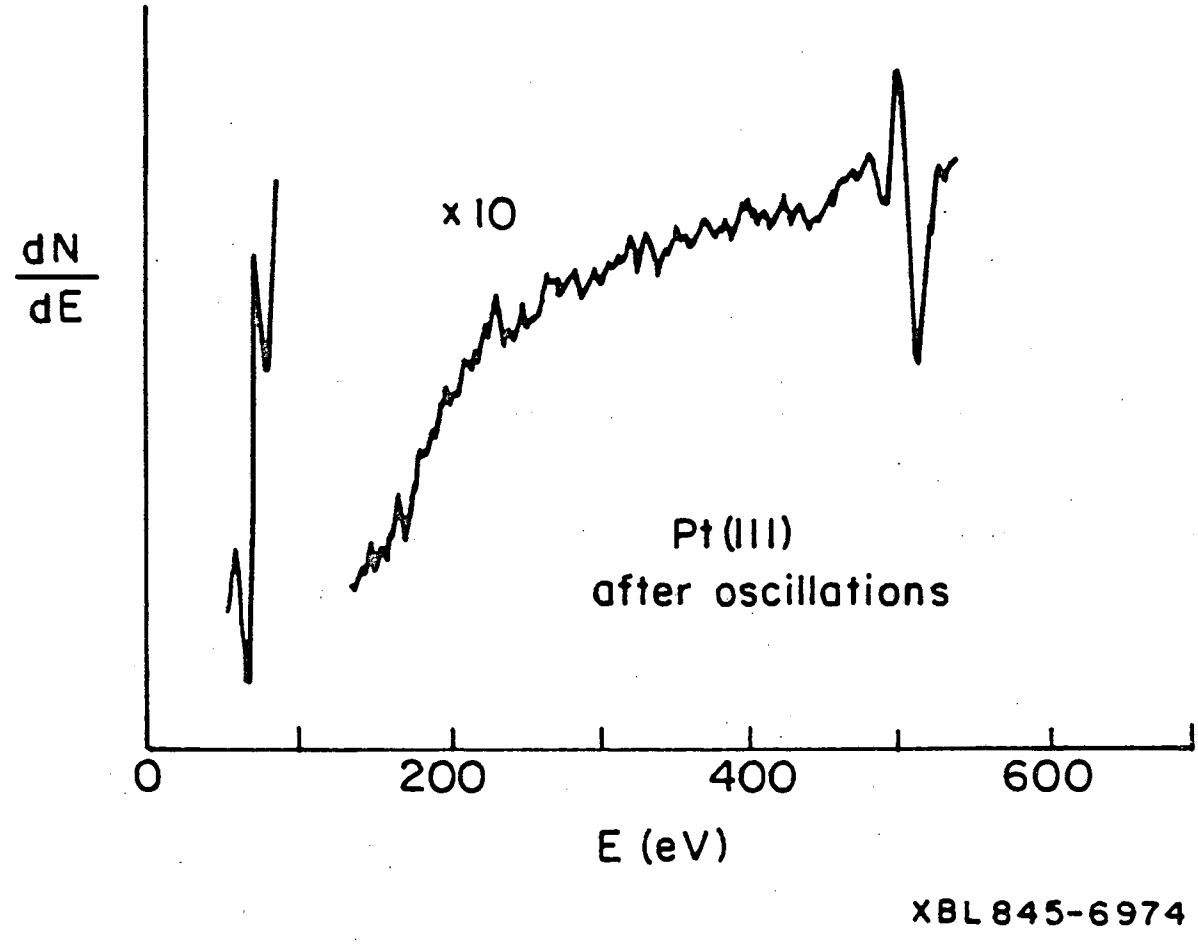

FIG. 6.4

A typical Auger spectrum of the platinum surface after the oscillatory reaction. The peak at 80 eV is due to silicon and the peak at 512 eV is due to oxygen.

Pt (111) with Si and O after Oscillation Reaction

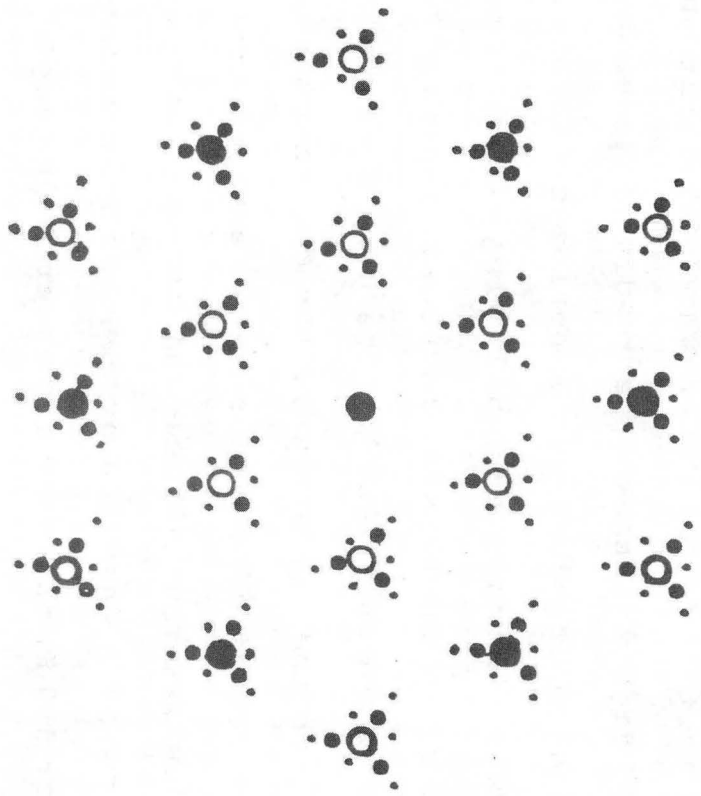

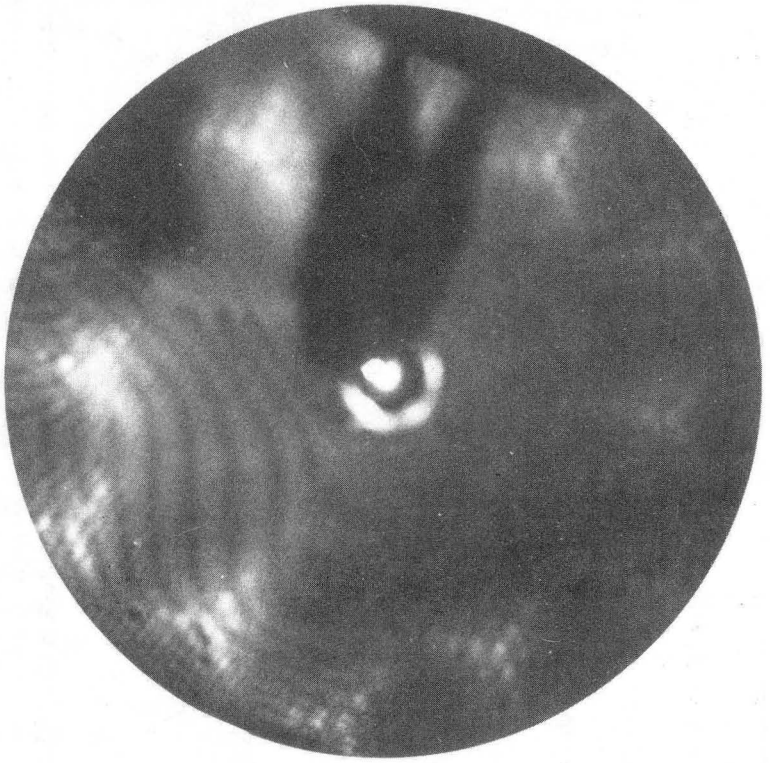

FIG. 6.5

A drawing and photograph of the LEED pattern observed for the Pt(111) surface after the oscillatory reaction. This pattern indicates a misfit ($\sqrt{3}$ X $\sqrt{3}$)-R30° surface structure.

spectrum could not be obtained. It was noted, however, that desorption of oxygen began at ~ 800 K. It appears that the amount of near surface oxygen was substantial. Even after heating the crystal at 1000 K for one minute in vacuum, the decomposition rate of PtO_2 (as monitored by mass spectrometry) remained constant and the oxygen Auger peak had decreased by less than 10 %.

3. The Effect of Surface Oxidation and Reduction on the Oscillatory Reaction Behavior

Fig. 6.6 shows the effect of pure carbon monoxide and pure oxygen treatments on the catalytic reaction behavior of a Pt(111) surface which had exhibited oscillatory behavior. After the reduction or oxidation of the surface, the reaction gas composition and current passed through the sample were restored to the values under which oscillations had been observed. Fig. 6.6a shows the result of leaving the crystal in flowing CO at 550 K for a period of 40 minutes. When oxygen was introduced following this treatment the temperature of the crystal increased rapidly from 550 K to 630 K and began oscillating. The base temperature drops off gradually to the value before the CO treatment. Fig. 6.6b shows the result of a more severe reducing treatment. The oxygen flow was shut off and the crystal was heated to 720 K for 5 minutes. When the oxygen was reintroduced with the crystal at 550 K, the crystal temperature jumped to 670 K and then gradually dropped off to 600 K without beginning to

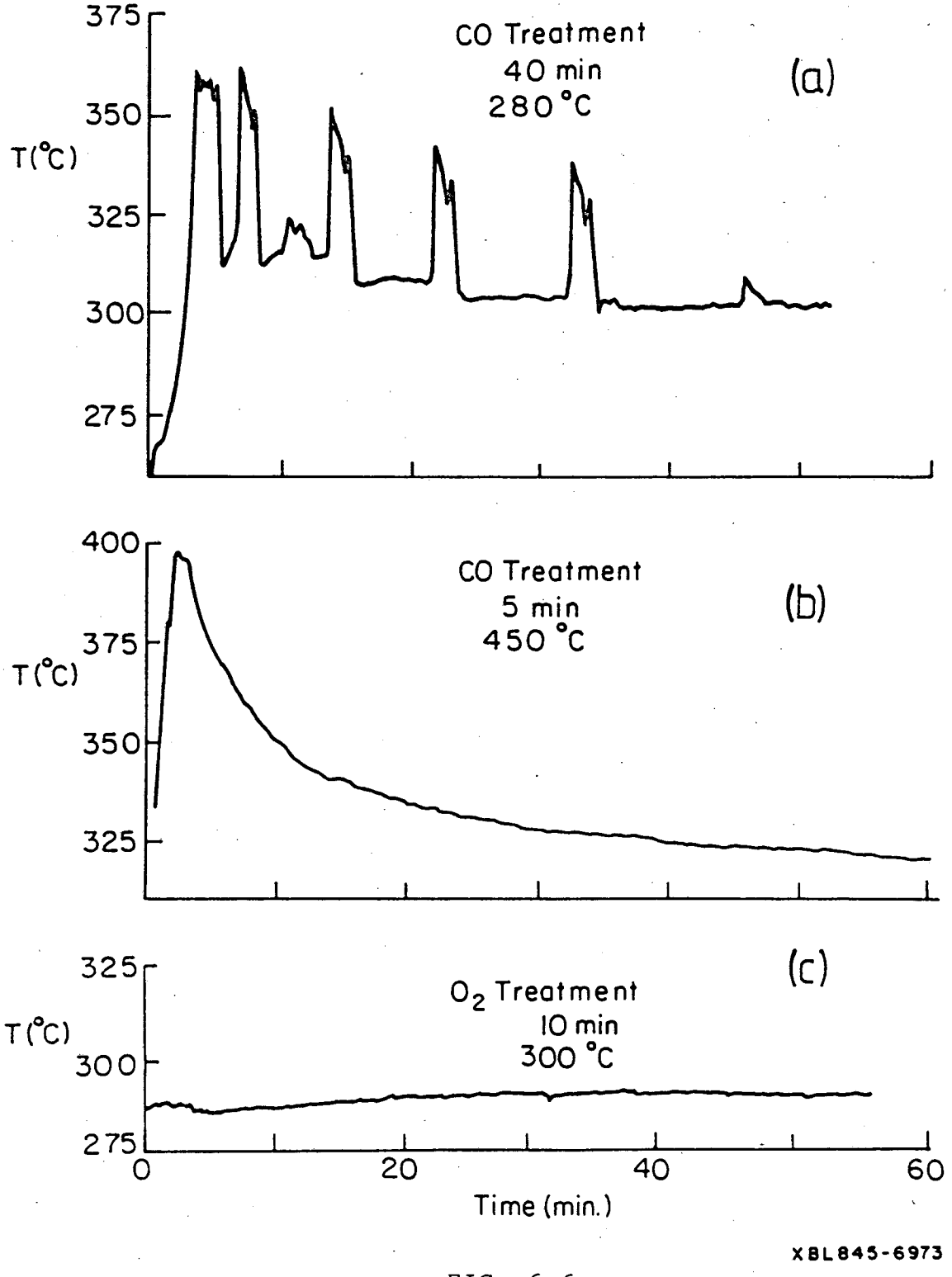

FIG. 6.6

Plots of sample temperature versus time under oscillatory conditions after treatments in (a and b) pure CO and (c) pure oxygen.

oscillate for at least an hour. In general, a mild CO treatment resulted in an initial temperature jump when oxygen was introduced followed by oscillations. A more severe CO treatment resulted in a large temperature jump upon the addition of oxygen, with the resumption of oscillatory behavior after a considerable time period, this period being longer the more severe the CO treatment.

Fig. 6.6c shows the effect of an oxygen treatment of the crystal surface which had exhibited oscillations. The CO flow was shut off for a period of 5 minutes, exposing the crystal to pure oxygen, with the crystal at 570 K. When the CO flow was resumed, there was no increase in the temperature of the crystal for a period of at least 1 hour. In general, an oxygen treatment resulted in little or no temperature jump upon the addition of CO and the period of time which elapsed before the oscillations resumed was longer the more severe the oxygen treatment.

These results seem to be consistent with the model proposed by Sales, Turner, and Maple (STM) in which the oscillations are driven by a cyclic oxidation and reduction of the surface. A heavily oxidized surface results in a low reaction rate, while a high rate is observed on a reduced surface.

C. DISCUSSION

The results of these experiments indicate that the mechanism for the oscillatory behavior of the CO oxidation reaction at atmospheric pressure differs from that at low pressures. In the low pressure regime, the oscillations appear to be driven by a periodic phase transformation of the Pt(100) surface [6.11 - 6.13]. At atmospheric pressure, the absence of observable oscillations on the clean, annealed Pt(100) crystal surface and their presence on the silicon contaminated Pt(111) and Pt(100) surfaces indicates that the mechanism of the oscillations at atmospheric pressure is not the same as that proposed for the reaction at low pressure. This is not surprising since it is doubtful that the surface would be reconstructed when exposed to a mixture of CO/O_2 at atmospheric pressure.

The kinetic model for the high-pressure reaction is presented in the appendix. The model considers the presence of three surface species: molecular CO, atomic oxygen, and a platinum oxide which is only slightly reactive towards CO. The solution to these equations for a given set of parameters is shown in Fig. 6.7. When the reaction rate is high, the oxygen coverage is relatively high, the CO coverage is relatively low, and the oxide coverage is increasing. The converse is true when the reaction rate is low. The behavior of the reaction can be seen more clearly when the rate of CO oxidation is plotted versus the oxide coverage. A plot of this type is shown in Fig. 6.8 where the solid line indicates

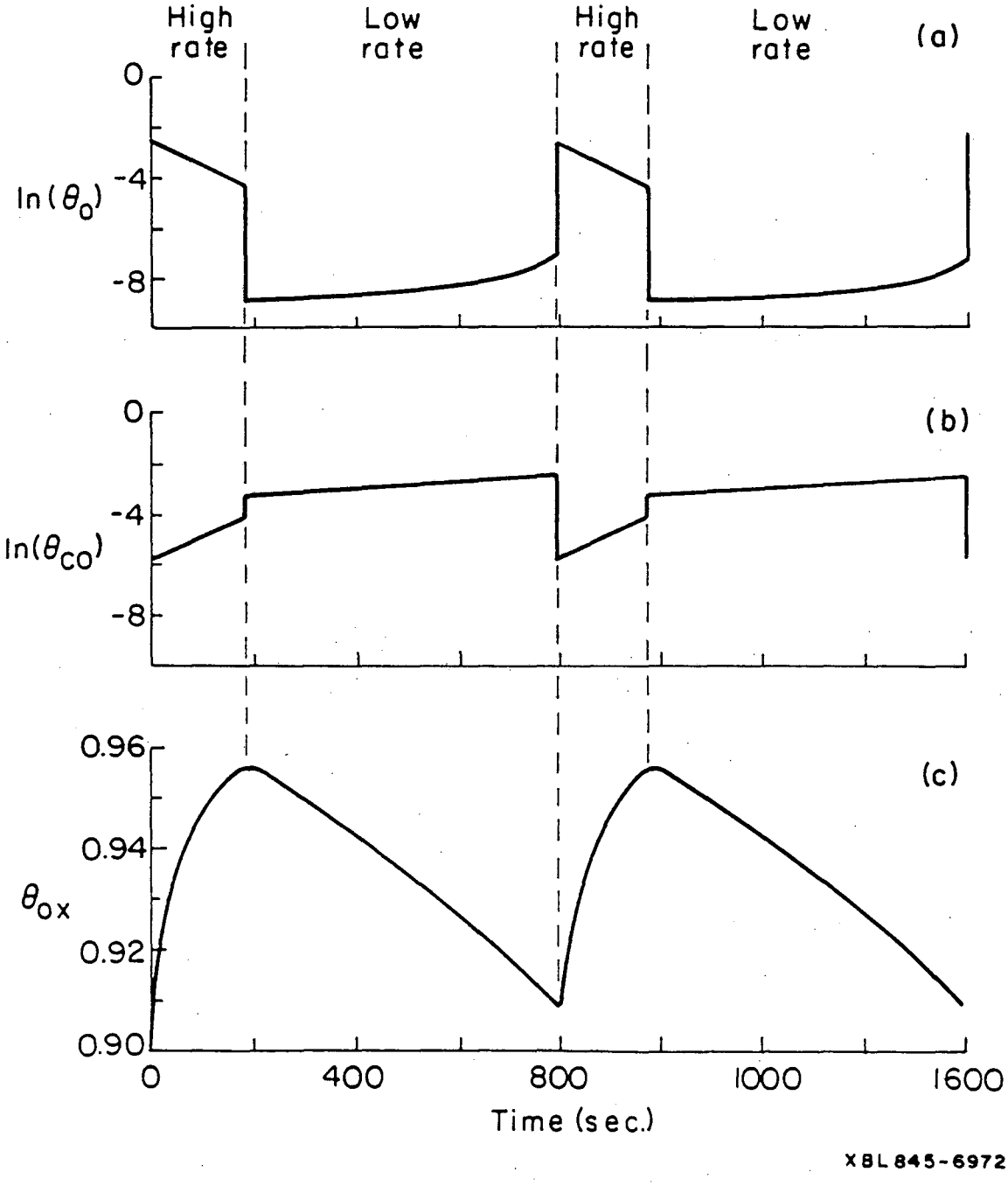

FIG. 6.7

Solutions to the kinetic equations showing $\ln(\theta_O)$, $\ln(\theta_{CO})$ and θ_{ox} as a function of time. See Table 6.2 for rate constant values.

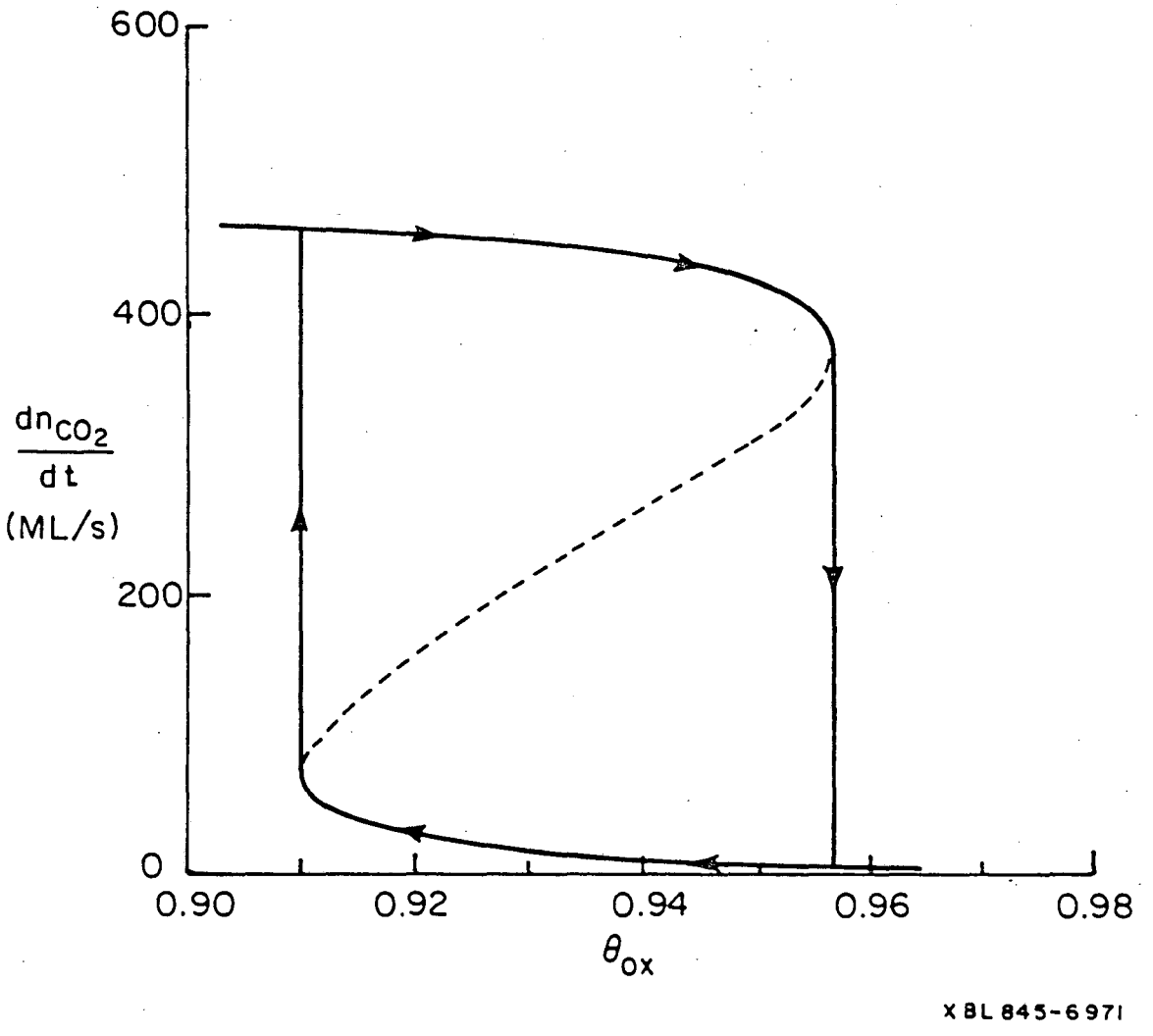

FIG. 6.8

Solutions to the kinetic equations plotted as the rate of CO_2 production versus θ_{ox}. The solid line shows the reaction path and the dotted line is an unstable solution. Values for the rate constants are listed in Table 6.2.

the path of the reaction and the dotted line is an unstable solution to the kinetic equations.

When the reaction is proceeding at a fast rate (in the upper branch), the time derivative of the oxide coverage is positive. Thus, the surface oxidizes while the rate of CO oxidation and catalyst temperature slowly decrease. This is due to a reduction in the number of sites on the platinum which are not oxidized. This continues until the cusp is reached, and at this point, CO builds up on the surface and the reaction drops into the lower branch. The time derivative of the oxide coverage in the lower branch is negative due to the abundance of CO on the surface, so the surface begins to reduce. The reaction rate and catalyst temperature gradually increase due to an increase in the number of platinum sites available. This process continues until the next cusp is reached, at which point the reaction jumps back to the upper branch and the cycle repeats itself.

In an attempt to experimentally verify this hypothesis of changing oxide coverage, the reaction was stopped at various points in the oscillation, the high pressure cell opened and the surface was examined by Auger spectroscopy. The spectra obtained were identical within experimental error. Several factors may have contributed to our inability to detect changes in the oxide coverage : 1) the surface present at atmospheric pressure is unstable under UHV; 2) the oxide is several layers thick; 3) the silicon is in the form of SiO_2 and remains oxidized; 4) adsorbed CO can react with

the oxide before a measurement can be made; and 5) the absolute changes in the coverages are less than 5 % of a monolayer.

The parameters determining the length of time which the reaction spends in the upper and lower branches are the rate constants for the oxidation and reduction of the surface. Within the context of the model, these parameters determine the point at which $d\theta_{ox}/dt = 0$ on the Z-shaped curve (Fig. 6.8). Oscillatory behavior will occur if this point falls between the two cusps (on the dotted line). If the surface oxidation rate constant is too large relative to the surface reduction rate constant, the reaction will reach a steady state in the lower branch. If the surface oxidation rate constant is too small relative to the reduction rate constant, the reaction will reach a steady state in the upper branch.

Changes in the other rate constants affect the shape of the Z-shaped curve. As the rate of oxygen adsorption is increased,i.e. an increase in the partial pressure of oxygen, the change in θ_{ox} during an oscillation decreases, the magnitude of the temperature jump decreases, and the curve shifts toward higher oxide coverages. A similar effect is observed when the CO desorption rate is increased. An increase in the adsorption rate of CO has the opposite effect. As the CO oxidation rate constant is increased, the change in θ_{ox} decreases, the magnitude of the temperature jump increases, and the curve shifts to higher oxide

coverages. These effects are summarized in the form of temperature versus time plots in Fig. 6.9.

For a given set of conditions, the rate of reaction clearly depends on the oxide coverage. If the amount of oxide on the surface is less than the amount of oxide present at the left cusp, the reaction will start off in the upper branch. This is illustrated experimentally in Fig. 6.6b where the crystal was treated in flowing CO at 730 K for 5 minutes, lowering the surface oxide coverage to less than that of the oscillatory region. When oxygen was introduced the temperature of the crystal jumped up 100 K very rapidly and remained in the high branch for at least one hour. Fig. 6.6c shows the result of oxidizing the surface past the oscillatory region. When CO was introduced, there was no jump in crystal temperature and the reaction remained in the lower branch for at least one hour.

The silicon always present on the surface after the initiation of the oscillations appears to play an important role in the oscillatory behavior. While a clean, sputtered Pt(13,1,1) surface was found to yield only small, erratic oscillations, the same surface with Si present yielded large, regular oscillations (Fig. 6.3). It appears that this impurity either increases the sticking coefficient of oxygen or catalyzes the formation of the platinum oxide. We believe that the silicon provides an adsorption site with a higher sticking probability than that for platinum, and after adsorption, the oxygen can spill over to the Pt surface.

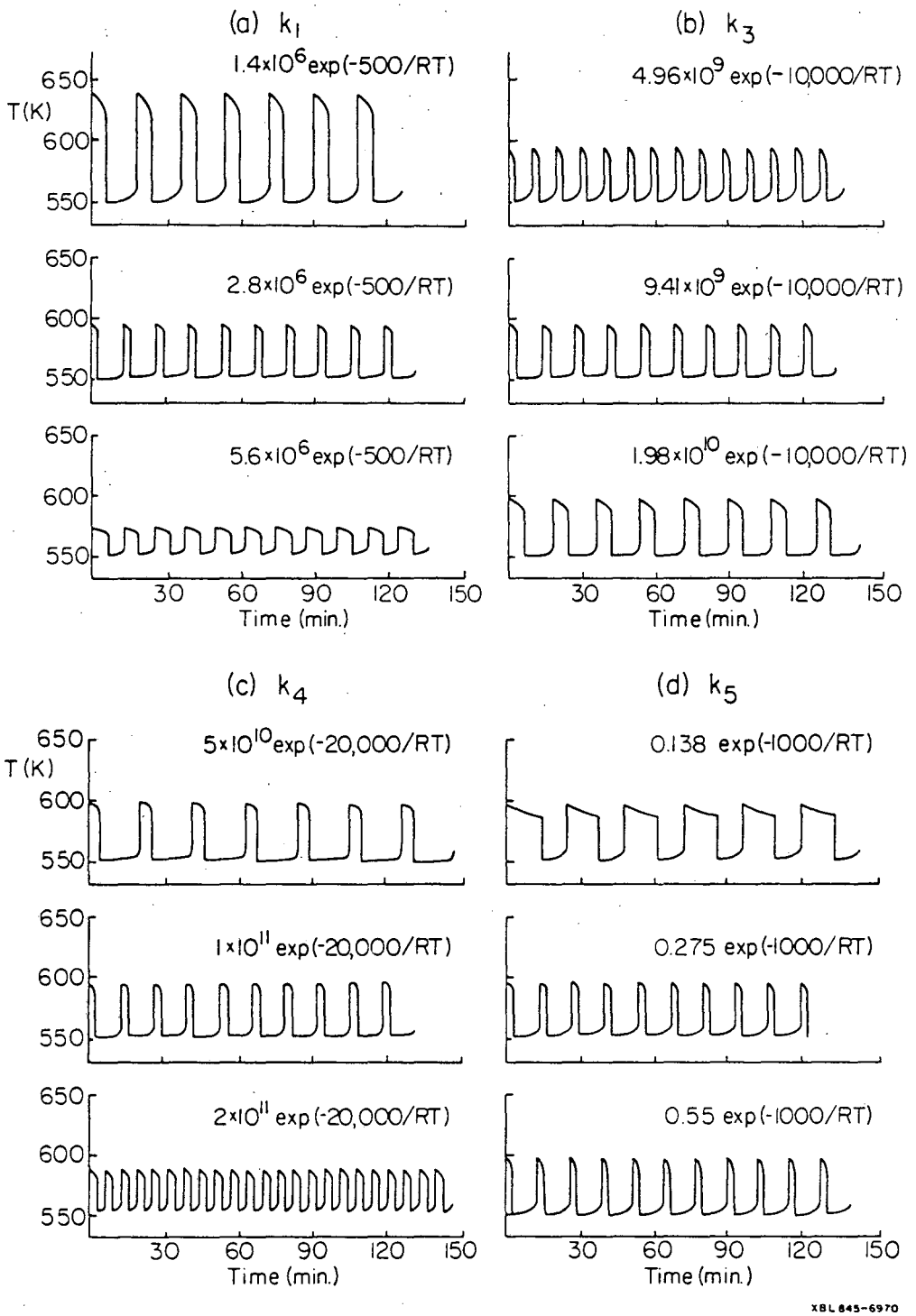

FIG. 6.9

Theoretically generated oscillations of the sample temperature as a function of time. Values of the rate constants listed in Table 6.2 were used in the calculations except where indicated in the figure.

These results are consistent with the earlier modeling results of STM and other independent studies of the formation and reduction of PtO_2 [6.22]. Oxide formation rates measured over platinum black were an order of magnitude smaller then those necessary to sustain oscillations in the model. The presence of Si impurities which segregate to the Pt surface may increase this oxide formation rate to values which will support oscillatory behavior. This increase in the rate of oxide formation may be due either to an increase in the coverage of atomic oxygen (θ_O), or an increase in the rate constant for oxide formation.

While the Pt/Si/O system [6.23] has not been extensively studied, work by Salmeron et al. gives an indication of the instability of Si at a Pt surface when exposed to oxygen [6.24]. This work shows that even low partial pressure of oxygen may induce either surface segregation or bulk diffusion of Si into Pt. Thus the Pt/Si/O system might be expected to be unstable in an UHV environment. Fig. 6.10 shows the effect of exposure of an oscillating Pt crystal to UHV conditions. The gas composition and temperature are the same for the two sets of oscillations shown. The only difference was that the high pressure cell had been opened to UHV between the two. This change in oscillatory behavior may be ascribed to the instability of the Pt/Si/O system in vacuum. Changes in the surface which occur when the system is exposed to vacuum may result in a change of the surface oxidation or reduction rate resulting in the effect shown

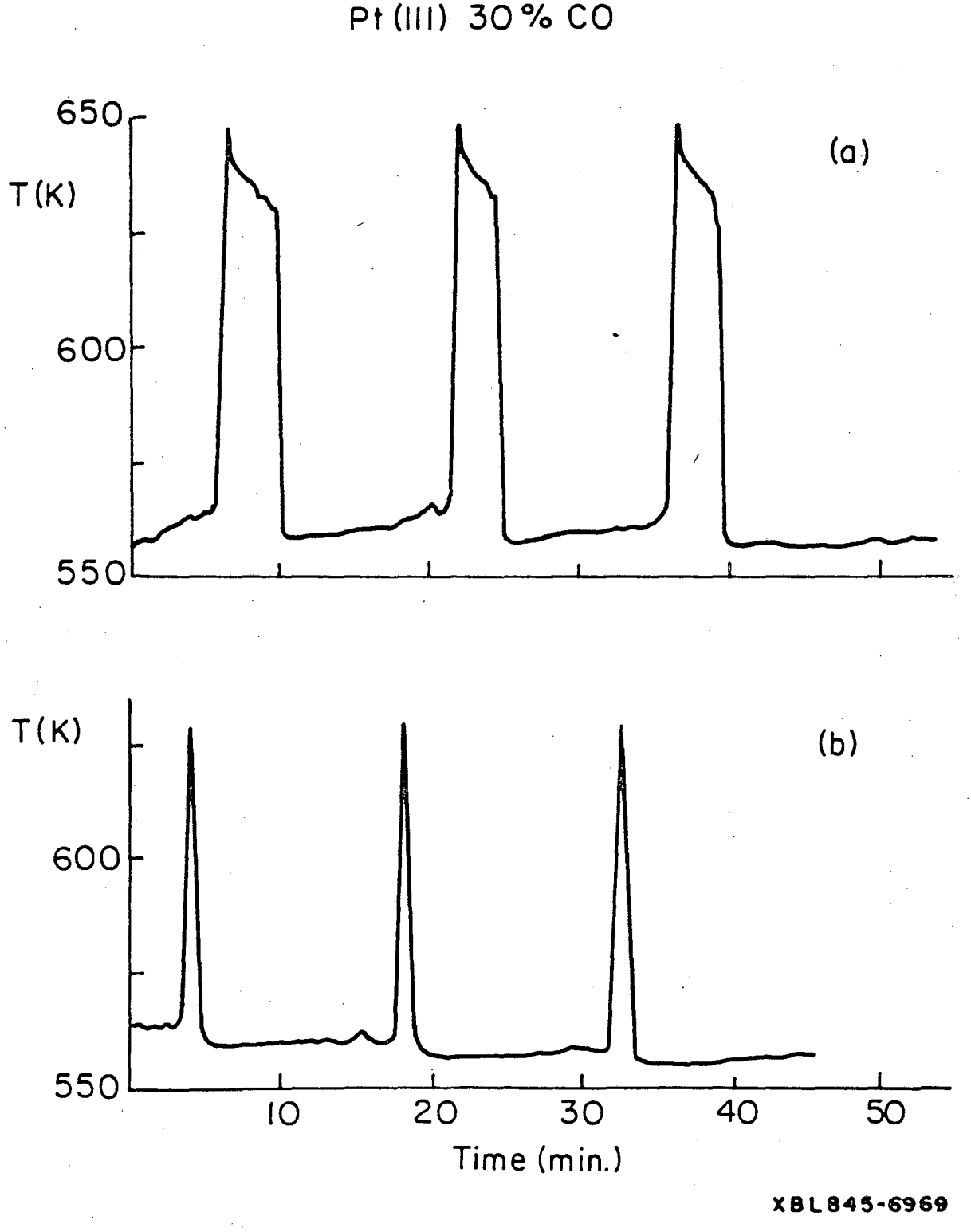

FIG. 6.10

Sample temperature as a function of time a) before and b) after exposure to ultra-high vacuum.

theoretically in Fig. 6.9d. Unfortunately, there was no observed change in the relative Auger intensities for these three species. Thus one may assume that induced changes probably do not involve large scale diffusion of species, but instead minor structural rearrangement in the near surface layers, or coverage changes too small to detect by AES.

An alternative explanation for the results of Fig. 6.10 may be a slow diffusion of oxygen from the bulk of the Pt. One might assume that exposure of the Pt to UHV conditions results in the decomposition of the PtO_2. This would certainly affect the CO oxidation kinetics on the surface and might result in the changes shown in figure 9. Thermodynamically PtO_2 would certainly dissociate in UHV for temperatures higher than 400 K. From the standard enthalpy of formation (-41.8 kcal/mole) and the standard entropy of formation (-48.9 cal/mole/deg) one can calculate that PtO_2 will dissociate for $P(O_2) < 1.3 \times 10^{-17}$ torr at 300 K and for $P(O_2) < 9.1 \times 10^{-4}$ torr at 550 K. Nevertheless, the kinetics of oxygen diffusion in Pt are very slow. Although the kinetic data for the diffusion of oxygen through Pt are not very precise, the data which is available ($D_o = 9.3 \pm 1.8$ cm^2/sec, $E = 78 \pm 25$ kcal/mole) [6.25] indicate that the diffusion of oxygen through 10 Å of Pt would require 6×10^{33} years at 300 K and 200 seconds at 1000 K.

CONCLUSIONS

1) Oscillatory reaction rates have been observed for the catalyzed oxidation of carbon monoxide over platinum single crystal surfaces of (111), (100), and (13,1,1) orientations at atmospheric pressure.

2) The Pt(100) surface is know to undergo a (5 X 20) to (1 X 1) phase transformation upon the adsorption of carbon monoxide. Cox et. al. have proposed that oscillations which they have observed at low pressure (1×10^{-4} torr) are due to this surface phase transformation. Since the Pt(111) surface does not undergo any such reconstruction, this mechanism cannot be responsible for the oscillations at atmospheric pressure which are reported here.

3) Reaction rate oscillations at atmospheric pressure are believed to be driven by an cyclic oxidation and reduction of the platinum surface. A model incorporating this process and including the temperature variation of the catalyst as the driving force of the transition between reaction branches step shows excellent agreement with experimental results.

4) While oscillations have been obtained over clean platinum single crystal surfaces, it appears that silicon impurities are usually present on a surface supporting oscillations. These impurities play an important role in the oscillatory behavior by either catalyzing the formation of the platinum oxide or by increasing the sticking coefficient of oxygen on the platinum surface.

APPENDIX

A Kinetic Model for the Oscillatory Behavior of the CO Oxidation Reaction Over Platinum

The following assumptions are made in the model :

1) The molecular adsorption rate of CO and the dissociative adsorption rate of O_2 depend only on the number of sites available for adsorption, the partial pressures of the gases, and the temperature.

2) CO_2 is produced from the reaction between adsorbed CO and adsorbed atomic oxygen and desorbs instantaneously upon formation.

3) The desorption energy of CO is independent of coverage. Desorption of oxygen is ignored.

4) The number of CO and O_2 adsorption sites are the same.

In the STM model, all calculations were made for isothermal conditions. In reality, due to the high exothermicity of the reaction, the crystal temperature, T, is dependent on the reaction rate. We have modified the STM model by assuming a temperature with a reaction rate dependence of the form : $T = T_o + a\ r(CO_2)$. The magnitude of the constant 'a' would depend on the surface-to-volume ratio of the catalyst, the rate of thermal conduction from the sample, and other thermodynamic factors. It was not the intention of the authors to model the temperature exactly, and we feel that this simple model is sufficient.

There are three surface species whose coverages were considered : atomic oxygen (θ_O), molecular carbon monoxide (θ_{CO}), and oxygen in the form of an oxide (θ_{ox}). The kinetic equations which define these coverages are as follows:

$$d\theta_O/dt = k_1\theta_s^2 - k_3\theta_O\theta_{CO} - k_5\theta_O(1 - \theta_{ox}) \quad (1)$$

$$d\theta_{CO}/dt = k_2\theta_s - k_4\theta_{CO} - k_3\theta_O\theta_{CO} - k_6\theta_{CO}\theta_{ox} \quad (2)$$

$$d\theta_{ox}/dt = k_5\theta_O(1 - \theta_{ox}) - k_6\theta_{CO}\theta_{ox} \quad (3)$$

where $\theta_s = 1 - \theta_O - \theta_{CO} - \theta_{ox}$

and the rate constants are temperature dependent.

Values for the rate constants are shown in Table 6.2.

In eqn. 1 the first term represents the rate of dissociative adsorption of O_2, the next term the reaction between adsorbed, atomic oxygen and adsorbed carbon monoxide, and the last term the formation of the oxide from adsorbed, atomic oxygen. Similarly, the terms in eqn. 2 describe the molecular adsorption of CO, the desorption of CO, the reaction between adsorbed CO and adsorbed, atomic oxygen, and the reaction of CO with the oxide to form CO_2, respectively. The third equation consists of the rates of formation of the oxide from adsorbed, atomic oxygen and the reaction of the oxide with adsorbed CO to form CO_2. Reactant pressures have been included in the rate constants.

This set of equations was solved using two different methods. One was an iterative method in which the time

TABLE 6.2

		A (sec^{-1})	E_a (Kcal/mol)
k_1	Oxygen Adsorption	2.8×10^6	0.5
k_2	CO Adsorption	3.0×10^4	0
k_3	Langmuir-Hinshelwood	9.4×10^9	10
k_4	CO Desorption	1.0×10^{11}	20
k_5	Surface Oxidation	0.275	1.0
k_6	Surface Reduction	12	10

increment was weighted inversely proportional to the sum of the rates of the individual simple processes involved in the reaction (rate of O_2 adsorption, rate of CO adsorption, etc.) with a proportionality constant on the order of 10^{-4}. The other method was similar to the quasi-steady state solution reported by STM [6.17]. In this solution, the derivatives $d\theta_O/dt$ and $d\theta_{CO}/dt$ were set equal to zero and the terms $k_5\theta_O(1 - \theta_{ox})$ and $k_6\theta_{CO}\theta_{ox}$ were ignored in equations 1 and 2. The justification for these approximations is the rates of adsorption, desorption and CO_2 production are much larger than the rates of oxidation and reduction of the surface ($k_1,k_2,k_3,k_4 >> k_5,k_6$. The difference between this method and that reported by STM is that this solution is not isothermal. The solutions obtained by the iterative and quasi-steady state methods were very similar. The only difference between the solutions obtained by the two methods occurred when the reaction approached a points of transition between branches. This is because $d\theta_O/dt$ and $d\theta_{CO}/dt$ become relatively large at these points and the steady state approximation no longer holds. Since the later method required much less computer time, it was the primary method utilized in this work.

REFERENCES

6.1) M. Sheintuch and R.A. Schmitz, Catalysis Rev. Sci. Eng. 15 (1977) 107.

6.2) J.E. Turner, B.C. Sales and M.B. Maple, Surface Sci. 103 (1981) 54.

6.3) J.E. Turner, B.C. Sales and M.B. Maple, Surface Sci. 109 (1981) 591.

6.4) P. Hugo, Ber. Bundsenges. Physik. Chem. 74(1970)121.

6.5) J.P. Dauchot and J. Van Cakenberghe, Japan. J. Appl. Phys. Suppl. 2, Pt. 2 (1974) 533.

6.6) J.P. Dauchot and J. Van Cakenberghe, Nature (Phys. Sci.) 246 (1973) 61.

6.7) R.T. Plichta, Ph.D. Thesis in Chemical Engineering (1976), University of Illinois at Urbana, obtained through University Microfilms, Ann Arbor, MI.

6.8) R. Gray, J.F. Griffiths and J.S. Rogerson, presented at the Joint ASME/AIChE 18th Nat. Heat Transfer Conf., San Diego, CA, August 6-8, 1979.

6.9) E. McCarthy, J. Zahrdnick, G.C. Kuczynski and J.J. Carbery, J. Catalysis 39 (1974) 29.

6.10) M.B. Cutlip and C.N. Kenney, in: Proc. 5th Intern. Symp. on Chem. Reaction Eng., Houston, ACS Symp. Ser. 65 (1978) 475.

6.11) M.P. Cox, G. Ertl, R. Imbihl and J. Rustig, Surface Sci. 134 (1983) 517.

6.12) G. Ertl, P.R. Norton and J. Rüstig, Phys. Rev. Lett. 49 (1982) 177.

6.13) P.R. Norton, P.E. Binder, K. Griffiths, T.E. Jackman, J.A. Davies and J. Rüstig, J. Chem. Phys. 80 (1984) 3859.

6.14) D.M. Haaland and F.L. Williams, J. Catal. 76 (1982) 450.

6.15) D.J. Kaul and E.E. Wolf, J. Catal. 91 (1985) 216.

6.16) W. Beusch, P. Fieguth and E. Wicke, Adv. Chem. Ser. 109 (1972) 615.

6.17) B.C. Sales, T.E. Turner and M.B. Maple, Surface Sci. 114 (1982) 381.

6.18) P. Gray and S.K. Scott, Chem. Eng. Sci. 38 (1983) 29.

6.19) A. Uppal, W.H. Ray and A.B. Poore, Chem. Eng. Sci. 29 (1974) 967.

6.20) H.P. Bonzel, A.M. Franken and G. Pirug, Surface Sci. 104 (1981) 625.

6.21) M. Salmeron, L. Brewer and G.A. Somorjai, Surface Sci. 112 (1981) 207.

6.22) B.C. Sales, J.E. Turner and M.B. Maple, Surface Sci. 112 (1981) 272.

6.23 P. Légaré, L. Hilaire and G. Maire, Surface Sci. 141 (1984) 604.

6.24) M. Salmeron and G.A. Somorjai, J. Vac. Sci. Technol., 19 (1981) 722.

6.25) L.R. Velho and R.J. Barlett, Met. Trans. 3 (1972) 65.

LAWRENCE BERKELEY LABORATORY
TECHNICAL INFORMATION DEPARTMENT
UNIVERSITY OF CALIFORNIA
BERKELEY, CALIFORNIA 94720